Prebiotic Organization of Biomolecules on Mineral Surfaces

Hagop Abadian

Sorbonne Université

Ecole doctorale 397

Laboratoire de Réactivité de Surface

Prebiotic Organization of Biomolecules on Mineral Surfaces

M. Hagop ABADIAN

Thèse de doctorat de Chimie Physique des Matériaux

Dirigée par M. Jean-François Lambert ET Mme. Christel GERVAIS

Présentée et soutenue publiquement le 1 Mars 2021, Devant un jury composé de :

M. Bruno ALONSO	*Directeur de Recherche (ICG Montpellier)*	Rapporteur
Mme. Gloria BERLIER	*Professeur (Universita di Torino)*	Rapportrice
M. Florent BARBAULT	*Professeur (Université de Paris)*	Examinateur
Mme. Christine MÉNAGER	*Professeur (Sorbonne Université)*	Examinatrice
Mme. Dominique COSTA	*Directrice de Recherche (Chimie ParisTech)*	Examinatrice
M. Jean-François LAMBERT	*Professeur (Sorbonne Université)*	Directeur
Mme. Christel GERVAIS	*Professeur (Sorbonne Université)*	Co-Directrice

Dédicace

Acknowledgements

I would like to thank my supervisors M. Jean-Francois LAMBERT and Mme. Christel GERVAIS for their consistent support and guidance during the running of this project. I value the knowledge and the outstanding conversations with my supervisor M. Jean-Francois LAMBERT about the theories of the origins of life which gave me admiration and the needed motivation to complete my research project, I would also provide exclusive thanks to my Co-supervisor Mme. Christel GERVAIS for her upmost dedication and perseverance in analyzing and conducting alongside me the NMR experiments throughout the years, her contribution provided me with the ultimate enthusiasm and courage to face the challenges with a smile and optimism.

A warm-hearted appreciation to the assistance of M. Alberto MEZZETTI in accompanying me at the beginning of my IR experiments and providing me with additional knowledge in analysis and interpretation.

A special thanks to my Origin of life team, Louis TER-OVANESSIAN and Lise BEDOIN. I appreciate your group effort and cooperation throughout the years.

I thank all the permanent staff members who pulled out a helping hand in giving advice and showed sympathy towards my work, I thank all the non-permanent members and the friends I made during the past 3 years including Oscar, Ricardo, Marwa, Laura, Priyanka, Louay, Elisa, Antoine, Nawal, Vincent, Mathieu, Abdallah, Leila, Aya, Ola, Judy and Silvia with whom I have shared wonderful moments inside and outside out of the laboratory. A special shootout to my childhood friends in Lebanon who still think that I roam around in Paris eating croissant and drink wine every day.

I would like to express my deepest appreciation to Mme. Hélène PERNOT and M. Christian BONHOMME for welcoming me and giving me the opportunity to work in their respective laboratories; Laboratoire de Réactivité de Surface (LRS) and laboratoire de Chimie de la Matière Condensée de Paris **(**LCMCP).

I would like to express my gratitude to M. Bruno ALONSO and Mme. Gloria BERLIER, the reporters, for agreeing to judge my thesis as well as to M. Florent BARBAULT, Mme. Christine MÉNAGER and Mme. Dominique COSTA for agreeing to be my examiners.

Finally, the sincerest thanks goes to my loving family; my parents and my brother for always supporting me and having my back. When times are trying, knowing that my family is in my corner gives me the strength to carry through. Thank you for always being there.

I cannot finish my acknowledgement without mentioning my late uncle Mr. Hratch Demirdjian, who was a mentor and a great teacher. On a personal level, he has been a great inspiration to me as well as to my scientific career.

Table of Contents

Abstract

This thesis reports on the adsorption of two amino acids (AA) with different properties, Leucine and Glutamic acid, on the amorphous silica surface. It exemplifies a general approach to hybrid systems that combines experimental information and molecular modeling in order to characterize at the molecular level the interaction of organic molecules with adsorption sites on the surface of inorganic minerals.

State-of-the-art spectroscopic techniques, chiefly IR spectroscopy and solid-state NMR, were used to gather information on the functional groups of the amino acids and the way they were modified by the adsorption. In conjunction with macroscopic characterization techniques such as X-Ray Diffraction (XRD) and Thermogravimetric Analysis (TGA), which allowed the identification of the parameters that govern surface speciation – chiefly the activity of water, explaining the importance of a controlled drying step – and the competition between site adsorption and precipitation as a separate crystal phase.

For both amino acids, experimental data indicate that adsorption involves the formation of specific H-bonds with groups of surface silanols. DFT modeling showed that stable H-bonded adducts can indeed be formed involving silanols, one amino acid molecule and several molecules of water – anhydrous models did not correspond to the experimental observations, especially regarding the observed prevalence of zwitterions. Theoretical values of NMR chemical shifts were calculated and corresponded quite well with the experimental values, once again favouring microsolvated models. Tentative conclusions can be proposed regarding the topology of the H-bonded lattice, i.e. the H-bond connectivity between functional groups, water molecules, and surface silanols.

The thermal evolution of AA/SiO_2 systems was also investigated. Amide formation occurred at moderate temperatures. When adsorbed alone, Glu mostly converted to the cyclic form, pyroGlutamic acid, while Leu was mostly transformed to the cyclic dimer, cyclo(Leu-Leu). Both forms may be considered as “dead ends” with regard to the rise in biomolecules complexity that occurred at the origin of life on Earth. In contrast, when they were adsorbed together on the silica surface, they gave rise to the formation of linear oligopeptides that may be considered as a first step towards the emergence of proteins.

Chapter I : Origins of Life

I.1 Origin of small biomolecules; amino acids

I.1.1 The origins of Amino Acids

In 1924, Alexander Oparin proposed that the abiotic synthesis of organic compounds over a long period of time was the precondition for the emergence of life on earth,[1] hereby establishing a link between fundamental biochemical and prebiotic chemical processes, and laying down some intriguing questions for generations to come. It took almost 30 years until Oparin's model of reducing primordial atmosphere was tested experimentally by Miller and Urey, in the 1950s. Biochemists Stanley Miller and Harold Urey attempted to simulate these hypothesized conditions of the Archean Earth, by performing a spark discharge experiment in a custom-built experimental device containing a mixture of water, ammonia, methane and hydrogen (that were supposed to mimic the primordial atmosphere). The apparatus also simulated evaporation and precipitation through the use of a heating mantle and a condenser respectively; after some weeks of running the experiment, it eventually yielded numerous molecules including amino acids and became the cornerstone of prebiotic chemistry[2] (Figure 1.1). The Miller-Urey synthesis emphasized the importance of considering plausible environments that could have accommodated the primordial chemistry and directed the molecular evolution towards the building blocks of life on our planet.

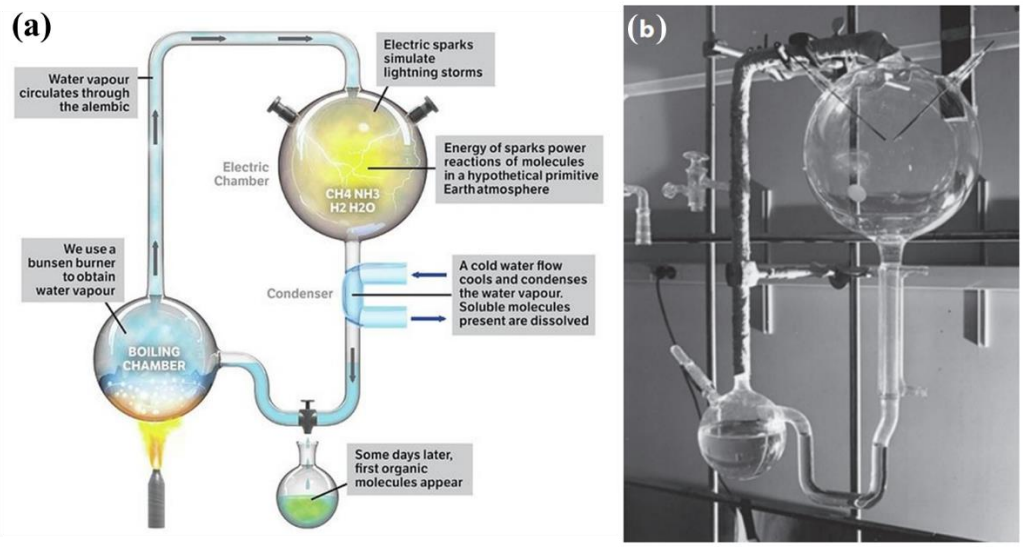

Figure 1.1. Spark-discharge apparatus used in the Miller-Urey experiments. (a) Schematic drawing of the apparatus. (b) Photo of the apparatus taken by Stanley Miller.[3]

The Miller-Urey experiment pioneered modern research on the molecular origins of life but their gas mixture postulated a reduced atmosphere, where hydrogen is present but oxygen is absent, since an oxidized atmosphere make the production of organic compounds thermodynamically unfavorable. Even in the presence of a neutral atmosphere (the primordial atmosphere is now believed to have been close to neutral[4]), most recent results suggest that

the yield of amino acid may have been highly underestimated due to a possible oxidizing step of the final amino acid product. Indeed, nitrite and nitrate also produced by spark discharge destroyed the amino acids produced.[5] However in the presence of a pH buffer and the right redox balance, this destruction of amino acids could be prevented; some additives such as Fe^{2+} could also play the role of oxidation inhibitors.

The changing views of the atmosphere inspired experimentalists to investigate the potential for synthesis of organic compounds in the presence of different atmospheric elements that could have been present in the primordial world. In their later work, Miller and coworkers continued with the scheme of the electrical discharge, but they integrated new geochemical knowledge about the Archean atmosphere: N_2 was used as an initial source of nitrogen, with only slight traces of ammonia (NH_3): these adjustments made possible to yield 10 proteinaceous amino acids (Ala, Asp, Glu, Gly, Ile, Leu, Pro, Ser, Thr, Val).[6]

Subsequent to Miller-Urey's experiments, other ones have involved energy sources different from electric discharge: one source that was popular was UV radiation since there would have been some UV light reaching the ground level due to the absence of an ozone layer. Under UV irradiation and mild conditions, formaldehyde (HCHO) and hydrogen cyanide (HCN) were generated : they are the precursors of amino acid formation since they react by Strecker synthesis to form prebiotic amino acids[7,8] (Figure 1.2). The production of amino acids from precursors such as formamide has been envisaged for a long time. In the 1910s, Walther Löb exposed wet formamide to UV light and electrical discharge and obtained the simplest possible amino acid, glycine.[9]

In summary, one can easily conclude that amino acids are relatively easily produced regardless of the source of the input energy as long as the light elements H, C, N and O are contained in a reducing or neutral atmosphere. The crucial condition is the absence of any oxidizing agent such as oxygen.[10]

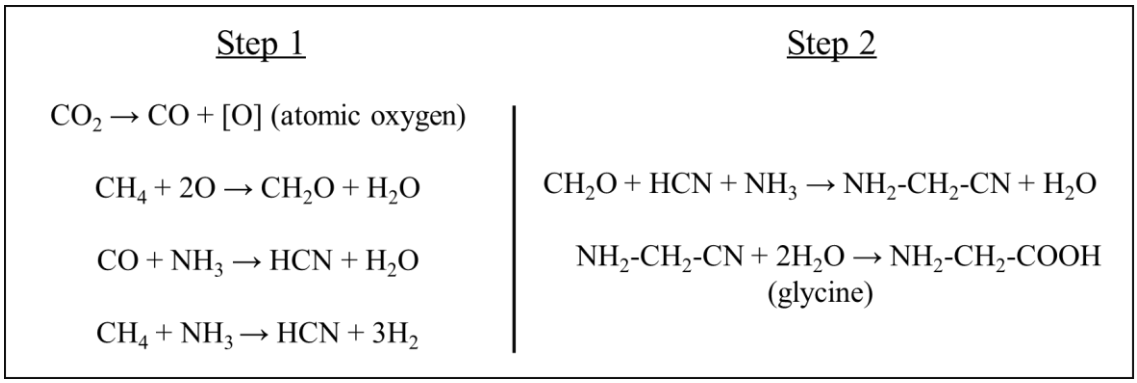

Figure 1.2. Some reactions involved in the formation of organic molecules such as glycine from atmospheric gases such as formaldehyde and hydrogen cyanide[11,12]

This groundbreaking event (Miller-Urey's experiment) has exerted a great influence over the origins-of-life field until the end of the 20th century: Stanley Miller was the initiator of the experimental study concerning the origins of small biomolecules from a mixture of atmospheric gases and later their evolution to even more complex bioorganic molecules. Many textbooks still state today that bioorganic molecules necessary for the emergence of life were formed by lightning (electrical discharge) on the primitive earth.

In spite of this, we have seen that Miller's scenario has raised some objections and as an alternative, many researchers studied meteorites.[13] They could have provided a source of small biomolecules in the frame of the "impact theory" in which meteorites containing significant traces of organic carbon including amino acids somehow formed in the interplanetary space, impacted the Earth and came in contact with the primordial surface: they burst out and led to the formation of organic molecules such as amino acids[14] or even more complex ones such as peptides; some have even claimed that living cells may have reached the earth's surface through meteorites.[15]

The theory of meteorites bringing life on earth may have its weak points: for instance, the organic molecules previously formed may be degraded once entering or coming in contact with the earth's atmosphere. Under high temperature flux, the molecules entering will have to endure enormous amounts of heat to reach the earth's surface; this implies that those meteorites should contain substantial amount of organic carbon to initiate life on impact. An additional point that further raises complications is that meteorites perhaps can 'give' life, but one must not forget what happened with the dinosaurs when a meteorite came into impact with them.

I.1.2 The 'RNA World' and the origins of nucleotides

Whether the first organic molecules were produced by Miller-Urey experiment-like syntheses or by meteorites or comets, many questions remain on the way to life.

To be able to answer these questions, we need to go back to the simplest autonomous living organisms, made up of cells, each composed of phospholipid bilayers containing, inter alia, a genetic molecule known as DNA (deoxyribonucleic acid). The genetic information located inside DNA can be transcribed into RNA (ribonucleic acid) which is mostly a messenger molecule, a process catalysed by a protein enzyme. Finally, this RNA is translated to proteins, a process yet again catalysed by protein enzymes. This description is famously referred to as "The Central Dogma of molecular Biology"; it is to be noted that nucleic acids require specific enzymes for the transcription and the translation process to be even possible, but at the same time proteins require nucleic acids to code for them.

Some researchers have assumed that life started from a double helixed DNA strand due to its role in heredity: they have predicted a sort of a "DNA world", however this concept was quickly discredited after it was well established that a DNA molecule cannot operate alone in a biological setting.[16]

RNA became the focus of more interest after understanding its cellular role as rRNA, mRNA and tRNA as well as its importance as a mediator in the genetic information pathway during transcription and translation. The phrase "RNA World" was first used by Walter Gilbert[17] in 1986, and quickly followed up by Lazcano[18] in 1996 and most recently by Sutherland[19] in 2015. The overall idea grasped by all scientists is that the feasibility of RNA world relies on the dual ability of RNA molecules. First, they can have a catalytic role like the enzymes discussed previously. For instance, RNA molecules have the potential capability to cleave organic molecules including themselves. This catalytic activity of RNA was also underlined by Thomas R. Cech[20] in the case of ribosomes, the molecular engines of peptide bond

formation. Second, RNA is of course a vector of information, even if in current cells long-term information storage has been taken over by the more resilient DNA.

RNA is a polymer and is the result of nucleotides polymerization. Nucleotides themselves consist of three chemically different parts: a sugar (ribose), a "nucleobase" (N-containing heterocycle) and a bridging phosphate group.

Phosphates play an important role in signal transmission, a useful process in genetic coding, and in metabolism, suggesting an important contribution to the origin of life. Among a network of phosphate-dependent reactions, nucleobases or ribose (an essential component for RNA) are produced (phosphate-independent[21] reactions are also possible), hence indicating a possible source and a clear route for the RNA world.[22]

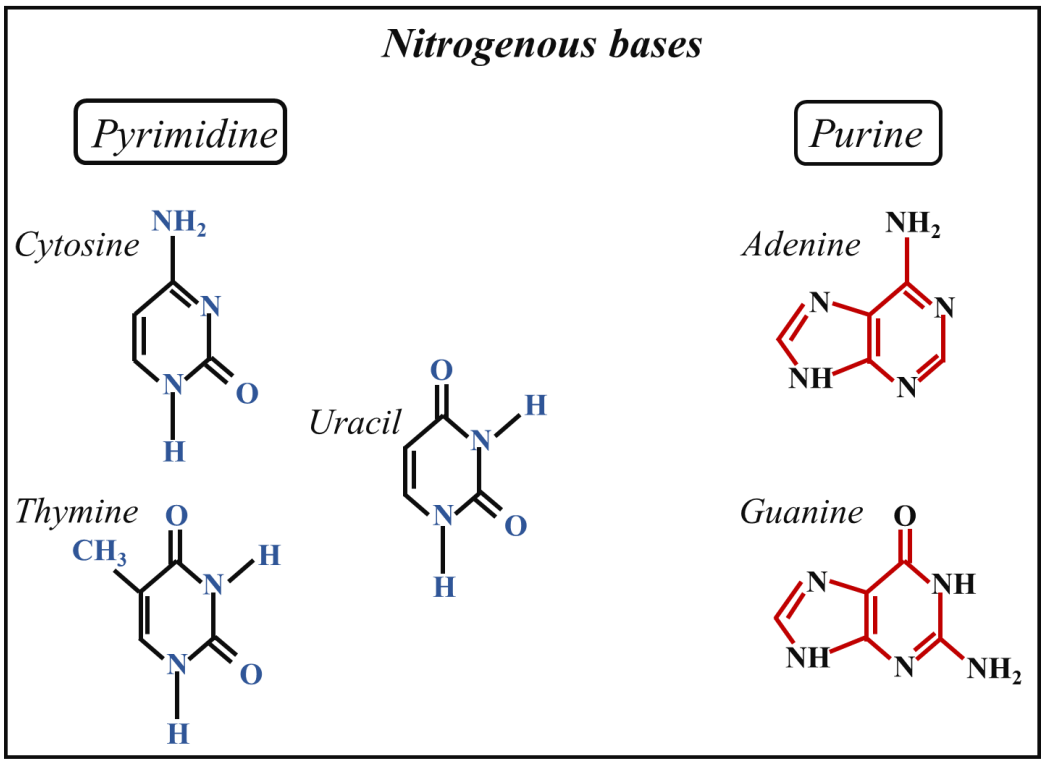

Figure 1.3. Structure of the various canonical nucleic bases: Cytosine, Thymine, Uracil, Adenine and Guanine

Nucleobases are another component of the nucleotides. They are either purines or pyrimidines[23] and the nature of the heterocycle (Figure 1.3) is crucial for base pairing, that has existed for some 3.6 Gya (Gigayears ago) [24]. The pioneering work done in the 1960s by Oró[25] showed the prebiotic synthesis of nucleobases: in 1961 Oró and Kimball[26] successfully synthesized adenine under primitive earth conditions from cyanide ions, which is considered as one of the milestones in prebiotic chemistry. The discovery happened shortly after the Miller-Urey's experiment (keep in mind that Oró had used a Miller-type experimental setup, i.e., a reduced atmosphere). The potential and pitfalls of this approach were reviewed by Leslie Orgel.[27]

Ribose, a component of nucleotides and sugars, could be generated from formaldehyde by chemical reaction known as formose reaction first observed by Alexander Butlerov.[28] Hydrothermal scenarios using the proposed reaction were also proposed in the past years by

Kopetzki *et al*.[29] The catalytic aspects of this reaction were reviewed by Delidovich as co-workers.[30]

Next, one must understand how ribose, nucleobases and phosphates were combined: this involves condensation reactions quite similar to those that will be treated in the part related to amino acid condensation (I.2). Other pathways leading towards nucleoside formation, that do not involve the previous synthesis of these three components have been proposed as well.[31]

The RNA world postulates that later on, the primitive polynucleotide chains were able to act as a functional template or even like a catalyst for promoting the polymerization of the complementary nucleotides to build up an initial strand of molecule, which is known as the RNA like polymer, hence providing its place in the emergence of life hypothesis.[17] We will not review further those steps that lie « downstream » of our research activity.

I.1.3 Other primordial biomolecules : lipids

Another essential requirement for life to start is the formation of some amphiphilic molecules such as lipids, able to self-assemble into vesicles. Their major interest is their barrier function, preventing “death by dilution” of the first prebiotic systems[32]. But they may also have enabled the formation of ion gradients. An early life would take advantage of these gradients as a source of energy for replicative process[33]. A “Lipid world”[34] would emerge, kick-starting metabolism before the advent of biopolymers. The advantage seen in the “RNA World” was the catalytic abilities of nucleic acids have. But lipids and other simple amphiphilic, generally only considered for their structural role, exhibit other remarkable qualities, such as substantial catalytic capacities[34–36]. A recent update on “Lipid world” developments may be found in Deamer [32]. Nevertheless, its limitations are clearly obvious as the availability of phospholipids, the lipid world precursors, on the primordial Earth is questionable. In fact, every scenario when studied closely may contain a point advantageous to the origins of life, but also another one that is detrimental to it. The goal of the prebiotic scientist may be to merge different scenarios in order to reach an ultimate possible answer.

In this thesis, I am going to focus on amino acids that may have built an ‘amino acid world’;[37] and indeed amino acids have played an interesting and important role in the origins of life scenarios (OoL), but how they have interacted with other constituents of life is another story. Among the numerous scenarios that have been proposed, some of the soundest and least complicated ones can be related to the Miller-Urey experiments in which a series of elementary biomolecules including amino acids were obtained under a reducing atmosphere. What makes this pathway more plausible than the popular “RNA World” is because amino acids are much easier to synthesize than RNA in the primitive earth. The Miller-Urey experiments have produced more than 40 different amino acids, likely to have been present and acted as initiators in prebiotic chemistry world and those that are produced from an endogenous source fit well with the previous illustration.[38]

I.2 The next step: formation of biopolymers, towards peptides and proteins

I.2.1 Temperature increase

The production of amino acid is only a first step; for peptides to appear, amino acids need to accumulate and polymerize. It seems that this step cannot be bypassed in the rise towards complexity, and once they are formed there are plausible pathways towards more complex forms of organization such as collectively autocatalytic self-replicating sets. [39]

The condensation of amino acids into biopolymers such as peptides and proteins requires the formation of a peptide bond (CO-NH) with the elimination of one water molecule (Figure 1.4.a). This dehydration step is endergonic by +2 to +6 Kcal/mol, which makes this chemical reaction thermodynamically unfavorable in free solution in ambient conditions. As a consequence, attempts to find a plausible path for the origin of life focused on other environments in the 1990s, first suggesting hydrothermal conditions since the temperature on the Earth's surface was slightly higher than nowadays. In this context, it is interesting that the oldest recognizable prokaryotes are the anaerobic sulfur-reducing chemosynthetic hyperthermophiles, organisms that grow optimally at 90° and above, like the ones found today in deep-sea hydrothermal vents.[40]. This possible connection between temperature and the occurrence of biomolecules in hydrothermal conditions has encouraged hypotheses connecting origin of life to near deep sea vents.[41] Similar temperatures and even higher ones are reached near sedimentary basins as well. The theory of the hydrothermal origins of life postulates that temperature increase along geothermal gradients induces a thermodynamically favored oligomerization over hydrolysis between two amino acids. It was shown by E. Shock[42] that condensation of amino acids in aqueous solutions is possible at high temperature, and as the temperature increased further, the cyclic form of the peptide is more stable than the linear ones in terms of Gibb's free energy.

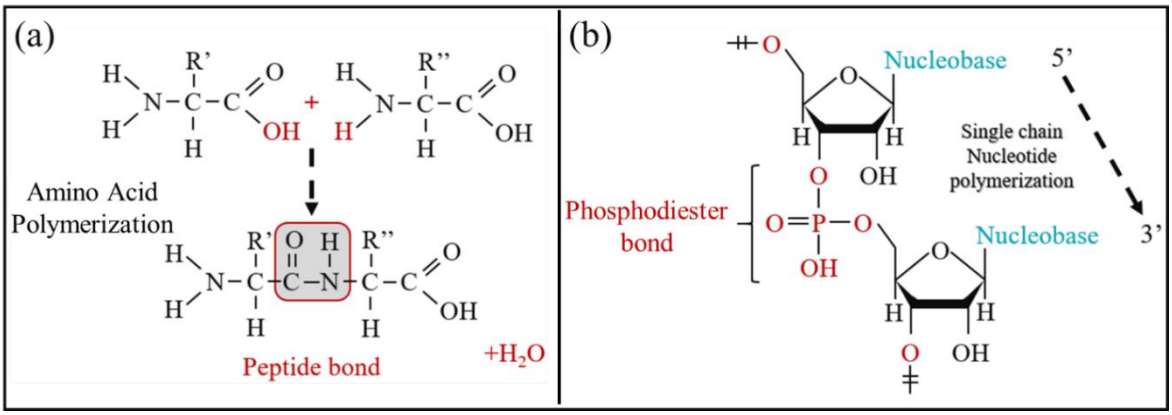

Figure 1.4. (a) Amino acid polymerization, (b) Nucleotide polymers showing the phosphodiester bonds (3', 5' refer to the numbering of the ribose OH groups)

Needless to say, origin of life proponents of the "RNA World" (Figure 1.4.b) are caught up with the same competitive and challenging debates, such as the "water problem" because thermodynamically, it is not possible for these bonds to form in an aqueous mixture. Hence, the thermal stability of peptides and proteins is controlled by the temperature-dependent equilibrium between the amino acids and the products of their binding to each other, i.e. the peptides. Their elongation to more complicated peptides (and finally to proteins) is subject to the same thermodynamic limitations as during the initial phase of peptide bond formation.[43]

An important role of temperature in the origins of life was also postulated by the 'flash heating' phenomenon,[44] based on the heating of the earth's surface by very large impact events that resulted in a sudden increase in the surface temperature. In addition to releasing some atmospheric gases (e.g. methane) that may have taken part in Miller's synthesis, this temperature increase could help polymerization of amino acids provided that it does not cause the complete degradation of the amino acids.

In a different approach, Rode[45] proposed that amino acids are able to oligomerize via the salt induced peptide formation (SIPF) reaction in aqueous solution at temperatures between 60° and 90° in the presence of a high concentration of NaCl (sodium chloride) and especially Cu^{2+} ions (here temperature mostly plays a kinetic role, the favorable kinetics being induced by complexation to the metal cations). Such high salt concentrations could have been reached on the primitive earth in lagoons and puddles before being rediluted with rain. The SIPF reaction shows some specific properties, like a preference to α-amino acids and even stereospecific differentiation in favor of the L-form enantiomer of the prebiotic amino acids.

In another application of the meteorite delivery model, some also suggest that peptide-like proteins are formed on interstellar dust grains and imported to our solar system via the impact of comets.

I.2.2 "Polymerization on the rocks"

It has been long postulated and suggested that mineral surfaces have played a crucial role in the chemical evolution of life, acting as a promising location for the transition from chemical geochemistry to biochemistry. The primary role of inorganic materials in the origins of life was first proposed by J. D. Bernal in 1949 in his influential lecture titled *"The Physical Basis of Life"* which was published later on in 1951. We will come back to Bernal's proposal in the following paragraph. Let us concentrate here on the justification he gave for a potential positive role on life. The formation of a peptide bond between two amino acids can be written as:

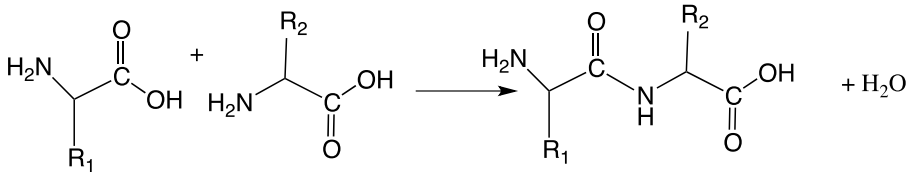

or in a more condensed way:

A + B ⟶ A-B + H_2O, with an equilibrium constant $K = \frac{a_{A-B}a_{H_2O}}{a_A a_B}$

Because this is a condensation reaction, concentrating the solution will increase the dimer/monomer ratio at equilibrium.• This also holds for any further polymerization step. Bernal argued that the effect of adsorption would be to increase the local amino acid concentration, and thus it would automatically favor the polymerization more in the "adsorbed phase" than in the solution. Indeed, in thermochemistry, adsorption is viewed as a local concentration increase in the vicinity of the surface and such an effect should take place. Not many data were available on amino acids adsorption when Bernal formulated his hypothesis, but it could be expected that e.g. minerals with positively charged surfaces, such as hydrotalcites, would adsorb and concentrate anionic amino acids such as Glutamate ions.

Unfortunately, when one tries to quantify this hypothesis by injecting experimental data, one finds that a significant displacement of condensation equilibria would require impossibly high concentrations of adsorbed molecules. And yet experimental evidence soon indicated that surfaces could have a promoting effect on amino acids, and then on nucleotides polymerization (cf. below, § I.3). Obviously, another explanation was required. In fact, it would be enough for adsorption to stabilize the polymers more than their monomers enthalpically due to some sort of specific bonding: the value of K would then increase and polymerization might be favored in the "adsorbed phase", although it would remain unfavored in the solution. There have been several arguments regarding this explanation. In 1991, de Duve and Miller[46] deduced from a theoretical analysis that for a dimer to be formed on the surface, it should have an adsorption enthalpy more negative than the two monomer reactants: and then the longer polymers would be so strongly adsorbed as to remain irreversibly adsorbed on the surface. Hill *et al*. confirmed experimentally that the free energy of adsorption of the oligomers increases regularly with their lengths; they adsorbed Glutamic acids oligomers on hydroxyapatite and then submitted them to a standard desorption procedure, noting that the longest ones remained "stubbornly adsorbed" [47]. Others such as Gerstner[48] strongly opposed this idea. Studying the adsorption of various biomolecules on a cation exchanger, they observed that the Gibbs free energy of the additional monomer unit being bound on the surface is approximately constant as the chain grows, which should eventually result in a less efficient surface polymerization.

Oddly enough, the simple explanation of AA polymerization through an increase of K in the adsorbed phase remained untested for more than twenty years after it was proposed. Only in 2010 did Marshall-Bowman *et al*[49] measure equilibrium glycine polymerization in aqueous dispersions of various minerals and compare it with minerals-free polymerization: no significant variation of K was observed, invalidating this explanation.

Yet there is still a simple thermodynamic explanation to surface-induced amino acids polymerization, and it rests on the role of water. If we can decrease the activity of water (a_{H2O}), then for $K = \frac{a_{A-B}a_{H_2O}}{a_A a_B}$ to be constant, $\frac{a_{A-B}}{a_A a_B}$ has to increase proportionally. In other terms,

• Let us write the equilibrium relation for a solution with constant water activity, $K = \frac{[A-B]}{[A][B]}$. Suppose for instance that we initially introduce both amino acids in concentration C°, and define *x* as the relative rate of dimerization, then $K = \frac{x/2}{(C°-x)^2}$; it is easy to solve for *x* and show that this quantity increases with C°, almost linearly when *K* is small - and the value of *K* is a few times 10^{-3} for A.A. dimerization.

speciation favors the monomers in “wet” conditions, but the polymers in dry conditions. And indeed, successful polymerization procedures all involved at least one drying step. The effect of the removal of water is a simple application of Le Châtelier's principle: removal of one of the reaction products automatically drives the amino acids condensation in the forward direction, favoring the polymerized peptides.[50]

But then, if the trick was only to dry the system, the mineral surface would not be indispensable. It has in fact been observed by several authors that bulk amino acids can polymerize without any mineral being present[51,52]. However, this only happens at rather high temperatures, higher than when they are deposited on a surface (e.g. 240°C instead of 150°C for glycine vs. glycine on silica) – and high enough to cause significant biomolecules degradation. Thus, surfaces do have an important role: they increase the reaction rate at a given temperature, in other words they have a catalytic effect. The ability of mineral surfaces to catalyze chemical reactions is well-known and they could have played the role that is now devolved to enzymes in living cells.

Here we see the all-important distinction between the two aspects of every chemical reaction, the thermodynamics and the kinetics. Thus, if we want to answer the question asked by Zaia: was amino acid adsorption on the mineral surface such an important parameter for life to emerge and evolve?[53] The answer is “yes”, but mostly to explain the reaction kinetics; the favorable thermodynamics on the other hand seem to be a straightforward consequence of Le Châtelier’s principle.

Then, what can be said about the biomolecules/surface interaction? For an efficient catalysis, it has to be “just right”, according to another general rule known as Sabatier’s principle. A good catalyst must interact strongly enough with the reagents in order to activate them, but not too strongly or they would be trapped in the formation of a stoichiometric compound. This takes an additional meaning in the case of the origins of life. Life is a metastable state of matter in which activated molecules are maintained for a long time, in conditions where, thermodynamically, they should be unstable. In amino acids polymerization, drying at moderately high temperatures provides conditions where the biopolymers are thermodynamically stable, and the kinetics of polymerization are fast enough for it to proceed; if, later on, the system is rehydrated at low temperatures, the polymers are metastable – but the reaction is so slow that they can persist for a long time. If the catalyst was too active, on the other hand, the polymers would be degraded immediately. This shows the importance of characterizing the biomolecules/surface interaction, which is the task we have undertaken in this thesis.

I.3 Mineral surfaces at the origins of life

In this paragraph, I will focus on the different minerals that have been proposed and/or tested for biopolymers formation since Bernal’s hypothesis was formulated.

I.3.1 Clay Minerals

Bernal anticipated that clays provide chemically active sites at which the first prebiotic reactions could take place.[54]

Clays are probably the most geologically relevant and abundant minerals on the primitive earth surface.[55] They are highly reactive due to their massive surface area to mass ratio, and clay minerals can adsorb large amounts of many biomolecules; they may have played a role to protect them from degradation against the harsh conditions of the early Earth (or of Mars[56]). Furthermore, their interlamellar space could have played a role in confining biomolecules to a well-defined region of space before they were encapsulated by biological membranes.[57]

Cairns-Smith went much further than that in a provocative book where he advocated the idea that clay minerals actually were the first living organisms, discussing ways in which they could have mimicked the first functions of life (information storage, growth and duplication, metabolism)[58] before a "takeover" by biochemical systems; however, there was never a convincing experimental demonstration of any part of his scenario.

The fact that origins of life model can include a hypothetical clay based explanation for any desired catalytic reactions makes it perhaps too convenient for comfort. As Robert Hazen[59] writes: "these 'magic powder' aspects of clays leave me frustrated".

Still, there were indeed some successful studies of clay-based prebiotic chemistry. Lahav[60] observed the polymerization of glycine on a montmorillonite submitted to "fluctuating environments", i.e. to alternating wetting and drying treatment. Wetting and drying experiments were popular with researchers in geochemistry, because they mimic the process of evaporation and precipitation (rain) in the early atmosphere. We have exposed the rationale for the success of procedures involving drying steps in the preceding paragraph. Later on, these systems were extensively studied by Bujdák and Rode.[61–63] Peptides up to 5 amino acid residues in length were obtained; the yields were often quite low, but this was probably due to insufficient activation temperatures and/or heating times.

In the frame of the "RNA world", Ferris and co-workers[64] showed that activated nucleotides are able to polymerize to RNA oligomers up to 55 nucleotides long through the formation of phosphodiester bonds on catalytically active surfaces such as montmorillonite clays. It should be noticed that nucleoside 5-phosphorimidazolides were used in the experiments, which are not prebiotic molecules and circumvent the thermodynamical problem by using an activated monomer, so that drying is not required.

Non-clay silicates have sometimes been considered for Origins of Life scenarios. Smith[65] has suggested that dealuminated zeolites and feldspars might scavenge organic species for catalytic assembly into specific polymers protected from prompt hydrolysis and photochemical destruction, due to their microporous structure. Several works were devoted to amino acids adsorption and reactivity on the surface of various zeolites, but they are not part of a systematic and coherent approach.[66–73]

A very different class of candidate materials for amino acids polymerization are metal sulfides, which will now be examined.

I.3.2 Pyrite and other sulfides

The first mineral surfaces included many volcanic rocks due to numerous volcanic eruptions that occurred on Earth, and these rocks included sulfides.

The idea of life emerging from a 'prebiotic soup' was strongly opposed by both Bernal and Wächtershäuser since many biochemical reactions are thermodynamically forbidden in a free solution, as we have mentioned. At the end of the 1990s, Wächtershäuser[74] proposed that a mineral surface based on pyrite (a crystalline iron sulfide, FeS_2) could have played a major role in the origin of life in an 'Iron-Sulphur world'. In short, hydrothermal vent systems, where volcanoes interacted chemically with oceans, provide the conditions required for the "Iron-Sulphur" reactions to take place at the surface of pyrite. The latter is positively charged,• inducing the concentration of anionic constituents such as polyionic coenzymes, nucleic acids and also some polypeptides, that could have given rise to a primitive metabolism on surfaces. The Iron-sulphur World attracted its share of criticism[46], mainly due to its unproven conjectures that have been pointed out through the years. The theory proposed by Wächtershäuser predicted a number of testable chemical reactions but lacks experimental studies. Nevertheless, it drew the attention of many researchers to sulfide surfaces, and peptide formation on metal sulfides has been demonstrated.[41] The reactivity of amino acids on sulfides was also the object of a series of high-quality molecular modeling studies.[75–78]

I.3.3 Chirality of the surface

Robert Hazen alongside his work on clay minerals performed adsorption of both types of amino acid enantiomers (L and D) on calcite crystals and observed that the chiral crystalline surfaces provide effective discriminative environments for left and right handed molecules. This links the chirality of the mineral surface with the problem of the organization of the prebiotic world.[79]

I.4 Amino Acid polymerization on oxide surfaces

Attempts at empirically testing Bernal's hypothesis of amino acids polymerization on a mineral surface have been carried out by a number of scientists since the 1970s. Lahav[80] studied the reactivity of non-activated amino acid in a fluctuating environment with clay as the mineral surface. He observed that under successive wetting and drying cycles (mimicking climate fluctuations), it was possible to obtain oligomers of glycine without any activating agents. By controlling the rate of cycles, it is possible to control the extent of polymerization.

In his experiments, Bujdák was able to expand the observation of amino acids polymerization to silica as well as on alumina[62,63], where he adsorbed and condensed Glycine (Gly), Alanine (Ala), Proline (Pro), Valine (Val) and Leucine (Leu). Like Lahav, he applied wetting and drying consecutively and found out that hetero-oligomerization does not only depend on the reactivity of each monomer introduced onto a surface but also on the stability of the final polypeptide product. He claimed that amino acids selectively polymerized with amino acids of the same kind rather than with another amino acid. Co-adsorption of more than one amino acid may indeed lead to sequence selectivity which is difficult to investigate due to the complexity of potential oligomers formed.[81] In fact, selectivity in amino acids polymerization is a very important question for the origins of life because any functional role of the short proteins formed on surfaces would be dependent on their exhibiting the 'right" sequences. In spite of this, it has been only little studied so far.

• This is at least what Wächtershäuser assumed; more recent data on pyrite surfaces indicate that they can often be negatively charged instead.

It was confirmed in the 1990s by Basiuk[82] that amino acids can form linear peptides on silica and alumina surface, by using IR vibrational spectroscopy : water vibrations clearly disappeared over drying procedures, which was a prerequisite for peptide bonds formation. Later on, he proceeded with follow up experiments on dehydrated silica surfaces by using HPLC and MS techniques. He showed that more severe thermal treatments of amino acids on the surfaces can cause not only sublimation but also decarboxylation and deamination as well.[83]

In the LRS team at Sorbonne Université, Stievano [81] combined thermogravimetric analysis, vibrational spectroscopy (IR) and macroscopic measurements to study the adsorbed forms of Glycine and Lysine and their reactivity on the surface. Meng[84] had already shown that glycine molecules deposited on a silica surface, led to peptide bond formation at high temperatures between 120 °C and 160 °C, although the main product was the relatively unpromising cyclic dimer ("DKP", i.e., diketopiperazine). Solid-state NMR was introduced as a tool for adsorbed amino acids characterization by Lopes *et al*. in 2009.[85] Later on, several studies were devoted by the same team to applying multi-technique characterization approach to several supported amino acid systems, on silica[86] and other supports[50,87], including TiO_2[88], clay minerals[89] and iron oxyhydroxides.[90] Two articles are of particular significance for this thesis. The first one, by Folliet *et al*.,[91] was a collaboration between LRS and LCMCP and contained the first application of the joint NMR-DFT characterization procedure to a supported amino acid system, namely glycine on mesoporous silica. The second one[92] only contained experimental data, and did not use NMR, but still played an important role in the choice of the systems we have studied. It focused on the behavior of couples of amino acids co-adsorbed on non-porous amorphous silica and found that the Glutamic acid + Leucine (Glu+Leu) couple exhibits interesting properties: formation of rather long linear polymers in a single activation step, and hints of stoichiometric and sequence selectivity. As a consequence, two Ph.D. thesis were devoted to the understanding of this system, the present one which is concerned with the molecular-level characterization of adsorbed Glu and Leu, and that of L. Bedoin[93] which deals with the identification of complex peptide mixtures obtained by their thermal activation through advanced mass spectrometric techniques.

Other groups that recently focused on the molecular level characterization of silica-supported amino acids using the same general approach as in the LRS are those of Guo and Holland.[94–97] and, for solid-state NMR, Ben Shir *et al*.[98–100] Their main findings will be reviewed in § I.5.3 below.

The preceding paragraphs mostly listed experimental studies, but the surface reactivity of adsorbed amino acids has also been tackled by molecular modeling methods since an early stage of the development of these techniques. The DFT technique has been applied in the LRS team[101–103], but the most systematic theoretical investigation of supported amino acids, on several silica polymorphs and also on apatites, is due to Rimola and Ugliengo. These references will also be commented below after the molecular modeling techniques have been introduced.[104–117]

As this short summary shows, intensive investigations have been made to understand amide bond formation both experimentally and by computational means. However, no full understanding has been reached in this frame yet, due to the fact that different amino acids on different surfaces are investigated by different scientific groups, and sometimes using different deposition and activation methods which makes it difficult to compare the results. For instance, several spectroscopic studies carried out by Lambert and co-workers[86,118,119] indicate that glycine adsorbs, from an aqueous solution, on amorphous silica as a zwitterion and reacts at

160 °C to give diketopiperazine (DKP), the cyclic dimer product. In contrast, IR measurements of Martra *et al*[120], who performed surface adsorption from the gas phase reactants, show the formation of long oligomers from successive feedings on amorphous silica at mild temperatures. Obviously the results obtained from these two different research groups are not incompatible, but they underline that very different outcomes may follow from a difference in the adsorption procedure – and thus, they also underline the need for a thorough *in situ* characterization of the state of adsorbed molecules.

I.5 Molecular-level characterization of adsorbed biomolecules

I.5.1 Solid state NMR spectroscopy

I.5.1.1 Introduction to solid state NMR spectroscopy

Since its discovery, 70 years ago, independently by Bloch[121] in liquids and Purcell[122] in solids, Nuclear magnetic Resonance (NMR) has revolutionized the way molecules and materials are analyzed and characterized at the molecular level. It was indeed observed that when a nucleus with non-zero spin such as ^{1}H, ^{31}P or ^{19}F is placed in a magnetic field and excited with a radiofrequency (RF) field, it responds uniquely with a specific frequency of absorption. Furthermore, for a given nucleus, changes in the local environment (bond length, angles, symmetry) modify its surrounding magnetic field inducing a significant effect on the NMR spectrum. Consequently, solid-state Nuclear Magnetic Resonance (ssNMR) spectroscopy has proven to be a powerful and complementary tool to crystallographic techniques for the structural characterization of disordered solids (glasses, amorphous solids and biological samples). In addition to informations on the structure, dynamics in solids can also be investigated.

Nowadays, NMR spectroscopy is considered as one of the most important techniques in chemistry in a wide range of applications as *(i)* identification of organic and inorganic compounds ranging from the very small molecules (organic and inorganic drug molecules[123]) to the very large molecules such as proteins[124,125] as well as elucidating their form and function simultaneously, *(ii)* determination of chemical reaction mechanisms in organic and polymer chemistry, *(iii)* determination of solid materials structural reactivity (ceramics, wood and glass materials), *(iv)* imaging as shown by Lauterbur who investigated the internal structure of an object by placing it in an intense magnetic field gradient[126], a technique now known as MRI.

I.5.1.2 General Principles of ss-NMR Spectroscopy

The theory behind NMR is that most nuclei possess an intrinsic angular momentum called spin[127], one of the fundamental physical properties of matter alongside mass, electric charge and magnetism[128]. It should be furthermore noticed that electrons also possess a spin, a property used in EPR spectroscopy for example. The nuclear spin I [129–131] is responsible for the magnetic moment μ_I (μ_s) as given by :

$$\mu_I = \gamma I \quad (1)$$

where γ is the gyromagnetic ratio, characteristic of the individual isotopes of nuclei. For NMR spectroscopy, the spin of the nucleus must be non-zero : when placed in a magnetic field, the nuclei's magnetic moments interact with the external magnetic field B_0 [132]. For I = ½ nuclei (^{1}H, ^{13}C and ^{15}N for example), each nucleus has two linearly independent spin states, with m = 1/2 or $m = -1/2$ (also referred to as spin-up and spin-down) for the z-component of spin. In the absence of a magnetic field, these states are degenerate. If the nucleus is placed in a magnetic field, the two states have no longer the same energy as a result of the interaction between the nuclear magnetic dipole moment and the external magnetic field called "Zeeman interaction"[133]. More generally, the Zeeman interaction results in a distribution of single state into 2I+1 non-degenerate state values between +I and –I in integer steps.

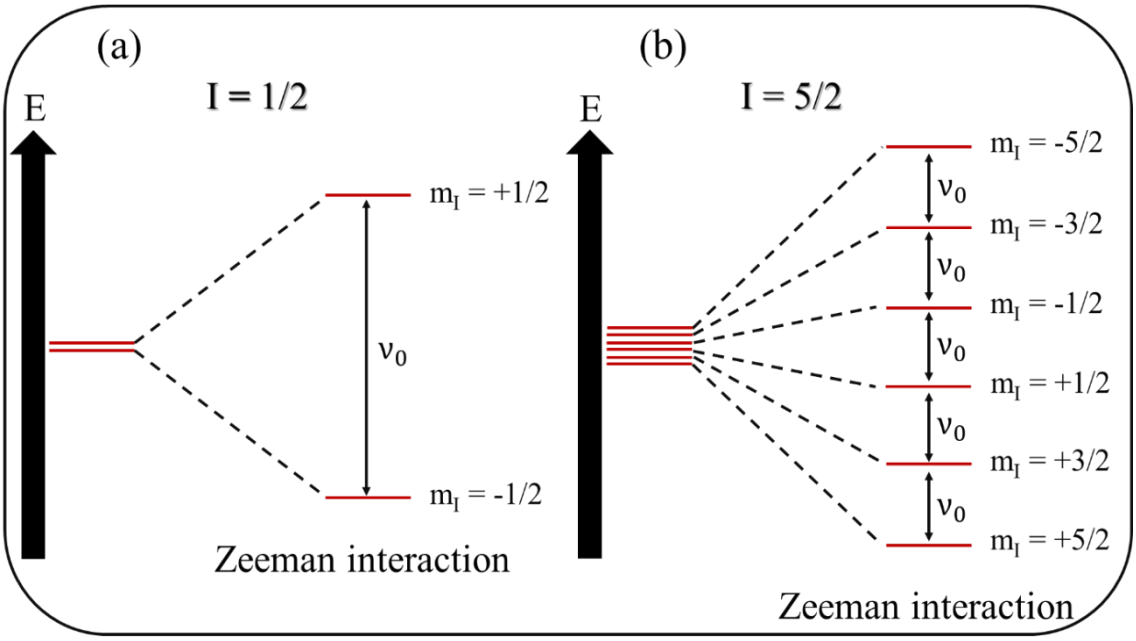

Figure 1.5. Splitting of (a) I = 1/2 and (b) I = 5/2 nuclear energy levels by the Zeeman interaction with the application of an external magnetic field. The frequency difference between the energy levels is defined as the Larmor frequency, ν_0, and is quoted in Hertz (Hz)

The external magnetic field B_0 is considered to lie along the z axis, the projection of the spin I of the nuclei onto a specified axis, arbitrarily the z axis, is given by $I_z = mI\ \hbar$, where I_z is the z component of I. mI is the magnetic quantum number and has (2I + 1) values as discussed earlier: hence this induces a 'z' propagation effect on each of the energy states:

$$E_{|m_I\rangle} = \mu_z B_0 \quad (2)$$

$$E_{|m_I\rangle} = -\gamma m_I \hbar B_0 \quad (3)$$

As an example, the splitting of the energy levels for a spin I = 1/2 and a spin I = 5/2 by the Zeeman interaction is shown in Figure 1.5. The selection rule for observable transitions in NMR spectroscopy is ΔmI = ± 1, which allows transitions to occur between adjacent energy levels. When an electromagnetic radiation of energy interacts with such a system, the nuclear spins change their state undergoing resonant absorption. The resonance condition is given by :

$$\omega_0 = \frac{\Delta E}{\hbar} = -\gamma B_0 \quad (4)$$

Where ω_0 is the '*Larmor frequency'* in rad/s or in Hz

$$\nu_0 = \frac{-\gamma B_0}{2\pi} \quad (5)$$

The presence of an electronic cloud around the nuclei (depending on the chemical environment of each atom) induces a small magnetic field aligned and opposed to B_0. A shielding tensor σ can therefore be described as $B_{ind.} = -\sigma . B_0$, where B_{ind} is the induced magnetic field created by the response of the electronic cloud of the nucleus to the external magnetic shield. This small contribution is nonetheless very important because it is responsible for the chemical shift which is different for each nucleus. Indeed, the nucleus doesn't feel "B_0" but an effective field B_{eff} = $(1-\sigma)B_0$ and the resonance frequency isn't ν_0 anymore but $\nu = \frac{\gamma B_{eff}}{2\pi}$
Furthermore, the chemical shift, the value commonly used by chemists, can be defined by:

$$\delta_{iso} = \frac{\nu - \nu_{ref}}{\nu_0} \times 10^6 \quad (6)$$

where ν_{ref} is the resonance frequency of a reference compound (for example Trimethylsilane TMS for ^1H and ^{13}C). Chemical shift is expressed in ppm.

I.5.1.3 Techniques in solid state NMR spectroscopy

In solution, sharp well-resolved NMR signals are usually observed due to averaging of anisotropic interactions (such as chemical shift anisotropy, dipolar and quadrupolar couplings) thanks to the rotation and tumbling of molecules (Brownian motion). In the solid state, broad line features are observed as a consequence of non-averaging of large anisotropic interactions[134], eventhough NMR signals were first observed in solids.[122] Over the years, development of methods to increase resolution such as magic angle spinning (MAS) but also sequences to increase sensitivity as cross polarization (CP), or spectral edition as 2D HETeronuclear CORrelation (HETCOR) have made solid state NMR spectroscopy a successful and promising technique for organic, inorganic and biological solids. A selection of the techniques and sequences used in this study will be briefly highlighted and explained in the upcoming parts.

I.5.1.4 Magic Angle Spinning (MAS)

At the preliminary stages of the NMR spectroscopy, most studies were focused on solution samples because most of the interesting information in solids was hidden under the broad

unresolved signals. The major breakthrough in solid state was the Magic Angle Spinning (MAS) technique in the 1950s by Lowe[135] and Andrew[136], combined with other sequences such as spin echoes known as the Hahn echo[137], high resolution NMR spectra were obtainable from solid samples by the 1970s.

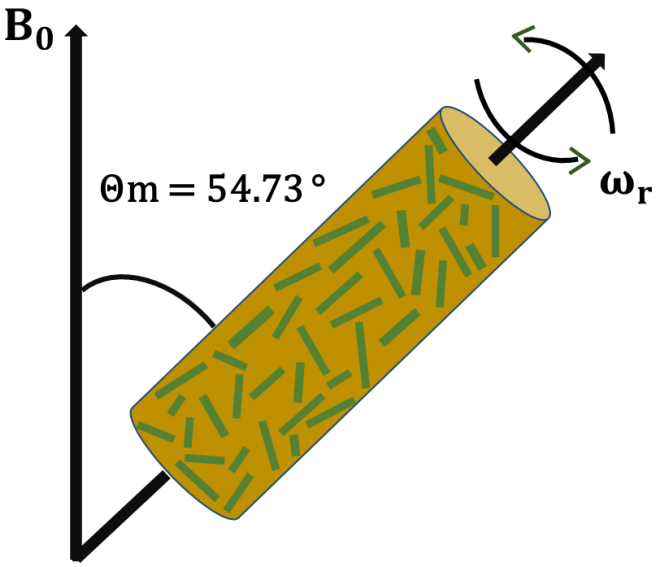

Figure 1.6. Sample rotation at magic angle 54.73° with respect to magnetic field B_0 in MAS technique where ω_R is the spinning frequency

Broad features of static spectra due to anisotropic interaction such as chemical shift anisotropy and dipolar coupling could be narrowed by combining MAS with the NMR spectroscopy.[138] The technique involves spinning rapidly the powdered sample in a rotor (typically in zirconia) at an angle θm = 54.7° (called the magic angle) with respect to the external magnetic field B_0 as shown in Figure 1.6. Indeed, this angle cancels to zero the second order Legendre Polynomial ($P_2(\theta) = ½(3\cos^2(\theta)-1)$ while chemical shift and dipolar coupling interactions can be expressed as $\omega = \omega_{iso} + \omega(\alpha,\beta,\gamma).P_2(\theta)$ where ω_{iso} and $\omega(\alpha,\beta,\gamma)$ are the isotropic and anisotropic contributions of these interactions. Consequently, MAS allows averaging these interactions to their isotropic value. If the spinning frequency is inferior to the amplitude of the interactions, residual spinning sidebands will be observed. Furthermore, in combination with high spinning speeds, the use of high field spectrometers can be of importance to gain resolution in proton spectra.

I.5.1.5 Direct Polarization

An important technique for solid samples is the direct polarization[139] of the nuclei. For ^{13}C or ^{15}N, high power ^{1}H decoupling can be applied in addition. The spectra obtained allow the observation of the chemical environments and their quantification, provided that a suitable recycling delay is chosen. The latter has to take into account T_1 relaxation (also known as spin-lattice relaxation or longitudinal relaxation, which corresponds to the time for the magnetization to come back to equilibrium along B_0). Typically, the recycle delay is given by :

$$D_1 = 5\ T_1 \qquad (7)$$

On the other hand, as will be described in chapter 3, choosing a short relaxation delay can be a way to select signal of a disordered phase and get rid of a crystalline one since T_1 values are known to be longer for crystals.

Nonetheless, to address the recurring problem of NMR lack of sensitivity, in particular in organic molecules since the natural abundance and the gyromagnetic ration of both ^{13}C and ^{15}N nuclei are low, specific NMR sequences were proposed, as Cross Polarization.

I.5.1.6 Cross Polarization

Hartmann and Hahn[140] discovered a double resonance condition allowing the polarization transfer from an abundant spin system (such as the proton ^{1}H) to a dilute spin system (such ^{13}C or ^{15}N). Later on, Pines and co-workers[141] succeeded in using this double resonance conditions to achieve higher ^{13}C sensitivity of adamantane NMR spectrum via a $\{^{1}H\}$-^{13}C transfer sequence which became known as the 'cross-polarization' technique. Initially, this method was developed for static samples, and later modified by Schafer and Stejskal for rotating solids.[142]

Transfer of polarization takes place between the two spins I (abundant) and S (rare) through I-S dipolar coupling, when I and S pulse frequencies satisfy, in the rotating frame, the Hartman-Hahn condition[140] given by:

$$\omega_{1I} = \omega_{1S} \tag{8}$$

However, when CP (Cross Polarization) is coupled with the MAS (magic angle spinning), time dependency will be introduced automatically and the Hartmann-Hahn conditions will be slightly altered as follows:

$$\omega_{1I} = \omega_{1S} + n\,\omega_R \tag{9}$$

Figure 1.7 shows a simple version of cross polarization pulse sequence with proton decoupling. Transverse magnetization is created on I spin (where I is typically a nucleus that has a high gyromagnetic ratio and high natural abundance like ^{1}H) through the application of a 90° pulse along the x-axis. Then, a spin-locking pulse is applied on both spins I and S for a certain time known as the 'contact time', where the magnetization of spin S is brought into equilibrium with the I spin in the rotating frame.

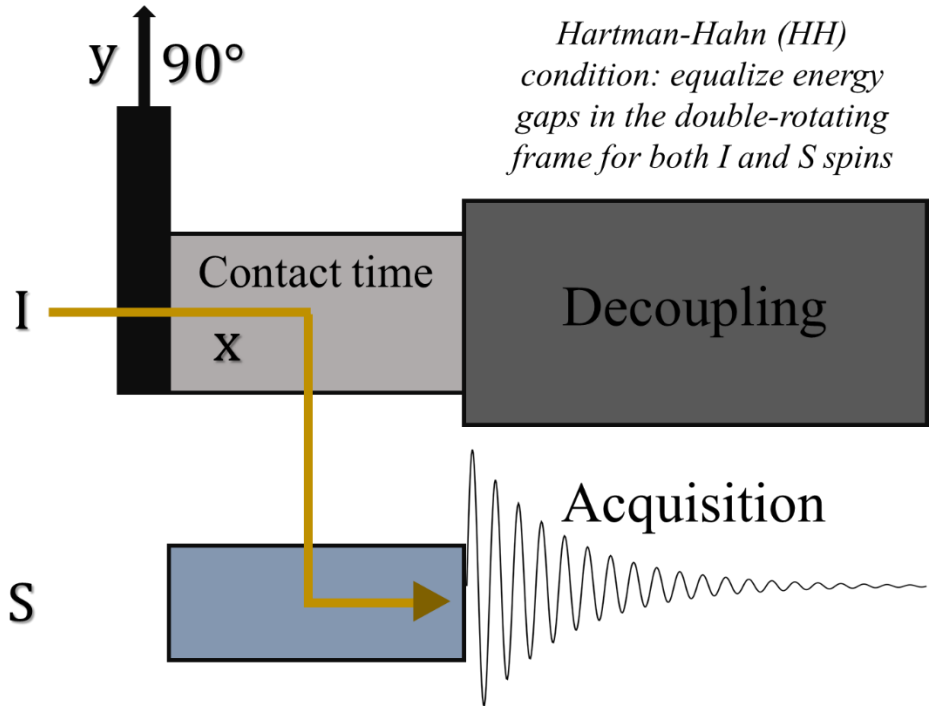

Figure 1.7. Pulse sequence of Cross Polarization with heteronuclear decoupling

One of the benefits of using the Cross Polarization experiment is that it offers a signal enhancement[143] of spin S by a factor N, depending on γ ratio between S and I spins, given by :

$$N = \frac{\gamma_I}{\gamma_S}\left(1 - \frac{N_S}{N_I}\right) \qquad (10)$$

where N_I and N_S are respectively, the numbers of abundant and rare spins in the sample. If γ_I/γ_s decreases, when $N_I > N_S$[144], hence N decreases. In other words, the magnetization transfer would not be possible if the gyromagnetic ratio of the abundant spin I was not larger than that of spin S (the less abundant nuclei). Consequently, an increase in the polarized factor (Ns) on the spins S after some contact-time is expected. Using ^{1}H as the I spin is therefore very efficient since it has the highest γ value.

An additional advantage in using CP-NMR pulse sequence is that recycle delay is now dependent on the I instead of the S spins, and protons show much shorter T_1 values than ^{13}C or ^{15}N. This allows therefore much shorter recycle intervals and quicker acquisitions. Hence more transients can be acquired in a given time, improving the signal-to-noise ratio (S/N).

CP also allows spectral edition in terms of degree of protonation since polarization is transferred from spin I (usually proton) to another spin S (^{13}C or ^{15}N) through dipolar coupling. Furthermore, information on dynamics (motion) can also be deduced since the magnetization transfer is governed by heteronuclear dipolar coupling which can be averaged by rapid motion.

I.5.1.7 Heteronuclear correlation, a 2D experiment

While high-resolution NMR spectra reveal information about the number of different species, their relative intensities, and respective chemical environments, in many cases more detailed

structural information can be obtained using two-dimensional correlation experiments. In these experiments, magnetization is transferred between nuclear spins, through either the dipolar coupling (a through-space interaction) or the J coupling (mediated by chemical bonds), providing information on spatial proximity, connectivity, and topology. In addition, using multiple dimensions can allow spectral edition to distinguish between the overlapping signals that exist in large molecules.[145]

In 1D pulsed Fourier transform NMR experiments, the signal is recorded as a function of one time variable and then Fourier transformed to obtain a spectrum. In 2D NMR experiments, the signal is recorded as a function of two time variables, t_1 and t_2, and the resulting data is Fourier transformed in both dimensions to obtain spectra. During the 1st period (t_1) also known as the preparation time, the sample is excited by one or more pulses, the resulting magnetization is allowed to evolve during t_1. Then another period follows, which is called the mixing time, after this period the signal is automatically recorded as a function of the second time variable t_2. It is important to realize that the signal is not recorded during the time t_1, but only during the time t_2 at the end of the sequence. The data is recorded at regularly spaced intervals in both t_1 and t_2.

Here I will focus on the ^{1}H-X (X being ^{13}C or ^{15}N in this manuscript) 2D CP-MAS HETCOR sequence (Figure 1.8.b), which consists in combining a cross polarization (CP) pulse experiment with a t_1 evolution. This second evolution time induces the acquisition of a series of FIDs which permits the reconstruction after Fourier Transform of an indirect dimension.

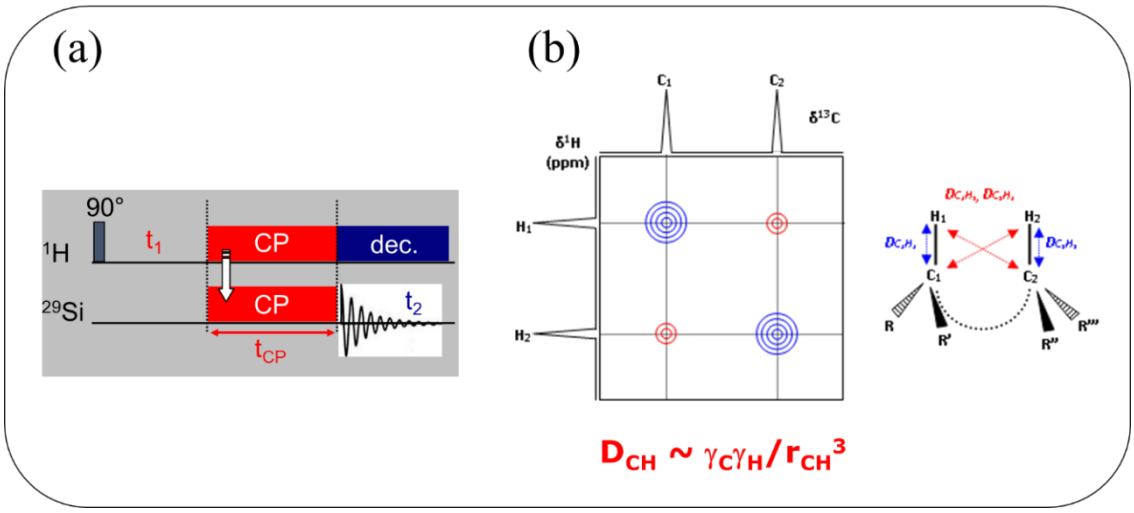

Figure 1.8. (a) Pulse sequence in {^{1}H}-^{29}Si CP-MAS HETCOR experiments (b) Scheme mapping in 2D ^{13}C-{^{1}H} CP MAS HETCOR for a simple system showing that correlation peak intensities are proportional to the intensity of the ^{13}C-^{1}H dipolar coupling and therefore to the C---H distances

^{1}H and X nuclei close in space and having therefore a strong dipolar coupling (proportional to $\frac{\gamma_H \gamma_X}{r_{HX}^3}$) will show correlation peaks on the two-dimensional map such as the one presented in Figure 1.8.b.

It should be noticed that S/N ratio in HETCOR experiments can be low when using naturally abundant ^{13}C or ^{15}N samples considering both the small natural abundance and gyromagnetic ratio of these isotopes. For that reason, isotopically enriched samples are useful to obtain a decent information in a reasonable acquisition time.

I.5.2 Study of Organic/Inorganic interactions by ss-NMR spectroscopy

The connection of NMR with 'origins of life' stands in the ability of this spectroscopy to study hybrid interactions between organic molecules and disordered mineral surfaces[146]; hybrid material or phase is considered as a disordered physical-chemical system that forms intricate organic and inorganic network. NMR offers a non-destructive way to analyze surfaces, adsorbed molecules but also modes of interaction between both components. This includes precise characterization of surfaces sites on which molecules will be adsorbed, dynamics and conformations of the molecules on the surface, H-bonding network, nature and hydration level of the interface between the molecule and the surface etc…. As described previously, NMR offers indeed a panel of sequences, both one- and two-dimensional to obtain these informations. In parallel of the NMR experiments, inorganic surfaces can be modelled by using *ab initio* approach with the aim to better characterize the reactive sites. In a second time, various modes of adsorption of the studied molecules can be studied to determine the most stable configurations. Finally, spectroscopic data and in particular NMR parameters can be calculated[147] and compared with experimental values. This theoretical approach can be crucial for the interpretation of NMR data as described at the end of this first chapter.

I.5.3 Literature examples of NMR investigation of amino acid adsorption on mineral surfaces

NMR spectroscopy has the ability to probe both the structure and the dynamics of biomolecules such as amino acids[148,149] alongside other characterization methods such as XRD. The biological activity of these biomolecules is governed by their interactions with other molecules, themselves influenced by their three-dimensional structure in space. Hence the knowledge of the 3D structure of a biomolecule is essential for a complete understanding of its function[150], and X-Ray diffraction is useless when crystallization is not possible. The earth's surface is mainly made of inorganic materials, able to interact with any organic molecule and have a catalytic activity as described at the beginning of this chapter. In this context, adsorption of amino acids as well as their condensation to peptides on silica surface has been investigated by NMR as summarized briefly in this paragraph.

I.5.3.1 Mesoporous Materials

Vega *et al*.[151] studied the mobility of deuterated Alanine molecules in mesoporous silica by ^{2}H NMR. The mobility was highly dependent on the hydration state; N-terminus hydrogen binding was seen for Alanine on the vicinity of SBA-15 and MCM-41 surfaces. Deuterium MAS NMR study of methionine and dialanine showed that the hydrogen binding of these molecules on the surface occurs via their N terminus and that a possible reorientation of the whole molecule at the surface binding site must be very slow.[152]As soon as the hydration reached one or two water molecules per (undefined) adsorption site, these waters could displace the adsorbed amino acid or peptide, and the latter became mobile.

Ben Shir and co-workers characterized the organic/inorganic interphase of Alanine encapsulated in a mesoporous silica[98] (SBA-15) by using an array of NMR techniques sensitive to dipolar couplings, $^{15}N\{^{13}C\}$ and $^{29}Si\{^{15}N\}$ REDOR NMR and $^{15}N\{^{1}H\}$ SLF. They identified

the presence of free and bound Alanine, both zwitterionic. The bound Alanine was engaged in an intermolecular hydrogen bond type of interaction between the ammonium (NH_3^+) moiety of Alanine and several surface silanol groups (3 or 4). Upon hydration, it changed into free Alanine, in an environment similar to an aqueous solution. The same battery of techniques, with the addition of $^{13}C\{^{15}N\}$ HETCOR was later applied to Gly on SBA-15,[36] and extended to Gly on MCM-41.[37] Very similar interpretations were proposed, including H-bonding of the (NH_3^+) moiety to silanols in the "dry" state, and the key role of the hydration state: even a limited number of water molecules cause the adsorbed amino acid to become more mobile, in a solution-like state.

We have already mentioned the work of Folliet *et al*. on Gly/MCM-41[91] as the first application of the joint experimental/modeling approach adopted in our thesis. In addition to a minor amount of crystalline Gly, the comparison of single-pulse (or direct polarization, DP) and CP spectra showed the coexistence of two glycine populations, one very mobile and one rigidly held on the surface. HETCOR results showed that the latter form was involved in a network of H-bonds involving both water and the surface silanols. As we will see later, comparison of experimentally observed chemical shifts with those calculated by molecular modeling allowed to propose more precise local structures for this adsorbed form.

I.5.3.2 Non-porous Silica nanoparticles

As we mentioned in § I.4, Lopes *et al*. were the first to perform solid state ^{13}C and ^{15}N NMR on glycine adsorbed on a silica surface, in this case an amorphous fumed silica (Aerosil 380, which was also used in our work). They could separately observe the crystalline and the adsorbed state of glycine, even in samples where XRD only gave an ambiguous response. Moreover, anionic and cationic forms of zwitterionic glycine could be distinguished in both ^{13}C and ^{15}N spectra. Finally both nuclei were sensitive to the presence of peptide bonds.[89]

A series of experiments using NMR were then performed by Lambert *et al*. at the LRS on amino acid adsorption on silica surfaces, to further understand the adsorbed amino acid signatures and their evolution with thermal activation. For example, glycine on silica was observed by ^{13}C NMR to form peptide bonds when heated at 160°C under a dry atmosphere, but not under a wet one[50], confirming the "Le Châtelier" interpretation of amino acid polymerization (cf. § I.2.2). The adsorption of Glutamic acid at low coverages gave a specific ^{13}C NMR fingerprint[81], and upon thermal activation, a cyclic form (pyroglutamic acid) was obtained rapidly at a temperature around 130°C.

Another team that systematically applied solid-state NMR to amino acids adsorbed on silica is that of Guo and Holland. Using ^{13}C and ^{15}N CP-MAS NMR, and also $^{1}H\{^{15}N\}$ and $^{1}H\{^{13}C\}$ HETCOR experiments, they distinguished between adsorbed and crystalline forms of Alanine on silica (although both were zwitterionic), as had been done for glycine.[95] Furthermore, they could observe modifications in the HETCOR correlations as a function of hydration: the carboxylate and ammonium interacted with water molecules in the hydrated state, but more likely with some silanols in the dry state (in opposition to the mesoporous silicas mentioned above, where only the ammonium seemed strongly bound to the surface). They also showed that thermal condensation, forming peptide bonds, from Alanine to the cyclic dimer, occurs within a small time and temperature range (170°C).[97]

Interestingly, they also studied the adsorption on the same amorphous silica of lysine, an amino acid that has an additional $–NH_3^+$ group in its side chain. Lysine was shown to interact through hydrogen bond between the side chain ammonium and the surface silanol groups[94,96] (instead of the ammonium of the amino acid moiety). Although we did not investigate lysine, we must remember that side chain groups can also play an important role in adsorption.

I.5.3.3 Clay Minerals

In an early application of solid-state NMR, Di Leo[153] could distinguish by ^{13}C NMR two different forms of Glycine in a Cd^{2+}-exchanged montmorillonite clay: a glycinum ion in cation exchanged position, and Glycine acting as a ligand coordinated to the remaining interlayer Cd^{2+}. Still by solid state ^{13}C CP-MAS NMR spectroscopy, Jaber *et al*. observed that arginine (Arg) mostly adsorbs as the H_2Arg^+ monocationic species by cation exchange into montmorillonite. The progressive formation of peptide bonds was obtained upon heating the system at 200°C. Both of these examples show the potential of ^{13}C NMR in the carbonyl region to discriminate the acid-base speciation of amino acids, and to observe their peptidic condensation.

I.5.4 Some general conclusions on NMR studies

Several conclusions seem to emerge from the various literatures studies and served as a guide for our investigations:

- 1D ^{15}N and ^{13}C solid-state NMR spectra (for the latter, especially in the C1, i.e. carboxylate/ carboxylic acid region) provide information on amino acid speciation: cationic or zwitterionic, crystalline vs. adsorbed. They also allow to observe the peptidic condensation reaction upon thermal activation. HETCOR and other dipolar coupling based techniques may provide information on the H-bonding state and proximities.

- On silica, both porous and non-porous, different non-crystalline forms are observed depending on the hydration state: a mobile one, comparable to amino acids in aqueous solution, in “wet” conditions, and a more rigid one, with limited molecular mobility, in “dry” conditions, with both co-existing at intermediate hydration. Therefore, control of the hydration state appears to be primordial to understand NMR results.

- The rigidly adsorbed form is engaged in a network of Hydrogen bonds with the surface. In particular, the ammonium ($-NH_3^+$) group of the zwitterion may form specific H-bonds with a group of silanols, “anchoring” the amino acid on the surface. Data are less clear for the carboxylate ($-COO^-$) group.

- However, when there is another functional group in the side chain, it may also be involved in bonding to the surface.

I.6 IR Spectroscopy

I.6.1 Significance of the vibrational spectroscopy of amino acids

Infrared spectroscopy is one of the classical methods for obtaining molecular structures and observing conformational changes of small molecules. This is due to its sensitivity to the chemical composition and architecture of the molecules. The IR spectrum is mainly separated into 3 different regions; *(i)* the higher-energy near-IR region, approximately 14000-4000 cm^{-1} (0.7-2.5 µm wavelength) where overtone or combination modes of molecular vibrations are observed ; *(ii)* the mid—IR region from 4000-400 cm^{-1} (2.5-25 µm) which is generally used to study the fundamental vibrations and the associated rotational-vibrational structure ; *(iii)* the far-IR region, approximately from 400-10 cm^{-1} (25-1000 µm) whose low energy corresponds to rotational spectroscopy and low frequency vibrations.

Fourier transform infrared (FTIR) spectroscopy is also relevant for biological systems. This makes IR spectroscopy a valuable tool e.g. for the investigation of protein structures.[154,155] For the determination of the secondary and tertiary structure, the individual properties of amino acids are of great importance. Recently, there has been a great deal of interest in understanding the specific vibrations of amino acids, especially amino acid side chains which play a fundamental role in stabilizing protein structures and catalyzing enzymatic reactions. These side chains vibrate at similar wavenumbers as amides vibrations I, II and III, that are dependent on the formation of the polypeptide backbone in proteins. It is estimated though that 10 to 30 % of the vibrations occurring in that region come from the side chain vibrations (Chirgadze *et al*[156]., 1975; Venyaminov and Kalnin[157], 1990; Rahmelow *et al*[158]., 1998). Investigations are often restricted to the 1800-1500 cm^{-1} spectral region and not to the whole mid IR region. (Goormaghtigh *et al*[159]., 1994; Wright and Vanderkooni[160]). When studying unpolymerized amino acids, this region is of utmost importance because it carries information regarding the carboxyl and the amine vibrations found within them.

Hence, peptide bond formation, and protein folding, can be investigated using IR spectroscopy.[161]

I.6.2 Literature on vibrational spectroscopy of amino acids on silica

IR spectroscopy of amino acid adsorption on surfaces started to gain interest in the 1970s, when it was observed that surface-supported amino acids induced vibrations, different from the reference bulk[162] ones. Furthermore, amino acid polycondensation has been studied with this technique by a number of authors who were interested in the prebiotic synthesis of peptides, generally in the bulk.[163–165] These two lines of research came together in the work of Basiuk *et al*., already cited in § I.4. In this work, mid-IR spectroscopy recorded *in situ* on supported amino acids and the products of their thermal treatment constituted the main characterization tool.[82,83,166–171]

These authors interpreted the IR data of individual amino acids on inorganic surfaces such as silica by the formation of specific hydrogen bonds between amino acid and the surface, but also of covalent bonds of the "surface ester" (Si-O-CO-R) type. While some of their interpretations may be challenged, these publications contain a wealth of data on the spectroscopic properties of supported amino acids.

Literature about the IR of amino acid adsorption on surfaces, and more particularly on silica, can be separated into two main parts: *(i)* those where amino acids were deposited from an aqueous phase – they were zwitterionic before adsorption on the surface, with recognizable $–COO^-$ and $–NH_3^+$ groups; *(ii)* those where amino acids sublimate to a vapor upon heating under reduced pressure, and thus are deposited from the gas phase where they were in the neutral form (with COOH and $–NH_2$ groups).

To the latter category belong the studies of Basiuk *et al*., already mentioned, but also the high-quality data of Martra *et al*.[120,172,173]

Previous work at LRS belongs to the first category, where IR was applied in the transmission mode after drying of the impregnated powder,[84,86,92] as do studies by Holland *et al*.[97] Kitadai *et al*.[174] used a different setting, with IR in the ATR mode, allowing to characterize the adsorption process in the presence of the aqueous phase.

The two preparation techniques gave very different results. When amino acids are adsorbed in the hydrated form, they remain zwitterionic until essentially all water is removed from the silica surface (definitely above 100°C), and only then do they condense to peptides.[84,86,175] In contrast, when they are adsorbed from the gas phase onto a dehydrated silica surface, the slight heating by the IR beam (around 50°C) is enough to cause condensation[167]. In summary, surface hydration, acido-basic AA speciation (zwitterionic vs. neutral) and peptidic condensation seem deeply connected.

I.7 Other experimental techniques

I.7.1 X-Ray Diffraction

A widely known method in the field of solid state or physical chemistry is X-Ray Diffraction (XRD), which is a non-destructive analytical technique to investigate crystalline phases. The nature, polymorphism[176] and size of the crystal phases[177] can be accessed by this technique. We have already stated that AA/SiO_2 systems often show the coexistence of a bulk crystalline phase with adsorbed amino acids. Usually, the bulk phase only starts to form when the adsorption sites on the surface are saturated. XRD then allows the identification of the saturation point: presence of Bragg peaks on the smooth amorphous background of silica is the sign of a crystalline the amino acid phase being formed (Figure 1.9).

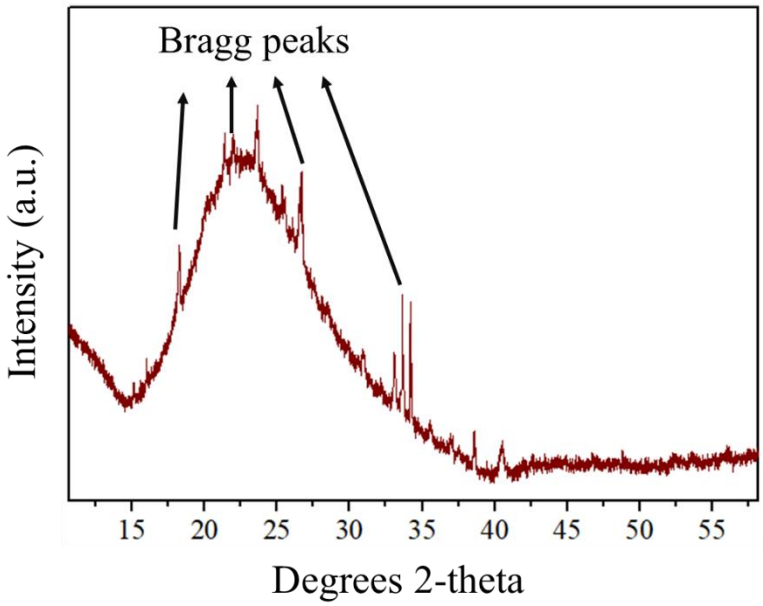

Figure 1.9. Example of an X-Ray diffraction pattern of a high Glutamic acid loading on SiO_2 showing the presence of several Bragg peaks superimposed on the broad diffusion baseline of amorphous silica

I.7.2 Thermogravimetric Analysis

The formation of peptides from amino acids usually cannot occur without thermal activation. Therefore, thermogravimetric analysis (TGA) is intensively used to separate the different thermal events occurring upon heat treatment. When heating an adsorbed amino acid, two main events are expected, peptide formation (leading to cyclic or linear forms) and decomposition. On silica, these events do not interfere with those that are attributable with the support (essentially, desorption of physisorbed water at T <100°C, as shown in Figure 1.10.[86]

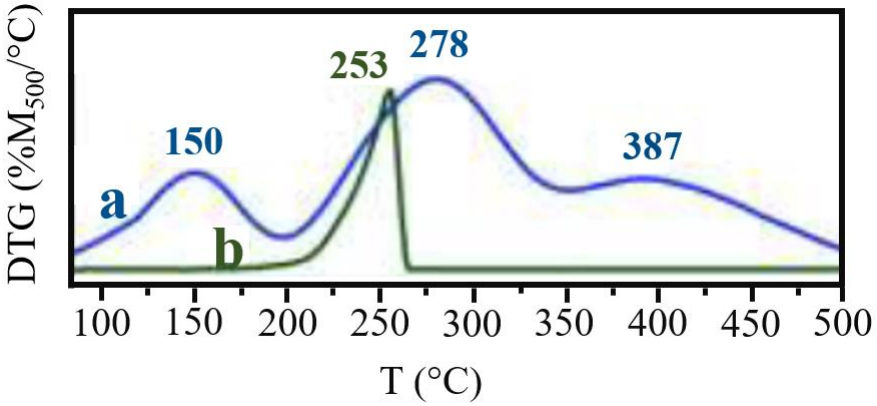

Figure 1.10. Thermogravimetry (TG) of (a) Leucine adsorbed on SiO_2, (b) Bulk crystalline Leucine

I.8 Computational Modeling

I.8.1 Theoretical Method

The aim of this work is to study the adsorption of molecules on a mineral surface. The latter is considered to be an infinite system, or at least to have an extension vastly greater than the size of individual molecules; hence a periodic approach is preferred to a cluster one, as discussed later. Moreover, we want to calculate electronic properties (in particular NMR parameters) which excludes classical approaches. For this reason, we used *ab initio* methods which try to solve the non-relativist time-independent Schrödinger equation. This allows to describe the electronic structure of atoms and molecules at the quantum level. The Schrödinger equation takes the following form.[178]

$$\hat{\mathrm{H}}(\mathbf{R})\,\Psi(\mathbf{r};\,\mathbf{R}) = \mathrm{E}(\mathbf{R})\,\Psi(\mathbf{r};\,\mathbf{R}) \qquad (11)$$

In this equation, $\hat{H}(\boldsymbol{R})$ is the Hamiltonian operator of the system that is dependent on the atomic coordinates (r) and the kinetic energy of the electrons, together with the electronic interactions[179]. The wavefunction $\Psi(\boldsymbol{r};\,\boldsymbol{R})$ contains information on the coordinates of the electrons **(r)** and nuclei **(R)**. The total energy (E) of the system is given by:

$$\mathrm{E} = -\,\mathrm{E}_{\mathrm{k}}^{\mathrm{e}} - \mathrm{E}_{\mathrm{k}}^{\mathrm{n}} - \mathrm{E}_{\mathrm{H}}^{\mathrm{ne}} - \mathrm{E}_{\mathrm{H}}^{\mathrm{ee}} - \mathrm{E}_{\mathrm{H}}^{\mathrm{nn}} \qquad (12)$$

In this equation, $\mathrm{E}_{\mathrm{k}}^{\mathrm{e}}$ and $\mathrm{E}_{\mathrm{k}}^{\mathrm{n}}$ describe the kinetic energy of the electrons and the nuclei respectively. $\mathrm{E}_{\mathrm{H}}^{\mathrm{ne}}$, $\mathrm{E}_{\mathrm{H}}^{\mathrm{ee}}$ and $\mathrm{E}_{\mathrm{H}}^{\mathrm{nn}}$describe the potential energies due to nucleus-electron, electron-electron and nucleus-nucleus interactions respectively.

The first approximation that was applied to the Schrödinger equation is that of Born-Oppenheimer[180,181], where the Hamiltonian of the system will be the electronic Hamiltonian and the wave function of the system will be the multi electronic. It states that the motion of electrons and nuclei may be considered independently and the wavefunction of the system decoupled into nuclear and electronic parts:

$$\Psi(\text{total}) = \Psi(\text{nuclei}) \times \Psi(\text{electron}) \qquad (13)$$

As a consequence, the problem is reduced to the motion of electrons in a fixed potential of the nuclei. The Hamiltonian of the system becomes :

$$\hat{H} = \hat{T} + \hat{V} + \hat{V}_H + \hat{V}_{XC} \qquad (14)$$

where, $\hat{\mathrm{T}}$ is the kinetic energy of the electrons, $\hat{V}$ is the interaction potential between electrons and nuclei, $\hat{V}_H$ is the Hartree potential of the electron-electron coulomb repulsion and $\hat{V}_{XC}$ is the electron-electron exchange and correlation potential.

Many methods were developed to solve the electronic Schrödinger equation by means of different types of approximations. They can be sorted in two categories: the methods based on the Hartree-Fock theory and those based on the Density Functional Theory (DFT). The latter

was used for the studies presented in this Thesis. In the following, I will be talking briefly about the Hartree-Fock method which will be followed directly by a more detailed description of the Density Functional Theory (DFT) method.

The Schrödinger equation remains much too complicated to be solved exactly for systems having a lot of electrons. One way to reduce this complexity is to treat the electrons in an averaged way[182]. The Hartree-Fock (HF)[183] approximation is a wavefunction-based, quantum-chemical method and calculates the energy of quantum many-body system in a stationary phase, directly in terms of wavefunction. In the HF approximation, each electron is described by an orbital and the total wavefunction is given as a product of these orbitals. Another consideration in the HF approximation, is that the electrons in the system are described by their respective orbitals. The equations in HF then strictly depend on their own solution and each HF equation must therefore be solved iteratively. Wavefunction methods provide a systematic path to improving the accuracy of the calculations. However, the improvement in the accuracy increases significantly the computational cost of the calculations. DFT calculations provide a practical balance between accuracy and computational cost and are now suitable for medium to large molecules.

I.8.2 Principles of periodic DFT simulation

Traditional methods in electronic structure theory, in particular Hartree-Fock theory are based on the complicated many-electron wave function. The main objective of the Density Functional Theory (DFT) is to replace the many-body electronic wave function by the electronic density as the quantity to be determined (Figure 1.11). DFT exploits the advantages of the density which is a simpler quantity to deal with.

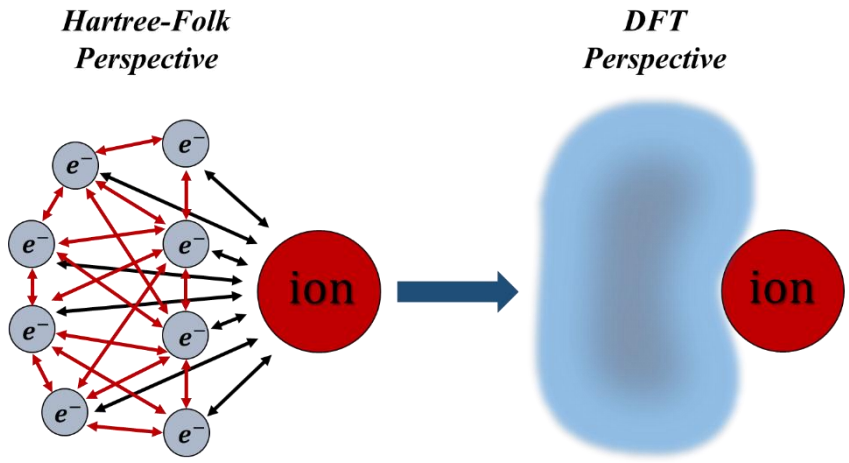

Figure 1.11. Hartree-Folk method (many-body theorem) vs. density functional theory (DFT)

The initial principle of this theory (DFT) comes historically from Thomas-Fermi model elaborated in 1927. According to that model, the kinetic energy of a non-interacting electrons gas depends only on the electronic density of that cloud. It was then completed by Dirac, who added an exchange energy also depending only on the electronic density of the system. Instead of working with a wave function, Ψ (like before), depending on the 3N cartesian coordinates of the N electrons of a system, one could easily use the electronic density, $\rho(\vec{r})$, which only

depends on 3 coordinates. The electronic density and the wavefunction are related by the following formula:

$$\rho(\vec{r}) = \int_{\vec{r}_2} \dots \int_{\vec{r}_N} \Psi(\vec{r}_1, \vec{r}_2 \dots \vec{r}_N)\Psi \times (\vec{r}_1, \vec{r}_2 \dots \vec{r}_N)\mathrm{d}\vec{r}_2 \dots \mathrm{d}\vec{r}_N \qquad (15)$$

In 1964, Hohenberg and Kohn[184] proved that determination of the electron density leads to a unique ground state energy and that this single variable (ρ) can be used instead of computing the full many-body wavefunction of the system. High accuracy can be achieved with the DFT approach, at a moderate computational expense. The founding principles of this theory can be illustrated in the form of two theorems.

The first theorem states that the properties of the system, including energy states, potentials and wave-functions are uniquely determined by the electron density $\rho(\vec{\mathrm{r}})$, Thus, the electronic energy of a chemical system can be written as:

$$E[\rho(\vec{r})] = T_e[\rho(\vec{r})] + V_{ee}[\rho(\vec{r})] + V_{Ne}[\rho(\vec{r})] \qquad (16)$$

where the potential of the nuclei V_{Ne} can be considered as a particular case of external potential v_{ext} , felt by the electrons. It is possible to generalize the equation 16 in the form of equation 17, where the F_HK function groups the kinetic energy of the electrons and their interactions. This latter functional is called universal functional as it does not depend on the external potential and therefore on the studied system.

$$[\rho(\vec{r})] = F_H K[\rho(\vec{\mathrm{r}})] + \int v_{ext}(\vec{r})\rho(\vec{r})\mathrm{d}\vec{r} \qquad (17)$$

However, with the first theorem alone, the electronic density of the ground state $\rho_0(\vec{\mathrm{r}})$ is unknown, and hence the second theorem (known also as the variational principle) is of importance. It states that the electron density $\rho_0(\vec{\mathrm{r}})$, for which the energy E is minimal is the true ground-state electron density. Thus, the energy of a system calculated with an approximate electronic density will always be superior to the exact energy obtained with the exact density.

$$F_H K[\rho(\vec{r})] + \int v_{ext}(\vec{r})\rho(\vec{r})\mathrm{d}\vec{r} \geq E_{exact}[\rho_{exact}(\vec{r})] \qquad (18)$$

The variational principle allows to select the electronic density the closest to the real one within a set of test densities. This selected density minimizes the total energy.

The two theorems of the Hohenberg-Kohn method predict that only the electronic density (ρ) of a system defines both the Hamiltonian and the resulting observable value. However, they do not help to determine the electronic density, as the interelectronic interaction term, V_{ee}, is still unknown.

However, Kohn and Sham developed a new method in 1965[185] to calculate the electronic density of the fundamental state (ground state), which is basically reducing the problem of interacting electrons (V_{ext}) in a static external potential to a problem of non-interacting electrons moving in an effective potential (V_s), where the kinetic energy of the non-interacting electrons has a known analytical expression (T_s). The latter requires the introduction of the monoelectronic molecular orbital Ψ_i given in the following equation:

$$T_s = -\frac{1}{2} \sum_{i}^{electrons} \langle \Psi_i | \nabla_i^2 | \Psi_i \rangle \quad (19)$$

The objective is to compute the ground state energy for an N-electron system with ground state density ρ and external potential V_{ks} (also called Kohn-Sham potential) as a set of independent particle equation which is given as:

$$\left[-\frac{1}{2}\vec{\nabla}^2 + \mathrm{V_s}(\vec{\mathrm{r}}) \right] \Psi_\mathrm{i} = \mathrm{E_i}\Psi_\mathrm{i} \quad (20)$$

By applying the first Hohenberg-Kohn theorem to this non-interacting system, there is one external potential V_{ext} which generates the density of a ground state. One main advantage of this method is that it allows a straightforward determination of a large part of the kinetic energy in a simple way. Moreover, the two operators T_s and E_{ee} are universal for all systems, while V_{ks} is a time-dependent phenomena, such that the electronic density of the ground state remains invariant from one system to another.

In addition to the analytical expression of the kinetic energy given in equation 18, the total energy E can be given as:

$$E[\rho(\vec{r})] = T_s[\rho(\vec{\mathrm{r}})] + \int V_s(\vec{r})\rho(\vec{r})\mathrm{d}\vec{r} \quad (21)$$

and the energy associated with the real system is:

$$E[\rho] = T_s[\rho] + E_{ee}[\rho] + \int V_{ext}(\vec{r})\rho(\vec{r})\mathrm{d}\vec{r} \quad (22)$$

The classic Coulombic interaction between the electrons $J[\rho]$ can be written as:

$$J[\rho] = E_{ee}[\rho] - E_{non-classical}[\rho] = \frac{1}{2}\iint \frac{\rho(\vec{r})\rho(\vec{r}')}{|\vec{r}-\vec{r}'|}\mathrm{d}\vec{r}\mathrm{d}\vec{r}' \quad (23)$$

where $E_{non-classical}$ is the non-classical energy, and is composed of the exchange correlation energy, the Coulomb correlation and correlation of self-interaction. Using J, the energy in equation 21 can be expressed as the sum of two terms: the analytically calculable part and the exchange correlation part. The latter can be approximated. The simplest approximation is the LDA[186,187] (local density approximation), which assumes that the exchange-correlation energy at any point is equal to the exchange-correlation energy of a uniform electron gas:

$$E_{xc}^{LDA}[\rho] = \int \rho(\vec{r})\, \varepsilon_{xc}(\rho(r))\mathrm{d}\vec{r} \quad (24)$$

where ε_{xc} and is the exchange-correlation energy per particle of a homogenous electron gas of charge density ρ. An improvement in the accuracy provided by the LDA can be obtained by generalized gradient approximation (GGA) functional, which is a function of both the local density $\rho(\vec{r})$ and the density gradient $\Delta\rho(\vec{r})$ the gradient of the density [188] :

$$E_{xc}^{GGA}[\rho] = \int n(\vec{r})\, \varepsilon_{xc}\big(n(r)\big), |\nabla n(r)| \mathrm{d}\vec{r} \quad (25)$$

One example was developed by Perdew, Burke and Ernzerhof [189] (PBE) in 1996 and has been used throughout this work. It gives good results for geometries and atomization energies and reproduces well the hydrogen bonds.

The analytically calculable part and the exchange correlation part can be written as:

$$E[\rho] = \int v_{ext}(\vec{r})\rho(\vec{r})\mathrm{d}\vec{r} + T_s[\rho] + J[\rho] + T[\rho] - T_s[\rho] + E_{ee}[\rho] - J[\rho] \quad (26)$$

Thus, the exact energy of the real system including the classic Coulomb interaction $J[\rho]$ and the exchange correlation energy E_{ee} can be finally written under the form:

$$E[\rho] = T_s[\rho] + J[\rho] + \int V_{ext}(\vec{r})\rho(\vec{r})\mathrm{d}\vec{r} + E_{ee}[\rho] \quad (27)$$

Since there seems to be an analogy between the approximated and the real system, their densities and their energies are identical, hence equation 21 can be directly implemented in equation 27, and applying the variational principle on it, one can obtain the following equations 28 and 29:

$$\frac{\delta(T_s[\rho])}{\delta\rho(\vec{r})} + V_s(\vec{r}) = \frac{\delta(T_s[\rho])}{\delta\rho(\vec{r})} + \int \frac{\rho(\vec{r}')}{|\vec{r} - \vec{r}'|}\, \mathrm{d}\vec{r}' + vV_{ext}(\vec{r}) + \frac{\delta(E_{ee}[\rho])}{\delta\rho(\vec{r})} \quad (28)$$

$$V(\vec{r}) = V_{ext}(\vec{r}) + \int \frac{\rho(\vec{r}')}{|\vec{r} - \vec{r}'|}\mathrm{d}\vec{r}' + V_{ee}(\vec{r}) \quad (29)$$

Once $V_s(\vec{r})$ is determined, the Kohn-Sham equation (20) can be solved, i.e., the different molecular orbitals satisfy the following two conditions:

$$\sum_i^N |\Psi_i|^2 = \rho(\vec{r}) \quad (30)$$

and

$$\langle \Psi_i | \Psi_j \rangle = \delta_{ij} \quad (31)$$

In all of our models, the convergence energy criterion is such that the energy difference between the two electronic steps must be less than 10^{-4} eV: most of the DFT simulations to extract and separate the complex dielectric function of each individual layer of a multilayered system consist in a self-consistent iteration procedure. Moreover, the Kohn-Sham equations are solved in an iterative way consisting in choosing ρ_{in}, calculating the corresponding (V_{ext}, solving eq. 20 to obtain E_i and Ψ_i, then get ρ_{out}, compare $E_{in}$and $\rho_{out}$to know whether convergence is reached and if not, rerun the same process with an initial density being a mix of $\rho_{in}$and ρ_{out}.

I.8.3 Principles of *ab-initio* geometry optimization

Based on the existing literature, before calculation of any electronic properties, atomic positions of biomolecules as small as amino acids[190] and as large as proteins[191] need to be relaxed to the ground state by geometry optimization. More specifically, it has been reported previously that, prior to the calculation of NMR parameters, it is necessary to perform some optimization of the geometry in order to minimize the forces acting upon the atoms.[192]

The starting point of the optimization of a model may be obtained from a specific structure that has been already obtained by X-ray diffraction, derived from Bragg diffraction experiments (on systems such as single-crystal, powder X-ray diffraction or neutron diffraction)[193]. It is well known however that sometimes X-ray diffraction is not able to locate every atom in a configuration, such as hydrogen, isoelectronic atoms or those that are in the presence of heavier elements. Moreover, in the case of amorphous or aperiodic systems, atoms cannot be easily located by diffraction techniques. In these cases, the alternative is to simply construct the structure and then perform optimization.

Geometry optimization reduces the stresses caused by external and internal forces in a given molecule for example, in modifying the relative atomic positions.

In general, there are two possible types of molecular structures, the equilibrium geometry characterized as R_{eq} and the transition state geometry R_{ts}, both corresponding to a stationary point located on the potential energy surface (PES) (Figure 1.12) (molecular energy E(R) as a function of nuclear positions R= (R_1, R_2…)), our main focus however was towards the equilibrium geometry characterized as R_{eq}.

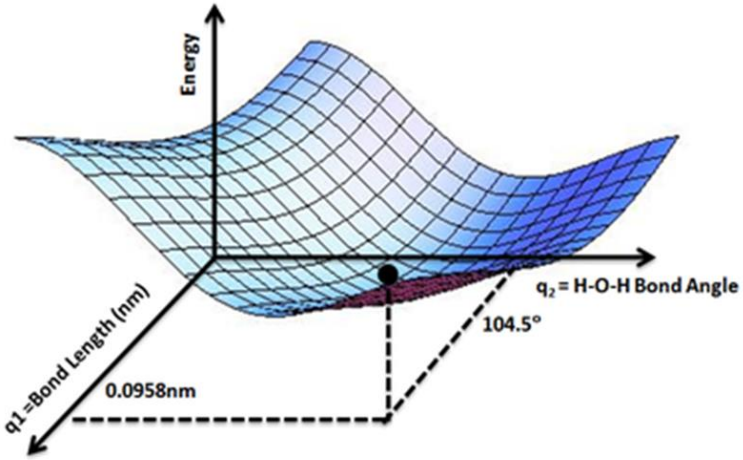

Figure 1.12. Random Potential energy surface adopted by MATLAB

The condition for the points determination is the cancellation of the first derivative of the energy with respect to the nuclei position. The second derivatives are all positive at the local minima; in contrast, one of them is negative at the saddle points (which is a minimal point on the potential energy surface PES).[194]

In the field of computational energy, energy minimization is the important process of finding a particular arrangement of atoms in space, resulting in bond lengths and bond angles that give rise to an overall minimization of the forces. This leads to a structure that can be used in various experimental and theoretical investigations.

Regardless of the choice of the material or the ability to determine the minimum-energy crossing points, geometry optimization cannot simulate the motion of molecules with respect to time, temperature and chemical forces. This requires molecular dynamics simulation.

I.8.4 Description of the silica surface

Different approaches can be used to describe a system: *(i)* the "cluster approach" is a common computational method used by theoreticians: it is performed on finite molecular systems selecting a limited number of atoms to represent a model of the active sites. To describe large materials, an appropriately sized cluster of atoms or molecules is constructed such that the atoms in the centre experience the same environment as in the true solid. *(ii)* the "periodic approach" is the most common and widespread method used for materials as it includes periodic boundary conditions and allows therefore infinite systems to be described. It involves the use of plane wave basis set and pseudopotentials as described more in detail in § I.8.6

There are many possible surface groups on silica nanoparticles that play a key role in the adsorption phenomena. Bridging points (matching point between the adsorbate and the adsorbent) can also be studied via structural modeling of surfaces, calculating the adsorption energy. Hence *ab-initio* methods are well adapted to characterize the reactive sites as well as the different possible favorable energy modes.[103]

For several decades, a great number of theoretical studies have been published on modeling mineral surfaces such as silica.[195,196]The surface approach at low coverage is said to be ideal when the catalytically active surface is only weakly perturbed by the chemical environments. It is sometimes mandatory to go beyond the ideal surface approach at low coverage.[197]

Further development of computing power at the beginning of the 1990s allowed scientists to get more and more realistic models thanks to the possibility of increasing the number of calculations in a reasonable duration. Further development in DFT made it possible to model much more complicated and complex strains of silica and surface ability.[198]

Finally, in the recent years, the extensions of this theoretical method has reached a phase, where it is possible to model an amorphous surface and not only a crystalline one, allowing access to realistic details.[199–202]

Complete/partial hydration and hydroxylation of the silica surface could also be modeled, since hydrated and hydroxylated surfaces respectively gained importance in the field of physical chemistry to understand the effect of water on silica properties (adsorption energies for example).[203,204]

I.8.5 DFT modeling of amino acid adsorption on mineral (mainly silica) surface

When modeling amino acids adsorption, two criteria need to be taken into account: *(i)* the amount of hydroxyl (OH) groups located on the surface, which can easily give rise to more local H-bonding with the surface; *(ii)* the nature of the amino acid, i.e. the chemical moieties of the side chain. Amino acids having a non-polar side chain show a common path of adsorption on silica surfaces via the ammonium $-NH_3^+$ group while the carboxylate ending pends back in the solution.[81]

Rimola *et al*. contributed a lot to studies on interactions between amino acids and hydroxylated silica. Many of their studies used models derived from one crystalline silica form, edingtonite. They first used limited clusters, then 1-D and 2-D slabs in a periodic approach. Their edingtonite (001) surface model exhibits a net 2.2 OH groups per nm^2 and they have compared the bonding of most biological amino acids on this surface, providing adsorption energies[113]. Many of their other published works, mentioned in §I.3 above, are concerned with elucidating the mechanism of peptide bond formation upon thermal activation, either with Glycine or smaller, model molecules. Later on, they also used clusters derived from zeolitic structures[205] and slabs of α-quartz (010).[173]

Edingtonite[206,207] and quartz[208] were also chosen by other authors who wanted to explore the effect of regular silanols networks on bonding with amino acids, as well as cristobalite.[209]

At the LRS, different models were used successively to represent the silica surface. The first attempts used isolated small clusters.[101,102] Later on, a slab representing a hydroxylated amorphous surface with 7.66 OH/nm^2 was developed and tested for Glycine adsorption[210]. However, this surface hydroxylation level was doubtlessly higher than that of the commercial Aerosil 380 non-porous silica used in most of the experimental studies (about OH/nm^2): it would rather constitute a relevant model for precipitation silicas, which have hardly been tested experimentally for amino acids adsorption and condensation. Finally, the work of Folliet *et al*.[91] made use of the previously developed model of amorphous fumed silica that we are also using in the present thesis.[200]

Silica surface cannot sum up the entire prebiotic chemistry, hence many other oxide surfaces[107,211] were simulated in the past decades showing signs of peptide bond formation possibilities.[106] A whole protein is challenging to simulate, but small peptide can be adsorbed on different mineral surfaces.[173]

I.8.6 NMR Calculations

One of the main physical phenomena intervening in experimental NMR spectroscopy is the ability of a nucleus to be either shielded or deshielded by its electronic cloud in a magnetic field. In order to calculate accurate magnetic shielding, both the core electrons and the given wavefunctions must be described in the most accurate possible way. For periodic systems, this is possible thanks to the projector-augmented wavefunction method (PAW)[212], which aims to

generalize pseudopotentials and linear augmented-plane wave method by introducing the transformation operator $\hat{T}$.

$$\Psi_{all\ electrons} = \hat{T}\Psi_{pseudo.} \quad (32)$$

For periodic systems, the PAW approach can be extended to the gauge-including projector augmented wavefunction (GIPAW)[212] method, including a translational invariance (mandatory when introducing a magnetic field) with the addition of a field transformation operator.[192]
In this work, calculations of NMR parameters were performed within the DFT framework, using the GIPAW method mentioned above for the NMR chemical shift calculation which is based on the plane wave theory and pseudopotentials.[213,214]

The chemical shift, δ, is certainly the most important NMR parameter. NMR chemical shift calculation was done after obtaining the absolute magnetic shielding tensor $\sigma(\vec{r})$, which describes the magnitude and orientation dependence of the chemical shift (CS) interaction and it is usually represented in 3D Cartesian space using a 3×3 matrix.

$$\sigma(\vec{r}) = \begin{bmatrix} \sigma_{xx} & \sigma_{xy} & \sigma_{xz} \\ \sigma_{yx} & \sigma_{yy} & \sigma_{yz} \\ \sigma_{zx} & \sigma_{zy} & \sigma_{zz} \end{bmatrix} \quad (33)$$

Absolute magnetic shielding tensor $\sigma(\vec{r})$ calculation is based on the determination of $B_{ind}(\vec{r})$, at each atomic position r, (because $B_{ind.} = -\sigma . B_0$). The latter is obtained from the current density at first order $j^{(1)}(\vec{r})$ induced by magnetic field B_0, on nuclei. The link between $B_{ind}(\vec{r})$ and $j^{(1)}(\vec{r})$ is obtained from the Biot-Savart relation :

$$B_{ind}(\vec{r}) = \frac{1}{c}\int dr' j^{(1)}(r') \times \frac{r - r'}{|r - r'|^3} \quad (34)$$

DFT calculations generate much information such as the absolute magnetic shielding tensor (σ) mentioned above and Electronic Field Gradient (necessary to get the quadrupolar coupling constant for nuclei of spin I > 1/2) as well as the relative orientation of both. Diagonalization of the symmetric part of the shielding tensor gives its three principal components (σ_{xx}, σ_{yy}, and σ_{zz})(39) and the average of these components, the isotropic magnetic shielding σ_{iso}^{calc}.The calculated isotropic chemical shift (δ_{iso}^{calc}) can finally be obtained from the following equation :

$$\delta_{iso}^{calc} = \frac{-(\sigma_{iso}^{calc} - \sigma_{ref})}{1 - \sigma_{ref}} \sim -(\sigma_{iso}^{calc} - \sigma_{ref}) \quad (35)$$

where σ_{ref} is the reference magnetic shielding value, estimated by calculating NMR parameters of a series of reference compounds as detailed in the next chapter.

NMR calculations have been used to interpret in details experimental results particularly for nuclei having low natural abundance (carbon or nitrogen), low sensitivity or very large anisotropic interactions.[215–218]

Furthermore, calculation of NMR parameters can be used to test and select the most relevant structural models that can't be obtained by diffraction methods, such as molecules adsorbed on surfaces. Comparing e.g. chemical shifts for well-chosen theoretical models with the experimental results allows to choose the model that gives the best fit with the experiment. New advanced basis sets allowed for a better precision in computing and executing simulation for different systems that would have been impossible to compute in the past, identifying complicated and highly scaled systems such as organic/inorganic frameworks. The interaction between the surface and the organic molecule is very important because it highly affects the NMR chemical shifts, especially for the functional groups of the organic molecule which allows a full interpretation of the spectrum.[219–223] This would be hard to accomplish otherwise since the relation between chemical shift and local structure is far from trivial, and it is the approach we have used in the present thesis.

The GIPAW method used for NMR calculations has already provided an interesting link between computation and experimental spectroscopic data for an amino acid adsorbed on silica. Folliet *et al*[91] performed ^{13}C and ^{15}N solid state NMR spectroscopy on Glycine in mesoporous silica and compared the results with calculated NMR parameters in models containing anhydrous or microsolvated Glycine adsorbed on an hydroxylated amorphous silica surface. The most relevant adsorption configurations could then be identified. Although several molecular structures could fit the observed chemical shifts, it was found that Glycine most likely interacted with vicinal silanols (a pair of silanols on two Si linked through a siloxane link, i.e. HOSi-O-SiOH).

Chapter II Materials and Methods

II.1 Materials

Fumed silica (nanoparticles, ~ 7nm) with BET (Brunauer, Emmett and Teller) surface area of 380 m^2/g was purchased from Evonik. In the following, "SiO_2" or "silica" refers to this particular fumed silica nanoparticle. ^{13}C and ^{15}N-enriched L-Leucine and L-Glutamic acid with enrichment levels of 97-99% were purchased from CortecNet. All materials were used as received.
Enrichments used were the following:

1) Leu (Figure 2.1.a)

- [$^{13}C_6$, $^{15}N_1$] referring to enrichment on all the Carbons and the nitrogen
- [1-^{13}C, $^{15}N_1$] referring to enrichment on C1 (carboxylate of the amino acid function) and the nitrogen
- [$^{13}C_6$] referring to enrichment on all the carbons, but not on the nitrogen

2) Glutamic acid (Figure 2.1.b)

- [$^{13}C_5$, $^{15}N_1$] referring to enrichment on all the carbons and the nitrogen
- [1-^{13}C] referring to enrichment on C1 only
- [5-^{13}C] referring to enrichment on C5 (carboxylic acid of the side chain) only

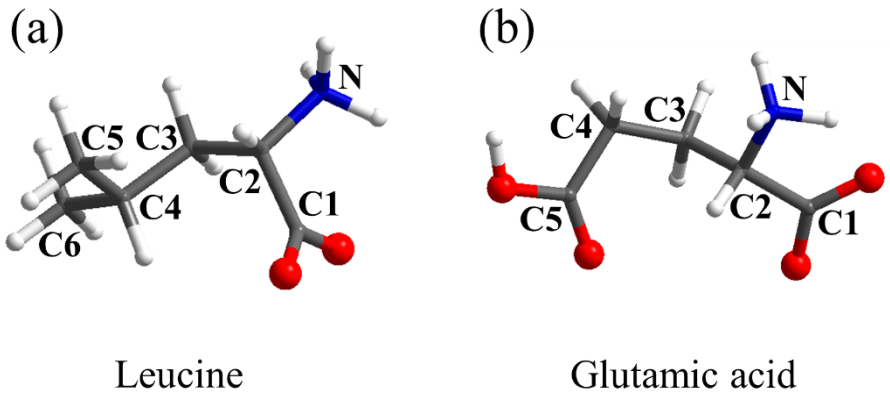

Figure 2.1. Carbon and Nitrogen positions and numberings for Leu and Glu amino acids

Apart from the commercial fumed silica nanomaterial already mentioned, two mesoporous silicas, MCM-41 and SBA-15, the synthesis was performed in the following ways:

- MCM-41 nanoparticles followed the protocol of Meynen *et al* through a modified conventional method[224]. An aqueous solution of cetyltrimethylammonium bromide (CTAB), mixed with aqueous ammonia was left under stirring at a constant temperature of 35°C. Then tetraethyl orthosilicate (TEOS) was added. The TEOS/CTAB/NH_4OH mixture was left at the

same temperature for 2 hours; afterwards, a hydrothermal treatment followed. After filtration, the final step was the removal of CTAB within the pores of the MCM-41 by calcination. The calcination process was the following: temperature was increased from 20°C to 300°C in 2 ½ hours. Then the temperature was kept constant at 300°C for 2 hours. Subsequently, temperature was increased from 300 to 550°C in 2 hours. Then the temperature was kept constant at 550°C for 12 hours. This liberated the mesoporous space of the MCM-41 silica material.

- SBA-15 nanoparticles also followed the protocol of Meynen *et al* through a modified conventional method[224]. An aqueous solution of pluronic acid (P123), mixed with the highly acidic HCl (hydrochloric acid) were left under constant heat (40°C) for around 3 hours. Then tetraethyl orthosilicate (TEOS) was added and the solution was set aside for 24 hours at 40°C, a hydrothermal treatment followed. After filtration, the final step included the removal of P123 within the pores of the SBA-15 by calcination. The calcination process was the following: temperature was increased from 20°C to 550°C in 22 hours. Then the temperature was kept constant at 550°C for 5 hours.

Nitrogen physisorption (Figure 2.2) was performed on the solid material at 77K. The BET analysis showed a high surface area for MCM-41, around 885m^2/g, and 832 m^2/g. The pore size distribution was determined using BJH (Barrett–Joyner–Halenda) treatment, resulting in a sharp peak for a pore size of 2.68 nm (MCM-41) and 9.23 nm (SBA-15). The porous volume was 0.8002 cm^3/g and 1.1898 cm^3/g respectively. In the following, Leu/MCM-41 or Glu/MCM-41, Leu/SBA-15 or Glu/SBA-15, $^{13}C/^{15}N$-Leu/MCM-41 or $^{13}C/^{15}N$-Glu/MCM-41 and $^{13}C/^{15}N$-Leu/SBA-15 or $^{13}C/^{15}N$-Glu/SBA-15 refers to the natural abundance Leucine or Glutamic acid and [$^{13}C_6/^{15}N$] or [$^{13}C_5$,^{15}N] refers to labeled Leucine or Glutamic acid adsorbed on mesoporous silica material (MCM-41 and SBA-15), respectively.

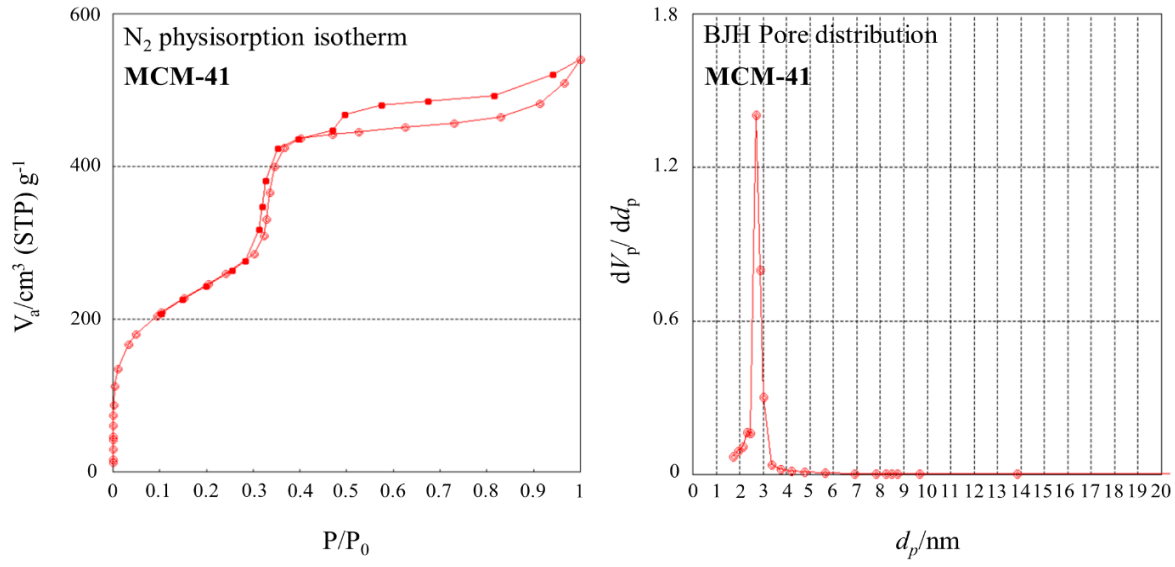

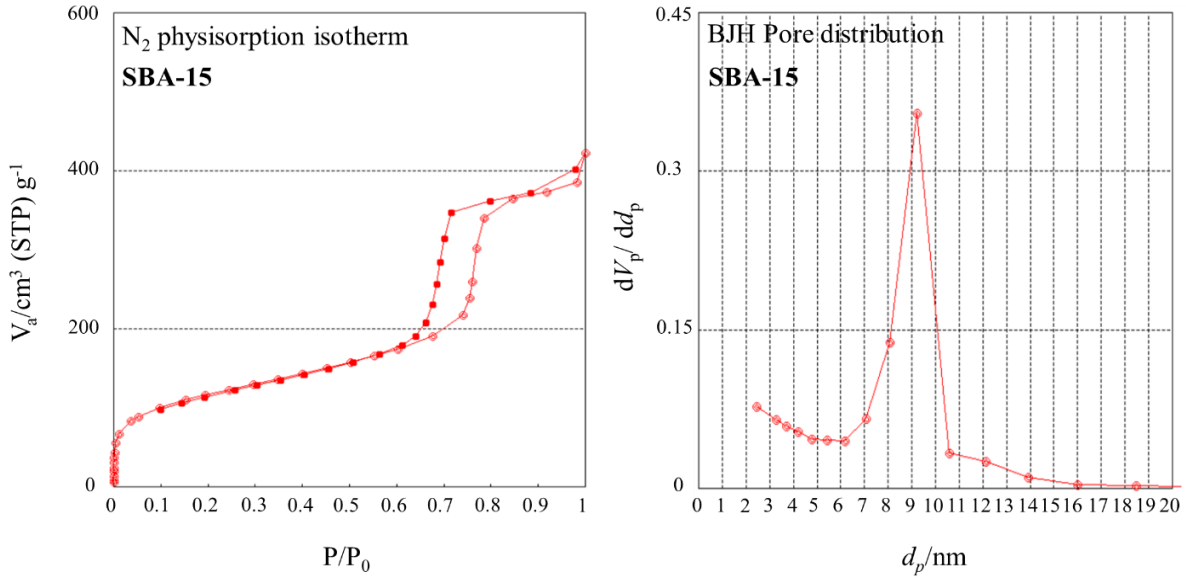

Figure 2.2. Full N_2 physisorption Isotherm and BJH pore distribution for MCM-41 and SBA-15

II.2 Samples preparation

Supported amino acid samples were prepared by loading the silica nanoparticles with the amino acid using the "incipient wetness" method. In a typical adsorption procedure, 1 g of SiO_2 was impregnated with a constant amount (10 mL) of aqueous solution of the amino acid at room temperature, where the amount of Leucine or Glutamic acid required to obtain the desired weight loading had been dissolved. For all loadings studied in this work, this amount remained inferior to the solubility of the amino acid. As an example, to obtain a loading of 3.0 wt. %, we used a 0.02 M Leu solution, resulting in the deposition of 0.200 mmol of Leucine per gram of SiO_2. A homogeneous slurry was obtained without a separate liquid phase. After careful mixing, two different drying methods were used: (i) 'nitrogen flow' consisting in drying the sample in a Petri dish at room temperature under nitrogen flow. This protocol of drying will be called 'dried under nitrogen flow' or **ND** for short in the rest of the manuscript. (ii) drying in a Schlenk tube connected to a rotary pump insuring primary vacuum. This will be called 'drying under vacuum' or **VD** in the rest of the manuscript. The two drying procedures are depicted graphically in Figure 2.3.

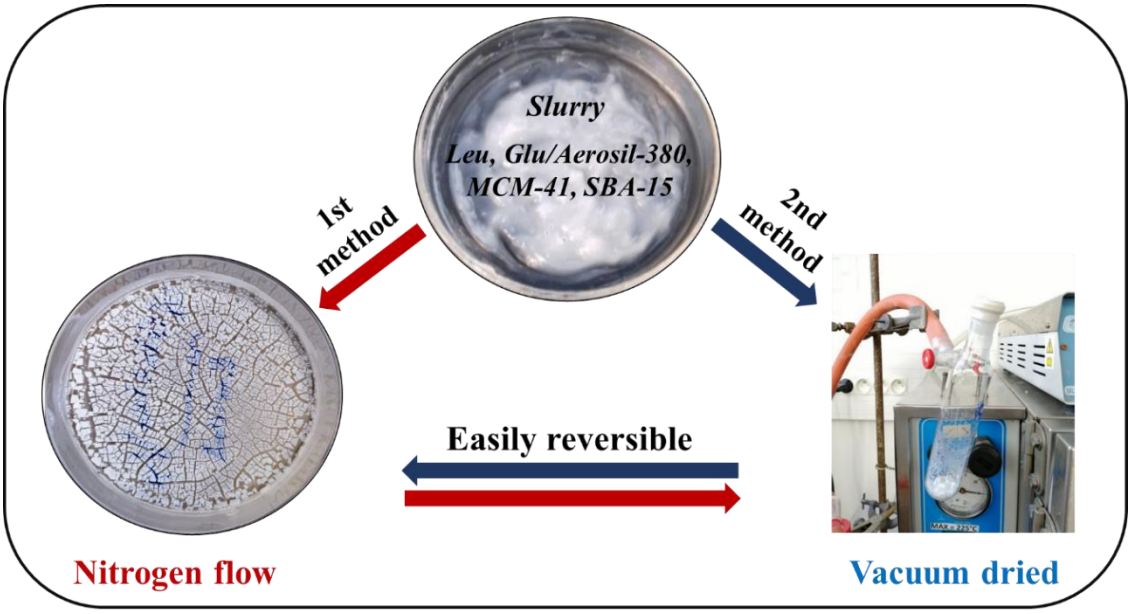

Figure 2.3. Drying methods used to prepare the sample of amino acids adsorbed on silica surface

These two drying procedures were chosen among five methods that had been tested and investigated by TGA (see Figure 2.5 below). We wanted to investigate the effects of surface hydration on amino acids, and we found that on raw Aerosil 380 silica, procedure ND gave the highest amount of retained water, and procedure VD the lowest. In addition, they were more reproducible than the other three.

In order to avoid rehydration under air, vacuum-dried samples were kept in a desiccator. They were filled in the NMR rotors inside a glove box immediately prior to recording the NMR spectra. Similarly, when performing IR spectroscopy, the samples were introduced in the sample holder inside the glove box to prevent water vapor readsorption. The samples prepared from solutions of various concentrations are noted x% A.A/SiO_2, where y% refers to the loading of the amino acid on expressed in weight % with respect to the bare support.

In the coming chapters, I am going to investigate mainly the adsorption of single amino acids Leucine and Glutamic acid as well as co-adsorption of (Glu+Leu) mainly on Aerosil 380 amorphous silica surfaces. The composition of all samples prepared is summarized in Table 2-1. More limited data were obtained for Leu and Glu on mesoporous silicas, and they are shortly presented at the end of each Chapter. The corresponding samples will be denoted as e.g. Glu/MCM-41 or Glu/SBA-15.

L-leucine loadings (%)	[L-leucine] (mmol)
1	0.07
2	0.15
3	0.22
4	0.30
5	0.38
6	0.45

L-Glutamic Acid loadings (%)	[L-Glutamic Acid] (mmol)
0.5	0.03
1	0.06
2	0.13
3	0.20
5	0.33
7	0.47
9	0.61

L-Glutamic Acid + L- Leucine (%)	[L-Glutamic Acid + L- Leucine] (mmol)
0.6	0.02 + 0.02
1	0.03 + 0.03
7	0.25 + 0.25
10	0.35 + 0.35

Table 2-1. Loadings of singly adsorbed and co-adsorbed Leucine and Glutamic acid on fumed silica nanoparticles studied in the upcoming chapters

Thermal activation was performed through two different methods (Figure 2.4) depending on the initial hydrated state on the amino acid (ND or VD). If the samples prepared followed the ND protocol, the samples were loaded inside a flow-through U-tube glass reactor (a-1) then transported to a thermal treatment unit where an Argon flow was circulated through the reactor; a circular furnace controlled by a thermoprogrammer (a-2) was used for heating the sample with a controlled temperature ramp. The heating rate was 5°/min and once the final temperature was reached, the heating was stopped and the sample was cooled down to room temperature.

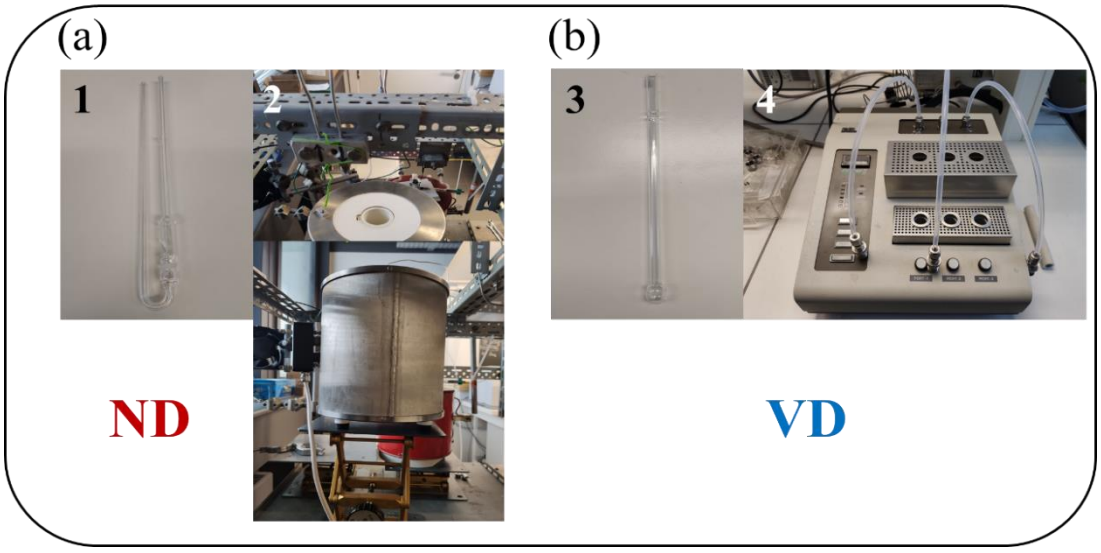

Figure 2.4. Thermal treatments performed under (a) Nitrogen dried conditions, (b) Vacuum dried conditions

If the samples followed a VD protocol, they are filled inside a long glass tube fitted with a rubber cap (b-3) inside the glove box to avoid any air contamination and later on transported to the BET pretreatment unit (Bel-prepII-vac unit, b-4) and thermally activated while being kept under vacuum. No control on the heating rate could be achieved in this setting. After being brought back to room temperature, samples are removed carefully and transported while being sealed back to the vacuum chamber to be later on used for further characterization techniques.

II.3 Experimental

Understanding the adsorption of these biomolecules on inorganic support and comprehending the mechanism of organic/inorganic interface is of great significance for developing novel bioinorganic composite systems for biomedical applications.[225–229] Investing thoroughly the interface is one the most difficult tasks physical chemists have to encounter, In the following text, the methodological approach and in particular the experimental and theoretical techniques used in this work will be described.

II.3.1 Experimental approach

II.3.1.1 IR Spectroscopy

IR spectra of amino acids adsorbed on the silica surface were collected by using a BRUKER Vertex 80 spectrometer (equipped with a MCT detector, Opus software and working in the rapid-scan mode), both on nitrogen dried and vacuum dried systems. The samples in powder form were placed between two transparent calcium fluoride (CaF_2) windows which are well suited for Infrared (IR)[230] The goal of the vibrational analysis is to identify vibrational modes attributable to a specific configuration of the adsorbed molecules, and their modifications due to the adsorption process. Because the silica support strongly adsorbs in the Si-O-Si, O-Si-O and O-H vibrational regions, the best observational window where molecules modes may be observed is in the 1700-1300 cm^{-1} region, although C-H and N-H stretching modes are also observable in the 3500-2800 cm^{-1} region.

Deuteration was often used as a method to replace the hydrogen atoms by deuterium in exchangeable groups. The preparation of D_2O samples were rather quick, the dissolution of the amino acids took place in D2O and not distilled water. After complete mixing, the solution was rapidly transported to the schlenk (Figure 2.3-Vacuum dried) and sealing was done after carefully pouring the aqueous solution (containing the amino acids + D_2O) into the schlenk filled with the inorganic silica nanoparticles.

II.3.1.2 X-Ray Diffraction

Low and wide angle measurements were performed with a Bruker D8 Advance diffractometer using the CuKα radiation (λ = 1.5408 Å). Low angle data were recorded for mesoporous silica based samples in the 2θ range between 0.5 and 7°, a step size of 0.01° with 1 s per step and operating at 30KV and 10 mA. Wide angle data were recorded in the 2θ range between 10 and 45° using 30KV and 10 mA conditions, a step size of 0.01° with 1 s per step.

Both low- and high-angle XRD depend on Bragg's Law: $n\lambda = 2\ d \sin\theta$ (where λ = wavelength of radiation used, in our case, Cu Kα radiation, λ = 1.5408Å, d = interplanar spacing in the crystalline lattice and θ = diffraction angle). At low angles, periodic distances of 20-500 Å will correspond to the arrangement of the mesoporous in MCM-41 and SBA-15 structures. At higher angles, XRD has the ability to distinguish between crystalline phases which gives characteristic "fingerprints" corresponding to organization of the hkl atomic planes.

II.3.1.3 Thermogravimetric Analysis

Thermal gravimetric analysis (TGA) experiments were performed with a TA SDT Q600 (TA Instrumental Inc.) instrument under dry air flow (100 ml/min). For each experiment, 20 to 25 mg of sample was used and a heating rate of 5°C/min was applied up to 1000°C. When carrying out TG on the ND samples, before each experiment, the sample was kept under nitrogen flow for abound 15 min to remove weakly adsorbed water and to obtain a clear and stable baseline. For the VD samples, the sample was filled into the TG crucible inside the vacuum chamber beforehand and then transported quickly to the TGA with a cap to avoid any readsorption of water vapour. The experiment was then started likewise after a 15 min wait at RT under nitrogen flow.

As previously mentioned, TGA was used to determine the amount of remaining water after different drying procedures. Resulting DTG are compared in Figure 2.5: (1) under nitrogen flow (ND), (2) under synthetic air, (3) outgassed under vacuum for 1hr in the BelprepII-vac unit (BET apparatus), (4) vacuum dried using a Schlenk (VD), and (5) freeze dried. The weight loss assigned to physisorbed water removal is observed from ambient temperature to 100 °C. As already mentioned it is highest for ND, and lowest for VD.

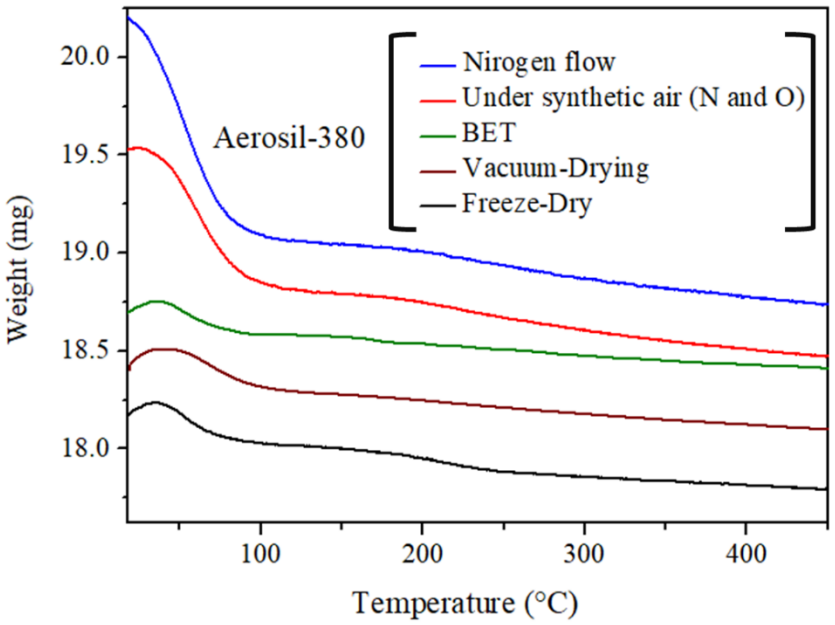

Figure 2.5. Thermograms (TGA) of different drying methods applied on Aerosil-380

II.4 NMR Spectroscopy

Solid state NMR spectroscopy measurements were carried out at room temperature with Bruker Avance 300 (field = 7 T, $\nu_0(^1H)$ = 300.29 MHz, $\nu_0(^{13}C)$ = 75.51 MHz, $\nu_0(^{15}N)$ = 30.44 MHz) and 700 (field = 16.4 T, $\nu_0(^1H)$ = 700.14 MHz, $\nu_0(^{13}C)$ = 176.08 MHz, $\nu_0(^{15}N)$ = 70.95 MHz) spectrometers using 7 mm and 4 mm Bruker MAS probes, respectively. The samples were spun at the magic angle at 5 and 14 kHz respectively. ^{13}C single pulse experiments were recorded using recycle delays between 2 and 500s. ^{13}C and ^{15}N CP MAS experiments were recorded with ramped-amplitude cross polarization in the ^1H channel to transfer magnetization from ^1H to $^{13}C/^{15}N$ (recycle delay = 3s, CP contact time = 1 ms, optimized ^1H spinal-64 decoupling). $\{^1H\} \rightarrow {}^{13}C$ and $\{^1H\} \rightarrow {}^{15}N$ 2D-HETCOR (Heteronuclear Correlation) CP MAS experiments were recorded at 7 T and 16.4 T and spinning speed of 14 kHz (64 increments of 71.4 µs were used with 312 (^{13}C) or 624 (^{15}N) scans per acquisition).

The experimental CP conditions, ^1H decoupling parameters and contact time CT (1ms) as well as recycle delays for 2D $\{^1H\} \rightarrow {}^{13}C$ and $\{^1H\} \rightarrow {}^{15}N$ NMR experiments were identical to 1D CP-MAS NMR experiments.

In all solid state NMR experiments, the chemical shift values of ^1H, ^{13}C and ^{15}N were indirectly referenced to adamantane ($\delta_{iso}(^1H)$ = 1.63 ppm and $\delta_{iso}(^{13}C)$ = 38.6 ppm) and NH_4NO_3 ($\delta_{iso}(^{15}N)$ = -4.6 ppm for the NO_3 group) respectively.[231,232] The line broadening factor (lb) was set to 25 Hz for ^{13}C CP-MAS spectra, ^{15}N CP-MAS spectra and 2D $\{^1H\} \rightarrow {}^{13}C$ HETCOR spectra (on the ^{13}C dimension), and 50 Hz for 2D $\{^1H\} \rightarrow {}^{15}N$ HETCOR spectra.

To get as much resolution as possible on proton spectra, in particular when recording HETCOR experiments, high magnetic fields were used. Indeed, considering the small amount of amino acid compared to silica, using very small rotors to reach very high spinning speed was not the best choice to get a reasonable S/N ratio for ^{13}C and ^{15}N spectra.

Liquid state NMR of the bulk Leucine and Glutamic acid was performed by preparing a 600 µL deuterated water solution previously purchased from Sigma Aldrich, both Leu and Glu were added (at the saturation concentration based on their solubility, 23.7 g/1L for Leucine and 7.2 g/1L for Glutamic acid) into the NMR tube containing the deuterated D_2O solution.

Liquid state NMR spectroscopy measurements were carried out at room temperature with Bruker Avance 500 (field = 11.6 T, $\nu_0(^1H)$ = 500.07 MHz, $\nu_0(^{13}C)$ = 125.76 MHz, $\nu_0(^{15}N)$ = 50.68 MHz) spectrometer using the glass tube containing the sample amino acid.

II.5 Molecular modeling methods

II.5.1 Structural Models

The study of these interfaces can also be approached from a theoretical angle by structural modeling of adsorption configurations of molecules. Using state of the art *ab-initio* methods makes it possible to characterize the reactive sites and to determine the most energetically efficient adsorption models. Later on a link can be established between these accepted models and the experimental data.[103]

For geometry optimization, all performed calculations were based on the Density Functional Theory (DFT) approach, using plane-wave pseudopotentials implemented in the VASP code.[233,234] The Perdew-Burke-Ernzerhof (PBE) functional[235,236] was chosen to perform the periodic DFT calculations.[200] The Projected Augmented Wave (PAW) method [237,238] was used for electronic structure calculations where the electrons with their interactions with the ionic cores were treated explicitly[237] allowing for DFT simulations to be performed with greater computational efficiency and precision[239]. An energy cutoff of 400 eV for the plane-wave basis is used. Static calculations were performed at 0 K for geometry optimization.

The adsorption of these amino acid models were performed on the fumed silica surface model previously published by Tielens *et al.*[200] The model consists of a $Si_{27}O_{67}H_{26}$ slab. The silanol density at the surface is 5.8 nm^{-2}, and unit cell dimensions are 12.77 × 17.64 × 25.17 $Å^3$. The slab has a density of approximately 1.7 g/cm^3. The number of Si atoms belonging to tetrahedra exposed on the surface is approximately 8 nm^{-2}. The surface silanol groups are composed of vicinal silanols having the highest density, a geminal group located at the corner of the supercell and isolated groups dispersed on the surface between the two former groups. The nature of these different silanol sites is recalled in Figure 2.6.

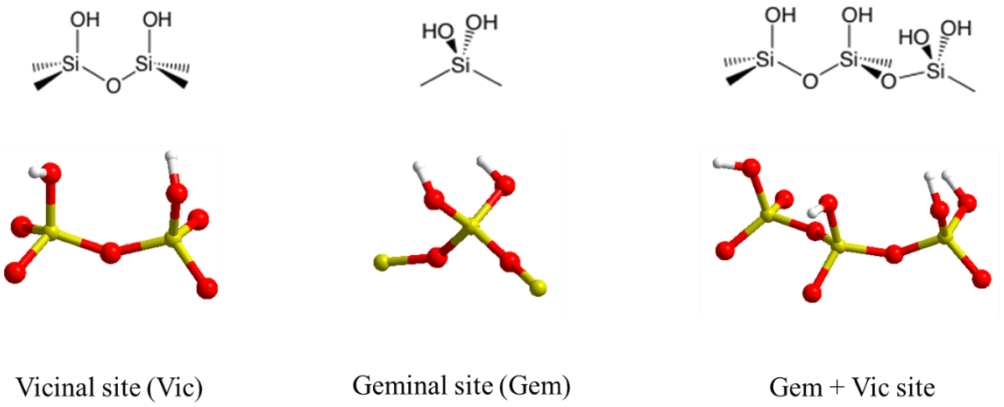

Figure 2.6. A schematic view of the main silanol adsorption sites in our model

Note that the vicinal and geminal groups are close enough to be considered as forming a "silanol nest". The OH density is 5.8 OH nm^{-2}, the same for the upper and the lower face. The ratios between geminal, vicinal and siloxane silanols are 0.23, 0.92 and 0.38 for the top surface, and 0.46, 1.00 and 0.31 for the bottom surface.

In our simulations two different approaches in molecular designing were applied. In order to mimic the experimental modeling systems containing the studied amino acid on the silica surface were undertaken, models containing no trace of water molecules were designed and systems containing water molecules were also modeled based on the number of the functional groups an amino acid may have.

The energies of amino acid interaction and adsorption on the silica surface were calculated by subtracting from the energy of the system as a whole the energies of neutral Leucine or neutral Glutamic acid (NL or NG), the silica surface E(Sil), and, when present, water molecules $E(H_2O)$. These electronic energies were obtained after separate geometry optimizations. E(L, Sil) is the energy of the optimized (Amino acid + silica + *n* water) system with Leucine or

Glutamic acid adsorbed on the silica surface. The number of water molecules in the models varies. The adsorption energy ΔE_{ads} was calculated as follows:

$$\Delta \mathrm{Eads} = \mathrm{E(L{:}\,G, Sil)} - \mathrm{E(NL{:}\,NG)} - \mathrm{E(Sil)} - \mathrm{nE(H_2O)} \quad (36)$$

II.5.2 NMR Calculation by Quantum Espresso (QE)

Quantum ESPRESSO (QE) is the major open source code for quantum materials modeling using the plane-wave pseudopotential method, it has been the development platform for important methodological approach for computational systems.

Moreover, in the field of solid state NMR, a fundamental breakthrough has been made over the past decade by using the density functional theory method with a periodic approach. Hence using the PAW and GIPAW methods[216], it is possible to calculate the electric field tensors (EFT), CSA (Chemical shift Anisotropy) of all magnetically active nuclei of a given structure. The simple periodic approach of the DFT enables in obtaining a good description of the material, and further optimizing the pseudopotentials used, the calculation becomes relatively favored for large number of isotopes.

The shielding tensor is computed using the GIPAW[216] approach which permits the reproduction of the results of a fully converged all-electron calculation. The PBE generalized gradient approximation[189,236] was used and the valence electrons were described by norm conserving pseudopotentials[240] in the Kleinman-Bylander form[241]. The core definition for O, C, and N is $1s^2$ and $1s^2 2s^2 2p^6$ for Si. The core radii are 1.2 a.u. for H, 1.5 a.u. for O, 1.6 a.u. for C, 1.45 a.u. for N, and 2.0 au for Si. The wave functions were expanded on a plane wave basis set with a kinetic energy cutoff of 1088 eV. The integral over the first Brillouin zone was performed using a Monkhorst-Pack (1×1×1) k-point grid for the charge density and chemical shift tensor calculation for the adsorbed models. The isotropic chemical shift δ_{iso} is defined as $\delta_{iso} = -[\sigma_{iso} - \sigma_{iso}(\mathrm{ref})]$, where σ_{iso} is the isotropic magnetic shielding and $\sigma_{iso}(\mathrm{ref})$ is the isotropic magnetic shielding of the same nucleus in a reference compound. In the present case, referencing of the NMR chemical shield was accomplished by plotting a fit of the linear correlation between the experimental δ_{iso} and the calculated σ_{iso} values of 5 relaxed structures of amino acids :α-Glycine[242], L-Alanine[243], L-Leucine[244], α-Glutamic acid[245], β-Glutamic acid[246], enabled the determination of the relation between δ_{iso} and calculated σ_{iso} for the ^{13}C and ^{15}N nuclei (Figure 2.7). It should be noticed that the difference between the experimental chemical shifts and the regression line is at most 0.4 ppm in the case of ^{13}C and a bit more (1 ppm) in the case of ^{15}N, indicating a better accuracy of the calculations in the case of the carbon nucleus. The calculated Carbon and Nitrogen chemical shifts for the previously mentioned amino acids are shown in Table 2-2 and Table 2-3.

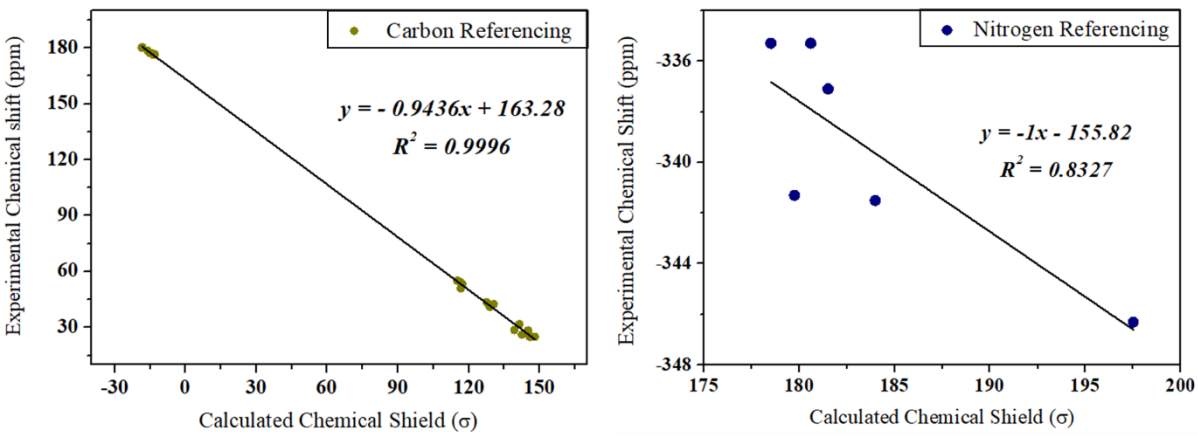

Figure 2.7. Comparison between GIPAW computed (total shielding) and experimental ^{13}C and ^{15}N NMR data for reference compounds (Leucine, α- and β-Glutamic acid, α-Glycine and Alanine)

Leucine	Calculated	δ_{iso} (calculated)	δ_{iso} (experimental)
	Sigma Total		
C1	-14.8	177.3	177.3
C2	116.1	53.7	54.4
C3	130.6	40.1	41.3
C4	145.9	25.6	25.3
C5	146.0	25.6	25.3
C6	146.1	25.5	25.3
C1	-13.1	175.6	176.5
C2	117.4	52.5	53.4
C3	128.8	41.7	42.9
C4	145.9	25.6	25.3
C5	148.0	23.6	25.3
C6	147.2	24.4	25.3

α-Glutamic Acid	Calculated	δ_{iso} (calculated)	δ_{iso} (experimental)
	Sigma Total		
C1	**-15.2**	**177.7**	**177.2**
C2	**116.2**	**53.6**	**54.4**
C3	**141.4**	**29.8**	**28.6**
C4	**139.2**	**31.9**	**31.6**
C5	**-18.4**	**180.7**	**180.1**
β-Glutamic Acid	**Calculated**	δ_{iso} **(calculated)**	δ_{iso} **(experimental)**
	Sigma Total		
C1	**-16.0**	**178.4**	**178.4**
C2	**115.2**	**54.6**	**55**
C3	**145.2**	**26.3**	**26.2**
C4	**142.5**	**28.8**	**28.3**
C5	**-18.3**	**180.5**	**180.4**

α-Glycine	Calculated	δ_{iso} (calculated)	δ_{iso} (experimental
	Sigma Total		
C1	**-13.4**	**176.0**	**176.2**
C2	**127.5**	**42.9**	**43.5**
Alanine	**Calculated**	δ_{iso} **(calculated)**	
C1	**-14.29**	**176.8**	**176.8**
C2	**116.5**	**53.3**	**50**
C3	**151**	**20.7**	**19.8**

Table 2-2. Calculated ^{13}C chemical shifts of L-Leucine, α–β Glutamic acid, α–Glycine and Alanine by using the referencing equation of ^{13}C mentioned in Figure 2.7, compared with the experimental chemical shifts

Amino Acids	Calculated	δ_{iso} (calculated)	δ_{iso} (experimental)
	Sigma Total		
Leucine	**178.5, 180.6**	**-334.3, -336.4**	**-335.3**
α-Glutamic Acid	**179.7**	**-335.5**	**-341.1**
β-Glutamic Acid	**183.9**	**-339.8**	**-341.1**
α-Glycine	**197.5**	**-353.3**	**-346.3**
Alanine	**183.6**	**-339.5**	**-337.1**

Table 2-3. Calculated Nitrogen chemical shifts of Leucine, α–β Glutamic acid, α–Glycine and Alanine by using the referencing equation of ^{15}N mentioned in Figure 2.7, compared with the experimental chemical shifts

Chapter III: Investigation of Leucine adsorption on Silica

III.1 Introduction

Among all possible amino acids that could (and sometimes already have) been studied, some present more interest than others.[38] Recently, workers at the LRS have observed that co-adsorption of Leucine (Leu) and Glutamic acid (Glu) on silica leads to rather long linear peptides that seem to present non-trivial sequence selectivity.[92] Thus, we have undertaken a joint experimental and theoretical characterization of the interaction of these two amino acids with a silica surface.

The present chapter concentrates on Leu/SiO_2. This particular system has been the subject of limited study so far, mostly at the macroscopic level: measurement of adsorption isotherms on quartz[247] and mesoporous silica[248] or measurement of adsorption enthalpies for chromatographic applications.[249]

Leucine is an amino acid with a non-polar side chain. It is represented in Figure 3.1, with the atom numbering scheme we will use throughout. Also represented are the forms that exist in aqueous solution – the cation, denoted as H_2Leu^+, the zwitterion or $HLeu^{\pm}$, and the anion or Leu^-. The zwitterion is the predominant form in the 2.36–9.60 pH range. The neutral form, $HLeu^0$, exists in the gas phase; it has been calculated that the addition of at least two water molecules per Leu is necessary to make the zwitterionic form more stable than the neutral one.[250] Thus, with respect to its acid-base speciation, Leu behaves much like Glycine, which has been studied a lot more.

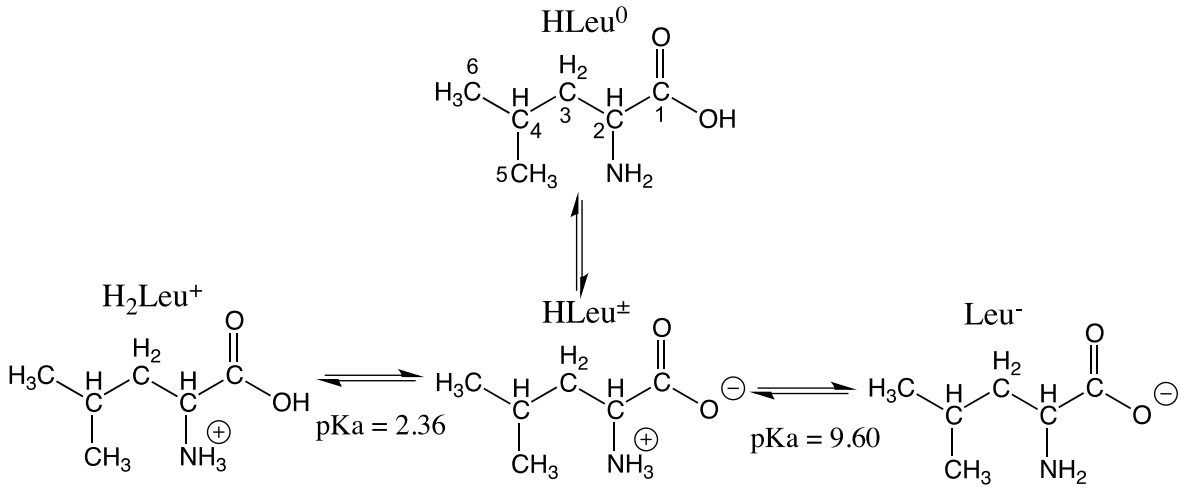

Figure 3.1. Leucine and its acido-basic speciation

To understand the adsorption of Leucine species, a combination of multiple spectroscopic techniques was applied. The objective was to get a picture at the molecular level of Leucine interaction with fumed silica (Aerosil 380) surfaces. For this purpose, IR and solid state NMR spectroscopies were chosen, using in particular 2D Heteronuclear chemical shift correlation (HETCOR) experiments to trace out the proximities and proton-carbon or proton-nitrogen

connectivities in the hope of understanding and identifying the type of bonding of Leucine with the surface. Moreover, high and low hydration levels were investigated and quantified by TGA, in order to understand the influence of water on Leucine speciation and adsorption behavior.

Experimental data were combined with theoretical models obtained by using periodic DFT simulations, considering both anhydrous and microsolvated Leucine adsorbed on a hydroxylated amorphous silica surface. The aim was both to propose a description of the local organization of the amino acid at the surface and to help interpreting experimental data. Indeed, adsorption energies could be compared between the different models and corresponding NMR parameters calculated. This allowed to select the models giving the best agreement with experiments but also to try to extract possible correlations between NMR parameters of moieties interacting with the surface and their local environment, in particular the H-bond network.

III.2 Macroscopic Characterization

III.2.1 X-Ray Diffraction

As seen in Figure 3.2, bulk commercial Leucine and bulk enriched [$^{13}C_6$, 1-^{15}N] Leucine show the same Bragg peaks positions (the assignment of Miller indices is reported on the figure). This proves that the crystal structure of Leucine is preserved after isotopic enrichment. Data on bulk Leucine (Bragg peaks) were previously reported by Elfassy *et al.*[251] The most intense peaks are the (0 0 l) ones. The corresponding lattice planes are parallel to the Leucine layers (Figure 3.10).

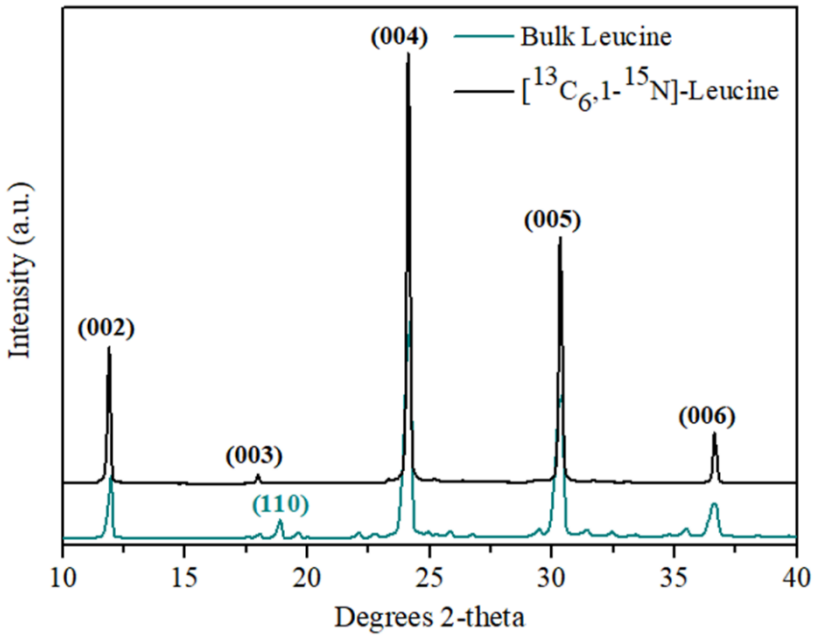

Figure 3.2. X-ray diffraction of bulk Leucine vs enriched [$^{13}C_6$, 1-^{15}N] -bulk Leucine

XRD data on Leucine adsorbed on fumed silica nanoparticles at different loadings were previously reported by Sakhno *et al.*[92] In conformity with this work, in the present one, we recorded the XRD of Leu/SiO_2 (under Nitrogen dried conditions) at different loadings. The X-Ray Diffractograms of our samples show that Leucine loadings above 3% led to the appearance

of sharp Bragg peaks consistent with bulk Leucine crystals. Focusing on the region of 2θ between 18° and 32°, peaks can be assigned to (-1 1 0), (-1 0 3), (0 0 4) and (0 0 5) reticular places at around 19°, 19.7°, 24.3° and 30.3° respectively (Figure 3.3). Hence, as mentioned in Chapter II, a 3% loading is considered as the upper limit for the saturation coverage of molecularly adsorbed Leu on the silica surface. Above this loading, crystallites of bulk Leucine are present in addition to the adsorbed form(s), complicating the characterization of the latter.

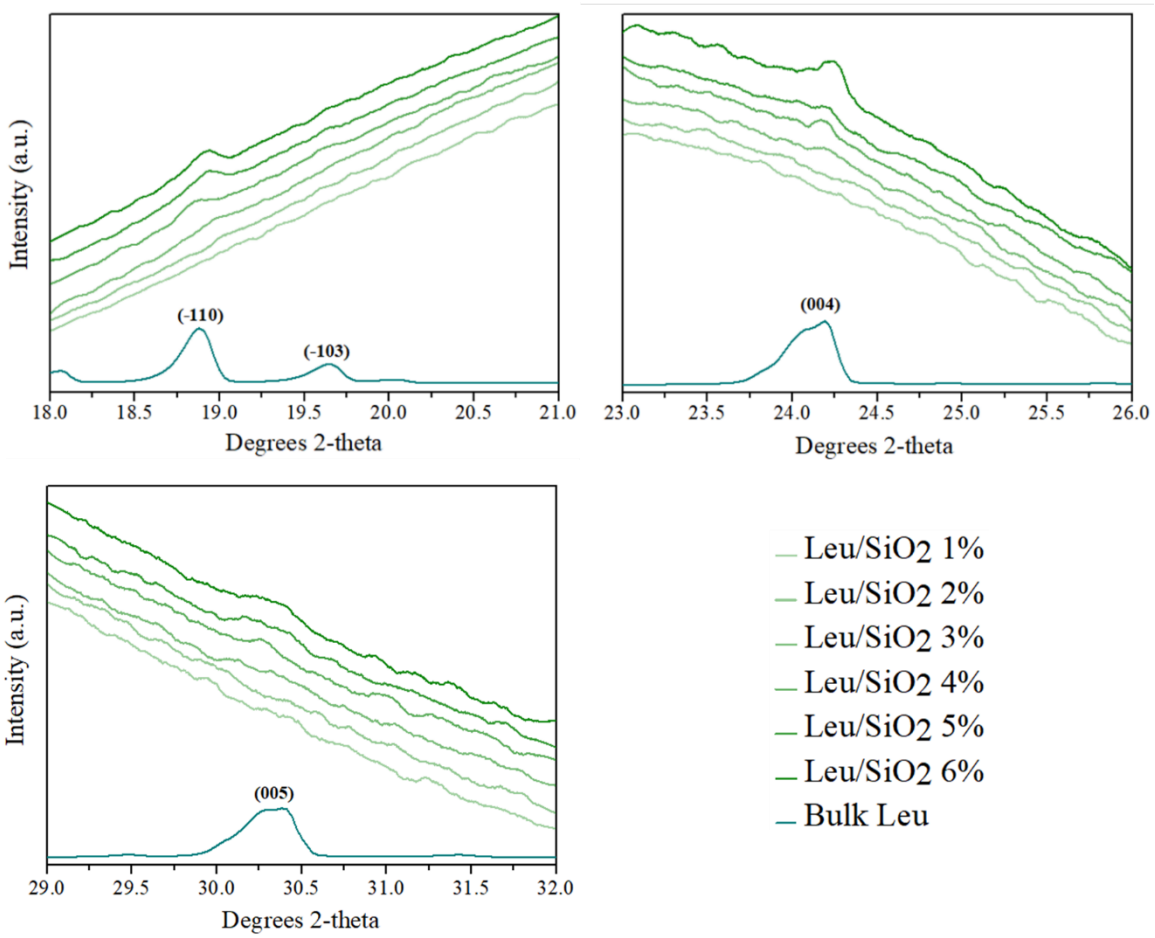

Figure 3.3. XRD patterns of pure bulk Leu and Leu/SiO_2 systems with increasing loadings

III.2.2 Thermogravimetric Analysis

Leu/SiO_2 at different loadings were analyzed by thermogravimetry after both nitrogen drying (ND) and vacuum drying (VD) (Cf Chapter II). The DTG curves are presented in Figure 3.4 and Figure 3.5. They show three thermal events in clearly distinct temperature ranges. Based on previous work[92], the first, endothermal event between RT and 120°C (T_{max} = 50-60°) may be assigned to physisorbed water elimination, the second one (T_{max} = 176-182°C) to amino acids peptidic condensation releasing water, and the third one (above 250°C, composite, with a maximum around 300°C) to oxidative degradation of supported organic molecules (since the TGs were carried out under air flow, O_2 is available for organic molecules oxidation). After the physisorbed water elimination, both ND and VD samples have essentially the same DTG.

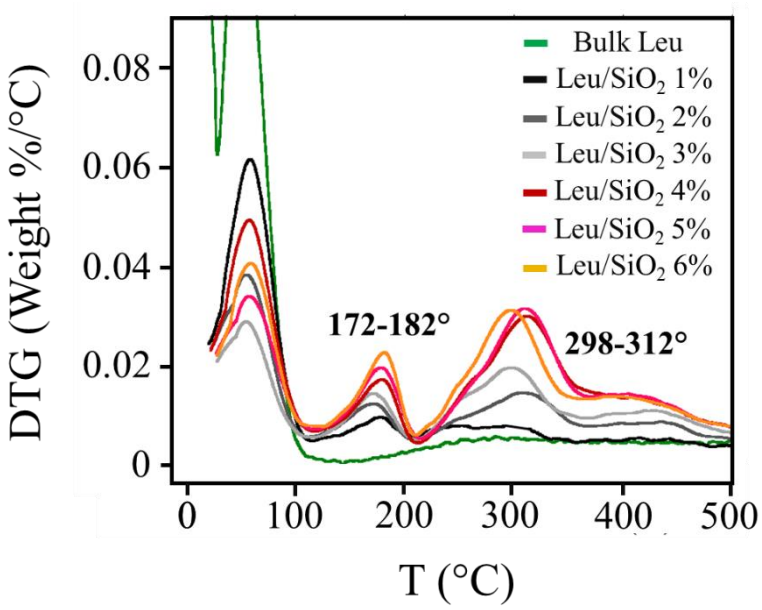

Figure 3.4. DTG curves of Leu/SiO_2 at different weight percentages loadings, after ND treatment (green trace corresponds to the raw SiO_2 support)

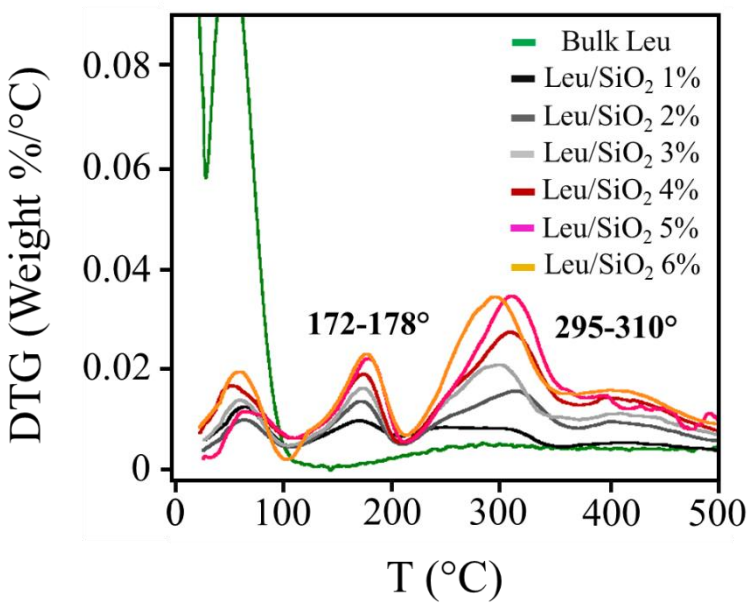

Figure 3.5. DTG curves of Leu/SiO_2 at different weight percentages loadings, after VD treatment (green trace corresponds to the raw SiO_2 support)

If the above assignment of thermal events is correct, then integrating the weight losses corresponding to the second and third events (after correction for weight loss of the raw support) should give the weight loading of the amino acid – which is known since the deposition procedure we used results in complete retention in the final sample of the amino acids initially introduced. This was done for ND (two repeats-blue and green) and VD treated samples (red) (Figure 3.6). The agreement is indeed quite good overall; possibly, for the highest loadings, the organic matter is not completely removed at 650°C (the upper limit we used for integration) and its quantification would need continuing the TG to higher temperatures.

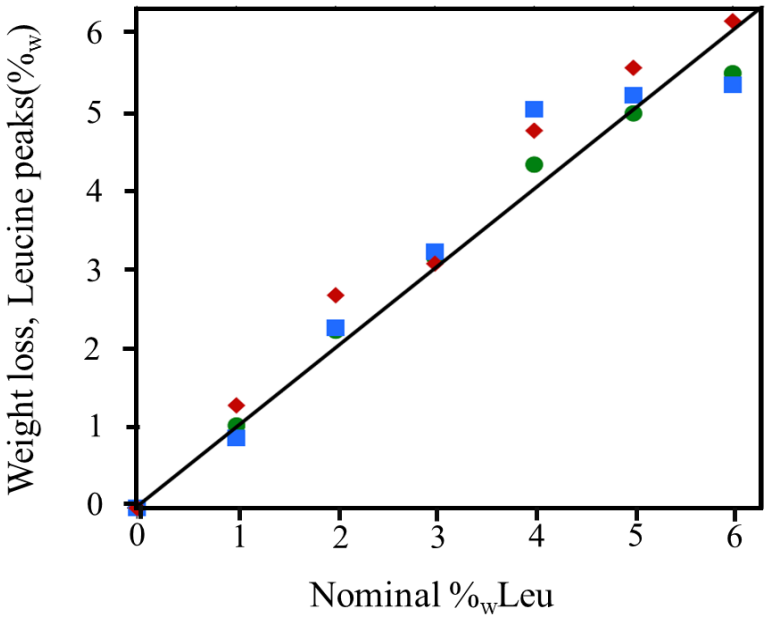

Figure 3.6. Weight losses in events attributed to Leucine degradation (corrected for support losses), as a function of the nominal Leucine weight loading. (blue and green correspond to ND system while red corresponds to VD)

The amount of physisorbed water can be estimated by quantification of the first event (weight loss before 100°C), since amino acid decomposition does not interfere in this range.
The calculation of the number of water molecules/nm^2 was done according to the following formula:

$$\text{Number of water molecules/nm}^2 = \frac{(\%\ \text{weight of water}/100) * \text{N}_\text{A}}{\text{M}(\text{H}_2\text{O}) * \text{A} * 10^{18}} \qquad (37)$$

where N_A is Avogadro's number, and 'A' is the specific surface area of Aerosil silica particles (380 m^2 /g).

Figure 3.7 shows the amount of physisorbed water remaining after nitrogen and vacuum drying, as a function of the Leucine loading. Unsurprisingly, it strongly depends on the drying method applied prior to analysis as well as the amount of Leucine on the surface.

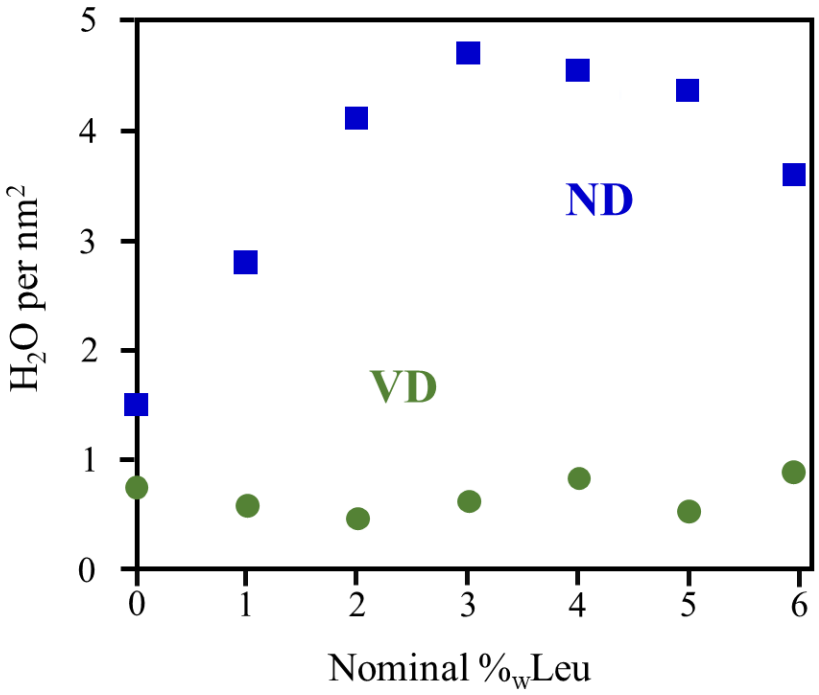

Figure 3.7. Quantification of physisorbed water in Leu/SiO_2 as a function of Leucine loading after VD and ND treatments. 3% Leu corresponds to 0.36 Leu molecule per nm^2.

After VD, less than one water molecule per nm^2 stays adsorbed on the bare silica: this is four times less than the total number of silanols, and thus water must be strongly adsorbed on a limited number of special silanols sites. Noticeably, the amount of water remains almost constant for samples containing deposited Leucine. Therefore, Leucine does not "displace" adsorbed water molecules: either it is adsorbed on different surface sites, or (more likely, as we shall see later), it interacts with water-covered sites, resulting in H_2O acting as a bridging molecule between the surface and Leu. The molar ratio between strongly adsorbed water and Leucine depends of course on the Leucine loading. For 3% Leu (which is a rough estimate of the saturation coverage according to the XRD data in § III.2.1), H_2O: Leu would be about 2.8, and 4.2 for 2% Leu.

After ND, the amount of residual water on raw silica is somewhat higher, at about 2 molecules per nm^2. Interestingly, it increases proportionally to the Leucine loading until 3%, i.e., until saturation of the adsorbed sites is reached, then reaches a plateau and levels off. This suggests that there is a co-adsorption of Leucine with a number of water molecules that, in view of the proportionality constant, is about 10 water molecules per adsorbed Leucine – an amount sufficient to provide an aqueous-like environment.

III.3 Spectroscopic Characterization

III.3.1 Infrared Spectroscopy

Figure 3.8 shows the IR spectra of Leu/SiO_2 at different loadings and after ND or VD treatment. Spectra of VD samples with a D_2O exchange were also recorded to help interpretation. Three separate regions can be observed: the fingerprint region of amino acids between 2200-1350 cm^{-1}, the region containing OH, NH and CH stretching bands (4000-2000 cm^{-1}) and finally the NIR region between 6000-4500 cm^{-1} that can show a diagnostic combination band of water, and is useful to estimate the extent of hydration. The Leucine bands may be attributed with confidence on the basis of isotopic exchange, together with a comparison with literature data and the spectrum of bulk Leucine. Their assignments are listed in Table 3-1.

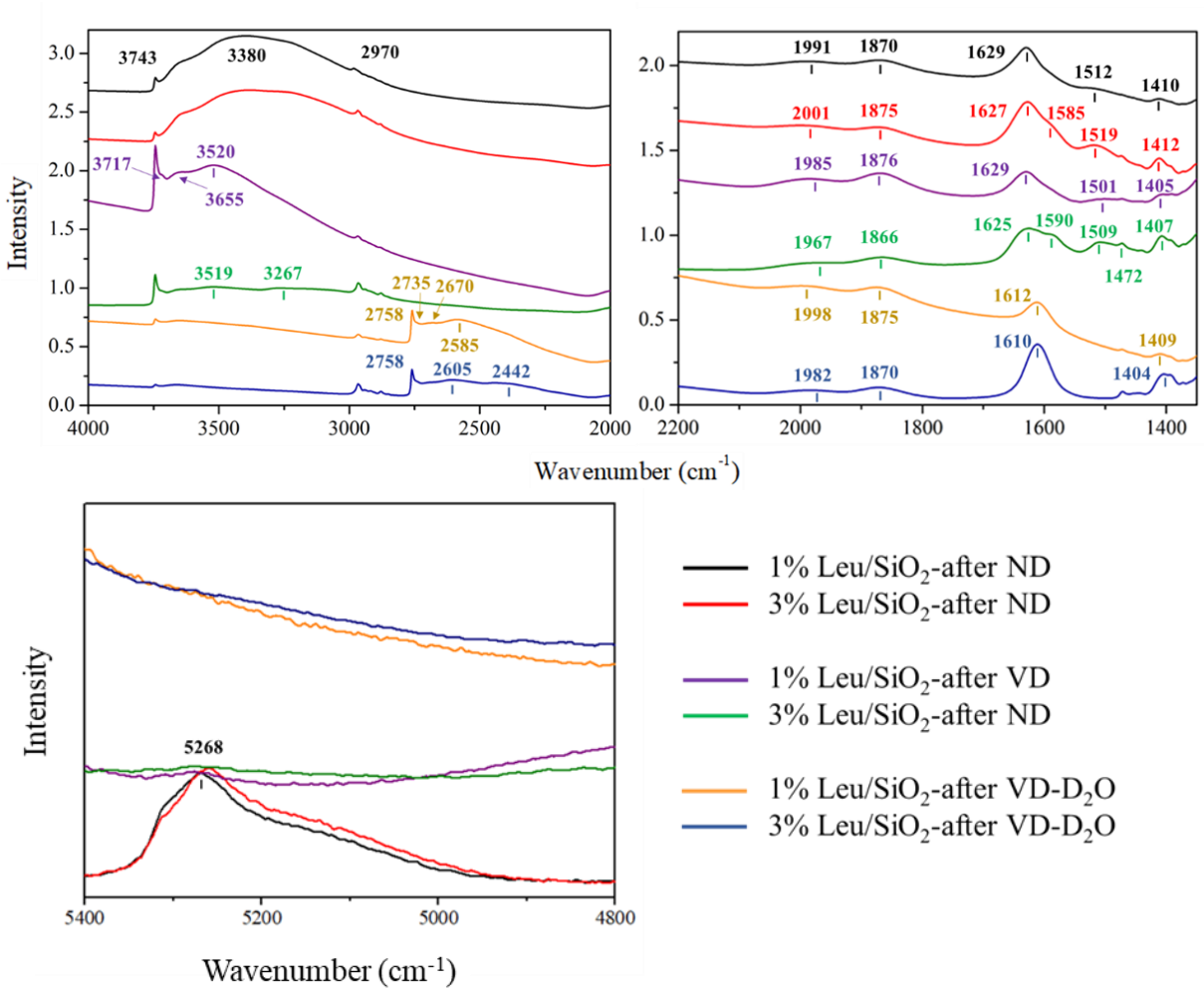

Figure 3.8. IR spectra of Leu/SiO_2, at different percentages (1% and 3%), and after drying in different conditions (Nitrogen dried, ND and Vacuum dried, VD). D_2O exchange was also performed on the VD samples

Assignment	Wavenumber (cm^{-1})				
3%Leu/Silica Nitrogen-dried (ND)	1625	~1590	1518	1411	1351
3%Leu/Silica Vacuum-dried (VD)	1627	1590	1508	1407	1347
Leucine Solution H_2O (Derbel et al. JPC B 2007, 111, 1470	1644	1594	1514	1410	1350
Vibrations	$\delta_a(NH_3^+)$	$\nu_a(CO_2^-)$	$\delta_S(NH_3^+)$	$\nu_s(CO_2^-)$	ν(CH+NH)

Table 3-1. Positions of main IR bands attributable to Leucine (in cm^{-1}) in water solution (literature data) and in Leu/SiO_2, vacuum-dried and nitrogen-dried

With the exception of $\delta_a(NH_3^+)$, which is hard to locate because of overlap, band positions in the strongly hydrated ND samples are close to those in water solution. When going from ND to VD samples, the $\delta_s(NH_3^+)$ band is downshifted by -10 to -11 cm^{-1}, the $\nu_s(COO^-)$ band by -4 to -5 cm^{-1}, and the ν(CH+NH) band by -4 cm^{-1}, respectively. This means that the NH_3^+ moiety has its environment most affected by thorough drying. It would be compatible with the establishment of bonding with surface silanols in VD samples, instead of water molecules in ND samples.

The silica support itself shows two combination bands at 1870 and 1990 cm^{-1} that are often used for spectra normalization since they do not overlap with the range of most organic vibrations. In addition, there is a medium intensity band at ~1630 cm^{-1}, which is an overtone of ν_{sym} Si-O-Si[252]; it is superimposed with the asymmetric bending of the amine moiety $\delta_a(NH_3^+)$. In high-water content samples, there is also a contribution of the H_2O bending mode at the same position.

Upon H/D exchange, the 1625 and 1590 cm^{-1} bands disappear, and are replaced by a strong band at 1610 cm^{-1}. The disappearance of the 1625 cm^{-1} band is understandable if it is mainly due to NH_3^+ asymmetric bending: the exchange produces ND_3^+ moieties whose bending vibrations absorb below 1300 cm^{-1}, out of the observed spectral window. On the other hand, the band at 1590 cm^{-1} is mainly due to COO^- asymmetric stretching but DFT calculations on the Leu zwitterion in aqueous solution have shown that deuteration induces a blue shift of this band (which is found at 1594 cm^{-1} in water). In fact, this vibrational mode in non-deuterated Leu contains considerable contributions from the NH_3^+ bending and when the molecular group is deuterated to ND_3^+, this contribution disappears, resulting in a pure COO^- asymmetric stretching and thus in the vibrational mode absorbing at a higher energy.[161]

At lower wavenumbers, the 1508 cm^{-1} band disappears upon H/D exchange, consistent with its attribution to the symmetric bending of the NH_3^+. The 1407 cm^{-1} band (COO^- symmetric stretching) is slightly downshifted to 1404 cm^{-1}, in agreement with previous experiments in

water and D_2O. The 1471 cm^{-1} band does not change position upon H/D exchange, since it is due to vibrations of the unexchangeable CH_3 groups.[161] The 1394 cm^{-1} (attributed mainly to CH_3) and the 1347 cm^{-1} (mainly localized on the aliphatic side chain of Leu) do not shift upon H/D exchange either.

In ND samples, the 4000-2000 cm^{-1} region is dominated by the contribution of the OH of adsorbed water molecules, a broad and intense band that has a maximum at low wavenumbers (around 3400 cm^{-1}) due to inhomogeneous H-bond interactions in the multilayered adsorbed water molecules. The OH stretching of isolated silanols is also apparent at 3742 cm^{-1} and becomes better defined after VD; at the same time, other signals appear at 3717 and 3655 cm^{-1}, corresponding to different silanol types.[173] Broad features around 3300 cm^{-1} may be due to NH stretching in Leu. All of these features shift to lower wavenumbers upon D_2O exposure, indicating that the corresponding groups are easily D-exchanged as expected. In contrast, the band at 2970 cm^{-1} corresponding to C-H stretching does not shift.

In the NIR region, the band assigned to the combination mode of water is clearly visible for the ND samples. It has a maximum at 5288 cm^{-1} and appears composite: it might be interesting to try to identify its components as they could correspond to different types of adsorbed water. After VD, it is hard to notice any signal left in this region, confirming a successful dehydration. Of course, exposure to D_2O does not restore this signal, as adsorbed D_2O will vibrate in a different spectral region.

The above attributions are confirmed by experiment on differently isotopically labelled 3% Leu/SiO_2 (Figure 3.9). In particular, [1-^{13}C, 1-^{15}N] Leu/SiO_2 shows a red shift (bathochromic shift) of the 1590 cm^{-1} and 1407 cm^{-1} bands (to 1563 cm^{-1} and 1372 cm^{-1} respectively), confirming the attribution of these bands mainly to COO^- vibrations. Smaller red shifts are observed for the other bands (1508 cm^{-1} shifts down to 1500 cm^{-1}; 1392 cm^{-1} to 1386 cm^{-1}) that have only small contributions from COO^- vibrational modes. Interestingly, the 1627 cm^{-1} band shifts down to ~1613 cm^{-1}, suggesting a non-negligible COO^- character in this vibrational mode, The IR spectrum of (^{13}C)$_6$ Leu/SiO_2 is also compatible with the above assignments as seen in Figure 3.9.b where it shows downshifts for the 1625 (to ~1611 cm^{-1}), 1590 (to 1563 cm^{-1}), 1508 (to 1500 cm^{-1}). The 1407 cm^{-1} band undergoes a stronger downshift (to 1364 cm^{-1}) compared to Leu [1-^{13}C, 1-^{15}N], confirming that the band is not due to a pure COO^- symmetric stretching but also reflects contributions from motion of other carbon nuclei. The 1392 cm^{-1} and 1347 cm^{-1} bands also undergo a more pronounced shift (to 1372 cm^{-1} and 1333 cm^{-1}, respectively)

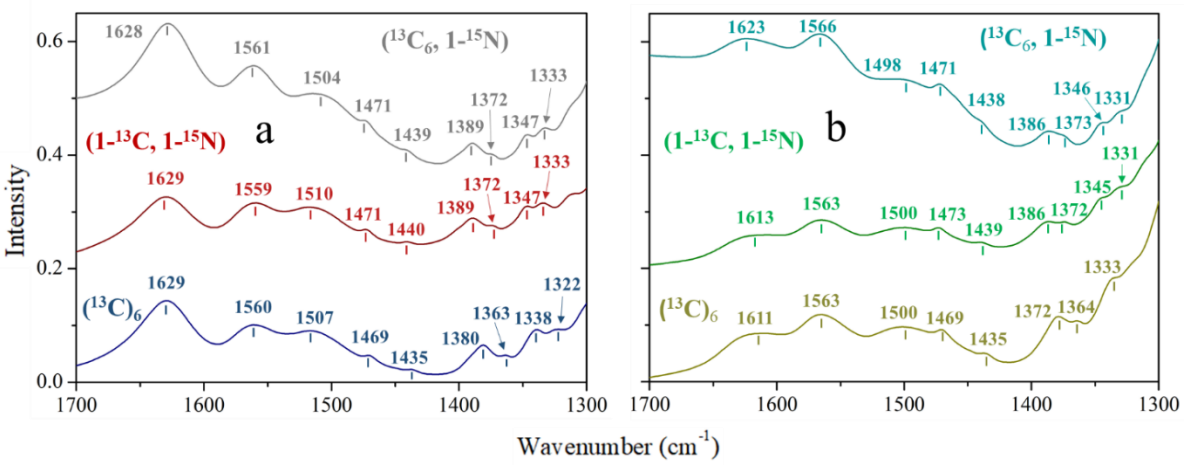

Figure 3.9. Isotopically enriched samples of 3% [$^{13}C_6$,1-^{15}N] Leu; 3% [1-$^{13}C_1$,1-^{15}N] Leu and 3% [^{13}C]$_6$ Leu adsorbed on SiO_2, (a) After Nitrogen flow drying (ND), (b) After Vacuum drying (VD)

compared to [1-^{13}C, 1-^{15}N] Leu/SiO_2, showing that these two vibrational modes involve several C atoms. Finally, the 1472 cm^{-1} band undergoes a slight shift to 1469 cm^{-1} providing evidence for its assignment to the CH_3 groups of the side chain of Leu.

The main difference between the ND and the VD enriched samples is in the amino acid region, where water removal has led to a significant decrease in the asymmetric bending of the ammonium as well as in the symmetric stretching of the carboxylate group, especially in the samples where the enrichment was on the carbon atoms only; however, in the case where the enrichment was on both carbon and nitrogen ([1-^{13}C,$^{15}N_1$] Leu/SiO_2), the difference was not as noticeable.

Important lessons may be drawn from IR results:
- Even after VD, Leucine is zwitterionic, as it is in water solution.
- There is no evidence of covalent bond formation between the Leucine molecule and the surface since all vibrations of Leucine are clearly conserved.
- Changes in band positions between ND and VD treatments suggest that the environment of the supported amino acid is similar to the aqueous solution after ND, while after VD specific interactions are established between silica surface groups and amino acid moieties, chiefly the ammonium group (-NH_3^+).

III.3.2 Solid-state NMR spectroscopy

Solid-state NMR spectra were recorded for the amino acid L-Leucine in its bulk form as well as adsorbed on Aerosil-380 silica. Enrichments in ^{13}C and ^{15}N were used in order to obtain intense signals in a reasonable acquisition time. 1D-Direct polarization (DP) as well as 1D-Cross polarization (CP) experiments were performed to distinguish bulk-like from adsorbed Leucine molecules; furthermore, 2D HETCOR NMR experiments were carried out to obtain information on nuclear connectivities.

III.3.2.1 NMR signatures of bulk crystalline Leucine and Leucine in solution

In principle, the NMR spectra of bulk Leucine crystals may be used as reference points to understand the relation between NMR parameters and local structure, since the latter is precisely known from diffraction analysis. However, the data on the crystal structure of L-Leucine is surprisingly complex. After initial works by Harding and Howieson[253] and Coll *et al*[254], Görbitz & Dalhus[244] found by single-crystal XRD that L-Leucine has a monoclinic crystal structure at 120K with parameters a = 9.562Å, b = 5.301Å, c = 14.519 Å, β = 94.20° and two non-equivalent Leucine molecules (called A and B in the following) per unit cell. On the other hand, when using a powder diffraction method, it was reported that L-Leucine undergoes several phase transition at 150 and 275 K,[255] with subtle changes involving variations in functional groups mobility.

Later on, Binns *et al*. precisely located the H atoms by using neutron diffraction and did not confirm any phase transition. Interestingly, they used the PIXEL quantum calculation method to identify separate components of the cohesion energy[256]. Very strong hydrogen bonds were identified between Leucine molecules, with total energies ranging between -146 kJ/mol and -46 kJ/mol. Each Leucine molecule forms eight hydrogen bonds, but while the carboxylate in Leu A has three H-bonds from the ammonium groups of other molecules, Leu B has four, one

of which is a bifurcated hydrogen bond. Figure 3.10 shows the crystal structure and the difference in local H-bonding between the two inequivalent Leu molecules.

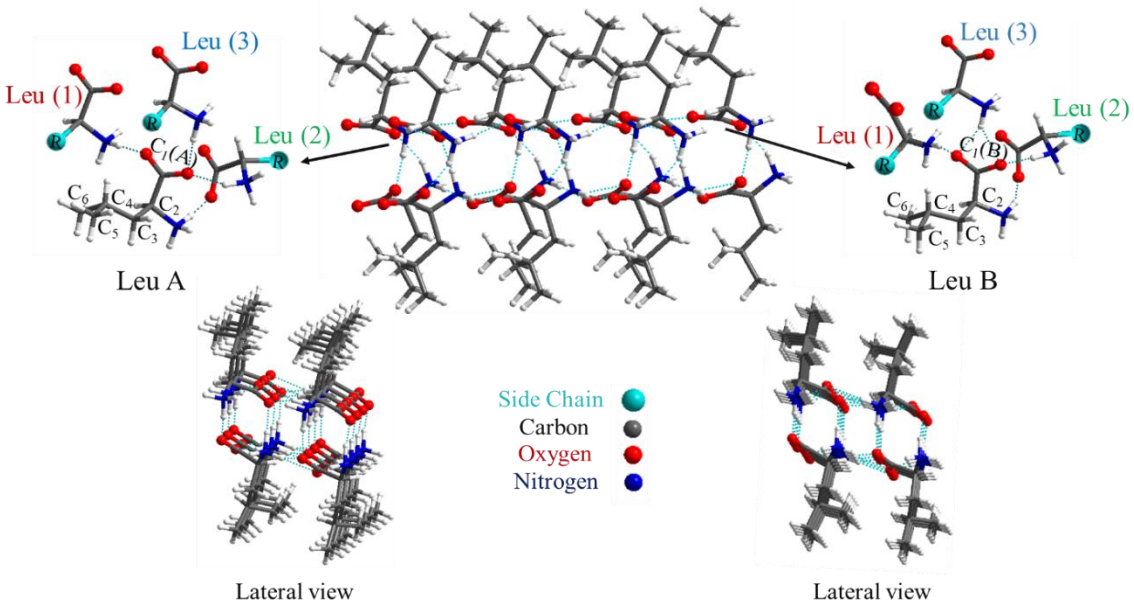

Figure 3.10. Two L-Leucine molecules **(Leu A and Leu B)** in the assymetric unit cell[256]

i ^{13}C CP-MAS

Figure 3.11 shows the ^{13}C CP-MAS NMR spectrum of bulk polycrystalline L-Leucine, as well as the liquid-state ^{13}C NMR of a Leucine solution. The bulk Leu spectrum is in agreement with previously published ones[257,258] and shows two narrow signals in the carboxylate region, at 176.5 and 177.3 ppm, due to the presence of the two inequivalent molecules in the crystalline structure.[257] Thus, the small differences in H-bonding environment outlined above are sufficient to give rise to two clearly separated signals. This was well reproduced by our computations, that foresaw two peaks in the carboxylate region at 177.3 and 176.5 ppm, respectively (See Tables 2-1 & 2-2 of Chapter II). Aqueous Leu has only one carboxylate signal at 176.4 ppm.

In the aliphatic region, the signals observed for bulk Leu at 53.9 ppm, 42.1 ppm and 25.3 ppm are assigned to C2-H (methine), C3-H_2 (methylene, and the 2 CH_3 (in C5 and C6) overlapping with the C4-H, respectively (See Tables 2-1 & 2-2 of Chapter II). The former two signals are split, as observed for carboxylates, corresponding to the two inequivalent molecules in the unit cell.[259] In aqueous solution, well-separate signals are observed for C4-H (25.0 ppm) and CH_3 (C5 and C6) (22.8 and 21.7 ppm - two non-equivalent methyl groups are observed, probably due to restricted rotation around the C3-C4 bond).

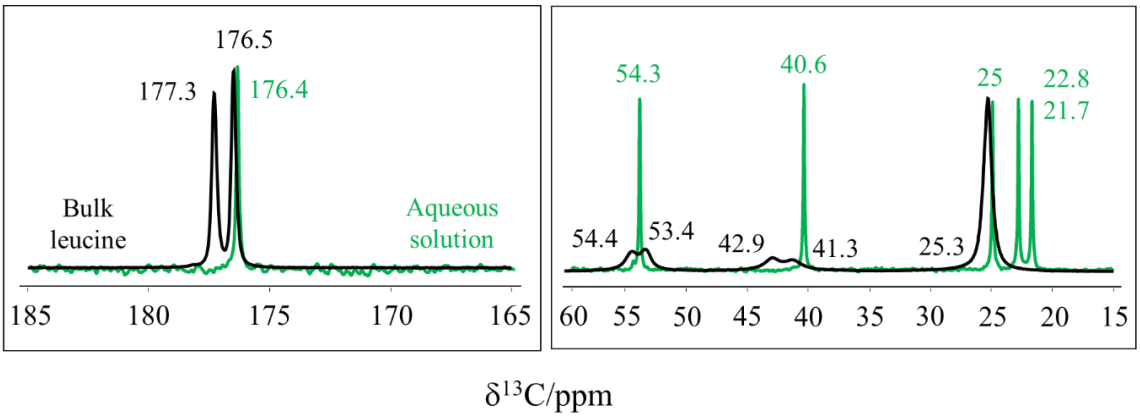

Figure 3.11. ^{13}C CP MAS NMR spectra of bulk [1-^{13}C,^{15}N] Leucine (black) and (natural abundance) Leucine in aqueous solution (green) in the carboxylate and aliphatic region

^{13}C CP MAS NMR spectra of the isotopically enriched Leu samples were recorded at different magnetic fields. As seen in Figure 3.12, spectra obtained at high field (16.4 T) show two signals corresponding to the two non-equivalent carboxylic environments as already discussed (although a slight splitting of each signal is apparent in the spectrum of [$^{13}C_6$] Leu). In contrast, at 7 T, a more complex signal is obtained for the samples enriched on all carbons ([$^{13}C_6$] and [$^{13}C_6$,^{15}N] Leu) – but not for the natural abundance Leu. These observations can be explained by the effect of J_{CC} coupling between the carboxylate carbons and the fully ^{13}C enriched neighboring CH (C2) that causes splitting into a doublet. At low fields, one should then observe two doublets instead of two singlets but coincidentally, two of the resulting four signal overlap, giving rise to the shape observed in Figure 3.12 (right part, green and red spectra). At higher fields, the effect of J coupling is minimized and only detected for the [$^{13}C_6$] Leu sample. The conclusion is that high fields may be necessary to obtain easily interpretable ^{13}C spectra for Leucine samples. Moreover, it will bring resolution on the proton dimension when recording $^{1}H \rightarrow {}^{13}C$ 2D-HETCOR as discussed later.

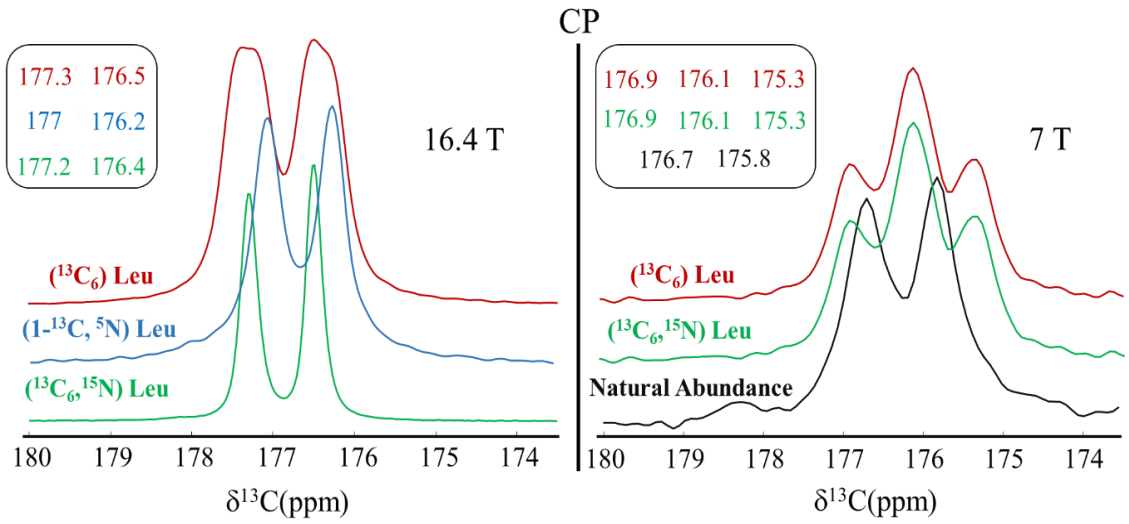

Figure 3.12. ^{13}C Cross polarization (CP) of isotopically [^{13}C,^{15}N] enriched bulk L-Leucine and for natural abundance bulk L-Leucine at different magnetic fields (16.4 T and 7 T)

ii ^{15}N CP-MAS

The ^{15}N CP-MAS of bulk Leucine (Figure 3.13) shows a signal at -335.3 ppm. By comparison with the ^{13}C spectrum, it could have been expected to observed two signals corresponding to the ammonium moieties in A and B Leucine molecules in the unit cell. Possibly, their separation in ppm is not sufficient to distinguish them in view of the peak broadening – one can notice that the peak shape is rather asymmetric.

In comparison, the ammonium ^{15}N signal is observed at -341 ppm in solution. In the crystal, the ammonium group is bound as an H-bond donor to three oxygens of carboxylate groups, while in aqueous solution, it is presumably bound to several water molecules. This difference in the H-bonding environment is enough to result in a +5.7 ppm shift of the ^{15}N peak.

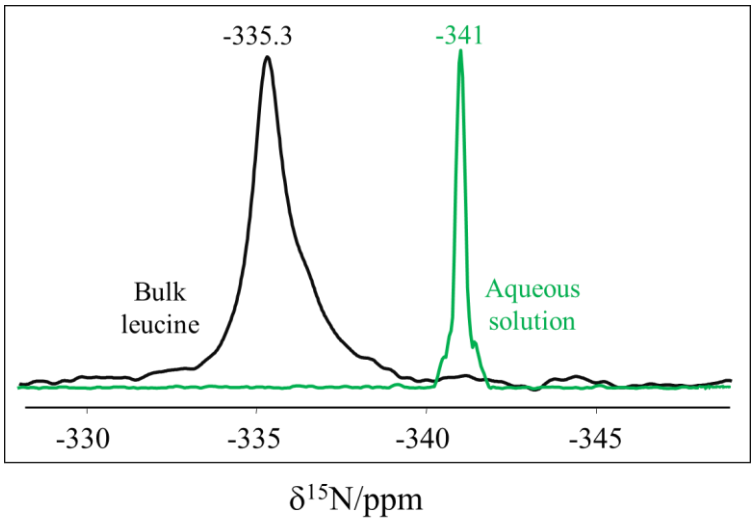

Figure 3.13. ^{15}N CPMAS NMR spectra of bulk [1-^{13}C,^{15}N] Leucine (black) and Leucine in aqueous solution (green)

iii ^{1}H MAS

Figure 3.14 presents the ^{1}H MAS NMR spectra of two bulk Leucine samples. The spectrum of fully enriched ([$^{13}C_6$, ^{15}N]) Leu was recorded at two field values, 7 T and 16.4 T. The first one is obviously too low to obtain a well-resolved spectrum, while at 16.4 T, three components are evidenced at 1.6, 5.0 and 9.3 ppm. We also ran at this higher field the proton spectrum of partly enriched Leu ([1-^{13}C, ^{15}N]). Its general appearance is very similar with three components of the same relative intensity, although somewhat shifted to higher fields. Thus, for proton as well as for ^{13}C NMR, it is desirable to work at high magnetic fields. In the case of ^{1}H NMR, high field is relevant specially to improve resolution by averaging strong ^{1}H-^{1}H dipolar couplings.

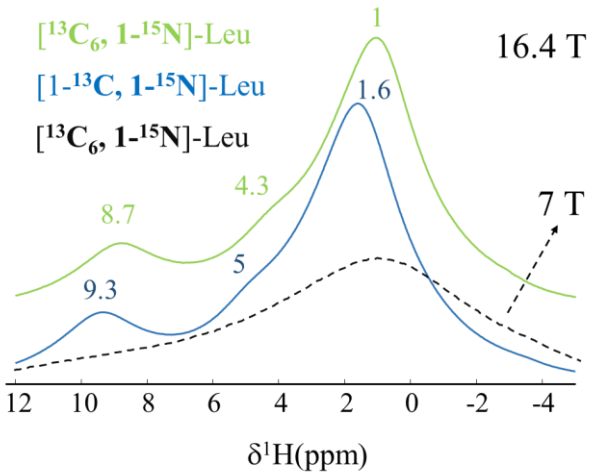

Figure 3.14. ^{1}H MAS NMR spectra for isotopically [^{13}C,^{15}N] enriched bulk L-Leucine at different magnetic field

Although there are no ^{1}H NMR studies of bulk Leu in the literature, based on NMR calculations, it is reasonable to propose that the main peak at 1.0 to 1.6 ppm contains contributions of the C3 methylene protons, the C4 methine, and the two methyl groups, the shoulder at 4.3 to 5.0 ppm is due to the C2 methine, and the signal at 8.7 to 9.3 ppm to the ammonium protons.

iv ^{13}C DP-MAS (Direct Polarization)

One should keep in mind that {^{1}H}-^{13}C CP-MAS experiments discussed above correspond to indirect detection of the ^{13}C signal by polarization transfer. Single Pulse (SP), also known as Direct Polarization (DP) experiments have been found useful to characterize different polymorphic structures as well as their dynamics, e.g. in the case of the α, β and γ polymorphs of glycine,[214,260] and so we also carried out DP ^{13}C NMR. For bulk Leu, the relaxation time (T_1) was found to be around 100s (Figure 3.15 and 3.16)

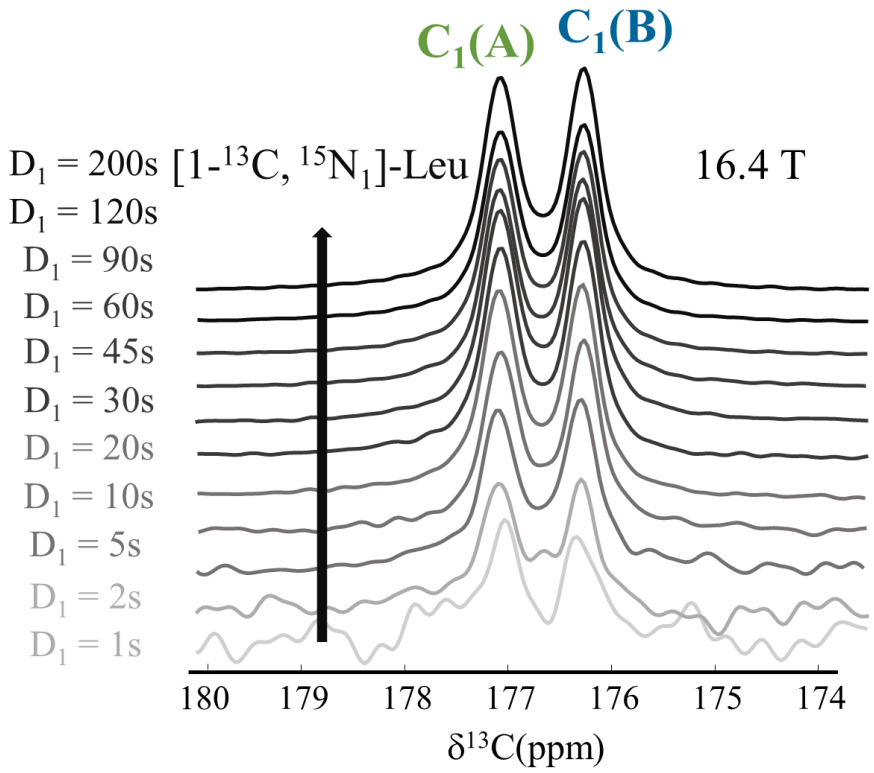

Figure 3.15. Direct Polarization ^{13}C MAS-NMR of bulk [1-^{13}C,^{15}N] Leucine, using variable recycle delays (D_1)

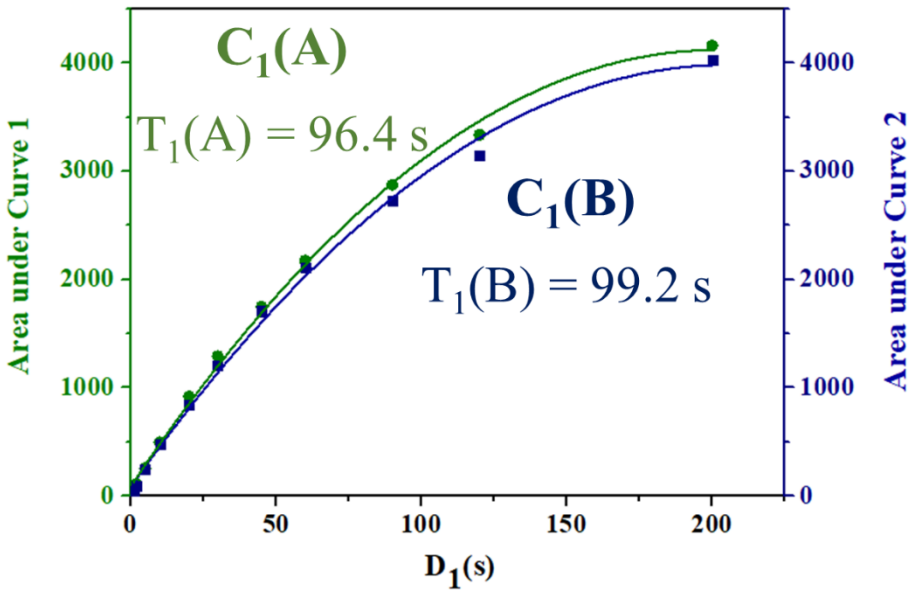

Figure 3.16. Fit of ^{13}C MAS NMR carboxylate peak intensities of [1-^{13}C,^{15}N] bulk Leucine (from Figure 3.14) as a function of the recycle delay D_1 using equation $M_{(D1)} = M_{(0)}(1-\exp(-D_1/T_1))$

III.3.2.2 NMR of Leu/SiO_2

i ^{13}C CP-MAS and ^{13}C DP-MAS

In the case of Leu/SiO_2 ND (see Figure 3.17), in the carboxylate region, two narrow ^{13}C peaks are observed at the same positions as in bulk Leu, probably due to a small amount of crystallized Leucine undetectable by XRD. They are superimposed with a large peak extending from 178 to 173 ppm. The broadness of the latter signal suggests a distribution of different conformations due to interaction with different environments on the surface (heterogeneous broadening). In the aliphatic region, a new ^{13}C peak at 21.1 ppm (not present in bulk Leu) is observed in Leu/SiO_2: this position is close to that observed in aqueous solution[261] and corresponds to the methyl groups of the side chain 5 (C5 and C6). Thus, C4 and C5-C6 signals are not superimposed for silica-supported Leu, contrary to bulk Leu, but in conformity with Leu in solution. This suggests that after adsorption followed by ND, the side chains are mostly interacting with water molecules. Upon vacuum drying, the main evolution is a significant broadening of the ^{13}C carboxylate signal while the aliphatic signals remain almost the same, suggesting that side chains are still surrounded by some water molecules, consistently with TGA results indicating that VD samples are not completely dry.

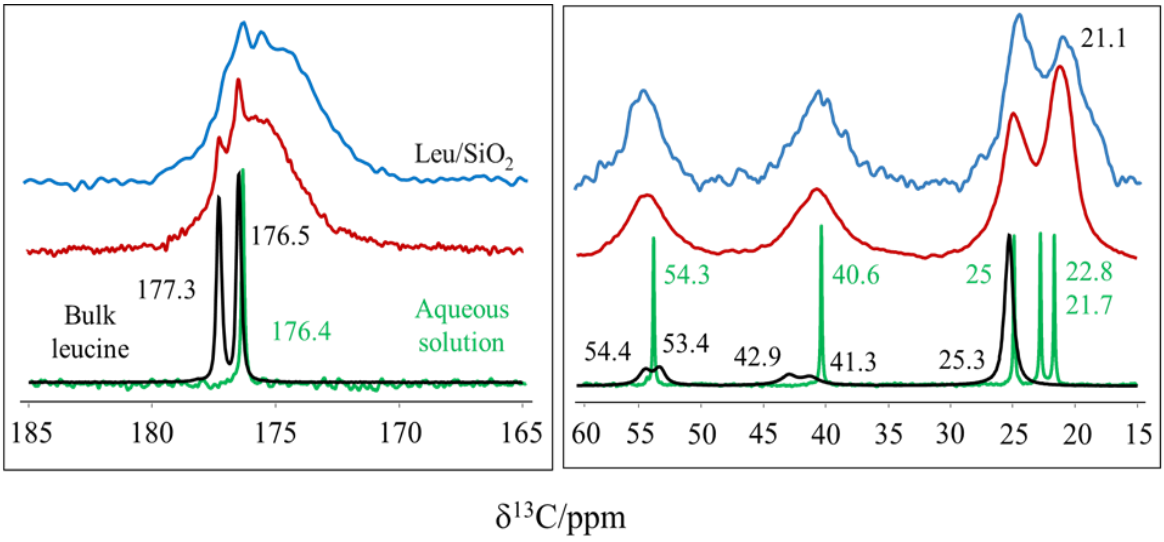

Figure 3.17. ^{13}C CP MAS NMR spectra of bulk [1-^{13}C,^{15}N] Leucine (black), Leucine in aqueous solution (green), 3%[1-^{13}C,$^{15}N_1$] Leu/SiO_2 after ND (red) and after VD (blue)

^{13}C DP- MAS spectra of ND Leu/SiO_2 was recorded at high magnetic field (16.4 T) with relaxation delays of 2s and 20s (Figure 3.18), which should be so short as to strongly suppress the signals of bulk Leu in view of the results in § III.3.2.1 iv. Indeed, the narrow signals are no longer observable, confirming that they are due to bulk-like Leu, in too small amounts to be detected by XRD, while the broad component is still present, compatible with its assignment to Leu in the "adsorbed state". Relaxation times for adsorbed species have indeed been found to be shorter e.g. for Alanine on fumed silica surface.[98]

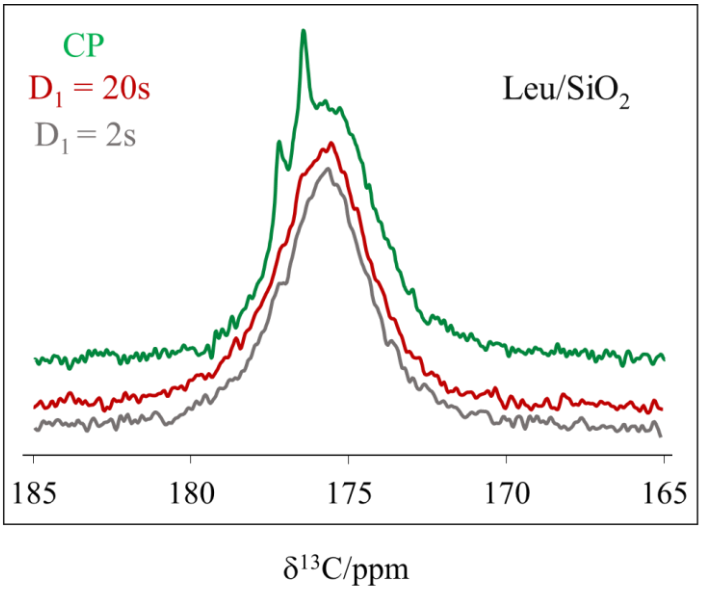

Figure 3.18. Direct polarization (SP) ^{13}C MAS NMR of ND 3%[1-^{13}C,^{15}N] Leu/SiO_2 in the carboxylate region at two different relaxation times (D_1 = 2s and 20s), compared with CP-NMR.

ii ^{15}N CP-MAS

The ^{15}N CP-MAS spectra of ND Leu/SiO_2 (Figure 3.19) shows a well-defined peak at -338 ppm, at a position shifted upfield as compared to bulk Leu (-335.3 ppm) : thus, it is shifted in the direction of H_2O-solvated ammonium, but without reaching the value of the latter (-341 ppm); in addition, a significantly smaller signal is observed close to the bulk position. The VD sample has a much broader signal that encompasses the two previous ones. This probably indicates a restricted mobility of the ammonium group.

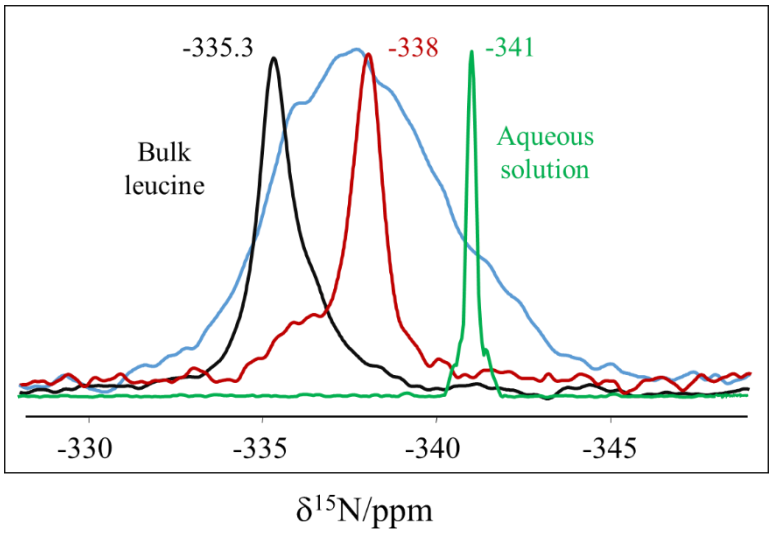

Figure 3.19. ^{15}N CPMAS NMR spectra of bulk [1-^{13}C,^{15}N] Leucine (black), Leucine in aqueous solution (green), 3%[1-^{13}C,^{15}N] Leu/SiO_2 after ND (red) and after VD (blue)

The broadening of both ^{13}C and ^{15}N signals after vacuum drying suggests that multiple possible configurations induce a distribution of distances and angles responsible for an increase in the number of possible adsorption configurations for the carboxylate and ammonium part of Leucine: this will be discussed in the modeling part.

The values corresponding to the fingerprints observed in the ^{15}N and ^{13}C CP- and DP-MAS NMR experiments, both in the carboxylate and in the aliphatic region, are summarized in Table 3-2.

A	^{13}C-carboxylate region			^{15}N
Samples	$C_{1(A)}O_2^-$	$C_{1(B)}O_2^-$	Broad band (178 to 173)	NH_3^+
$^{13}C_6/^{15}N_1$-Leu	177.3	176.5	-	-335.3
$^{13}C_1$-Leu/SiO_2-ND	177.2	176.4	175.3	-338
$^{13}C_6/^{15}N_1$-Leu/SiO_2-VD	177	176.3	175.6, 174.7	-332.5 to -345

B	^{13}C-Aliphatic region			
Samples	C_2H	C_3H_2	C_5H_3 C_6H_3	C_4H
$^{13}C_6$-Leu	54.4, 53.4	42.9, 41.3	25.3	
$^{13}C_6$-Leu/SiO_2-ND	54.3	40.7	25	21.1
$^{13}C_6$-Leu/SiO_2-VD	54.5	40.6	24.6	21.1

* Chemical shifts are reported in ppm

Table 3-2. Summary of ^{13}C and ^{15}N chemical shifts of enriched bulk L-Leucine and Leu/SiO_2 samples*

iii ^1H MAS NMR

Differences as a function of the drying treatment can also be studied by proton (^1H) NMR spectroscopy of Leu/SiO_2. Figure 3.20 compares the evolution between ND and VD drying of this sample and the raw silica support.

In both ND samples, the strong signal at around 4 ppm contains a predominant contribution of the "associated" silanols (silanols H-bonded to H_2O or other molecules). The chemical shift is probably the average of silanols and water molecules, as fast proton exchange is expected. This signal is rather sharp in ND SiO_2; in ND Leu/SiO_2, it has a "tail" up to 8-9 ppm that may be due to the Leucine protons, especially those of the ammonium moiety. The weak, sharp signal observed only in ND Leu/SiO_2 at 1.7 ppm could also be due to Leu, this time to the aliphatic protons, by analogy with Figure 3.14.

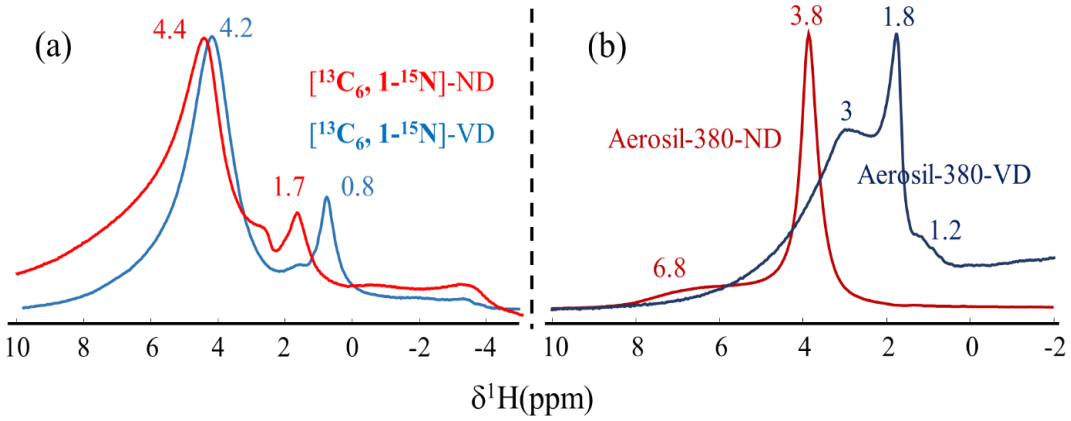

Figure 3.20. ^{1}H MAS NMR spectra of (a) 3% [$^{13}C_6$, ^{15}N] Leu/SiO_2, (b) the Leucine-free Aerosil-380 support, after ND and VD treatments

In VD SiO_2, the signal of the associated silanols weakens and shifts to lower δ values (3 ppm), as previously reported[262–265], due to the partial removal of H-bonded water molecules. At the same time, and again in coherence with literature data, a well-defined peak appears at 1.8 ppm, usually assigned to dehydrated isolated silanols. In VD Leu/SiO_2, the main peak remains at 4 ppm, and no strong component is observed at 1.8 ppm; however, a weak, sharp signal is observed at 0.8 ppm. Although we did not investigate proton spectra any further, both these observations may be connected with Leucine-silanol interactions.

iv $^{1}H \rightarrow {}^{13}C$ 2D-HETCOR

2D Heteronuclear chemical shift correlation (HETCOR) experiments were conducted to trace out the proximities and proton-carbon or proton-nitrogen connectivities in the hope of understanding and identifying the type of bonding of Leucine with the surface. The 2D $^{1}H \rightarrow {}^{13}C$ (carboxylate region) and $^{1}H \rightarrow {}^{15}N$ HETCOR CP-MAS NMR spectra are shown in Figure 3.21 and Figure 3.23, respectively, each time comparing the ND and VD systems with crystalline Leu.

The $^{1}H \rightarrow {}^{13}C$ 2D-HETCOR CP-MAS NMR spectrum of bulk Leucine shows three main cross-peaks, at 1.3, 4.0 and 8.8 ppm on the proton dimension, respectively corresponding to H in 3,4,5,6 positions, H in 2 position and ammonium protons. This 2D experiment is consistent with the previous ^{1}H MAS spectrum (Figure 3.14); all three proton signals observed in 1-D are observed as cross peaks, showing that they are correlated with the carboxylate. Indeed, the

distance between the carboxylate and the furthest protons (H5 and H6) are only about 5 Å according to the crystal structure.

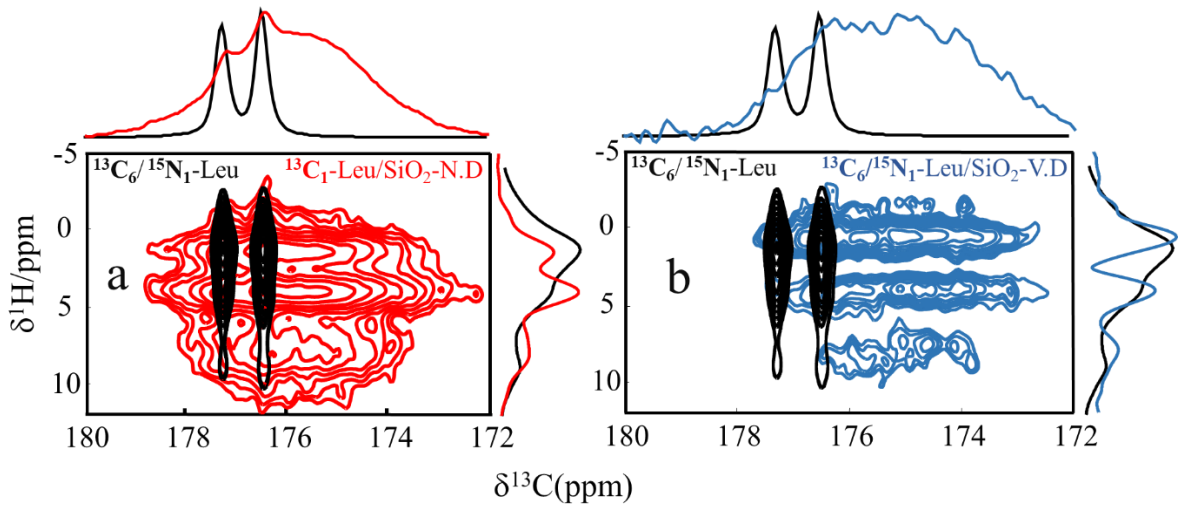

Figure 3.21. $^1H\rightarrow$ ^{13}C 2D-HETCOR CP MAS NMR spectra (16.4 T, 14 kHz) of 3%[1-^{13}C,^{15}N] Leucine/SiO_2 ND (red), VD (blue) and bulk L- [1-^{13}C,^{15}N] Leucine (black) in the carboxylic region

Leu/SiO_2 ND shows cross peaks more or less at the same position in the proton dimension, but the relative intensity of the signal at around 4 ppm is much higher, suggesting that it could be due to dipolar couplings not only with the methine proton of Leucine (H in position 2), but with the (silanol + water) OH protons typical of the silica surface (see discussion of Figure 3.20 above). After vacuum drying, this 4 ppm signal decreases, as water is removed; but it still remains rather strong, because this treatment is insufficient to remove all water from the sample, consistently with TGA results.

Upon vacuum drying, a significant broadening of the ^{13}C carboxylate signal is observed, while on the proton dimension aliphatic protons are slightly shifted to lower chemical shifts.

In the aliphatic region, Figure 3.22 shows that both ND and VD systems have indistinguishable HETCOR spectra. In particular, there are two ^{13}C signals at 21.1 and 24.7. We have previously said that the existence of two well-separate signals for the methyl and C4 methine groups was a “liquid-like” feature. Actually, those hydrophobic groups do not establish significant interactions with water; it is rather in the crystal phase that they have a special environment, due to the side-chains of Leucine being packed together in an arrangement reminiscent of the double layers made by the lipidic tails of surfactant molecules (see Figure 3.10).

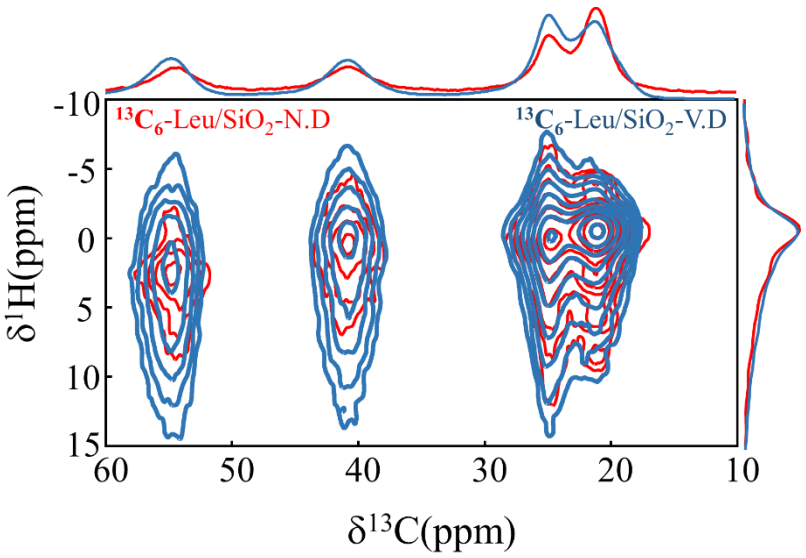

Figure 3.22. ^{1}H→ ^{13}C 2D-HETCOR CP MAS NMR spectra (7 T, 14 kHz) of 3%[1-^{13}C,^{15}N] Leucine/SiO_2 ND (red) and VD (blue) in the aliphatic region

In ^{1}H → ^{15}N 2D-HETCOR CP-MAS NMR spectrum of in bulk Leucine (Figure 3.23), the ^{15}N signal shows two main cross peaks at 1.1 and 8.7 ppm on the ^{1}H axis, the latter being due to the protons of the ammonium while the other signal corresponds to superimposition of most aliphatic protons - those of the C2 methine give a small shoulder at 4 ppm.

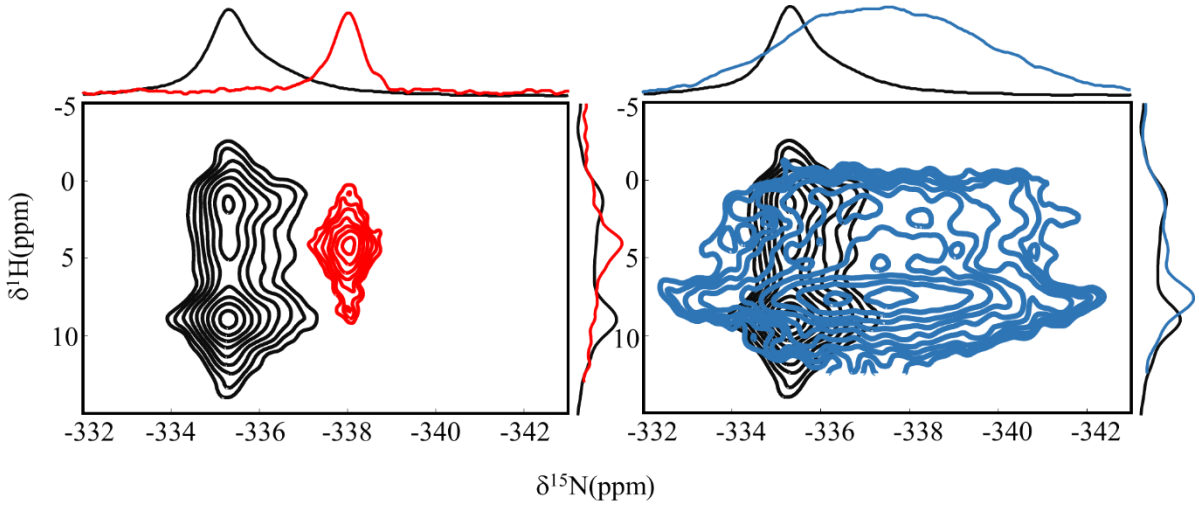

Figure 3.23. ^{1}H →^{15}N 2D-HETCOR MAS NMR spectra of bulk [1-^{13}C,^{15}N] L-Leucine (black), and 3%[1-^{13}C,^{15}N] Leu/SiO_2 after nitrogen drying (ND, red) and after vacuum drying (VD, blue)

For Leu/SiO_2 ND, the main cross peak is around 4 ppm in the ^{1}H direction. The near absence of a correlation that could be assigned to the ammonium protons is surprising at first sight but is in line with reported behavior for ammonium groups interacting with water. Indeed, Iwahara *et al*[266] showed that the characterization of the NH_3^+ group of aqueous proteins is rather challenging in aqueous solution due to a rapid proton exchange with water. Alternatively, or concomitantly, the ^{15}N-^{1}H interaction could be averaged out due to a high rotational mobility of the NH_3^+ as suggested by Ben Shir *et al*.[267] In any case, the behavior of the ammonium group

of Leucine in the nitrogen-dried sample is quite similar to that of an amino acid in aqueous solution.

After vacuum drying, the cross peak at 4 ppm decreases in intensity, as already observed for the $^{1}H \rightarrow {}^{13}C$ 2D-HETCOR. This is of course correlated to the smaller amount of water at the interface, but it must be underlined that the effect is stronger with ^{15}N than with ^{13}C: dehydration affects the environment of the ammonium group more than that of the carboxylate group. Moreover, the cross peak in the 7.5 to 8.8 ppm region corresponding to NH_3^+ protons reappears, indicating a lesser mobility of this moiety as well as limited proton exchange upon thorough drying. Both observations could be explained by the inception of a stronger interaction between the ammonium and the surface groups of silica.

III.4 Computational approach

Models containing the amino acid Leucine adsorbed on a silica surface are now presented. Anhydrous systems were prepared containing no trace of water molecules, but also microsolvated models in which 5 water molecules were added. The water molecules were placed surrounding the functional groups of Leucine (carboxylic acid $–COO^-$ and the ammonium $–NH_3^+$), and some were also placed along the side chain carbon skeleton.
Note that in both of the cases, the initial Leucine used before optimization was in the zwitterionic form.

Globally 29 different models were run, with 14 of them being anhydrous (containing no water) while the rest (15 models) are microsolvated (containing water as discrete molecules).

III.4.1 Adsorption Energies and molecular configurations

III.4.1.1 Anhydrous Models

For adsorbed Leucine, several models were investigated starting from different initial adsorption conformations and their geometry was optimized until a local energy minimum was reached. One Leucine molecule was placed in interaction with the surface sites mentioned in the description of the silica model (Chapter II; terminal, vicinal (Vic), and “silanols nest”, i.e. Gem + Vic). The amino acid was originally in the zwitterionic form, which constitutes a logical choice for comparison with an experimental setup where Leucine was deposited from an aqueous solution. The starting configurations were chosen with either the carboxylate or ammonium moieties, or both, interacting with the surface sites. Attempts to force the interaction of the hydrophobic side chain with the surface did not result in convergence upon optimization, and therefore these models were not considered any further. In this way, 12 different models were created, that are presented in Figure 3.24 and identified with a capital letter from A to L.

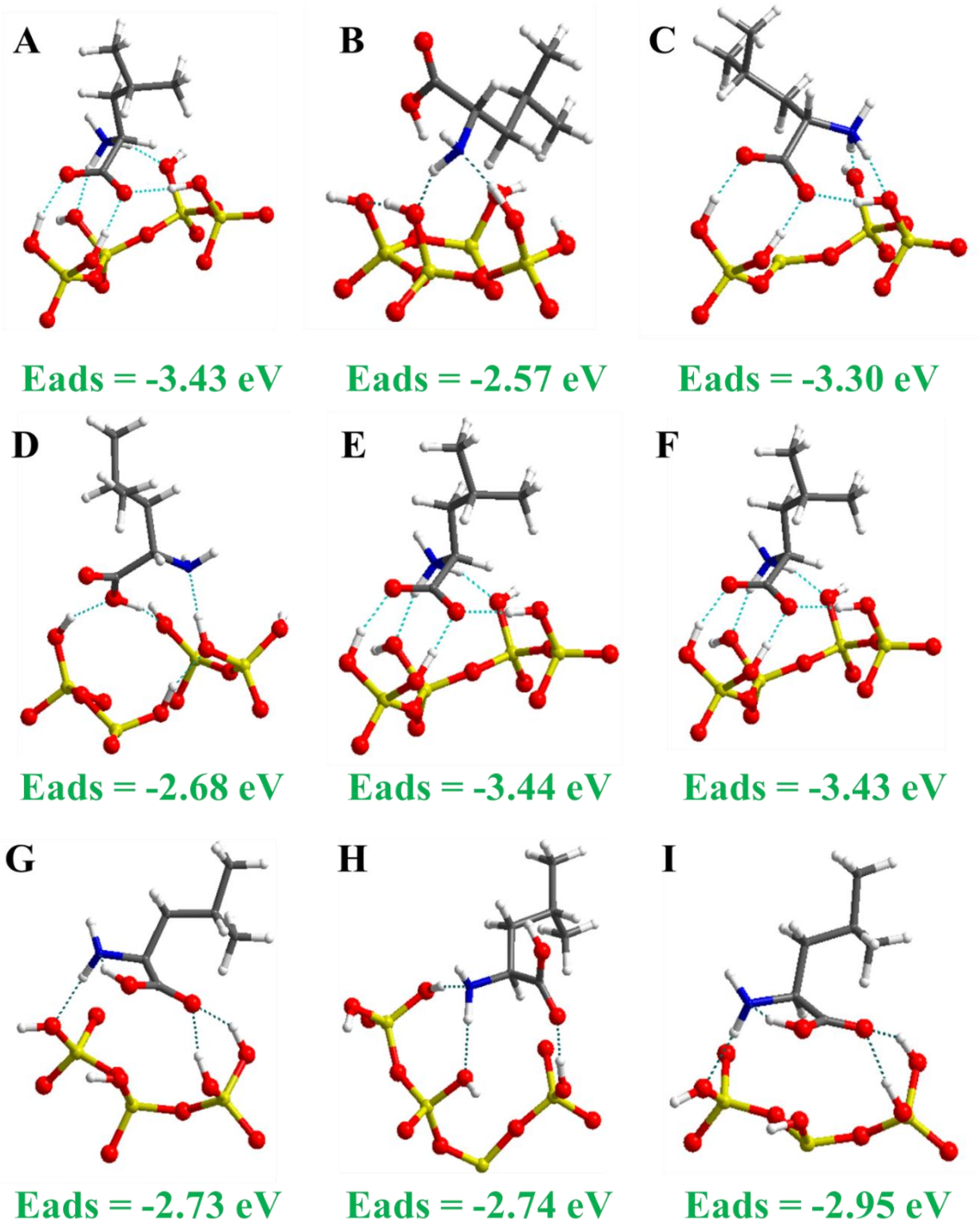
A
B
C
Eads = -3.43 eV
Eads = -2.57 eV
Eads = -3.30 eV
D
E
F
Eads = -2.68 eV
Eads = -3.44 eV
Eads = -3.43 eV
G
H
I
Eads = -2.73 eV
Eads = -2.74 eV
Eads = -2.95 eV

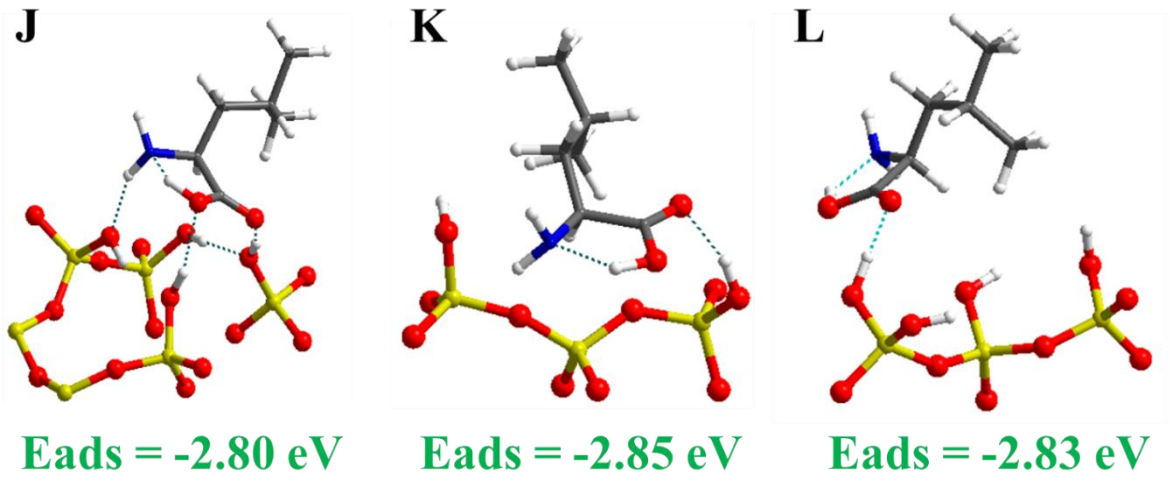

Figure 3.24. Anhydrous models with their E_{ads} (Energy of adsorption) after optimization under static property (O in red, Si in yellow, C in grey, N in blue and H in white)

For these anhydrous models, significant rearrangements sometimes occurred during the optimization. The carboxylic/carboxylate and the ammonium/amine groups systematically interacted with silanols through hydrogen bonding, stabilizing the adsorbed form. One first remark is that only hydrogen bonds were observed to form upon optimization, at the exclusion of any covalent bonds; nor was there any net proton transfer between the amino acid and the silica surface. Silanol groups may act as H-bond donors or H-bond acceptors towards Leucine functional groups, or both simultaneously.

Quite expectedly, the adsorption energy grew more negative when the number of H-bonds between the AA and the surface increased. The reader may follow this trend by looking e.g. at models B, I and A in Figure 3.24, that respectively have 2, 3 and 5 H-bonds. Adsorption energies become more favorable as more H-bonds are formed (-2.57, -2.95 eV, and -3.43 eV, respectively), with an almost linear trend. But a significant difference in behavior was observed when the number of H-bonds passed from 3 to 5. In models where Leucine formed at most 3 hydrogen bonds with the surface groups, it was found to isomerize the neutral form (N, with –COOH and $–NH_2$) after optimization, as opposed to the zwitterionic form (Z, with $–COO^-$ and $–NH_3^+$). In contrast, in models where 5 H-bonds were formed,• the zwitterionic form was maintained. This is illustrated in Figure 3.25**,** comparing the starting and optimized configurations for model A and I. Because the Z form prevails for the first one (model A) and the latter (model I) converts to the neutral form upon energy optimization, no significant energy barrier must exist between the two: proton transfer seems not to be an activated process. In the case of (trihydrated) glycine, it was found[268] that isomerization from the zwitterion to the neutral form by direct proton transfer had a small energy barrier, of 4 to 5 kcal/mol (about 20 kJ/mol).

• No models were observed with 4 H-bonds

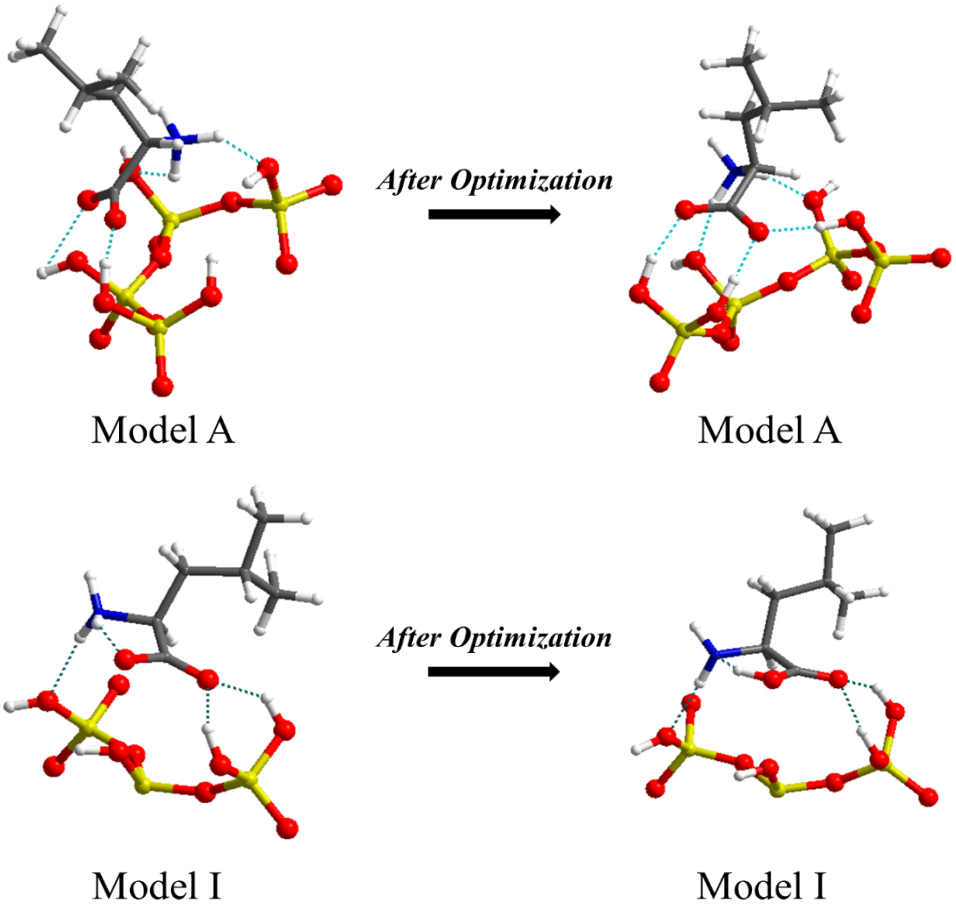

Figure 3.25. Comparison of the starting and optimized configurations of Leu/SiO_2 in anhydrous model A and I. Notice the isomerization from zwitterionic to neutral for model I

These results may be compared with those of Rimola *et al*. for glycine on eddingtonite silica.[269] On this surface with scarce silanols, glycine without co-adsorbed H_2O established at most 3 H bonds with the surface, and remained neutral. On the other hand, with more than two H_2O molecules co-adsorbed, more extensive H-bonds networks were formed and the zwitterion became the most stable form.

In all the anhydrous models presented in Figure 3.24, the initial starting Leucine molecule was in zwitterionic form, and the majority converted to the neutral form, while only few were stabilized and remained zwitterionic: this is probably due to the surface silanol site on which Leucine was adsorbed. To confirm this observation, two extra models were designed with a Neutral [COOH; NH_2] molecule as starting point (Models M and N). In Model N, the carboxylic group was placed on the geminal group, and in model M on an isolated silanol.

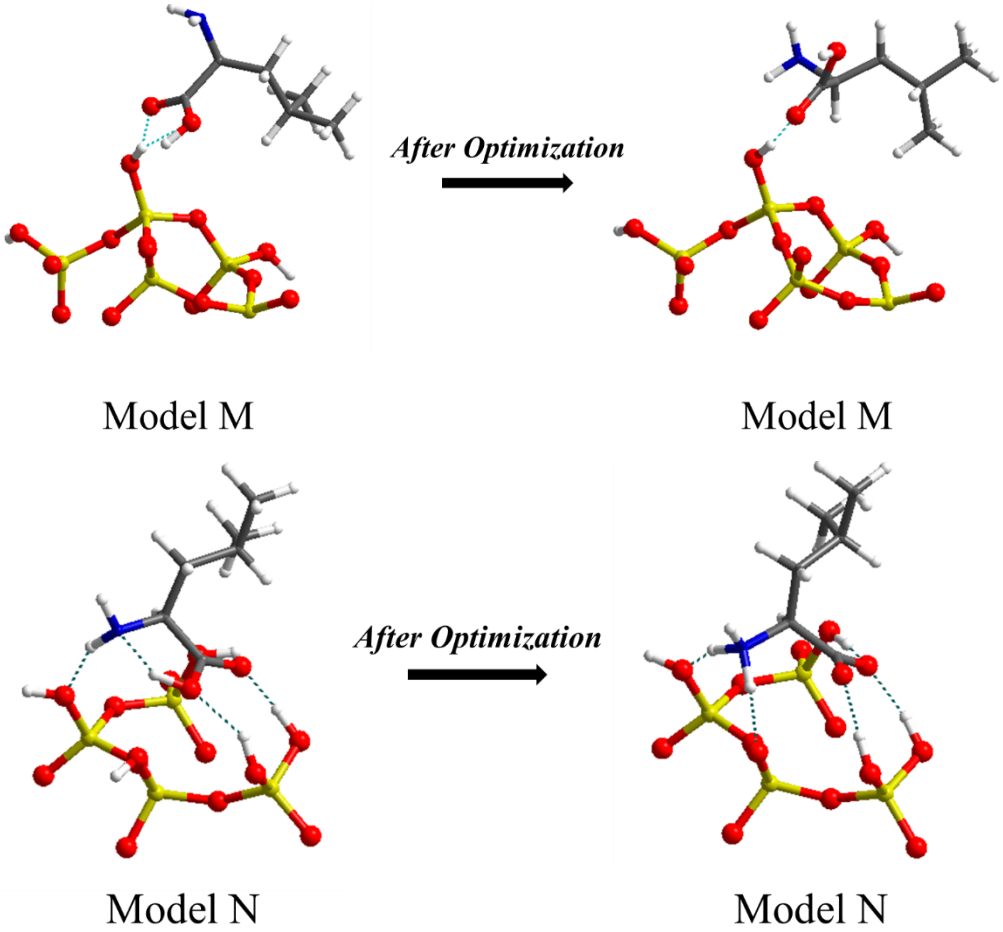

Figure 3.26. Comparing the starting and optimized configurations of Leu/SiO_2 in anhydrous models M and N. Notice the isomerization from neutral to zwitterionic in model N

Figure 3.26 illustrates the starting and optimized configurations for models M and N. When Leu was placed on the Isolated group of the Silica surface (model M), the molecule stayed neutral with an adsorption energy of -2.3 eV (again close to the activation energies obtained for most of the neutral models shown in Figure 3.24). On the other hand, in optimized Model N, Leu changes to zwitterionic with an adsorption energy comparable to models A, C, E and F (~ E_{ads} = -3.4 eV) shown above. This clearly indicates that the geminal group on the surface provides a stabilizing surface site for the Z form of Leu. We may also notice that while the initial neutral form in model N had an internal H-bond (COOH---NH_2), after isomerization to the zwitterion it did *not* contain the corresponding (COO^----H_3N^+) internal bond as both the ammonium and the carboxylate preferred to interact with the silica surface.

III.4.1.2 Microsolvated Models

The next step was to construct microsolvated Leucine models by adding water molecules to the systems previously studied (or devising new ones). In most of our models, we chose to introduce 5 water molecules per Leu. This number was compatible with the amount of water strongly held in vacuum-dried Leu/SiO_2 samples (at least 3 H_2O per Leucine at saturation

according to the data in Figure 3.7). The different hydrated models are listed in Figure 3.27 and labelled from A' to O'.

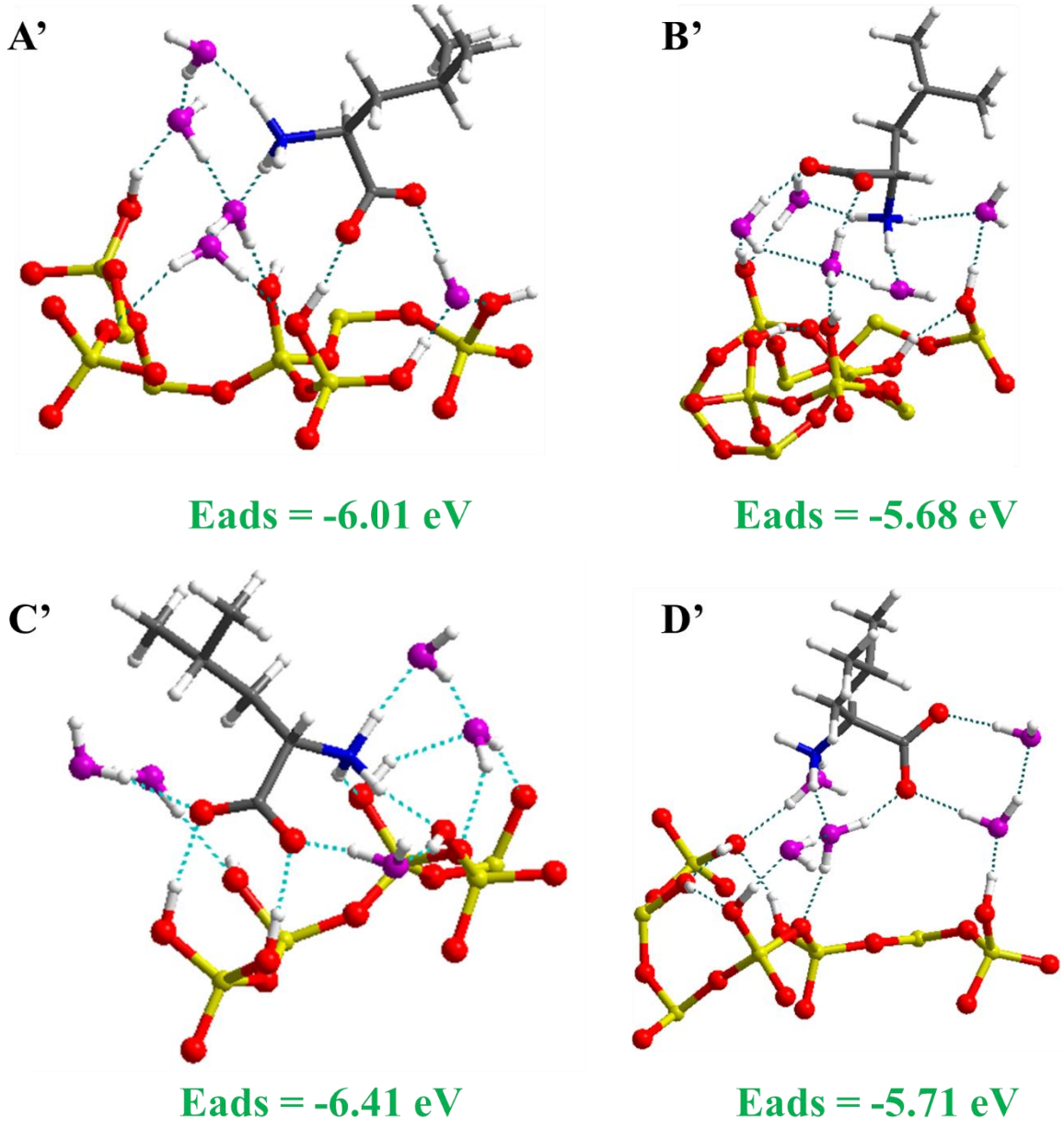

E’

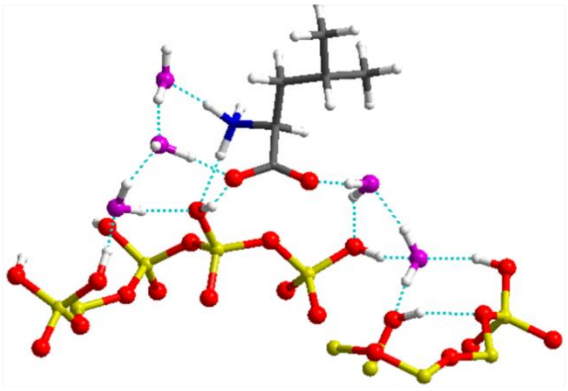

Eads = -6.08 eV

F’

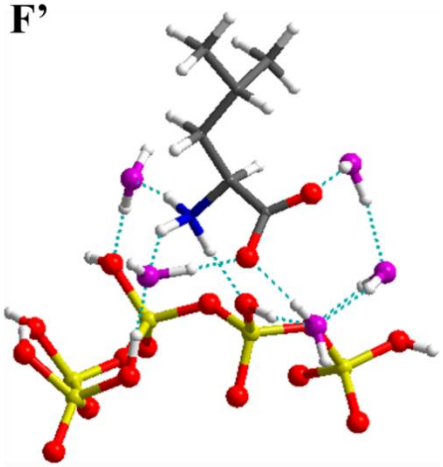

Eads = -5.68 eV

G’

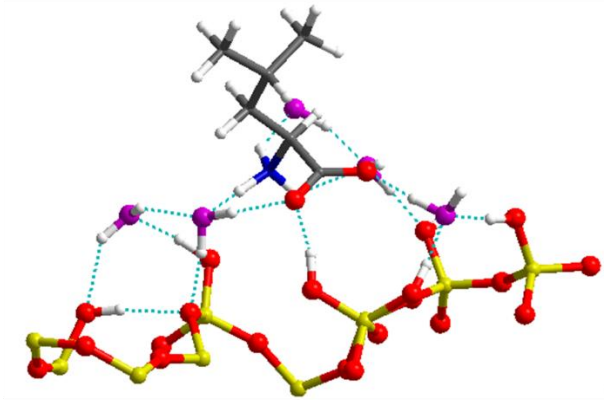

Eads = -5.82 eV

H’

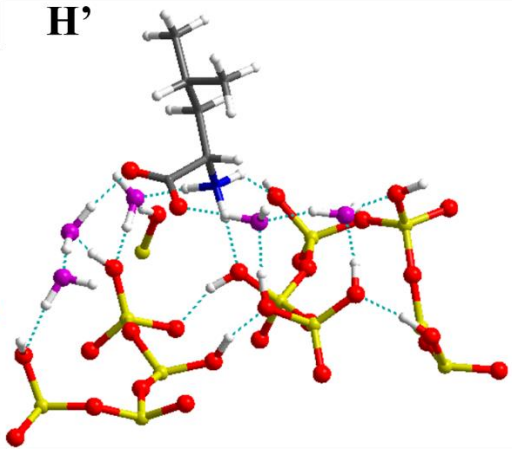

Eads = -6.60 eV

I’

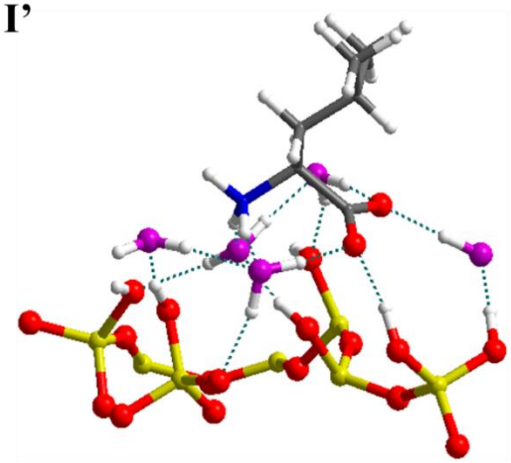

Eads = -6.65 eV

J’

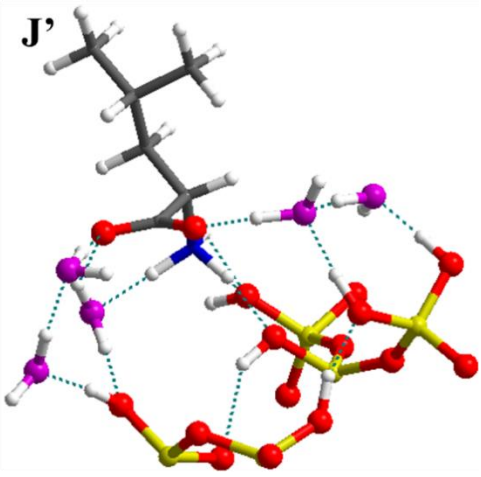

Eads = -6.26 eV

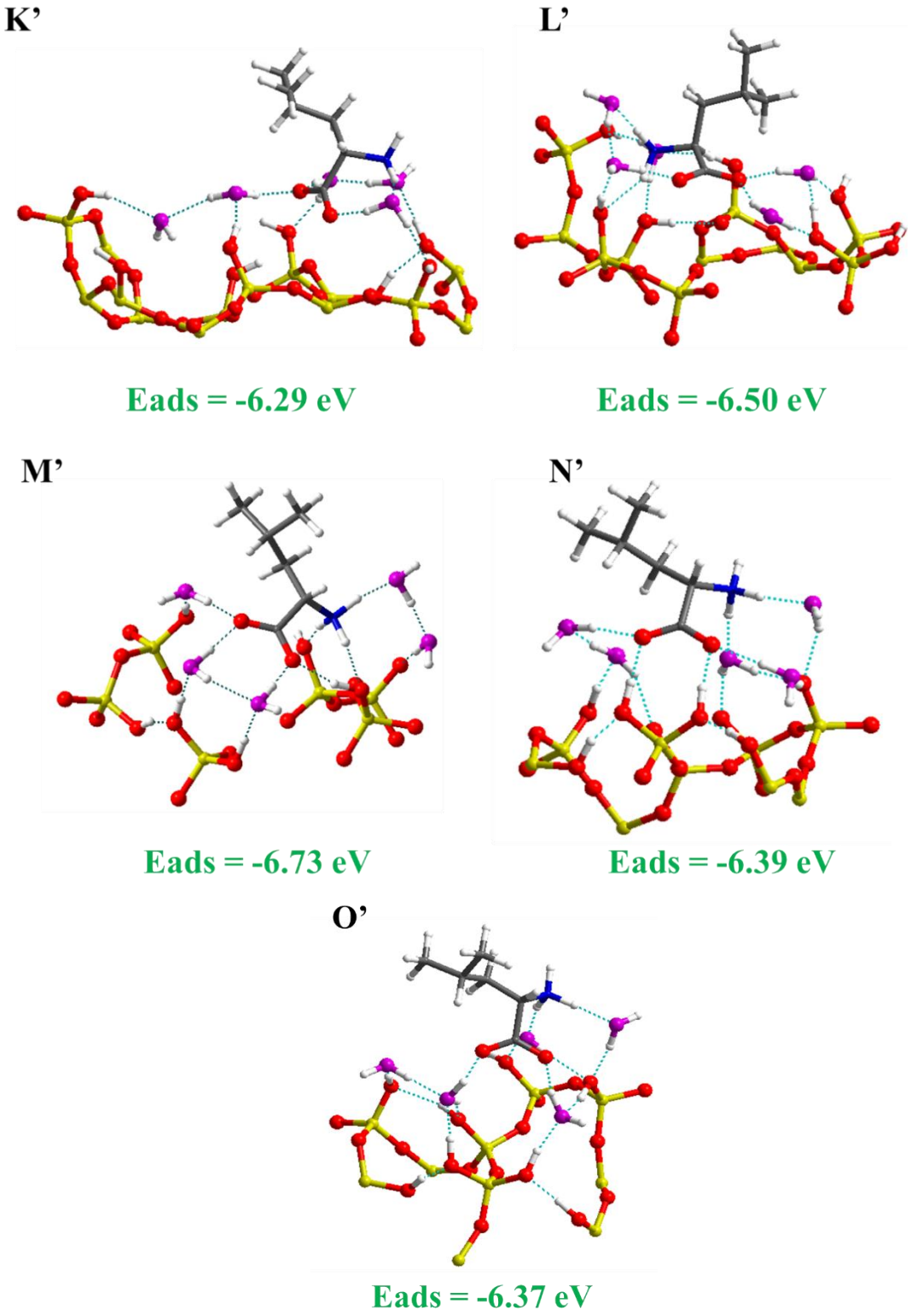

Figure 3.27. 15 microsolvated models (5 water molecules) with their E_{ads} (Energy of adsorption) after static optimization ((O of silica in red, O of water in purple, Si in yellow, C in grey, N in blue and H in white)

Our methodology for constructing the hydrated models was to separate the Leucine from the surface by breaking the H-bonds it had established in the unhydrated state, and then insert one bridging water between the two previously H-bonded partners for each H-bond. The

preferential location of water molecules between the amino acid functional group and the silanols groups is in line with previously published models,[269,270] although divergent results have been reported regarding the thermodynamic favorability of such bridging positions. After an initial [Leu-$(H_2O)_n$-surface] H-bonded lattice was formed in this way, the remaining water molecule(s) were left free to interact with it. It was found that optimization did not cause significant changes in the H-bonding connectivities, and therefore we created additional models that did not systematically have water in bridging positions, in order to check the validity of the initial assumption.

As for the anhydrous models, we only observed H-bonding interactions after optimization (no covalent bonds), and net proton transfers between the amino acid and the surface did not occur. In the microsolvated models, the Leucine molecule always remains in its zwitterionic form after geometry relaxation. Each water molecule is involved in 2 to 4 hydrogen bonds, with the surface as well as with the Leucine molecule.

i. Direct interaction with the surface vs. bridging water

Figure 3.28 compares the adsorption energies in models that differ through the bridging/non-bridging position of water. Five H_2O molecules are present in each case, but the interaction of the Leucine functional groups (carboxylate and ammonium) with the silanols is either by direct bonding, or through a bridging H_2O (mediated). Three of the models are almost degenerate (within 8.5 kJ/mol ~ 0.1 eV), but one is definitely more stable (by about 32.6 kJ/mol ~ 0.3 eV), namely the one where the carboxylate is adsorbed on the surface through bridging waters, while the ammonium directly interacts with surface silanols (model M'). In contrast, regarding the $-COO^-$ moiety, it is not energetically advantageous to have it directly interacting with the surface; in fact, it causes a slight destabilization. This is interesting because it suggests that a decrease of the activity of water will selectively lead to a fixation of the adsorbed amino acid to the surface through the ammonium moiety; as we have seen in Chapter I (§ I.1.6 and I.4.6), this type of preferential interaction of $-NH_4^+$ with the silica surface has been claimed from different lines of evidence for several amino acids on silica.

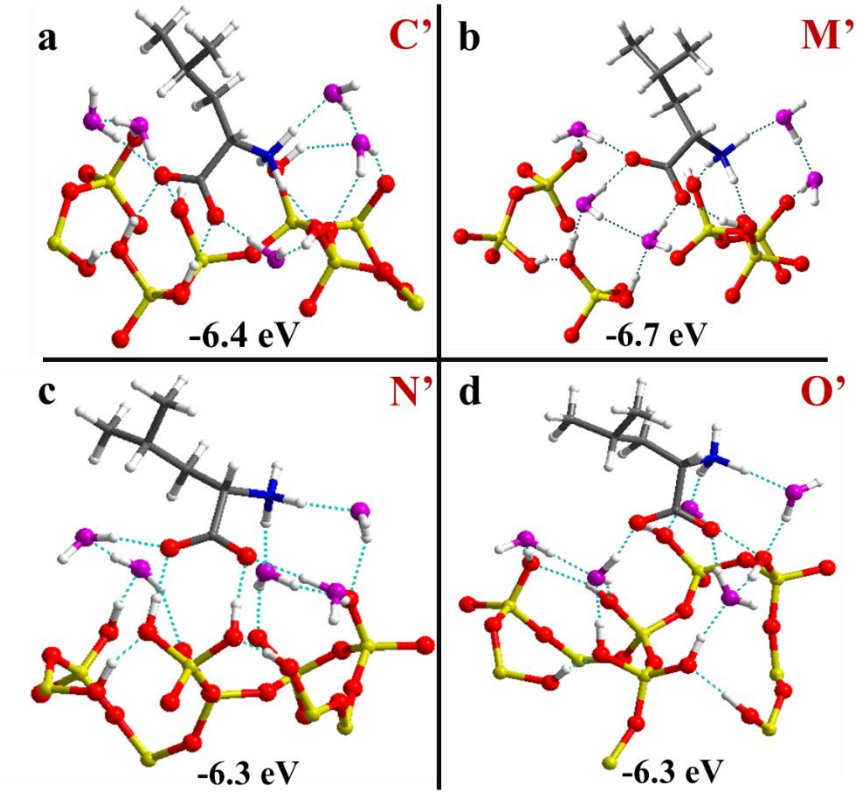

Figure 3.28. Possible configurations of water co-adsorbed with Leucine on the silica surface (5 water molecules per Leu): (a) direct interaction of both carboxylate and ammonium with the surface (all water molecules in non-bridging positions), (b) Carboxylate in interaction with the geminal silanols through two bridging waters, ammonium directly bonded to vicinal silanols, (c) carboxylate in direct interaction with the geminal silanols, ammonium with the vicinal silanols through two bridging waters, (d) both carboxylate and ammonium interacting through bridging water molecules

ii. Adsorption energies and varying the degree of hydration

Models with 5 water molecules per Leu show adsorption energies ranging between -5.6 and -6.7 eV (-540 to -646 kJ.mol^{-1}). These very negative values of course correspond to the adsorption not only of Leucine, but of all the water molecules. It is possible to compare the situation we tested here – co-adsorption with the formation of a three-partner Leu-$(H_2O)_n$-surface adduct – with the case of independent adsorption of each of the two partners, Leu and H_2O. In the latter case, i.e. for adsorption of water alone, experimental evidence and theoretical calculations are available. According to calorimetric data on the same type of silica, the adsorption enthalpy of water may reach values as negative as negative as -50 kJ.mol^{-1} per mole of water for low adsorbed amounts (< 0.8 nm^{-2}), but then levels off to -35 kJ.mol^{-1} per mole of water.[271] Adsorption energies may also be approached from molecular modeling. In fact, water adsorption was modeled on the same silica surface we used here,[200] yielding values of -46 to -50 kJ.mol^{-1} for isolated molecules - or -230 to -250 kJ per 5 moles – quite similar to the low-loading experimental data. In comparison, co-adsorption with Leucine of 5 water molecules resulted in additional stabilizations of -212 to -376 kJ.mol^{-1}, depending on the model. Thus, in some, but not all cases, co-adsorption induces a strong cooperative effect that stabilizes the 3-partner adduct.

In order to evaluate how far this additional stabilization extends, two models were created by adding 5 more water molecules, for a total of 10 per Leucine (see models G" and O" in Figure 3.29), an amount that would be in line with ND samples (see TG data in § III.2.2). Additional stabilizations amounted respectively to -69.5 kJ per mol H_2O (from G' to G"), and -52.1 kJ per mol H_2O (O' to O"). Thus, the 5 additional water molecules were still significantly stabilized in the first case with respect to the adsorption of water on silica, but not in the second one.

G'' and O'' were induced from G' and O' (Figure 3.27) respectively. The only difference between them is that:

- G' was adsorbed from the carboxylate, where one carboxylate oxygens is interacting with one Gem-OH group, and the other oxygen with the second Gem-OH but through a single water molecule acting as a bridge.

- O' was adsorbed from its two carboxylate oxygens to the two Gem-OH groups through 2 water molecules placed apart from one another.

Furthermore, G'' and O'' were obtained by simply adding 5 more water molecules onto G' and O' and performing a geometrical optimization making a system filled with 10 water molecules overall.

A consequence of these observations is that it should take significantly more energy to desorb water from the adduct (at least up to 5 H_2O per Leu), than from the bare surface of silica. Thus, dehydration of the adducts should take place at a temperature higher than the removal of ordinary physisorbed water. This, however, has never been conclusively evidenced from the TG data.

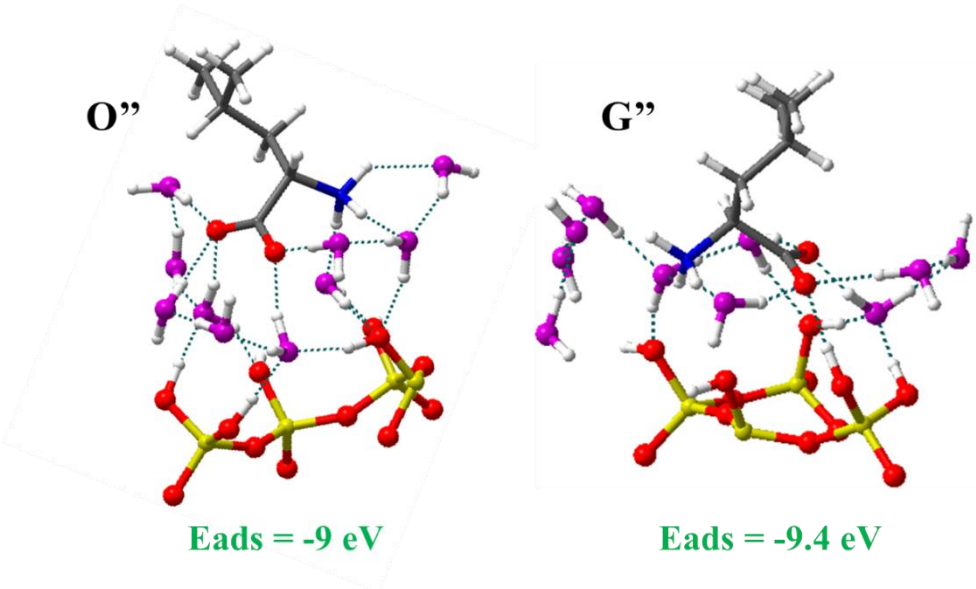

Figure 3.29. Possible configurations of water co-adsorbed with Leucine on the silica surface: (G'', O''), with 10 water molecules, Models G'' and O'' have the same initial arrangements as G' and O' and 5 water molecules were added near the interfacial interaction with carboxylate and geminal silanols and in bridging position between ammonium and vicinal silanols

iii. Effect of removing selected water molecules from the Leu/H_2O/SiO_2 adduct

Previously, we selected and discussed four models (C', M', N' and O') that differed in the bridging/non-bridging position of the microsolvating water molecules. A simple approach was applied in order to understand the difference in the adsorption energies among them, and especially the role of bridging water. We started from the optimized fully hydrated model and removed a single water molecule from it, keeping the other atoms in the same position. We then performed a single point calculation (during which no further optimization was carried out) of the new E_{ads} value. Figure 3.30 displays the water numbering scheme (in general, water molecules from 1 to 3 interact with the carboxylate group while 4 and 5 interact with the ammonium) and the energy changes for the removal of each water, which can be viewed as its contribution to the stability of the H-bonded network where ΔE_{ads} represents the energy difference between the initial hydrated E_{ads} (initial) containing 5 water molecules and the E_{ads} of each single point containing 4 water molecules (since each time 1 water molecule was removed).

$$\Delta Ea = Ea\ (Initial) - Ea\ (single\ point) \quad (38)$$

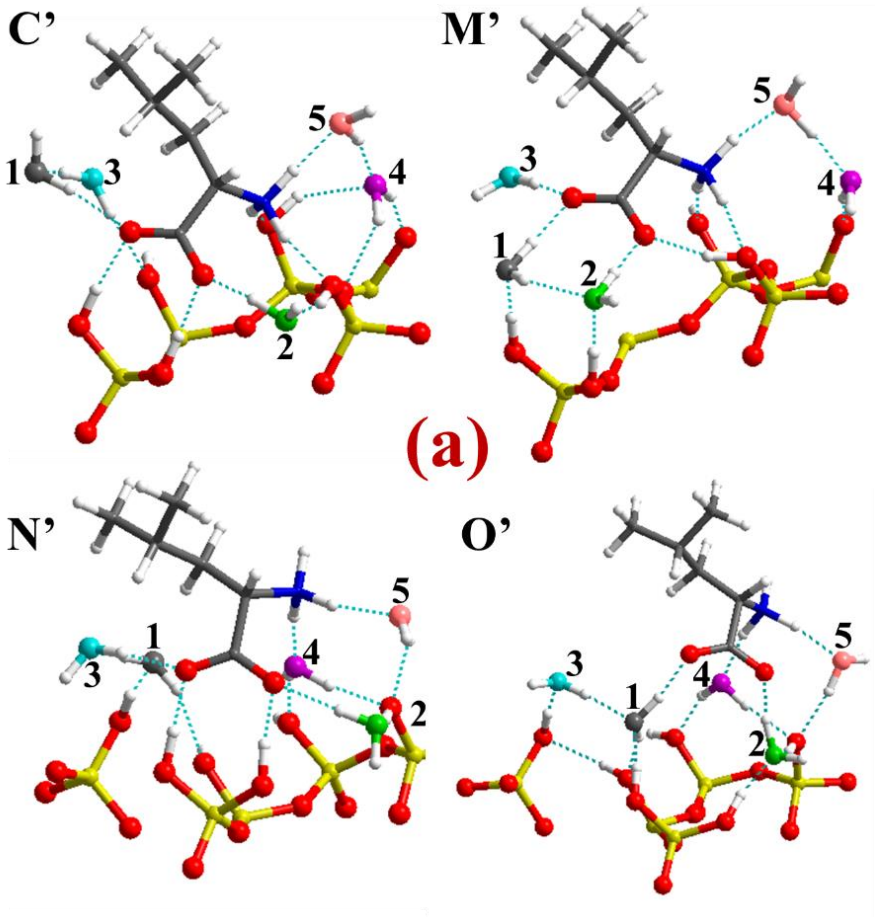

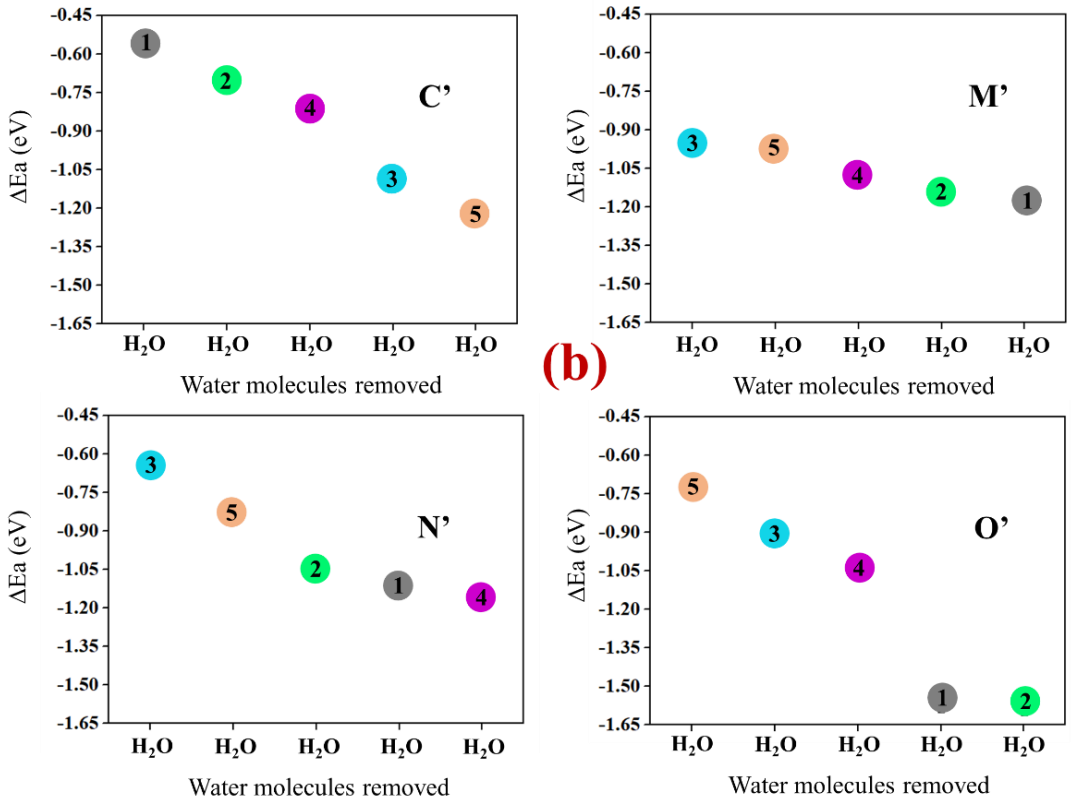

Figure 3.30. a) Models C', M', N' and O' with each water identified by numbering and specific coloring, (b) Changes in the adsorption energy of the system as a function of the water molecule removed

It might have been expected that the bridging waters would contribute more to the stability of the network than the other ones, since they are able to establish bonds with both Leu and the silanols. However, this is only obvious for water molecules that bridge the carboxylate terminal. Since the existence of this kind of bridging water brings extra stability to the system, there would be little tendency for the $-COO^-$ to lose them. In contrast, it would not be so unfavorable to lose the bridging water between the $-NH_3^+$ group and the surface, and the ammonium would be more prone to direct binding, in keeping with previous conclusions.

iv. Comparing Anhydrous and Microsolvated models

To further analyze the microsolvated models, they need to be compared with the anhydrous ones. It appears that some models that were less favored without water became highly favored when water was added. This may be explained by the fact that water interacts with the amino acid with less constraints than the surface itself, since surface silanol groups show specific type of conformations and orientations not always favorable to interact directly with Leucine functional groups. However, these constraints are relaxed when water is present.

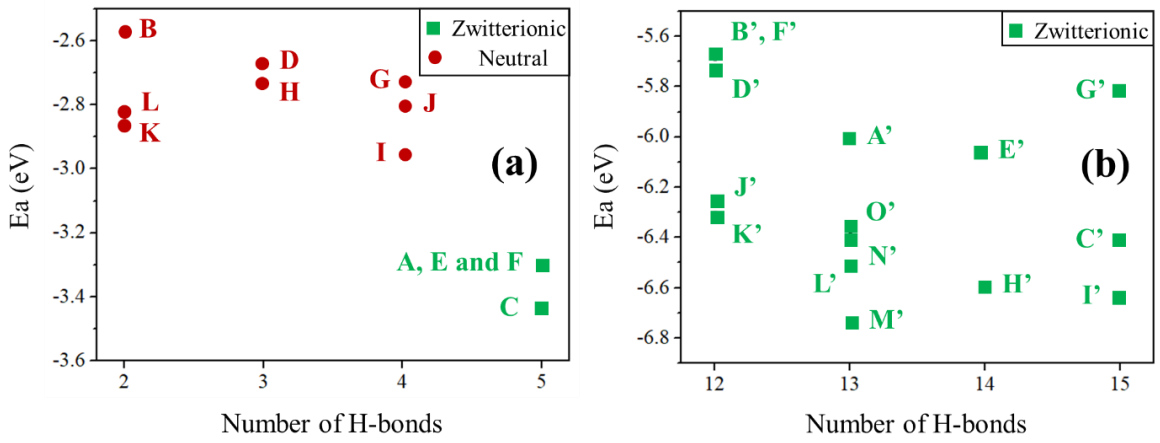

Figure 3.31. Adsorption energies as a function of the number of H bonds, (a) anhydrous models, (b) microsolvated models

Figure 3.31 shows the distribution of adsorption energies for the different models (both anhydrous and microsolvated), as a function of the number of H-bonds. Increased adsorption energies would be expected when the number of H-bonds increases, and this tendency is globally observed for the anhydrous models. For the microsolvated models, the correlation is much less clear, as the highest E_{ads} is found for a model with 13 H bonds, while some of those with 14 or 15 H-bonds have lower E_{ads} values. Globally, the linear correlation coefficient is only 0.37. Surely, microsolvated models are more complex: in addition to Leu-surface H-bonds, they also present water-surface, water-Leu, and water-water ones. Therefore, a naïve approach to estimate adsorption energies ("counting the bonds") is not sufficient, and more complex structural features must be taken into account: for the case of $Gly(H_2O)_n$ clusters, the consequences of different H-bonding topologies have recently been studied in detail by Marx *et al.*[272]

III.4.2 Calculation of NMR chemical shifts values

^{13}C and ^{15}N chemical shift calculations were performed on all 29 models of Leu/SiO_2. Figure 3.32 compares the calculated values with the experimental spectra, on a 2D diagram with the ^{13}C and ^{15}N spectra shown on the x and y axes.

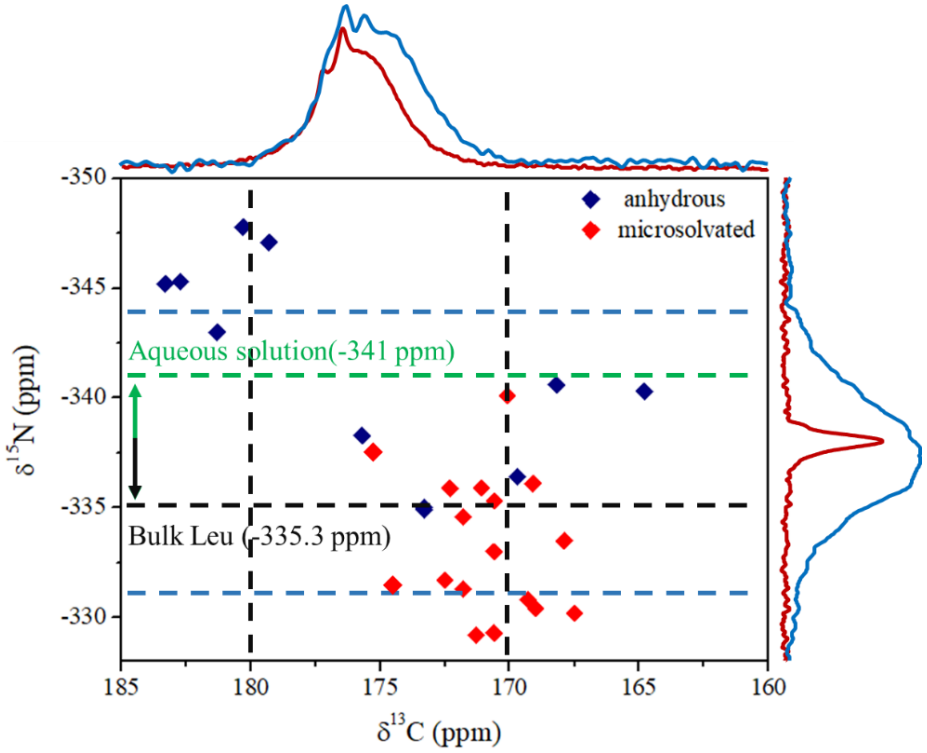

Figure 3.32. 2D map correlating ^{13}C and ^{15}N spectra of the adsorbed Leucine on silica, ND (red spectra) and VD (blue spectra), with the calculated ^{13}C and ^{15}N chemical shifts for the different adsorption configurations of Leucine (Blue points corresponding to anhydrous models, from A to L, and red points to microsolvated models, from A' to O', G'' and O'')

Beginning with the ^{13}C dimension for the N.D system, 4 models (G, H, I, J) show chemical shifts above 180 ppm and 8 models (B, C, D, A', D', K', L', O') below 170 ppm, definitely outside the experimental range. They include most neutral forms of anhydrous Leucine, which therefore seem to be incompatible with the experiments. This is in agreement with the IR results that indicate a predominance of zwitterionic Leucine.

Considering the ^{15}N chemical shifts, for the N.D sample, the experimental spectrum is quite narrow and almost none of the calculated values fall close to it. This would confirm that in such water-rich samples, the ammonium groups are in an aqueous-like environment and not strongly bonded to the surface. Indeed, none of our theoretical models reproduce these conditions.

The experimental vacuum-dried system fits better with the theoretical results (Figure 3.32-V.D, range indicated by the dashed blue lines), in particular with part of the microsolvated models (red dots). This is in line with the presence of remaining water even after vacuum drying, as observed by TGA. Incidentally, the only anhydrous model (model A) that shows acceptable agreement with experimental chemical shifts exhibits strong bonding between the carboxylate and the geminal silanols that stabilizes the zwitterionic form.

Beyond ^{13}C and ^{15}N, calculated proton chemical shifts are also of some interest. In table 1 of the Annex, calculated values of proton chemical shifts are shown together with the H-bonding distances involving these protons. Figure 3.33 shows a) the chemical shifts of the water protons (H_2O) as a function of their hydrogen bonding distances to acceptor groups and (b) the chemical shifts of the silanol protons as a function of their hydrogen bonding distance. With one or two exceptions, water protons are never found at chemical shifts < 2.5 ppm. H-bonded silanol protons (Figure 3.33.b) fall at even higher δ values; they often establish strong H-bonds with bonding distances between 1.6 and 1.8 Å (or even shorter) correlated with important downfield shifts (up to 12 ppm). Finally, Figure 3.33.c) shows the chemical shifts of H-bonded ammonium protons in the Leucine molecules –they too can be strongly shifted by H-bonding.

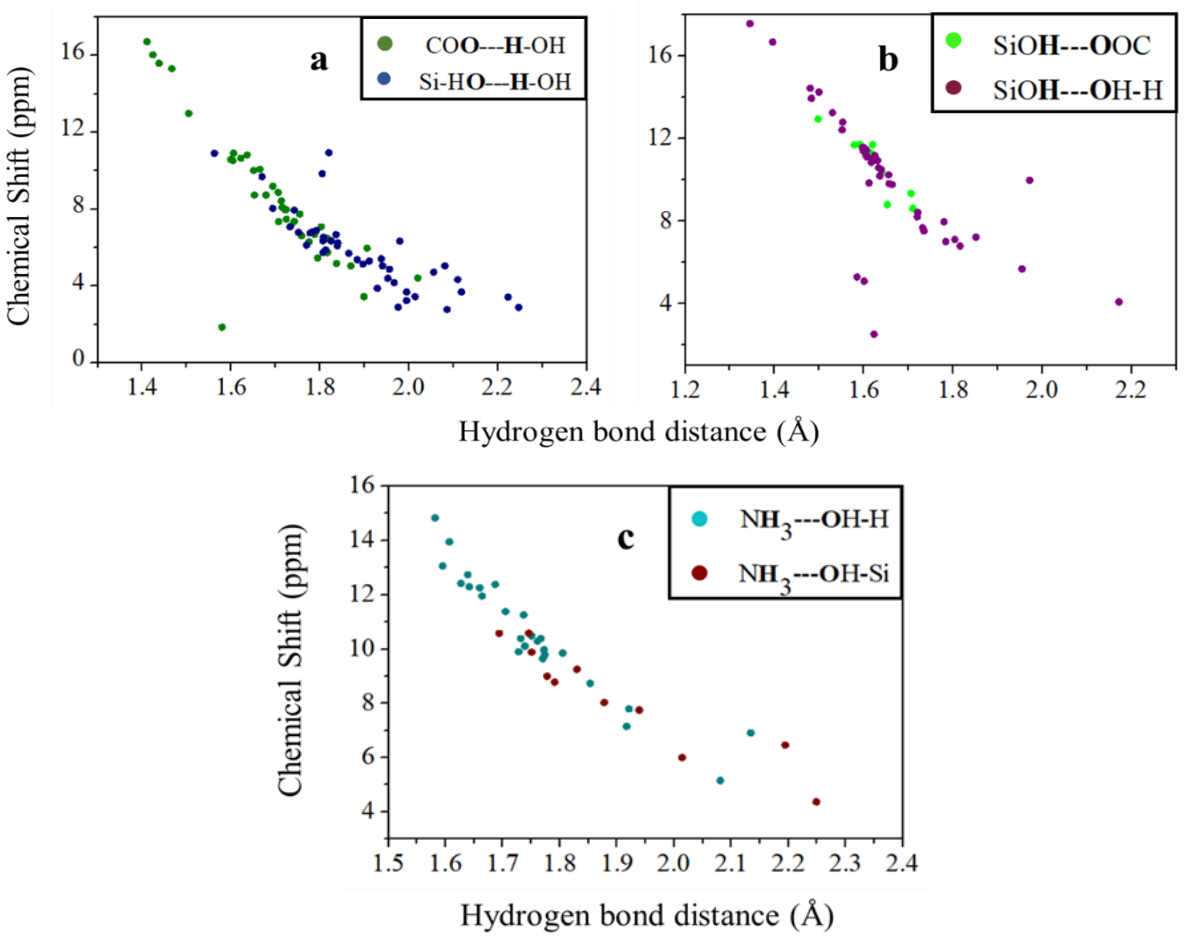

Figure 3.33. calculated ^{1}H chemical shift values as a function of H-bond distances in models A' to O', a) Protons of water H-bonded to the carboxylate or the silica surface b) Protons of surface silanols H-bonded to the carboxylate or water c) Protons of ammonium H-bonded to the silica surface or water

For all three sets of data, the chemical shifts exhibit a strong correlation with the H-bonding distance (with only a few conspicuous outliers). The evolution is almost linear for short H bonds, while the slope decreases for the weakest H-bonds (high *D**H***---*A* distances). A very

similar dependence has been reported previously for different systems, underlining that $\delta_{iso}(^1H)$ is highly sensitive to hydrogen bonding.[273]

Unfortunately, the proton chemical shifts in experimental NMR spectra are hard to interpret due to strong signal overlap, not only between silanols and water, but also with Leucine protons. Figure 3.34 presents the chemical shifts values calculated for the protons of Leucine for microsolvated models (A' to O'). All protons of the aliphatic side chain (those on C2, C3 and C4) fall within the same narrow range between 0.7 and 2.0 ppm, in keeping with the observation of a single peak. The methine C2-H proton on the one hand, and the ammonium ones on the other hand, are found in clearly separate ranges, but they may overlap with water and silanols protons, respectively.

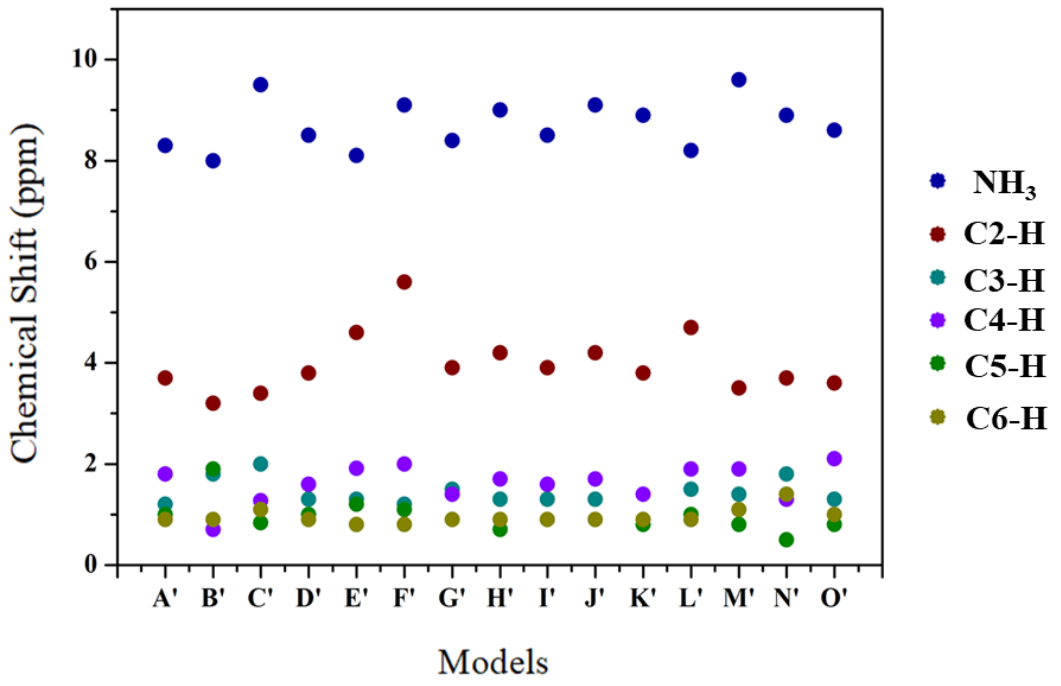

Figure 3.34. Calculated ^1H Chemical shift values of aliphatic protons for microsolvated models (from A' to O')

These results confirm the assignments we had proposed for the cross peaks of carboxylates in 2D $^1H \rightarrow {}^{13}C$ HETCOR CP-MAS NMR of N.D sample (Figure 3.21). The signal at 1.3 ppm can only correspond to coupling with aliphatic protons (on C3 to C6). Regarding the 4 ppm signal, it can be both C2-H and weakly H-bonded water superimposed: indeed, Figure 3.33.a shows around 4 ppm a rather concentrated set of points corresponding to water molecules with H---O distance between 1.9 and 2.25 Å (mainly Si**H**O---**H**$_2$O but also CO**O**$^-$---**H**$_2$O). Finally, the 8.8 ppm ^1H peak can correspond to proton of the ammonium group, but also to water strongly H-bonded to Leucine molecules.

The data in Figure 3.34 can also serve to exclude the existence of some particular configurations for adsorbed Leucine. Indeed, experimentally, there are no cross peaks for $\delta(^1H)$ above 9 ppm. Now, for models with direct SiO**H**---**C**OO$^-$ interactions, the silanols protons are generally found at chemical shifts higher than 8.8 and up to 12 ppm; thus, direct interaction of the carboxylates with the surface is not corroborated. In contrast, if the carboxylate interacts with water

molecules, COO---**H**OH with a distance around 1.7Å would give a proton chemical shift of about 8 ppm, so that the observed cross-peak at this value, previously interpreted as indicating a correlation with ammonium protons, may also contain a contribution of H-bonded (bridging) water.

In 2D ^{1}H-^{15}N HETCOR CP-MAS NMR of the VD sample (Figure 3.23), the ammonium peak mainly correlates with protons around 7.6 ppm that were supposed to be -NH_3^+ protons. Figure 3.33.c indicates that this value is more typical of ammonium protons H-bonded directly to silanols than H-bonded to water, as the latter are most often found at higher ppm values (in fact the calculated value is close to 7.6 ppm e.g. for configurations J' and M' where -NH_3^+ is in direct interaction with silanols). It will be recalled that in the ND sample, in opposition, the ammonium nitrogen only correlated to the protons of water.

In summary, first, the selected models, and among them especially the microsolvated models, show good consistency with the experimental results in terms of ^{13}C and ^{15}N chemical shifts as well as chemical shifts of the ammonium protons. Based on the observed chemical shifts in the carboxylate region, all neutral forms of the adsorbed Leucine can be excluded. In contrast, we obtained good agreement between the experimental data on the VD system and the ^{13}C and ^{15}N calculated values in microsolvated systems, strongly suggesting that VD systems consist in well-defined adducts involving zwitterionic Leucine solvated by a limited number of water molecules. Among microsolvated models, those with the -NH_3^+ directly H-bonded to the surface seem to give the best fit.

On the other hand, the experimental data for the ND systems did not correspond well to any of the investigated theoretical models. In fact, the NMR data for these incompletely dried systems are more akin to those of Leucine in solution, as observed by solution-NMR spectroscopy of aqueous Leucine. In the ND systems, ammonium groups are in an aqueous-like environment and only correlate with the protons of water.

III.4.3 Rationalizing ^{13}C Chemical shifts of carboxylates

Focusing on microsolvated systems (A' to O'), one can wonder why the carboxylate moiety (C_1) chemical shift is significantly different from the experimental ones in some cases. In general, the precision of carbon chemical shift calculations is better than that of nitrogen chemical shifts as shown by Dračínský *et al.*[274] Figure 3.35 summarizes the distribution of calculated carboxylate (C_1) ^{13}C chemical shifts obtained for all the models we tested.

Overall, in adsorbed Leucine models, the calculated chemical shifts of the carboxylates were lower than those in the bulk (178.2 and 178.3 ppm), in agreement with experimental data. The chemical shifts of ammonium ^{15}N were also lower than for bulk Leucine (-332.8 ppm). All carboxylate chemical shifts fall between 167 ppm and 173 ppm, with a high density between 170 and 172 ppm. For nitrogen, many results are concentrated in two regions, between -330 and -332 ppm (as for bulk Leucine) and between -334 and -336 ppm.

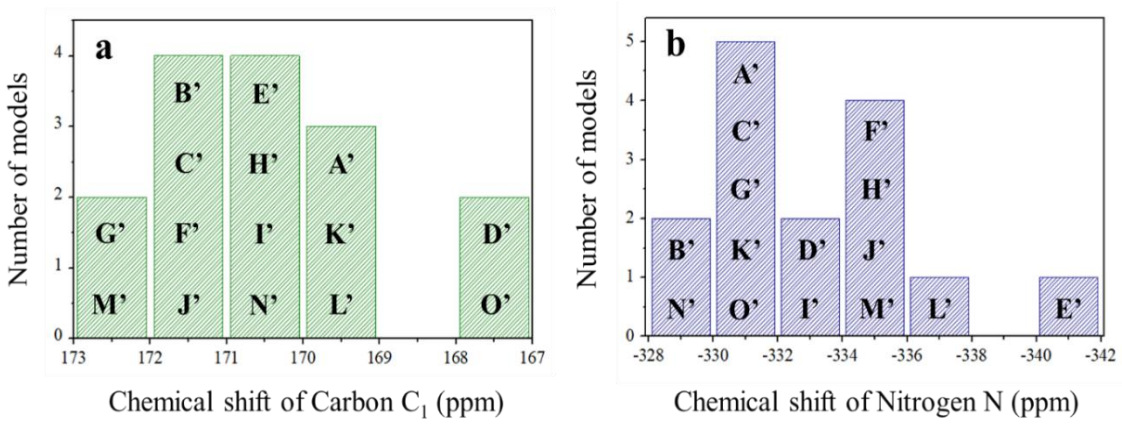

Figure 3.35. Histograms showing the distribution of calculated a) ^{13}C and b) ^{15}N chemical shifts in all microsolvated models

Several parameters could be responsible for carboxylate ^{13}C chemical shift (CS) variations in the different models: *(i)* the number of hydrogen bonds with the carboxylate moiety, *(ii)* C---O distances *(iii)* the number of hydrogen bonds involving the $-NH_3^+$ moiety. All these criteria are summarized in Figure 3.36.

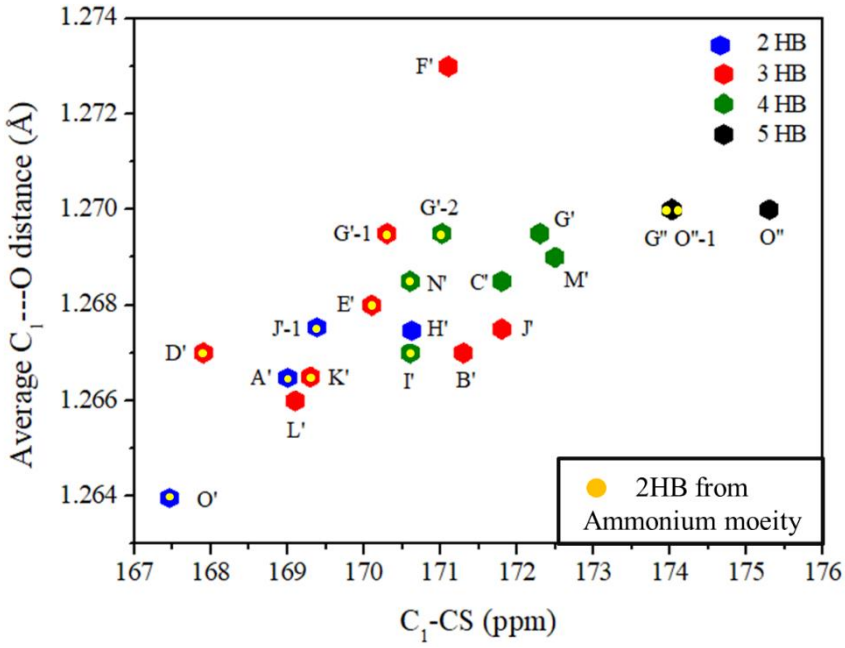

Figure 3.36. Correlation of the carboxylate C1 chemical shift values, the average C1---O distance and the number of hydrogen bonds to the carboxylate moiety (indicated by color codes), taking into account the bonding state of the amine (NH_3^+) moiety: without yellow points, the 3 protons are involved in a NH---O bond, with a yellow point only 2 protons are involved in a NH---O bond)

(i) The number of hydrogen bonds to the carboxylate groups in models A' to O' can be 2, 3 or 4. Models in which the carboxylate oxygens are involved in only 2 hydrogen bonds (blue points on Figure 3.36) show low chemical shifts (below 171 ppm) and the CS increases with the number of H-bonds: between 168 and 172 ppm for 3 bonds (red points), between 170.5 and 172.7 ppm for 4 bonds (green points). This is not unexpected based on the withdrawing effect of H-bonds on the electron density of the acceptor group. To confirm this tendency, five additional water molecules were added to two hydrated models: G' with 4 H-bonds having the most deshielded value (172.5 ppm), and O' with 2 H-bonds having the most shielded one (167.5 ppm). The two new systems obtained upon optimization, designated as G'' and O'' (see Figure 3.29 and black points on Figure 3.36) do indeed have 5 hydrogen bonds to their carboxylate moiety and show an increase in CS, moderate for G'' (+ 1.5 ppm for 1 additional H bond) and important for O" (+ 7.8 ppm for 3 additional H bonds).

Nonetheless, the strong overlap between models with different numbers of H-bonds indicates that this criterion is not sufficient to explain chemical shifts variations.

(ii) Figure 3.36 also seems to show that C_1 chemical shifts decrease with decreasing C---O distance: compare C', M' and G' among 4-HB models, or L', B', J' among 3-HB models. On the other hand, among 4-HB systems, models C' and N' have similar C---O distance but different CS, and the same is true for B' and D' among 3-HB models. Thus, some variations are still unaccounted for when taking *i)* and *ii)* into account, and we must look for additional criteria.

(iii) Models D' and B' have a 3.4 ppm CS difference while they do not differ according to criteria *i)* or *ii)*. Indeed, the most conspicuous difference between them lies in the H-bonding of the $–NH_3^+$ group: only two donor bonds from $–NH_3^+$ in the former (low CS), but three in the latter (high CS). Similarly, when comparing C' and N', there are only two $–NH_3^+$ donor bonds in N' (low CS) against 3 in C' (high CS). Thus, it seems that the higher the number of H-bonds donated by the $–NH_3^+$ group, the higher the chemical shift of the C_1 carbon. To confirm this hypothesis, one water molecule bonded to NH_3 group was deliberately removed from models O", G' and J' and NMR parameters were re-calculated, without performing any optimization to avoid change in H-bonding or in geometry. Removing one water molecule in this way ended up with systems that are microsolvated with 9, 4 and 4 water molecules respectively. As shown in Figure 3.36, the ^{13}C CS value of C_1 in these new models (denoted O"-1, G'-1 and J'-1 and represented in Figure 1 of the Annex is systematically smaller (NB: in model G'-1, the water molecule removed was also bonded to the carboxylate, so that two effects cooperate to decrease the CS). The existence of such long-distance effects on the chemical shifts has been observed e.g. for ammonium deprotonation of amino acids in solution[275]. Our data seem to indicate that even the H-bonding state of the ammonium can have a measurable influence on the chemical shift of C_1. This illustrates the potential of solid-state NMR as a tool for structure determination, even if the interpretation of data is not always straightforward. A similar analysis might be attempted for the side chain carbons.

III.5 Conclusions on the Leu/SiO_2 system

The first general conclusion on Leucine-silica interaction can be formulated in a simple way: water matters. Different drying methods lead to varying hydration states, that induce different Leucine speciations.

- Drying under inert gas flow at room pressure (ND) leads to still strongly hydrated samples. While broad NMR peaks indicate decreased mobility and exchange and significant heterogeneity of the local environment, other features (resolution of C4 and C5, C6 signals, ammonium mobility…) are comparable to those of Leucine in solution. The state of ND Leucine could be seen as that of a supported solution.

- Drying under vacuum (VD) causes a significant decrease of the residual water amount. Quantification by TG suggests that in this state, each Leucine molecule still retains a limited number of water molecules (of the order of 3 to 5 H_2O per Leu). This is corroborated by comparison of experimentally observed ^{13}C and ^{15}N chemical shifts with values calculated for microsolvated models on the one hand (Leucine co-adsorbed with a limited number of waters), anhydrous ones on the other hand (Leucine interacting only with surface silanols groups). Most of the models giving a good fit belong to the hydrated set. From an energetic point of view, co-adsorption of a water molecule with Leucine has a more negative $\Delta G°$ than its direct adsorption of it on the silica surface. The state of VD Leucine would then be an ensemble of 3-member surface adducts Leu.$(H_2O)_n$.(surface site), held together by a lattice of rather strong Hydrogen bonds.

A second conclusion regarding Leucine speciation is that, in samples dried without thermal activation, it is a zwitterion (as in aqueous solution) rather than a neutral form – in other words, it possesses a negative carboxylate as well as a positive ammonium group. This is strongly supported by IR data, as well as by the comparison of experimental and calculated chemical shifts – all among the models giving a good fit, even the anhydrous ones, have zwitterionic Leu. The adsorbed amino acid in this state should not be very reactive since the nucleophilic group present in the neutral form ($-NH_2$) is deactivated by protonation.

There are some hints of more specific information regarding the molecular structure of the (VD) adsorbed Leucine adducts. From theoretical calculations, models that have NH_3^+ directly interacting with the surface are definitely stabilized energetically. From experimental results, the observation of $\{^1H\text{-}^{15}N\}$ correlations involving ammonium protons indicate that this group has restricted mobility, as compared with ND samples, possibly due to the inception of a specific interaction with the surface. Also, the position of these ammonium protons on the ^1H chemical shift scale is more compatible with direct ammonium to silanols H-bonding, and IR indicates that the ammonium is more modified by adsorption than the carboxylate. Conversely, for the carboxylate moiety, the same criteria point instead toward an indirect interaction involving a carboxylate$\cdots H_2O\cdots$surface bonding. Beyond these features, the broad character of the NMR signals (excluding the small, sharp signals due to residual bulk Leucine) indicates some structural variability in the surface adducts. Not every silanol will do as an adsorption site, since the saturation coverage in adsorbed Leucine is about 10 times lower than the silanols density (0.36 nm^{-2} as compared to 4 nm^{-2}), but still many somewhat different silanols groups will provide slightly different molecular environments.

Chapter IV: Investigation of Glutamic acid adsorption on Silica

IV.1 Introduction

In the previous chapter on Leucine (chapter III), we have shown the relevance of comparing experimental and theoretical results to get a picture of the adsorption configurations on a molecular level. Hydration level of the system was varied (ND or VD procedures) and found to play a significant role on the overall adsorption phenomena. In this Chapter, we intend to implement the same approach and techniques on Glutamic acid and to observe results that can forecast an understanding on the adsorbed forms of Glu on the silica surface. Therefore, in this chapter, Glutamic acid adsorbed on fumed silica nanoparticle (Aerosil-380) surface will be studied with the same characterization techniques as previously (XRD, TGA, IR and solid state NMR spectroscopy); the theoretical approach will also be used to identify the possible adsorption energies as well as the possible binding localities on the surface by designing several models. Calculation of NMR parameters will then allow to make a link between experimental and theoretical results.

In addition to the Aerosil-380, some exploratory results have been obtained on two other, mesoporous silica supports (MCM-41 and SBA-15). They will be briefly presented in the Annex part of the thesis.

Leucine and Glutamic acid differ from one another in the nature of the side chain. Leucine has a hydrophobic side chain, while Glutamic acid has an extra functional group (COOH) that imparts it with a hydrophilic character – and with an additional acidity constant. Glutamic acid and its acido-basic speciation are represented in Figure 4.1.

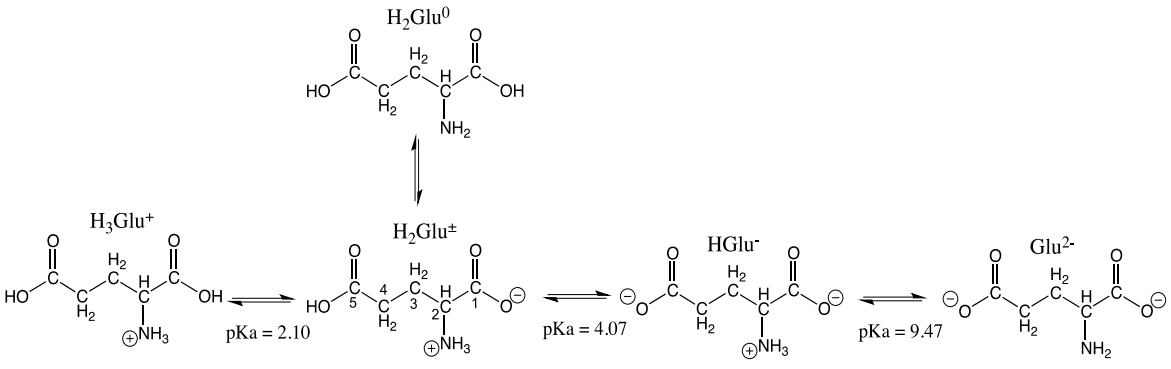

Figure 4.1. Glutamic acid and its acido-basic speciation

Like most amino acids, Glu is zwitterionic in solution. In Figure 4.1, the zwitterionic form $H_2Glu^{\pm}$ is represented together with its neutral isomer H_2Glu^0. Although the question has been less studied for Glu than for Gly or even Leu, it takes a minimum number of water molecules (3 in this case[276]) to stabilize the zwitterion with respect to the neutral form. In principle, the

anion $HGlu^-$ could also show protonation isomerism, but the question does not seem to have been addressed.

With respect to Leucine, Glutamic acid presents some additional challenges. The extra functional group in the side chain (-COOH) is able to interact with silica surface sites, like the COO^-, NH_3^+ of the amino acid moiety. This will increase the complexity of modeling its adsorption on silica. Glutamic acid is found to have two different crystalline polymorphs, noted as α and β forms, at room temperature. This is both a difficulty and an opportunity, since we have available two well-characterized structures that can serve as benchmarks for modeling and chemical shifts characterization.

Previous studies on Glu adsorption on silica mostly dealt with the effect of macroscopic parameters (pH, ion strength…) on adsorption isotherms[248], sometimes extracting thermodynamic constants for the adsorption phenomenon.[277,278] An exception is the work carried out at the LRS by Bouchoucha *et al*.[86] who applied many of the experimental techniques we used to this system. Among other conclusions, they found that Glutamic acid crystalizes at low loadings on surfaces hence making the characterization techniques challenging to selectively observe the signal of Glu adsorbed on the inorganic silica surface. This work will of course often be quoted here.

IV.2 Macroscopic Characterization

IV.2.1 X-ray Diffraction

Crystal polymorphism commonly occurs in organic compounds [279]. It is defined as the ability of a compound to crystallize in two or more distinct crystal structures, with the same chemical formula but different positions of atoms within the crystal lattice[280,281]. Due to variations in the physical properties of materials that exhibit polymorphism, e.g. stability, crystal habit, compressibility, density as well as dissolution rate and toxicity in drug context [282,283] it has gained considerable interest in certain fields such as bioavailability and drug efficacy in pharmaceutical compounds [284–287] and is therefore finely studied in pharmaceutical industry. Enhancement in process monitoring techniques are being developed in the drug industry to transform polymorph 'x' to polymorph 'y' with high rate or yield of transformation.[288]

The crystallization of polymorphs has a kinetic as well as a thermodynamic aspect. Transformations from the metastable to the stable polymorph takes place in a solvent by the process known as solution-mediated polymorphic transformation (SMPT). SMPT obeys the Ostwald "rule of stages", in other words, the metastable phase forms first; then dissolution of this phase is followed directly by the nucleation of the stable form (sometimes the surface of the metastable form acting as a favorable nucleation site). Finally, the growth and the persistence of the stable form takes place.[289,290]

L-Glu has two known polymorphs, the metastable α which has a granular or coarse pyramidal crystal form and the stable β form having a needle-like or leaflets form. The α form is one of the first crystalline structures of biomolecules to have been resolved by XRD [291]. It was studied by Hirokawa [246] and later by Lehmann et col.[243,245] Both structures are orthorhombic and belong to space group $P2_12_12_1$; the α form has a = 10.282, b = 8.779 and c = 7.068 Å, while the β form has a = 5.159(5) Å, b = 17.30(2) Å, c = 6.948(7) Å. [243,245,285,287,292] Controlling Glu

polymorphism requires extremely careful handling and precision. In the case of L-Glutamic acid, the metastable α form is rapidly converted to the β form upon direct contact with a solvent. Keeping in mind that the α form is not available commercially, the only way to synthesize it is through recrystallization from L-Glutamic acid solutions[293]. But this method requires the presence of an additive to promote the nucleation of the metastable form over the stable one. Indeed, in the presence of other amino acids (such as Alanine) and their co-existence with the L-Glu batch, it is relatively easy to obtain the α-form of L-Glu[294,295]. Consequently, several different approaches have been undertaken over the years to understand and locate the conditions for crystallization of the α form, as well as to elucidate the α–β transition.[296,297] Usually in industrial processes, it is crucial to obtain α-crystals of Glutamic acid and to prevent the transition to β-crystal.

Both forms of L-Glutamic acid (α and β) are related monotropically.[286] The XRD profiles of the two different polymorphs are significantly different, however,[176,298] and allow precise polymorph differentiation.

In this part, three different Glutamic acid samples were investigated:

- L-Glutamic acid purchased from Sigma-Aldrich.
- Three different isotopically enriched samples of L-Glutamic acid bought from CortecNet: [$^{13}C_5$, 1-^{15}N] enriched on all the atoms, [1-^{13}C] enriched only on the C1 carboxylic acid, [5-^{13}C] enriched on the C5 carboxylic acid of the side chain.
- α-Glu synthesized using the method previously published by Lai *et al* [299], who claimed that the α form nucleation is facilitated when a Glu solution is cooled down quickly from 80°C to 25°C or slightly lower. This results in the formation of pyramid-like crystals instead of needle-like ones (β phase).

Powder X-ray diffraction patterns of pure commercial L-Glutamic acid (non-enriched) and [$^{13}C_5$,1-^{15}N] L-Glu are shown in Figure 4.2.a. Commercial L- Glutamic acid is composed of the β-phase. The values of the Miller indices (hkl) were assigned from the following publications: Dhanasekaran et col.,[293] Srinivasan et col.,[300] Dharmayat et col., [298] Croker et col.,[301] Moshe et col.,[302] Quang et col.[303] and the crystal data for the α form has been reported by Bernal.[291]

The enriched sample is a mixture between the α and the β phases. It has already been reported that isotopically enriched samples give rise to a pattern where the metastable phase is found in equal amounts with the stable one. This may be due to the (unknown) procedure through which the enriched Glu was prepared, and/or to the presence of a minor impurity able to influence the crystallization process. After recrystallization was performed, Figure 4.2.c shows that only Bragg peaks of the α-phase appear: intense (0 0 2), (0 1 2), (2 1 1), (0 3 2) and (1 4 0) peaks are visible alongside the ones that were previously mentioned, which allows to say that recrystallization was successful and resulted in almost complete transformation from the β- to the α-form.

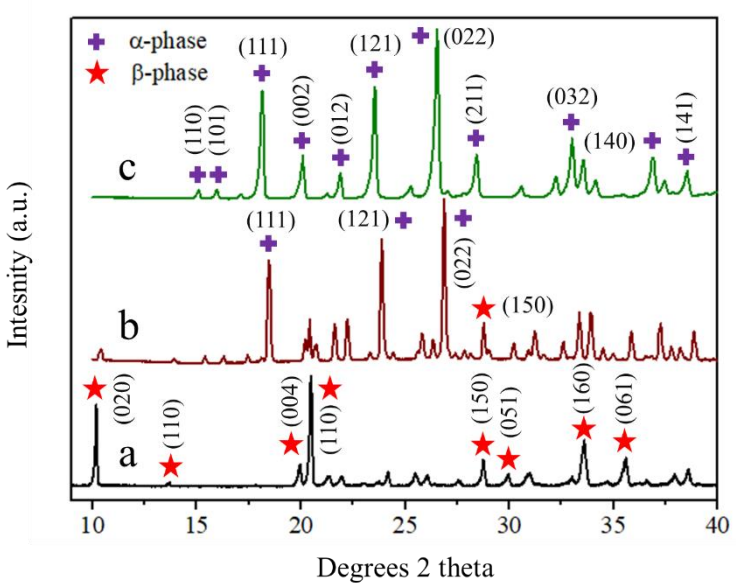

Figure 4.2. X-ray diffraction of a) bulk Glu, b) [$^{13}C_5$/1-^{15}N] -bulk Glu, c) α-phase obtained by recrystallization

Several different loadings of pure commercial L-Glutamic acid were adsorbed on fumed silica nanoparticles (Aerosil-380) to detect the maximum loading before bulk amino acid crystallization, as previously done for Leucine. Data on L-Glutamic acid adsorbed on fumed silica nanoparticles at different loadings had previously been reported by Sakhno *et al*.[92] The broad range X-Ray Diffractograms of our samples show that for loadings of 5% and above, Bragg peaks consistent with bulk Glutamic acid peaks are observed (Figure 4.3).

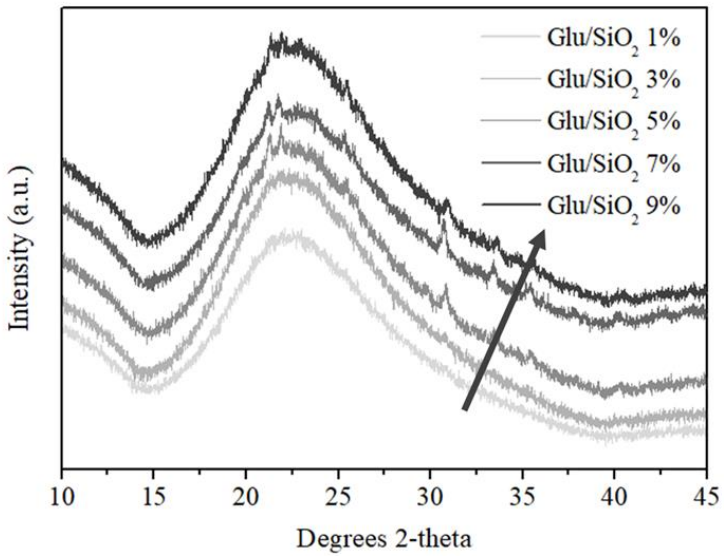

Figure 4.3. XRD patterns of pure bulk Glu/SiO_2 systems with increasing loadings

A closer look was taken at limited spectral ranges in order to define more precisely the saturation laoding.

Longer data acquisitions were performed (Figure 4.4), the first one for 2θ values from 20° to 27°, (which is the area strictly for the amino acids characterization), the second one from 29° to 33° and the last one from 32° to 37°.

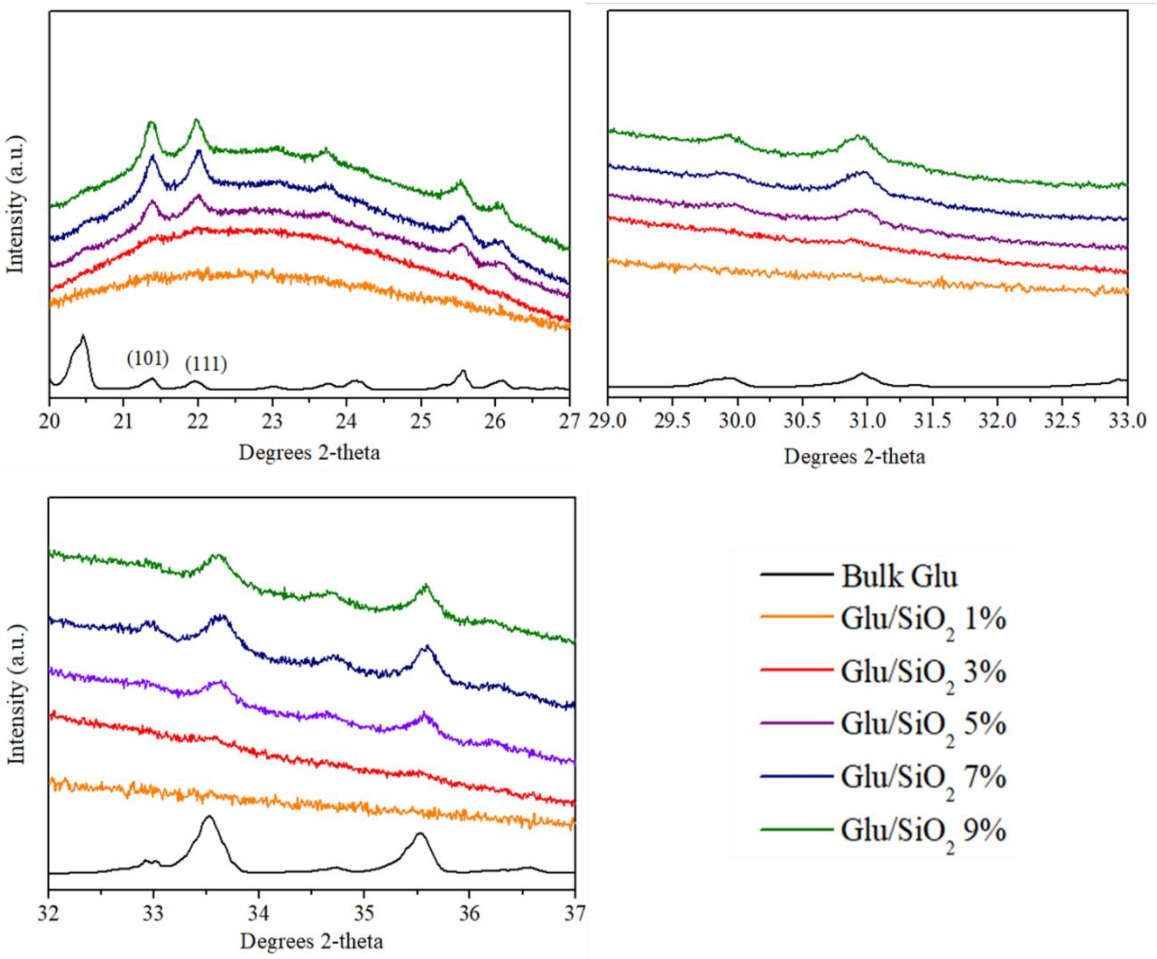

Figure 4.4. XRD patterns of pure bulk Glu and Glu/SiO_2 systems with increasing loadings

The close-up XRDs shown in Figure 4.4 indicate that bulk Glu peaks are already present, with low intensities, in the 3% Glu sample.

It is interesting to note that the relative intensities of peaks with different Miller indices in high-loading Glu/SiO_2 may be significantly different as compared to bulk: the peak at 2θ = 20.45° which corresponds to the Miller indices (1 1 0) is hardly seen in Glu/SiO_2, while the peaks at 21.3° and 21.9° are relatively more intense than in bulk Glu. In the 2θ =29° to 33° and 32° to 37° regions, no significant differences are observed. This phenomenon is not due to the simple dissolution/reprecipitation because when dissolving commercial Glu in the absence of the silica support followed by reprecipitation, the XRD patterns are superimposable. This may be due to preferential crystal growth in a special direction, induced by germination on the surface. Significant effects of a silica surface on the crystallization of amino acids have been reported before, e.g., when depositing glycine on silica, the metastable β form is nucleated instead of the stable α form.[84]

Finally, we compared two Glu/SiO_2 samples with a 7% loading, i.e. beyond the saturation coverage, prepared from either natural abundance Glu (β-form), or from the fully enriched Glu (equal amount of α- and β-forms; Figure 4.5). Unexpectedly, Glu seemed to keep some kind of memory of its initial crystalline form, since peaks of both α- and β-Glu were observed in the second case. This would be easily understood if undissolved crystals had been deposited on silica, but the deposition solution was limpid and there was no indication that dissolution was not complete. At any rate, here again, the (1 1 0) peak of the β form was strongly extinguished relatively to the other peaks, confirming the observation made above.

On the basis of this observation, we tried to see if it was possible to obtain a sample containing only α-Glu on silica. For this purpose, we prepared a deposition solution from the recrystallized enriched Glutamic acid that had been characterized as pure α-Glu (cf. supra). In this case however, the peaks of the α-phase were not present in the final Glu/SiO_2 sample and the diffractograms only contained the peaks of the β-phase, as for natural abundance Glu/SiO_2. These apparently puzzling observations may be understood if, as suggested above, the crystallization of the α-phase is due to the presence of an impurity, which might be eliminated in the recrystallization procedure.

Thus, for Glu/SiO_2 samples beyond the saturation limit, the precipitation of bulk Glu is a non-trivial phenomenon. It might be interesting to study it in more detail in another context, but in the frame of this thesis, we will not delve into its details.

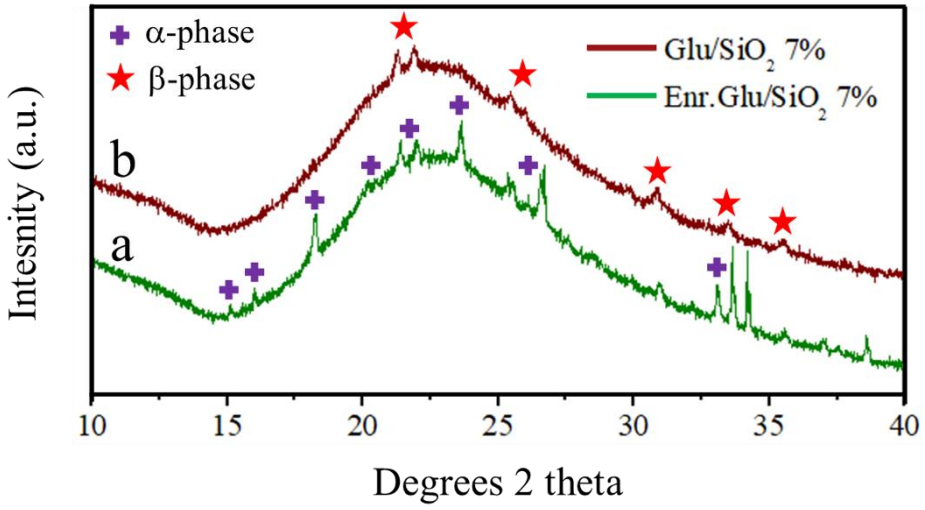

Figure 4.5. XRD patterns of a) [$^{13}C_5$/1-^{15}N]-7% Glu/SiO_2 and b) Natural abundance 7% Glu/SiO_2 systems

IV.2.2 Thermogravimetric Analysis

Thermogravimetric analyses were performed on samples with increasing Glu loadings and are shown in Figure 4.6 for samples dried under nitrogen flow (ND);

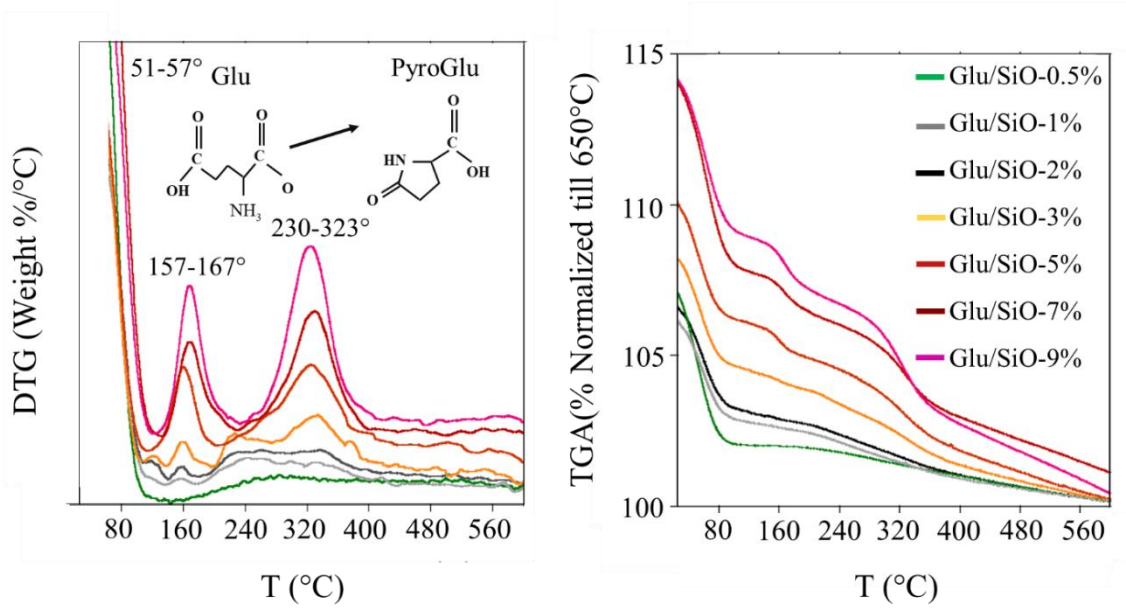

Figure 4.6. DTG and TGA curves of Glutamic acid adsorbed on silica (Aerosil 380) at different weight percentages loadings, after ND treatment (DTG traces offset for clarity; green traces correspond to the raw SiO_2 support)

The DTG traces show thermal events in three clearly distinct temperature ranges, unlike Leu/SiO_2. The first endothermal event between RT and 100°C, having T_{max} = 51-57°C, corresponds to the physisorbed water elimination. Then, a second endotherm at 157-167°C is assigned to peptide bond formation. It may be noted that a more complex DTG shape is observed in this region for the lowest loading samples (0.5, 1 and 2% Glu), with a first peak at around 120°. This had already been observed in a previous work[86], for loadings of 0.65 to 2.6% Glu, and attributed to an initial internal condensation of Glutamic to pyroglutamic acid, forming a five-membered lactam ring (scheme in Figure 4.6). The question of pyroglutamic acid formation will be discussed again in Chapter V. This reaction is also observed for bulk Glutamic acid[304], although at a considerably higher temperature (197°C in our conditions): thus, the occurrence of the 120°C event, or even those at 157-167°C, indicates a specific activation of Glu by the silica surface for the low loadings.

Figure 4.7 compares a typical DTG curve of Glu/SiO2 (7%) with that of bulk β-Glu.

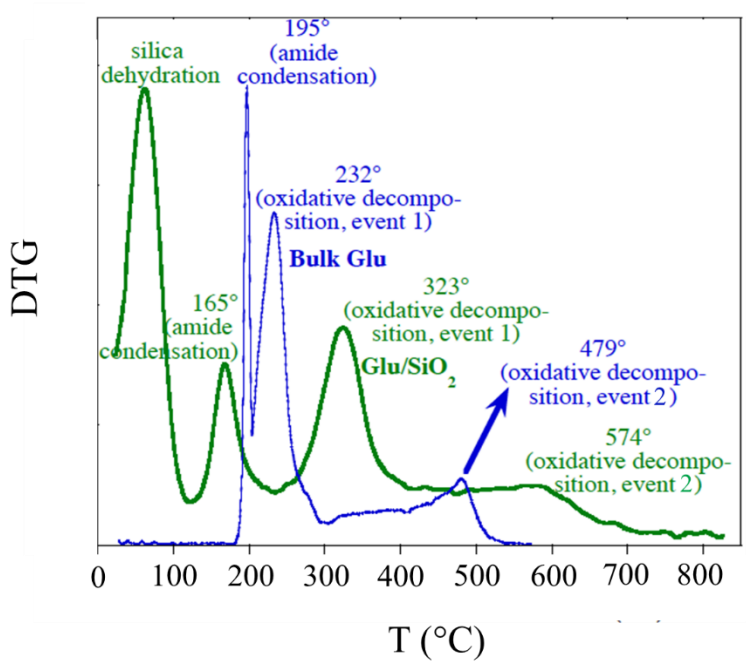

Figure 4.7. DTG curve of Glu/SiO_2 7% compared with that of bulk Glutamic acid (β phase)

On the topic of internal cyclization, it can be noted that the weight loss ratio between the first event and the total is almost constant, for an average of 0.27. This is close to the expected ratio if the first peak corresponds to the loss of two water molecules per Glu. Since extensive peptidic bonding between the amino acids (to give large linear polymers, or cyclic dimers) would only release one water molecule per Glu, with a weight loss ratio of 18 amu/147 amu = 0.122, this means that internal cyclization also takes place in most molecules at least.

The last two events are exothermic and may be attributed to the oxidative degradation of the supported peptidic material. Here too, the low loading samples show a different shape for this event, which starts shortly after 200°C and extends to 400°C, while for the higher loadings a sharper peak is observed with a T_{max} of 325-330°C. Overall though, interaction with the silica surface causes these degradation events to occur at higher temperatures than in the bulk, providing a significant temperature window where amide bonds may be stable.

In the case of the vacuum dried samples (Figure 4.8; color coding is the same as Figure 4.6), the general aspect of the DTGs is quite similar to that of the nitrogen-dried ones (Figure 4.6). However, and unsurprisingly, there is clearly less physisorbed water in the system, as shown by the lower intensity of the endothermic event at T_{max} = 58-78°C.

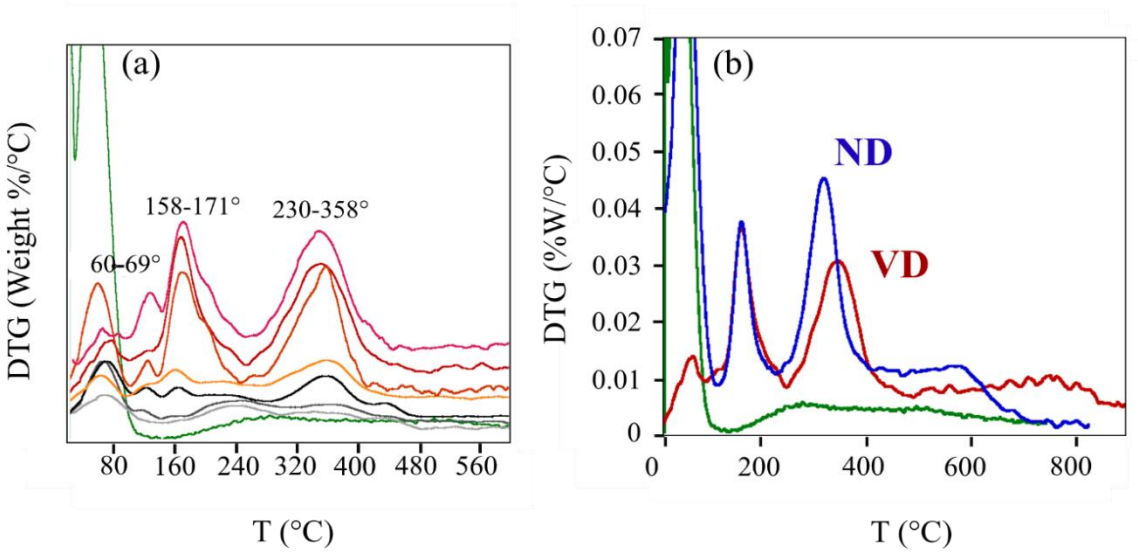

Figure 4.8. DTG curves of Glutamic acid adsorbed on silica (Aerosil-380) at different weight percentage loadings, after vacuum drying (DTG traces offset for clarity; the green trace corresponds to the raw SiO_2 support). Right: comparison of typical DTG traces for the same sample (Glu/SiO_2 7%), after ND and VD treatments

Although it would be expected for VD and ND samples to behave similarly after all physisorbed water has been removed from the system, there are some differences. In particular, the oxidative degradation events are shifted to higher temperatures after VD relative to ND treatments (see Figure 4.8 b) for an example). The elimination of organic matter after VD is not complete before 900°C; indeed, the integrated weight loss between 100 and 900°C, after correction for the silica contribution, corresponds well to the nominal Glu loading. We did not investigate this point further since we are mostly concerned with the low-temperature behavior of supported amino acids.

Quantification of the amount of physisorbed water in both series of samples was achieved, as in the case of Leu/SiO_2 (chapter III), from the weight loss corresponding to the first endothermic peak of the TGs. The amounts of physisorbed water remaining after both the ND and VD treatments are plotted in Figure 4.9, and compared with the corresponding values that had been found for Leu/SiO_2.

Just as for Leucine, a small amount of water (< 1 nm^{-2}) remains adsorbed after VD, and it is essentially independent of the amount of Glutamic acid in the system. In Chapter III, we had noted that this observation is compatible with the adsorption of the amino acid molecules on strongly retained water, which would then be in a bridging position. After ND in contrast, more water is retained (weakly held water): the amount of this weakly held water increases with the Glutamic acid loading until about 3% Glu, where this increase becomes less significant. For Leucine, it corresponded to about 10 water molecules per amino acid; for Glutamic acid, the increase is distinctly non-linear, which would mean that the number of weakly held H_2O per Glu is first quite high (as much as 15 H_2O molecules per Glu), and then decreases as more Glu is adsorbed.

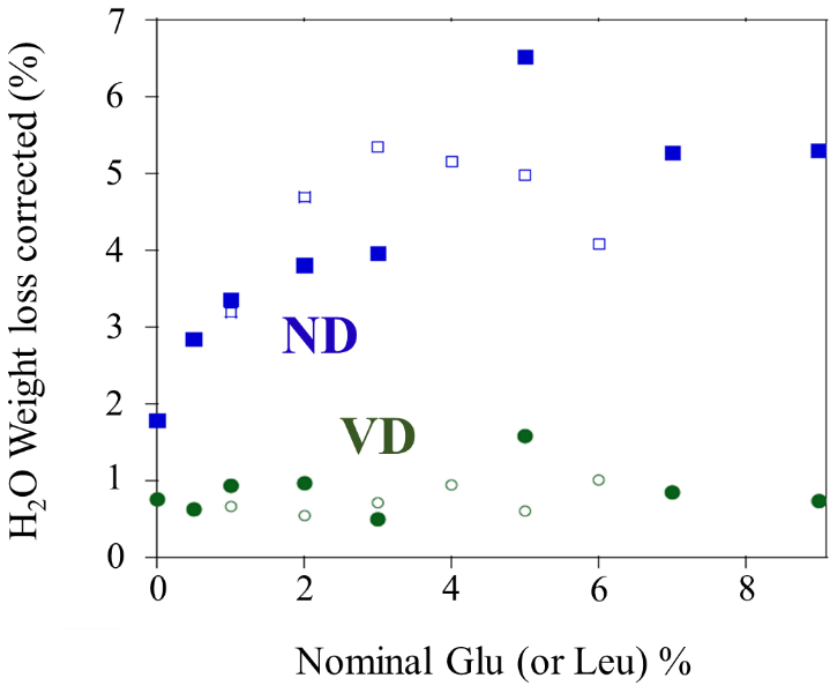

Figure 4.9. Quantification of physisorbed water in Glu/SiO_2 as a function of Glutamic acid loading after VD and ND treatments (full symbols); the corresponding data for Leu/SiO_2 (Chapter III) are displayed as open symbols.

IV.3 Spectroscopic Characterization

IV.3.1 Infrared Spectroscopy

IV.3.1.1 Variable loading Glu/SiO_2, effect of drying treatment

IR vibrational spectra of Glutamic acid adsorbed on the silica surface were collected both on nitrogen-dried and vacuum dried systems, for loadings of 1%, 3%, 5%, 7% and 9%. They are shown in Figure 4.10 (ND) and Figure 4.11 (VD), respectively.

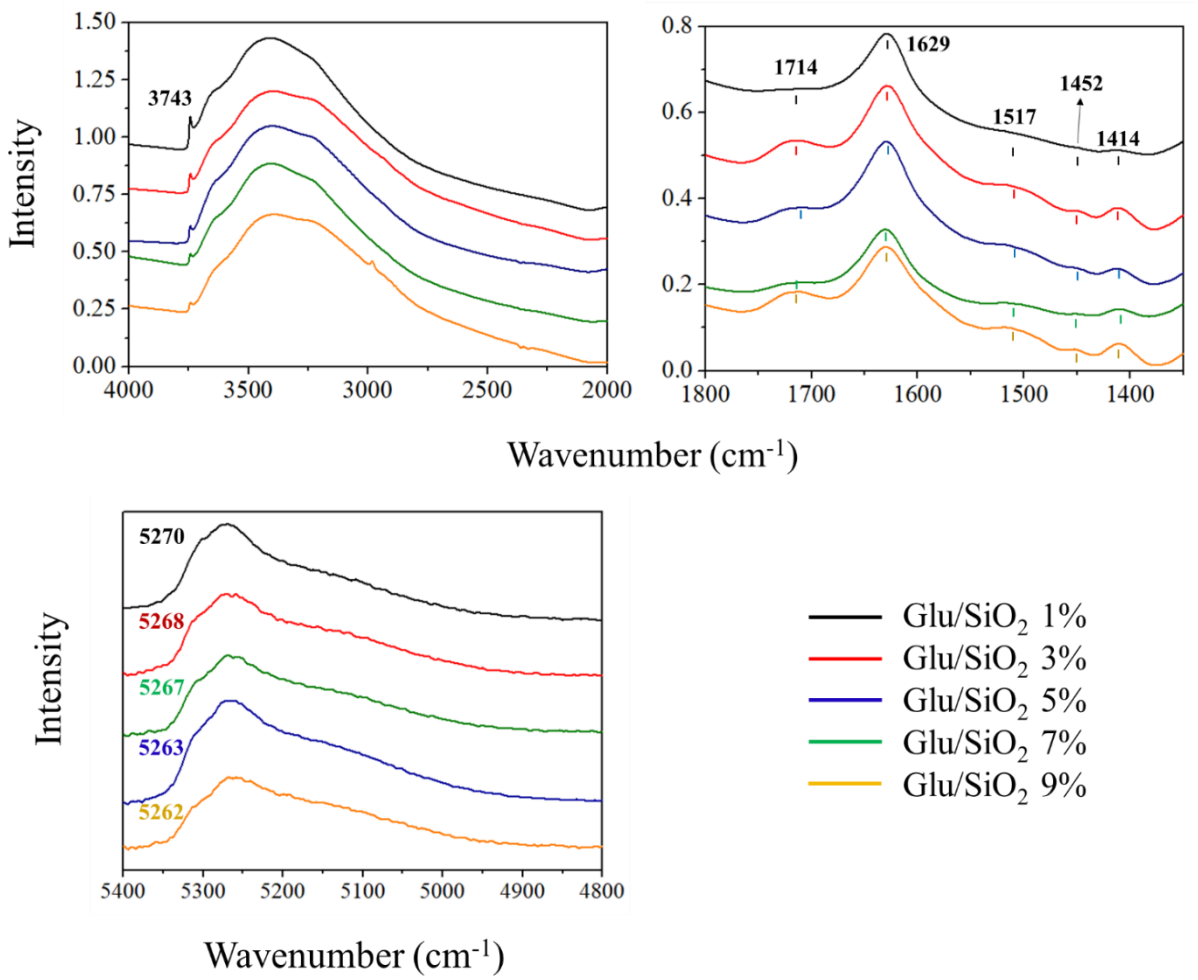

Figure 4.10. IR spectra of ND Glu/SiO_2 at different loadings in three spectral ranges (NIR data have been baseline corrected)

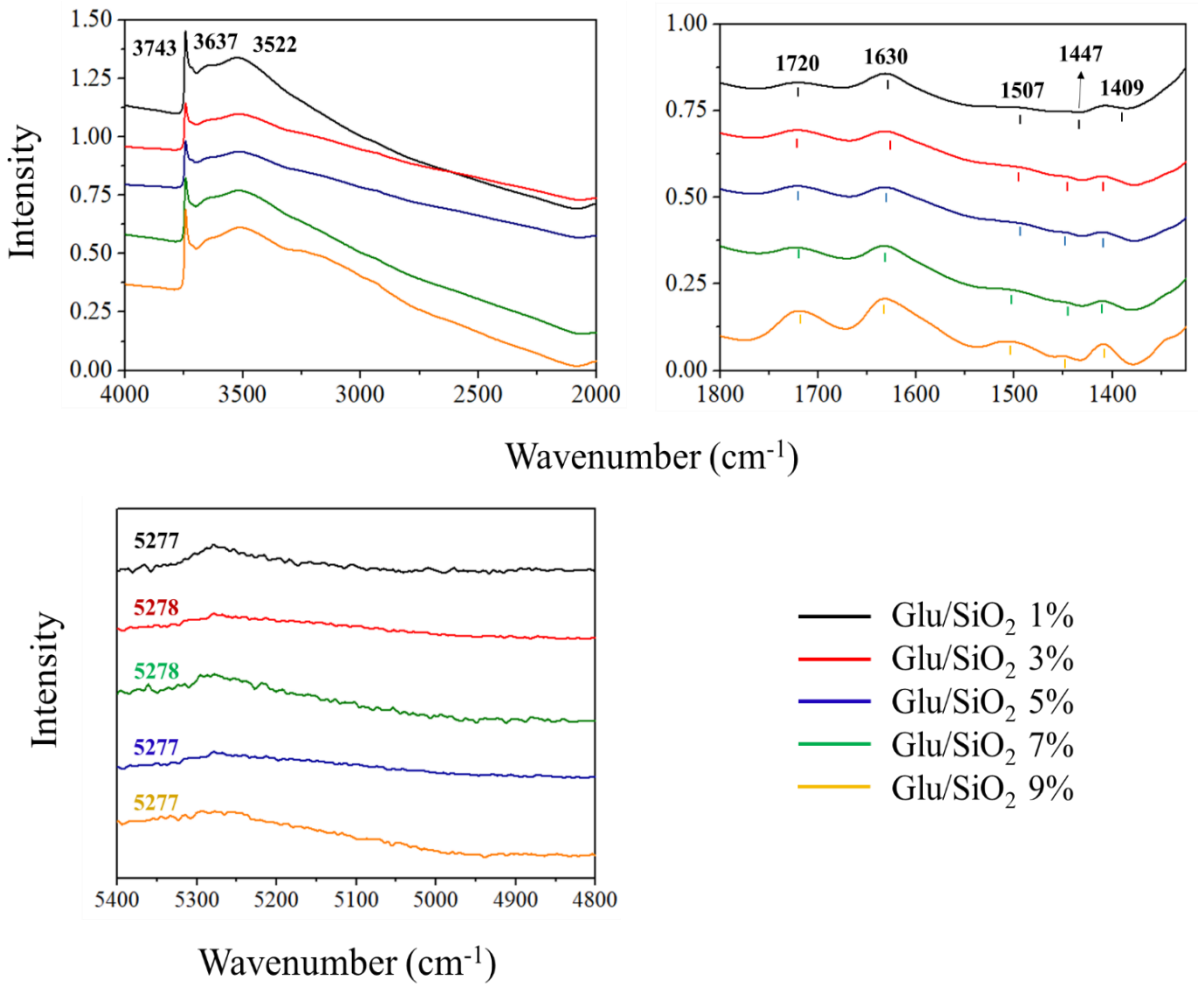

Figure 4.11. IR spectra of V.D Glu/SiO_2 at different loadings in three spectral ranges (NIR data have been baseline corrected)

In the 2000-4000 cm^{-1} region, as was the case for Leu/SiO_2, the spectrum is dominated by the O-H stretching of silanols (isolated silanols at 3473 cm^{-1}) and physisorbed water perturbed by H-bonding, the latter being significantly reduced after VD. Only for the highest loading does one observe broad components attributable to NH and CH stretching. In the fingerprint region between 1350-1800 cm^{-1}, several bands may be assigned to adsorbed Glutamic acid. A tentative assignment is proposed in Table 4-1 based on the previous work of A. Battistella.[305]

Assignment	Position in ND samples (cm^{-1})	Position in VD samples (cm^{-1})
ν (C=O) in COOH	1714	1720
δ_{as} (NH_3^+)	(1629	1630
ν_{as} (COO^-)	~1590 (shoulder)	~1590 (shoulder)
δ_{sym} (NH_3^+)	1517	1507
δ (CH_2)	1452	1447
ν_{sym} (COO^-)	1414	1409

Table 4-1. Main fingerprint bands in Glu/SiO samples, positions and assignments

Most of these bands are similar to the equivalent ones for Leu/SiO_2. The most conspicuous difference is the presence of a band at 1714-1720 cm^{-1} that clearly indicates the presence of a protonated COOH group. One can conclude that in the predominant adsorbed form, the side chain carboxylic function is protonated, while the amino acid moiety is zwitterionic – a speciation that, in water, is observed in the 2.1 to 4.1 pH range.

The symmetric bending mode of the ammonium group ($\delta_{as\ NH_3^+}$) is difficult to locate precisely as it overlaps with an overtone of the Si-O vibrations, and also with the bending mode of adsorbed water- this is why the intensity in this region significantly decreases when going from ND to VD samples. Besides this effect, slight shifts of the bands are observed between ND and VD treatments, the most important one concerning the $\delta_{sym\ NH_3^+}$ band.[86]

In the far IR region, the success of VD in removing the physisorbed water is evidenced by the decrease of the band at 5288 cm^{-1}.

VI.3.1.2 Effect of isotopic enrichment

Figure 4.12 shows the spectra of 1% Glu/SiO_2 with three different types of enrichment. The presence or absence of peaks for different isotopic enrichments can help check bands assignments. N.D and V.D raw spectra are presented, And the low loading should insure that we are observing effects pertaining to the adsorbed forms of Glu. Baseline correction (by subtraction of Aerosil-380-VD sample) was also applied to allow a better observation of the amino acid peaks. Only the region of importance for amino acid vibrations (1800-1325 cm^{-1}) is discussed here.

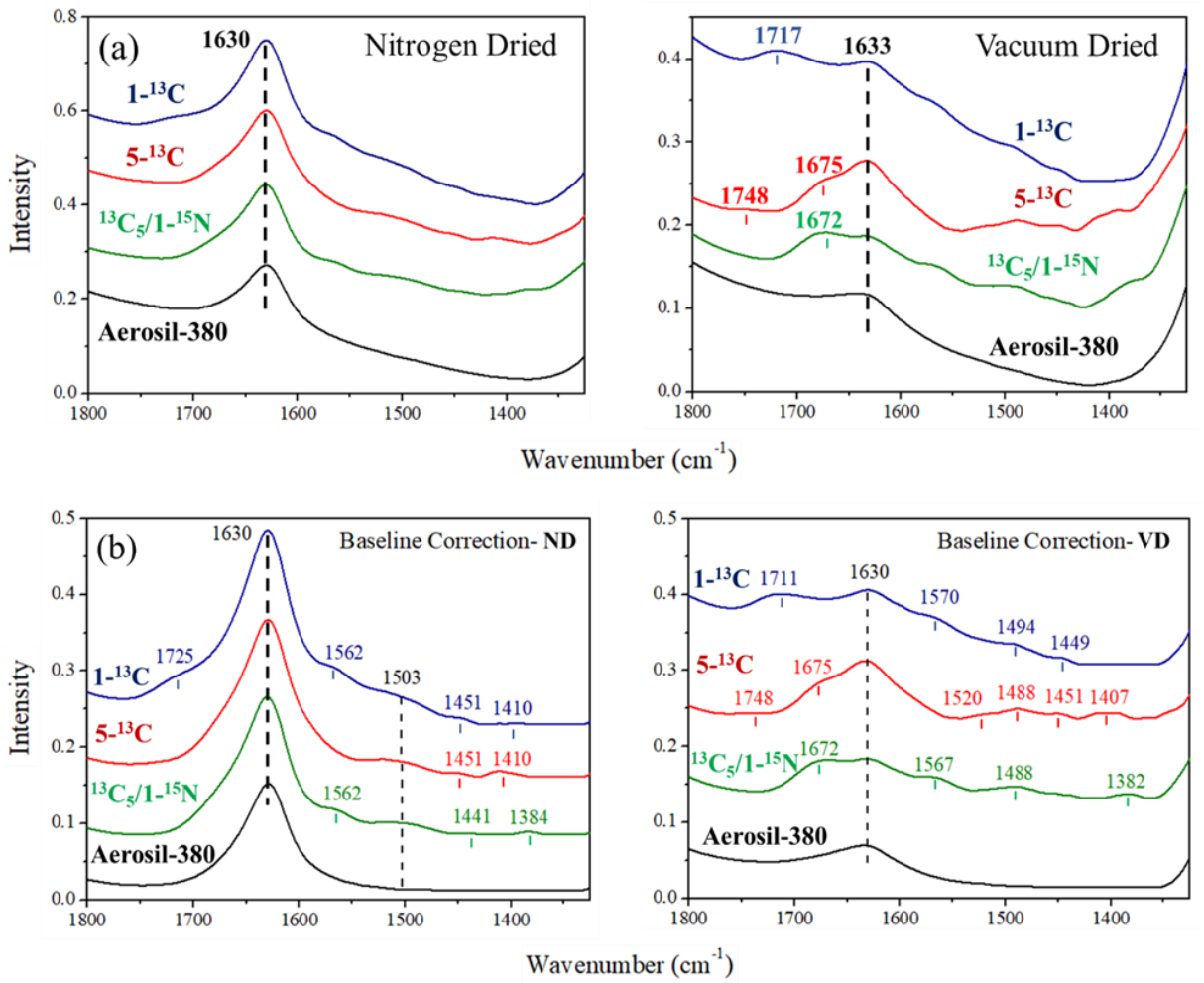

Figure 4.12. IR spectra of differently enriched Glu/SiO_2 performed under nitrogen flow (ND) and vacuum drying (VD) for 1% Glu/SiO_2, a) The original spectra, b) After baseline correction

Assignment	[1-^{13}C] Glu/SiO_2: Position (shift w.r.t natural abundance)	[5-^{13}C] Glu/SiO_2: Position (shift w.r.t natural abundance)	[$^{13}C_5$, ^{15}N] Glu/SiO_2: Position (shift w.r.t natural abundance)
ν (C=O) in COOH	1725 (+11)	n.o.	n.o.
$\delta_{as}(NH_3^+)$+ $\delta(H_2O)$	1630 (+1)	1630 (+1)	1630 (+1)
$\nu_{as}(COO^-)$	1562 (-28)	~1590 (0)	1562 (-28)
$\delta_{sym}(NH_3^+)$	1503 (-14)	1503 (-14)	1503 (-14)
$\delta(CH_2)$	1451 (-1)	1451 (-1)	1441(-11)

$\nu_{sym}(COO^-)$	n.o.	1410 (-4)	1384 (-30)

Table 4-2. IR band assignments and positions for the three enriched 1% Glu/SiO_2 samples in ND conditions, and shifts with respect to the natural abundance 1% Glu/SiO_2

Tentative band assignments and positions are listed in Table 4-2, which also indicates the shifts with respect to the natural abundance samples.

The intense band at 1630 cm^{-1} is probably dominated by the contribution of adsorbed water, so it is impossible to draw firm conclusions on the position of $\delta_{as}(NH_3^+)$. Some clear trends are apparent however. A band is present above 1700 cm^{-1} (although blue shifted with respect to natural abundance) only in the first sample, that has ^{12}C on the C5 carboxylic acid position; in the second and third samples, where the C5 position is exchanged with ^{13}C, this band disappears- we surmise that it is shifted to lower wavenumbers, where it is hidden under the other contributions around 1630 cm^{-1}. If this band is red-shifted by $^{12}C/^{13}C$ exchange at the C5 position, the corresponding vibration involves a movement of the C5 carbon, in conformity with its assignment to the ν (C=O) of the side-chain COOH.

Conversely, a band appears at 1562 cm^{-1} only when the C1 carboxylate position is exchanged with ^{13}C and, as far as one can say, the shoulder at 1590 cm^{-1} disappears. This band corresponds therefore to a vibration that involves a movement of the C1 carbon – we had assigned it to $\nu_{as}(COO^-)$ of the C1 carboxylate. Other effects are not so clearly explained, but these shifts confirm beyond reasonable doubt that the speciation of Glu adsorbed on the silica surface is predominantly zwitterionic after ND drying – the $H_2Glu^{\pm}$ form in Figure 4.1.

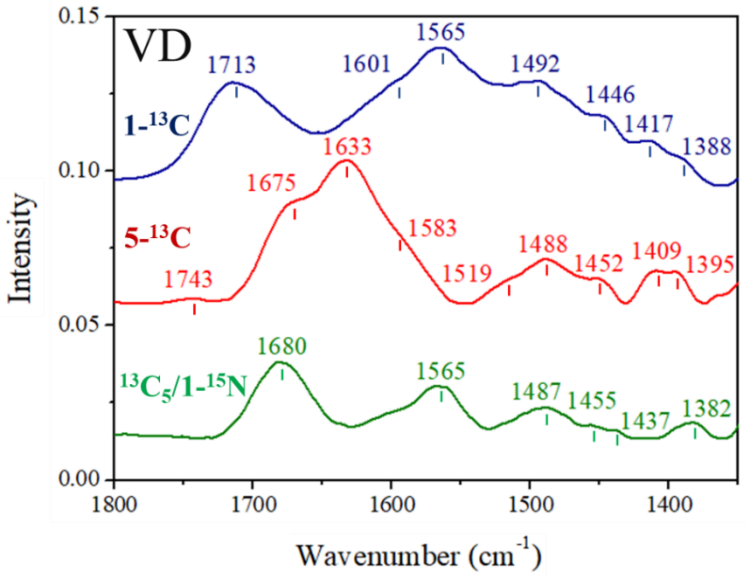

Figure 4.13. IR spectra of the three partially and fully enriched 1%Glu/SiO_2 samples in VD conditions, with baseline correction followed by subtraction from the signal of silica

We have also recorded the IR spectra of the same samples after VD drying. In these conditions, the interfering band at 1630 cm^{-1} band has decreased considerably due to water removal, but, as seen in Figure 4.12, a contribution at this position is still always present due to a SiO_2 combination band (see the spectrum of the raw Aerosil support). For this reason, we have tried

to subtract the spectrum of silica, after normalization to the overtone band at 1870 cm^{-1}. The results are shown in Figure 4.13.

This treatment reveals a lot of detail in the IR spectra, and a more extensive analysis would be needed to account for all observable spectrum components. Still, they very clearly confirm the two important observations we proposed above:

- The disappearance of the band assigned to ν (C=O) of the side-chain COOH in the two samples where C5 is isotopically exchanged: now, we can see its red-shifted counterpart at 1675 cm^{-1}-1680 cm^{-1}.
- The appearance of a band at 1565 cm^{-1} when the C1 carboxylate is exchanged, corresponding to the $\nu_{as}(COO^-)$ of the isotopically exchanged carboxylate.

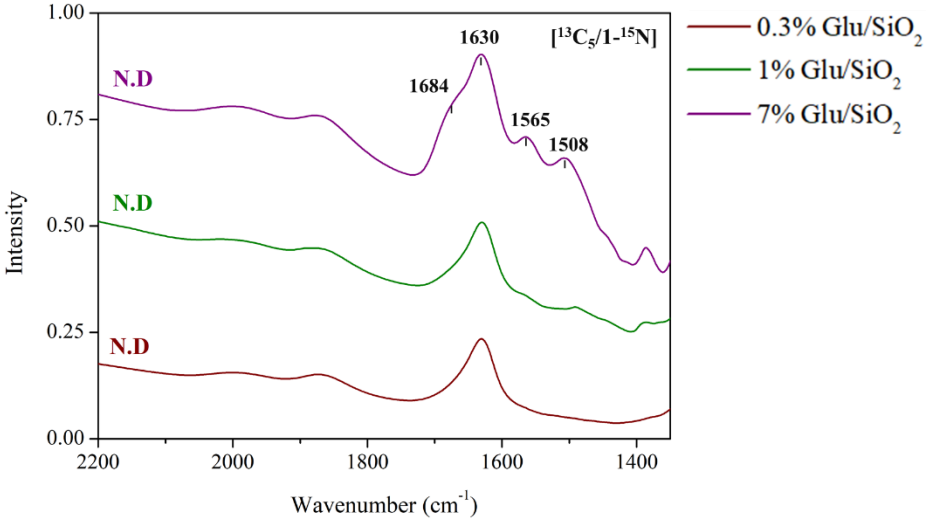

Figure 4.14. IR spectra of [$^{13}C_5$/1-^{15}N]-Glu/SiO_2 with different loadings recorded after drying under nitrogen flow (ND)

IV.3.1.3 IR of PyroGlu/SiO_2

We have mentioned in § IV.2.2 (TG results) that Glutamic acid can cyclize to pyroglutamic acid (PyroGlu) at rather low temperatures, and the matter will be important in Chapter V. In fact, we wondered if the rather harsh VD drying conditions might not be sufficient to start this transformation, which would compel us to rethink the interpretation of spectroscopic results. In order to check this point, we deposited genuine PyroGlu on the silica support and recorded the IR spectrum of the resulting system (Figure 4.15). They exhibit two strong bands at 1735 cm^{-1}, due to –COOH ν (C=O) of PyroGlu, at a position definitely higher than that of the side-chain -COOH of Glu; and at 1673 cm^{-1}, certainly an amide I band. These bands are never observed in Glu/SiO_2, either ND or VD, and thus we may conclude that the removal of water at room temperature is not enough to favor a cyclization of Glutamic acid to Pyroglutamic acid.

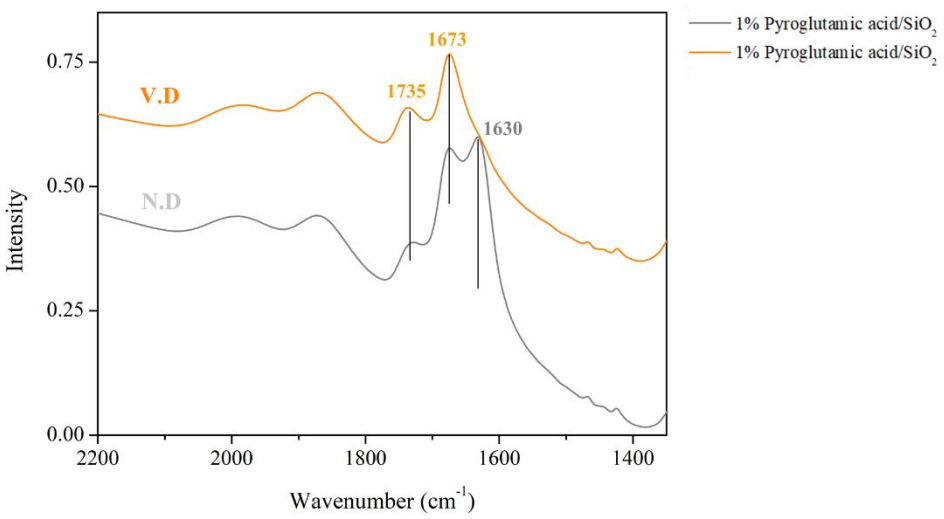

Figure 4.15. IR spectra of 1%PyroGlu/SiO_2 recorded under nitrogen flow (ND) and vacuum drying (VD), compared with bulk PyroGlu

IV.3.2 Solid State Nuclear Magnetic Resonance Spectroscopy

IV.3.2.1 Preliminary remarks on the molecular structures of Glu crystals

We have mentioned above (§ IV.2.1) the existence of two structurally different polymorphs (α and β) for Glutamic acid. In both forms, molecules are found in their zwitterionic form, where the C_5-carboxylic group located in the side chain is protonated whereas the C_1-carboxylate group is deprotonated as already suggested by Hirokawa (1955).[246] The structure of the two polymorphs was initially compared by Hirayama and coworkers[306] and Lehmann and Nunes [245], and later refined by Ruggiero and coworkers[307] who proposed a combined experimental and theoretical approach to discriminate the polymorphs. Both belong to space group $P2_12_12_1$, with Z = 4. The unit cell contains four Glutamic acid molecules, all in equivalent positions. This is in contrast with Leucine whose structure contained two non-equivalent molecules with slightly different environments.

There are some interesting similarities between the α and the β phase: the side chain carboxylic group show a distance between C_5---O_2H of 1.327 Å and 1.323 Å in α and β phase respectively, corresponding to a single bond, in contrast with C_5---O_1 of 1.241 Å and 1.245 Å in α and β phase respectively, corresponding to a double bond, while the C---O_1 and the C---O_2 distances in the carboxyl moiety show a minor difference of 0.02Å, which lies somewhere between the single and the double bond value. This is why it is known that the amino acid is in the zwitterionic form.

Some differences exist between the two phases of course. The shape of the carbon skeleton is different: extended in α, strongly twisted in β, as illustrated in Figure 4.16. Molecular shapes

can be quantitatively characterized by torsional angles. The O_1-C_1-C_2-C_3 torsion angles are close in both cases, -42.24° in the α-phase and -50.41° in the β-phase, and the same is true for the O_1-C_1-C_2-N angles, indicating that the amino acid moiety has a rather rigid shape; but the C_1-C_2-C_3-C_4 angle goes from 178.4 to -51.8° between the two phases. Furthermore, in β Glu, the carboxylate group follows the nearly linear arrangement of the other carbon atoms, having a dihedral angle of 8.70°, while in the case of α Glu, the dihedral angle is skewed out of the plane of the carbon backbone, exhibiting a 59.26° value (Figure 4.16). The different orientations of the side chain containing the C_5-Carboxyl group in the two polymorphs are characteristic for this part of the molecule that is highly flexible in nature.

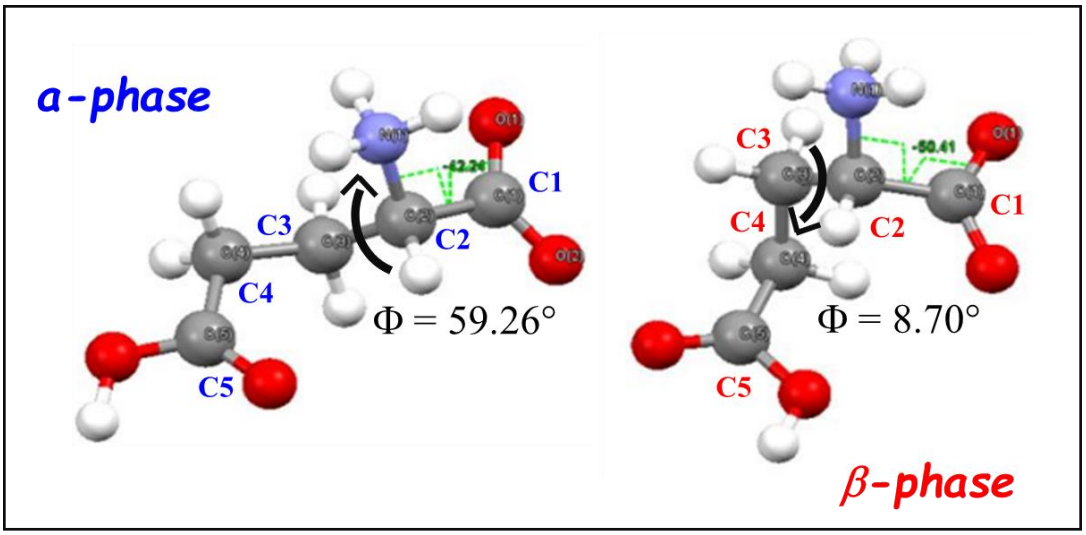

Figure 4.16. Scheme of the conformations of the Glu molecule in the α and β polymorphs

We may also compare the two structures from the point of view of H-bonding. No intramolecular hydrogen bond exists in either polymorph. In contrast, intermolecular H-bonds are well developed. Indeed, all possible H-donor groups (COO-H and $N(-H)_3$) participate in H-bonding. Each Glu molecule is involved in 4 H-bonds as a donor, and consequently• also in 4 H-bonds as an acceptor. The H-bond pattern is dominated by strong $–C_5OOH\cdots OOC_1$ bonds aligning the molecules into linear chains. The carboxylate oxygens accept two weaker H-bonds, and the carbonyl of the C5 carboxylic group accepts one, linking separate chains. The strong $–C_5OOH\cdots OOC_1$ bonds are characterized by a small OH···O distance, smaller for the β form (1.475 Å) than for the α one. This involvement of the carboxylate oxygen as a strong H-bond acceptor causes a lengthening of the covalent C-O bond.

The difference in H-bonding pattern lies in the distribution of H-bonds acceptor. In the α form, one of the carboxylate oxygens accepts one bond from a –COOH and one from a $–NH_3^+$, while the other oxygen of COO^- is H-bonded to a $–NH_3^+$; in the β form, the first carboxylate oxygen accepts two bonds from $–NH_3^+$ groups, the second oxygen accepts one bond from a –COOH. The H-bonding patterns are illustrated in Figure 4.17.

• This is because each H-bond involves one H-donor and one H-acceptor group, and all Glu molecules are equivalent.

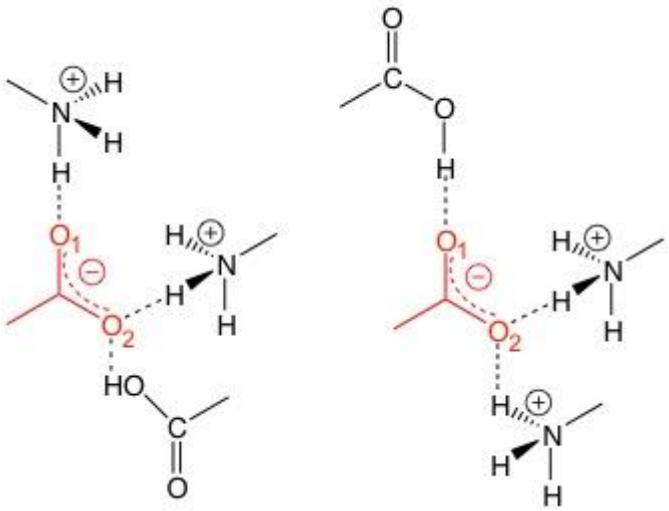

Figure 4.17. Differences in H-bonding pattern between α-Glu (left) and β-Glu (right)

Figure 4.18 shows the projection along 3 perpendicular directions as well as the perspective view of a single unit cell of Glutamic acid for the α-Glu form. The corresponding numerical values of the distances between different atoms and the dihedral angles related to these hydrogen bonds are summarized in Table 4-3.

Corresponding data for the β-Glu form are shown in Figure 4.19 and Table 4-4.

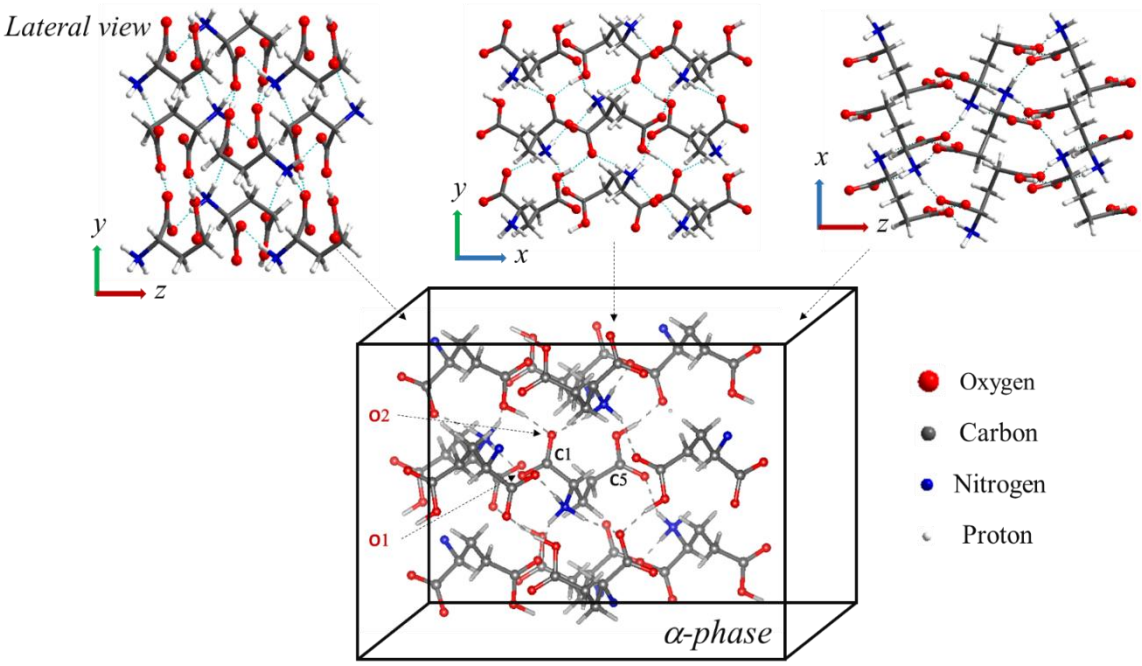

Figure 4.18. Crystal structure of L-Glutamic acid in the α polymorph

Atom-Atom interaction (H---X) Å	H-bond distance (Å)	Dihedral angle A-H---B (°)
NH_3---OC(5)OH	1.926	154.9
NH_3---O(2)C(1)O	1.794	170.4
NH_3---O(1)C(1)O	1.744	170.4
C(1)OO(2)---HOC(5)O	1.568	169.3

Table 4-3. Selected H- bond distances and dihedral angles in the α form of L-Glutamic acid

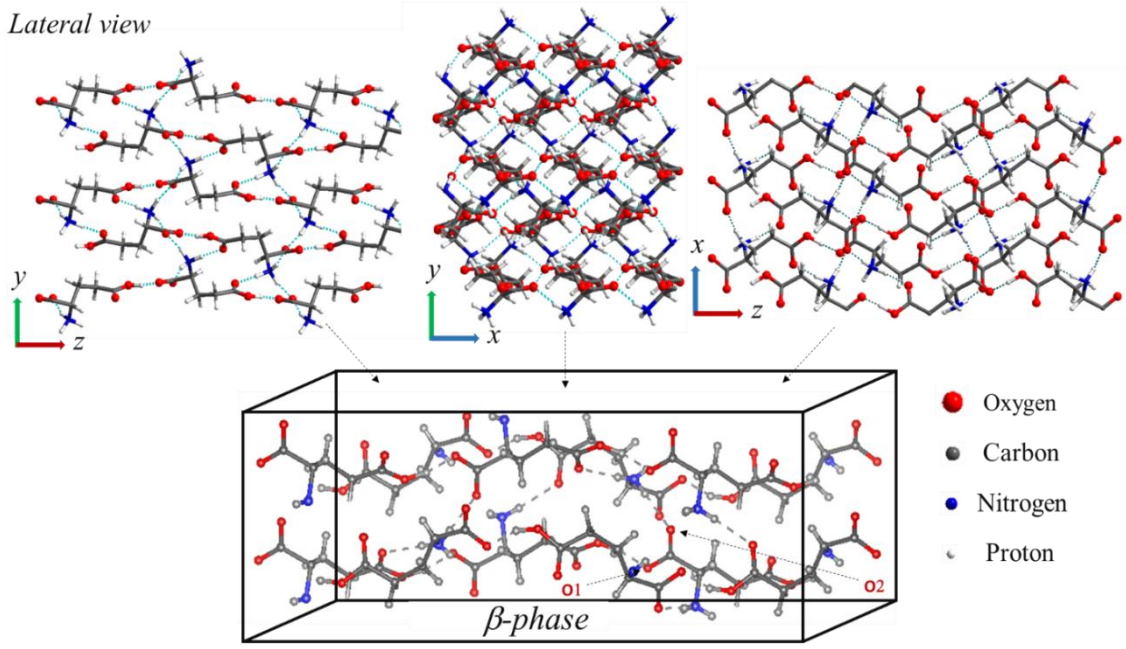

Figure 4.19. Crystal structure of L-Glutamic acid in the β polymorph

Atom-Atom interaction (H---X) Å	H-bond distance (Å)	Dihedral angle A-H---B (°)
NH_3---O(2)C(1)O	1.801	168.5
NH_3---O(2)C(1)O	1.834	165.4
NH_3---OC(5)OH	1.840	174.1
C(1)OO(2)---HOC(5)O	1.429	171.7

Table 4-4. Selected H- bond distances and the follow-up dihedral angles in the β form of L-Glutamic acid

IV.3.2.2 NMR of bulk Glutamic acid and Glutamic acid in solution

Several different samples of L-Glutamic acid were investigated by NMR, including the samples previously investigated by XRD.

- Natural abundance commercial L-Glutamic acid (β-form)
- Natural abundance recrystallized L-Glutamic acid (α-form)
- Fully enriched [$^{13}C_5$,^{15}N] commercial L-Glutamic acid (mixture of α- and β- forms according to XRD)
- [1-^{13}C] enriched commercial L-Glutamic acid

IV.3.2.2.i ^{13}C CP MAS and liquid-state NMR

Figure 4.20 shows the ^{13}C CP MAS spectra of commercial β-Glu (bulk Glu), enriched Glu ([$^{13}C_5$, ^{15}N]) both recorded at 16.4 T and recrystallized α-Glu (bulk Glu Recr.) at 7 T. The spectrum of the enriched Glu was obtained at a different field; in the case of a spin ½ nucleus, the effect on the chemical shifts should not be important, but it can still explain the slight upfield shift (0 to -0.4 ppm), the other possible explanation being a referencing problem. In the carboxylate region, bulk Glu shows two intense and narrow peaks at 180.4 ppm and 178.4 ppm, in agreement with previously published spectra.[148,308] According to the literature, these signals correspond to the two carboxyl groups of β-Glu : C5 and C1 respectively, an assignment that agrees with our calculated values, as shown in Chapter II (see Table 2-2).

The α-Glu polymorph shows a C1 signal slightly more deshielded than in β-Glu, at 177.2 ppm, while the side chain carboxylic acid (C5) is hardly affected. Finally, the enriched sample shows carboxylate peaks corresponding to both the α phase and β phases, confirming that it contains both polymorphs in equal amounts. It is interesting to notice that the H-bonding differences of

the C1 carboxylate moiety outlined above are sufficient to give rise to a -1.2 ppm shift of the C1 carboxylate signals; this constitutes a benchmark for the effect of H-bonding on the chemical shifts. It is probably a low-range estimate, since in both polymorphs the number of H-bond to the C1 carboxylate are the same, and even the nature of the H donors, the difference lying only in their spatial arrangement (see Figure 4.17).

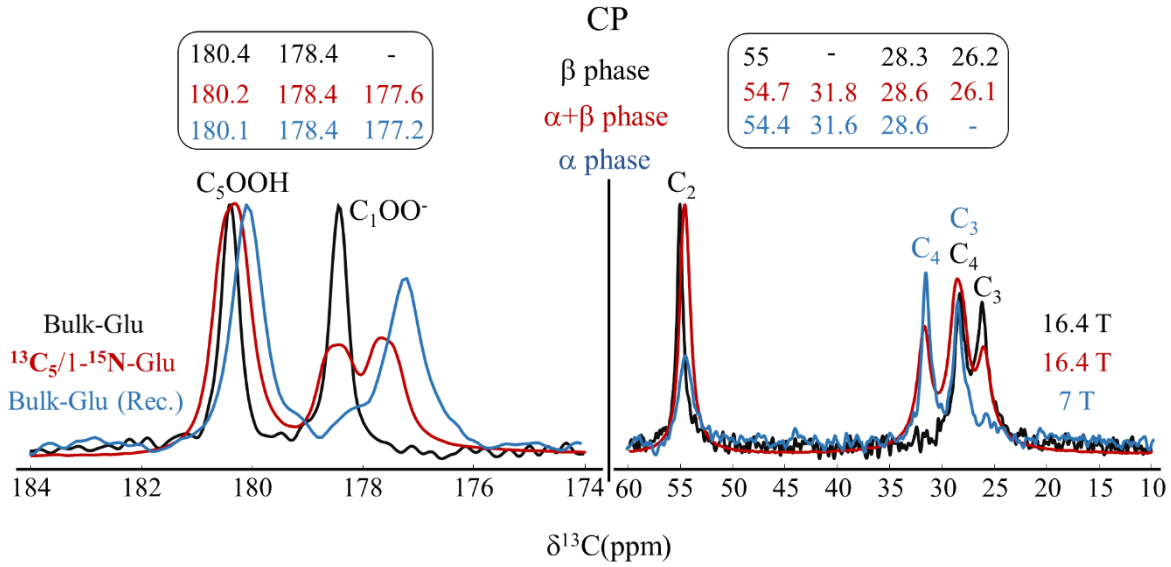

Figure 4.20. ^{13}C CP MAS NMR spectra of commercial bulk β-Glu (black), [$^{13}C_5$, 1-^{15}N] bulk Glu (red) and recrystallized commercial Glu (blue) in the carboxylate (left) and the aliphatic region (right)

In the aliphatic region, the signals observed for bulk β-Glu at 55.0 ppm, 28.3 ppm and 26.2 ppm are assigned to C2 (methine, CH group), C4 (methylene, CH_2), and C3 (CH_2).[86] In α-Glu, the methylene peaks are shifted downfield by a few ppm. This significant change in position of C3 is due to the effect of the torsion angle change that affects the environment of the methylenes (Figure 4.16). As expected, aliphatic signals of [$^{13}C_5$, 1-^{15}N] Glu show a superposition of the α and β phase signals.

When the spectrum of the samples enriched on all carbons was recorded at the lower field of 7 T, as already observed for bulk Leucine (Ch. III, § III-2.2.2), a significant J splitting of the C1 and C5 carbon signals induced a complex lineshape (not shown), where it was difficult to discriminate the contributions of the two phases. Thus, working at higher fields is preferable in this case too.

Beyond bulk solid Glu phases, another possible important reference for NMR chemical shifts is Glu in aqueous solution. This constitutes a reference point for “completely hydrated” Glu. The liquid-state ^{13}C NMR of Glu in solution (natural pH) is seen in Figure 4.21.

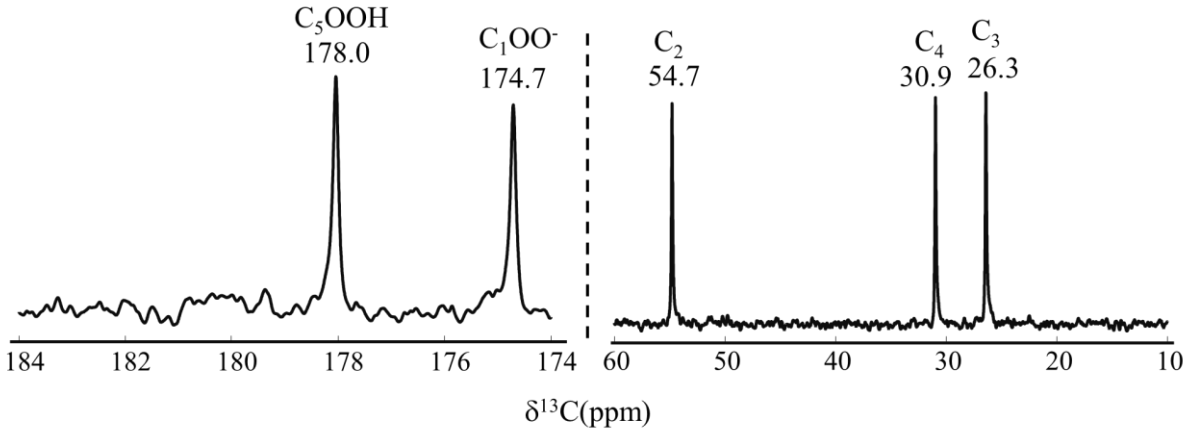

Figure 4.21. ^{13}C solution NMR spectrum of an aqueous solution of Glu (0.002 mol.L^{-1}) in the carboxylate and the aliphatic region

As expected, 5 peaks with approximately equal intensities are observed. The chemical shifts reported by Prabhu *et al.*[148] differ by a few ppm from the values reported here, possibly because of the use of a different chemical shift reference, and also in part because of a difference in solution pH (we observed unbuffered solutions, at the natural pH of ~3.4, while Prabhu *et al.* recorded their spectra at pH 7.3), but the successive assignments are the same and the order also corresponds to the attributions we made for the solid-state spectra. With respect to the solid, the chemical shift of the –C(5)OOH signal is not much affected, but the –C(1)OO^- is shifted upfield by 4 to 5 ppm, indicating a strongly different H-bonding pattern (indeed no H-bonds with ammonium moieties are expected in a dilute solution, as opposed to the solid – see Figure 4.18 and Figure 4.19). The methylene and methine carbons fall at values close to the solid-state ones.

IV.3.2.2.ii ^{15}N CP MAS NMR

The ^{15}N CP-MAS spectra of commercial bulk β-Glu and [$^{13}C_5$, ^{15}N] bulk Glu containing both the α and the β phase are shown in Figure 4.22. Enrichment enhances the signal to noise (S/N) ratio, which results in better-defined peaks. In both cases, the main signal is around -341 ppm, more precisely at -341.1 ppm for the sharp signal of the enriched Glu sample [$^{13}C_5$, 1-^{15}N], and therefore it may be assigned to nitrogen located in the β phases. The enriched sample, which is known to contain both the α and β phases, also exhibits a broader signal at -336.3 ppm. One might wonder if it corresponds to the α phase (or to impurities?). Unfortunately, no proper ^{15}N spectrum could be obtained from the pure α-Glu sample, for some unknown reason.

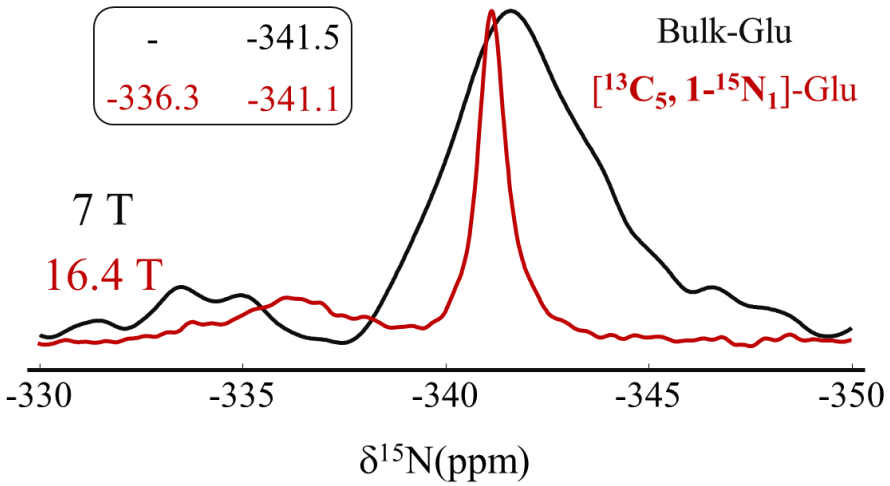

Figure 4.22. ^{15}N CP MAS NMR spectra of Commercial Bulk β-Glu (black) and [$^{13}C_5$, 1-$^{15}N_1$] Bulk-Glu (red)

For the Glu solution, a single ^{15}N signal was observed at -340.3 ppm, which can therefore be taken to characterize a fully hydrated ammonium group.

IV.3.2.2.iii ^{1}H MAS and liquid state NMR

The ^{1}H MAS NMR spectra of the two samples discussed above (bulk Glu and $^{13}C_5$, 1-^{15}N bulk Glu) are shown in Figure 4.23 and the ^{1}H chemical shifts values in Table 4-5; The spectrum of α-Glutamic acid (recrystallized from the bulk) was only available at a lower field and cannot yield useful information.

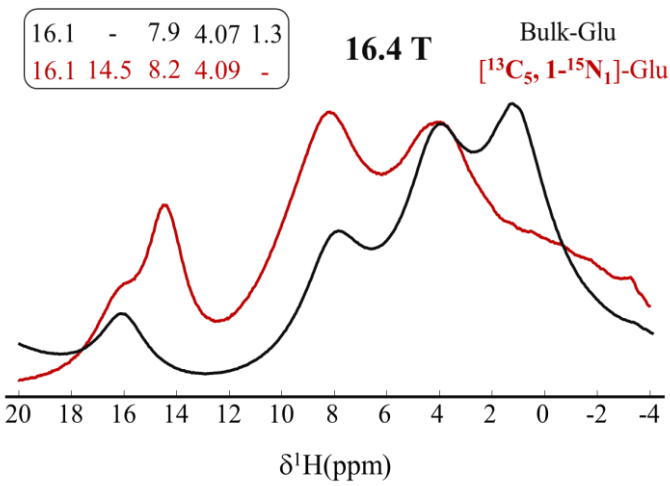

Figure 4.23. ^{1}H MAS NMR spectra of Commercial bulk β-Glu (black), and [$^{13}C_5$, ^{15}N] bulk Glu (red) recorded at 16.4 T (Spinning speed = 14 kHz)

Atoms	α-Glutamic Acid	β-Glutamic Acid
Calculated CS (ppm)		
H2	4.4	4.2
H3	2.6	2.4
H4	2.7	2.7
H5	16.7	19.1
NH_3	9.9	9

Table 4-5. ^{1}H chemical shift of α and β Glutamic acid

One way to assign the ^{1}H peaks is to compare the experimental spectra with the values we calculated for bulk α and β Glutamic acid (Annex-Table 2). This is done in Table 4-5. Four groups of protons in different chemical shift ranges are expected: the methylene protons between 2.4 and 2.6 ppm, the methine one at 4.2 to 4.4 ppm, the ammonium protons (-N**H**$_3$) above 9 ppm, and the acidic COOH at 16 to 19 ppm. The experimental spectra show maxima that correspond rather well with the first two groups (H2, H3 and H4) at 1.5 and 4.2 ppm while the peak at 8.2 ppm contributes to the ammonium protons (-N**H**$_3$) and the two peaks at 14.5 ppm and 16.1 ppm (in the enriched Glu) may correspond with the H5 of the carboxylic acid side chain of the α and β Glutamic acid respectively.

Figure 4.24 shows the superposition between the DP spectra shown in Figure 4.23 and filtrated ^{1}H spectra of [$^{13}C_5$, ^{15}N] bulk Glu extracted from the 2D HETCOR ^{1}H-^{13}C and ^{1}H-^{15}N CP MAS NMR spectra at 16.4 T.

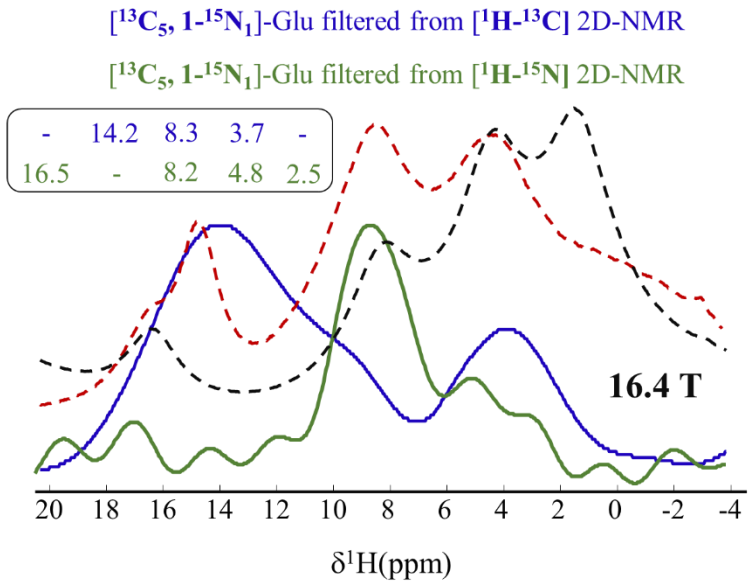

Figure 4.24. Superposition between ^{1}H MAS NMR spectra shown in the previous figure (red and black dotted lines) and ^{1}H projection from 2D HETCOR experiments on [$^{13}C_5$, 1-^{15}N] bulk Glu

The peak positions of ^{1}H projection of HETCOR spectra show an overall consistency with the ^{1}H MAS (Figure 4.23). The ^{1}H spectrum extracted from the 2D [^{1}H-^{13}C] NMR (blue) shows a peak at 3.7 ppm relatively close to the H2 of the methine observed in the 1-D proton spectrum (~ 4 ppm), and another strong one at about 14 ppm, corresponding to the proton of the side-chain –COOH (coupled with C5). The same peak is weakly observed at 4.8 ppm for the 2D [^{1}H-^{15}N] NMR spectrum, in which the NH_3^+ proton peak ~8.2 ppm is logically predominant.

Figure 4.25 shows the ^{1}H spectrum of Glu in aqueous solution. Three signals are apparent at 3.75, 2.49 and 2.09 ppm, attributable to the protons of C2, C4 and C3 respectively. The C**H** peak is a triplet as expected (it couples only to the neighboring methylene); the other two peaks show complex splittings.

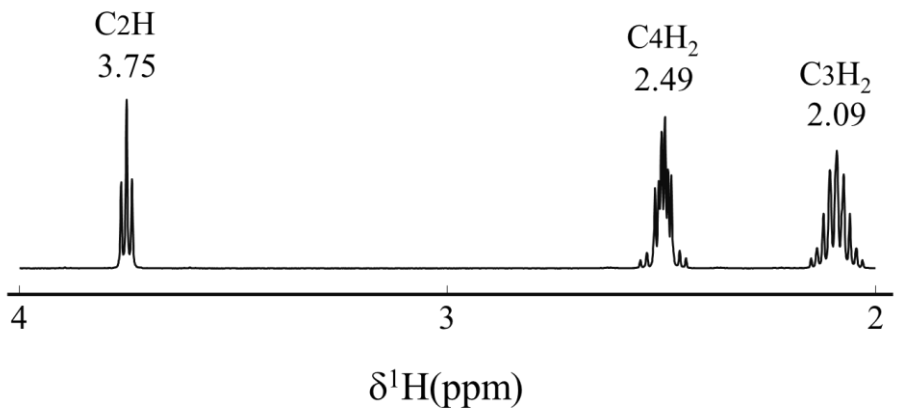

Figure 4.25. ^{1}H solution NMR spectra of an aqueous solution (0.002 mol.L^{-1}) of Glu, with assignments

IV.3.2.2.iv ^{13}C DP MAS (single pulse)

Direct polarization (single pulse) ^{13}C NMR was also performed on the enriched [$^{13}C_5$, ^{15}N] sample using different delay times. Relative intensities (area under the peak) of the C1 and C5 carbons of the α and β Glutamic acid, were plotted as a function of the recycling time (D_1) to extract T_1

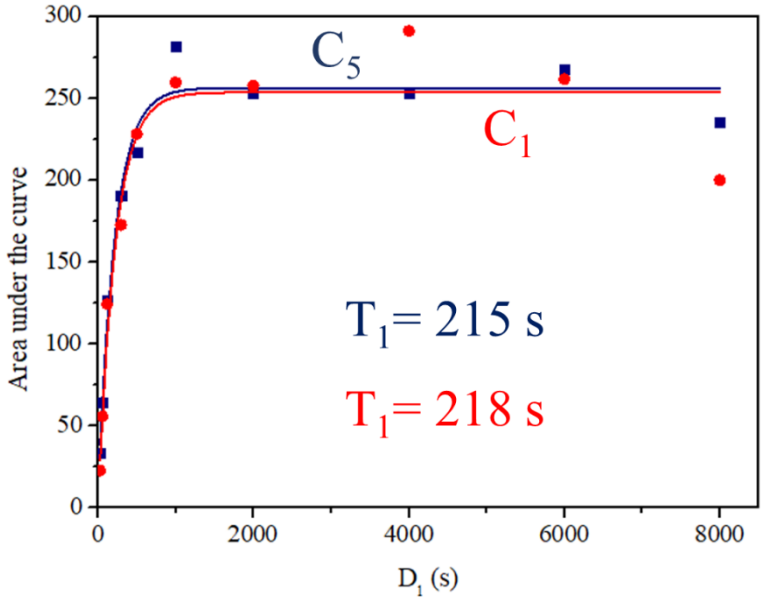

Figure 4.26. Experimental peak intensities for carbons C_1 and C_5 as a function of the recycling time D_1, and fits to the formula $M_{(D1)} = M_{(0)}(1-\exp(-D_1/T_1))$

Figure 4.26 shows the evolution of signals C1 and C5 for the sample $^{13}C_5$, 1-^{15}N bulk Glu as a function of D_1. The experimental curve was fitted with the following formula: $M_{(D1)} = M_{(0)}(1-\exp(-D_1/T_1))$, resulting in T_1 relaxation times of 215 s and 218 s for the C5 and C1 carbons respectively, i.e. very close to each other -and to the values found for the carboxylate of

Leucine. For both phases (α and β), T_1 value was the same for C1. It may also be the same for C5 which is trickier to verify since signals of both phases are superimposed.

Thus, single pulse ^{13}C NMR spectra of crystalline Glu may not be recorded with recycling times of reasonable lengths – one would need to wait at least $5T_1$, i.e. about 1000 s, before successive accumulations.

IV.3.2.2.v ^{1}H-^{13}C HETCOR

2D ^{1}H-^{13}C CP MAS HETCOR spectrum of [$^{13}C_5$, $^{15}N_1$] bulk Glu sample was recorded (Figure 4.27). The ^{13}C (horizontal) axis shows numerous correlations with the ^{1}H (vertical) axis. The carbon of the carboxylic acid moiety (C5) has a very strong correlation with the acidic proton in its –OH group, and a weaker one with the protons on the neighboring C4 methylene group. As for the carbon of the carboxylate moiety (C1), its behavior is different according to whether Glu is in the α or in the β phase. In the case of the α phase, correlation is with the neighboring H2 (methine) proton, but even more strongly with an acidic –COOH proton. This cannot be the –COOH in the same molecule which is too distant; rather, it is the –COOH of a neighboring molecule that acts as an H-bond donor to the carboxylate.

In the case of the β phase, the two correlations just mentioned are still observed, but in addition there is a strong cross-peak with the ammonium protons at 8.4 ppm. The C_1OO^- in the β phase shows a stronger interaction with the ammonium moiety; as shown in Table 4-6 , the distance between the carboxylate (C1) oxygens and the ammonium hydrogens are smaller than the distance between the carboxylic acid (C5) oxygen and the ammonium hydrogen. This indicates the hydrogen bond between the carboxylic acid (C1) and the ammonium hydrogens is much stronger in the β-phase in agreement with the intense cross-peak observed. It is an interesting example of HETCOR providing information on the H bonding pattern.

In the aliphatic region, the side chain carbons (C2, C3 and C4) show a common cross peak at 3.6 ppm contributing to their respective protons (H2, H3 and H4). Furthermore, a broader peak was seen around 10.6 ppm covering a much wider aspect of the ^{1}H (vertical) axis and according to the computational data performed on α and β Glutamic acids (ANNEX-Table 2), the position is closely related to the assigned ammonium protons (NH_3^+) even if slightly shifted compared to the corresponding cross-peak in the carboxylate region.

C-O---H-N (Å)	α-Glutamic Acid	β-Glutamic Acid
C(1)O-O(1)---H(1)-N	1.714	1.801
C(1)O-O(2)---H(2)-N	1.756	1.834
HO-C(5)O---H(3)-N	1.870	1.840

Table 4-6. C-O---H-N distance in Å for both α and β Glutamic acid

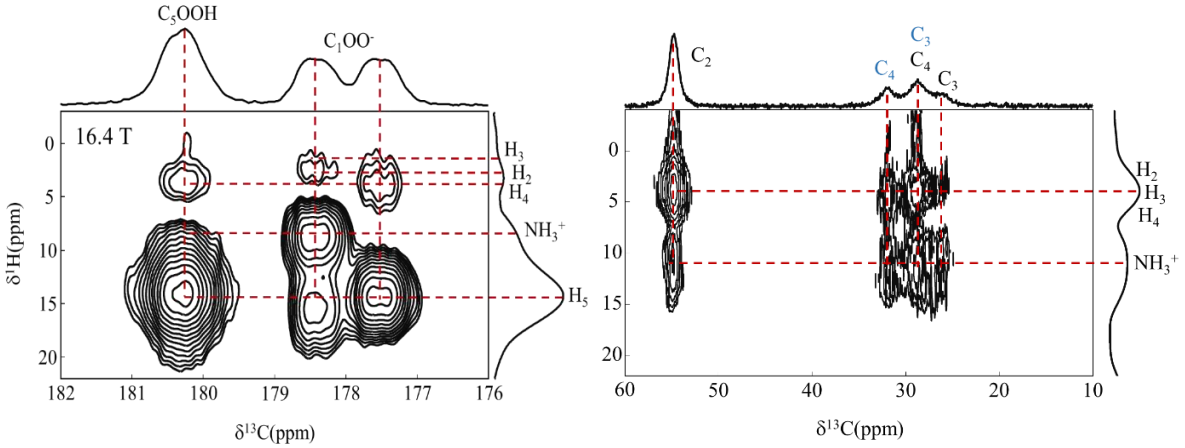

Figure 4.27. 2D ^{1}H-^{13}C CP MAS HETCOR experiment recorded at 16.4 T for [$^{13}C_5$, 1-$^{15}N_1$] bulk Glu in the carboxylic and the aliphatic region

IV.3.2.2.vi ^{1}H-^{15}N HETCOR

Figure 4.28 shows the 2D ^{1}H-^{15}N CP MAS HETCOR 2D spectrum of the fully enriched bulk Glu. While weak couplings with other protons may be present, the only intense one is with the protons resonating at about 9 ppm, which we have assigned to the $–NH_3^+$ group.

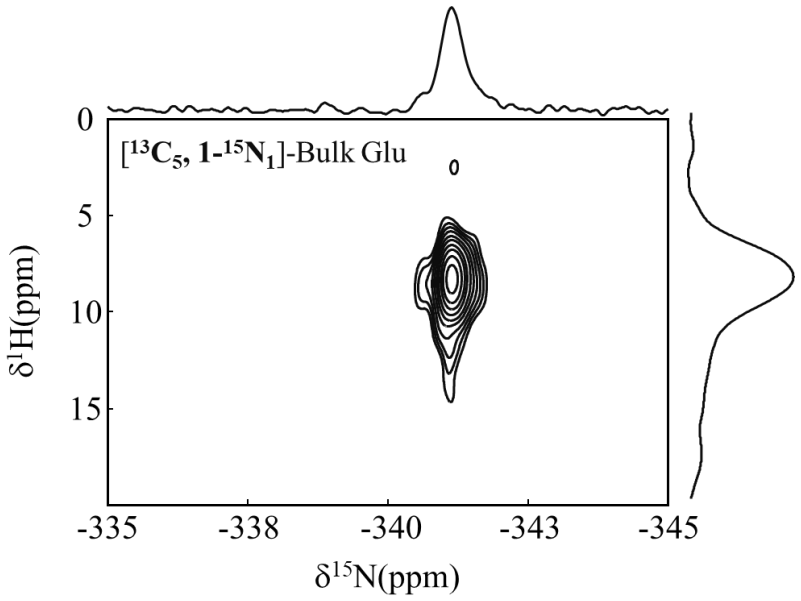

Figure 4.28. 2D ^{1}H-^{15}N CP MAS NMR HETCOR spectrum of [$^{13}C_5$, 1-^{15}N] bulk Glu

IV.3.2.3 Solid-state NMR of Glu/SiO_2 after ND treatment

For Glu/SiO_2, it was found expedient to first discuss the spectra of the ND samples. The effect of nitrogen drying (ND) will be treated in the following paragraph.

IV.3.2.3.i ^{13}C CP MAS NMR

Our aim was to study different loadings of Glu on SiO_2 in order to extract the maximum amount of information on the interaction between Glutamic acid and silica. According to Sakhno *et al*,[92] above 7%, Bragg peaks appear in the XRD. Figure 4.29 shows the ^{13}C CP-MAS NMR spectrum of 7% [$^{13}C_5$, ^{15}N] Glu/SiO_2 ND recorded at 16.4 T, compared with the bulk enriched Glu. They are very similar, indicating that the spectrum of this high Glu loading sample is dominated by the signals of the bulk Glu crystals, and any adsorbed forms are in too small amount to be observed. In fact, our own XRD study, detailed in §IV.2.1, later revealed that Bragg peaks of bulk Glu were already apparent for a 3% loading. Furthermore, we will show later that NMR may be sensitive to small amounts of crystallites (or very small crystallites) that are not visible by XRD, an observation that has also been made for Leu/SiO_2 (Ch. III, § III.3.2.2).

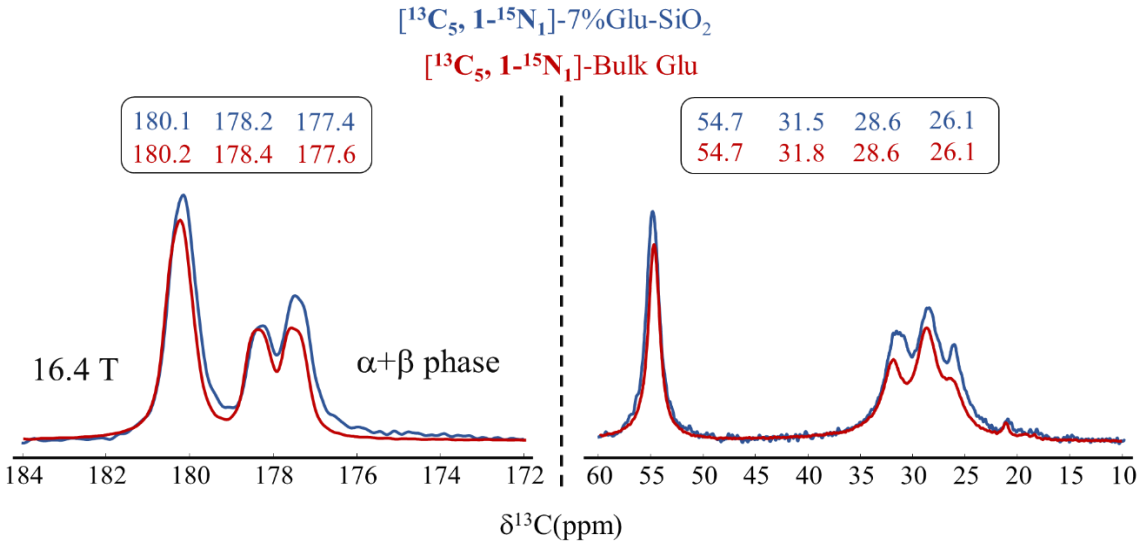

Figure 4.29. ^{13}C CP MAS NMR spectra of [$^{13}C_5$, $^{15}N_1$] bulk Glu and 7% [$^{13}C_5$, $^{15}N_1$] Glu/SiO_2 ND in the carboxylate and the aliphatic regions recorded at 16.4 T

It is intriguing to notice that a mixture of the α and β polymorphs is observed in the Glu/SiO_2 sample, in relative amounts very similar to the starting bulk Glu, although the latter has been completely dissolved in water prior to deposition on the silica surface. The α-phase is considered to be metastable and should readily transform to β-phase upon coming into contact with an aqueous solution: instead, the C1-carboxylate peak corresponding to the α-phase at ~177.4 ppm remains strongly evident even after Glu is adsorbed. Perhaps, although the deposition solution appears to be clear, some very small nuclei of each crystal phase remain present in solution.

Since we are interested in characterizing the adsorbed form, the percentage loading on the silica surface was decreased. Figure 4.30 compares the spectra of [$^{13}C_5$, ^{15}N] Glu adsorbed on the silica surface at 0.3% and 7% loadings. When decreasing the loading to 0.3%, three signals are apparent in the carboxyl region: most conspicuously, a new signal at 174.2 ppm was detected that does not correspond to any of the crystalline forms of Glu. In contrast, the C1 carboxylate of the bulk α form is absent (no signal around 177.4 ppm). This spectrum is compatible with that of 0.4% Glu/SiO_2 published by Bouchoucha *et al.*,[86] only better resolved due to the higher field.

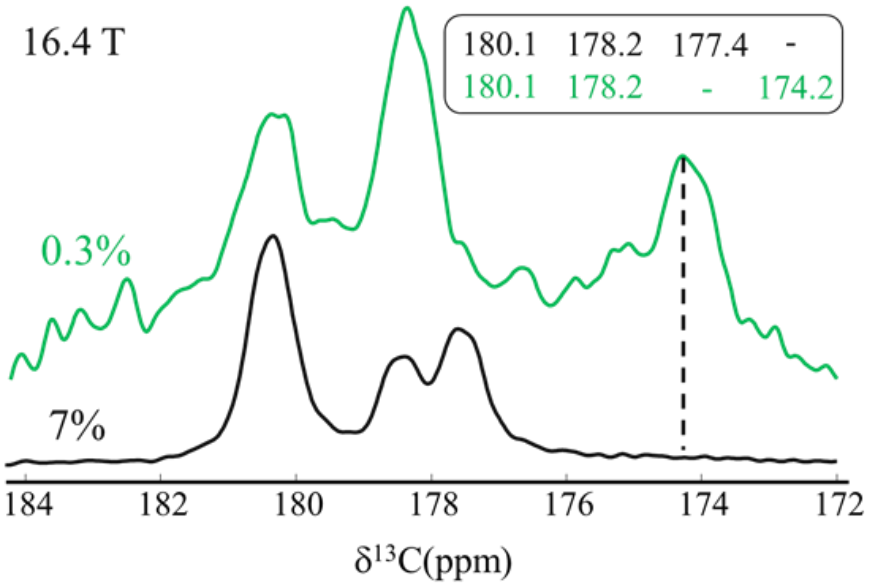

Figure 4.30. ^{13}C CP MAS NMR spectra at 16.4 T of [$^{13}C_5$, ^{15}N] Glu/SiO_2 in the carboxylate region at two different loadings – 7% (black) and 0.3% (green)

If the 174.2 ppm peak cannot be due to crystallized Glu, it falls close to the signal of the C1 carboxylate in aqueous solution. Since for the latter, the C5 carboxylic acid was found at 178.0 ppm, we hypothesize that the spectrum of this low-loading sample contains two components in approximately equal amounts, bulk β-Glu and Glu in hydrated environment. It should be noticed that the presence of this signal using the CP sequence indicates a reduced mobility (in opposition to the solution). The peak at 180.1 ppm would then correspond to the C5 carboxylic acid of β-Glu; the peak at 178.2 ppm, to a superposition of the C1 carboxylate of β-Glu and the C5 carboxylic acid of solution-like Glu, and the peak at 174.2 ppm to the C1 carboxylate of solution-like Glu.

For intermediate loadings (1% and 3% Glu), we only have low-field ^{13}C spectra (at 7 T). They are shown in Figure 4.31, together with the 7 T spectrum of the bulk [$^{13}C_5$, 1-^{15}N] Glu. As we have mentioned previously, strong J couplings result in a complex lineshape at low field. Both 3% and 1% Glu/SiO_2 exhibit spectra that look very much like that of bulk [$^{13}C_5$, ^{15}N] Glu, without any evidence of a solution-like signal around 174 ppm. Thus, insofar as the different magnetic fields allow to conclude, 3% and 1% [$^{13}C_5$, 1-^{15}N] Glu/SiO_2 look more like the 7% than the 0.3% sample.

.

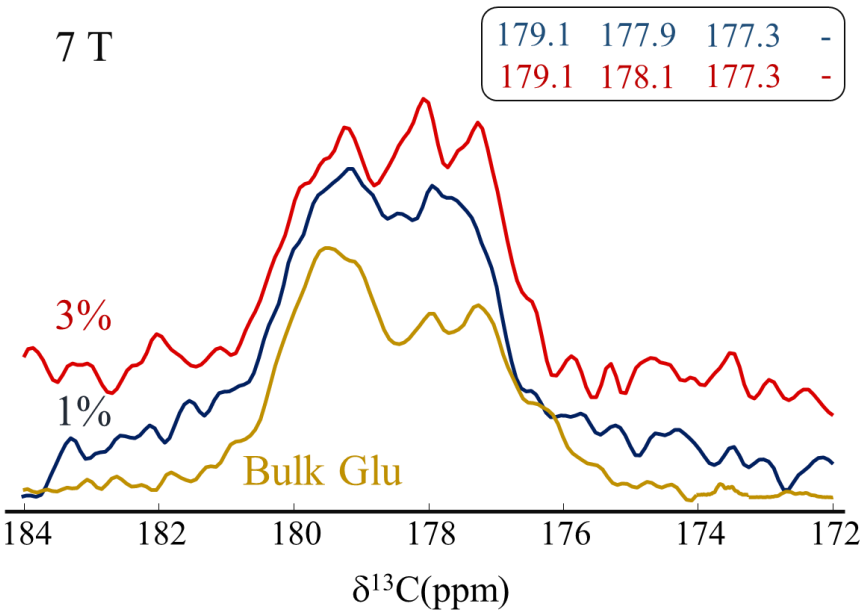

Figure 4.31. ^{13}C CP MAS NMR spectra at 7 T in the carboxylate region of bulk [$^{13}C_5$, 1-^{15}N] Glu and [$^{13}C_5$, 1-^{15}N] Glu/SiO_2 at two different loadings

Since the origin of peak splittings in low-field spectra lies in the J-coupling between neighboring ^{13}C nuclei, we also studied samples based on Glu molecules that were not fully enriched in ^{13}C. Figure 4.32 shows the low-field ^{13}C spectra of three Glu/SiO_2 samples prepared from natural abundance Glu. It must be noted that the 1% and 7% loadings were prepared from the β crystal form, and the 3% loading from the α form (Recr. Glu). Yet all three spectra are similar, and they only show the peaks typical of the β crystal form; neither those of the α form, nor the solution-like signal at 174 ppm are observed. It is particularly puzzling that while the mixture of the α and β phase in [$^{13}C_5$, 1-^{15}N] Glu seems to keep a "memory" of its initial crystal state, this is not the case of the pure α phase in natural abundance Glu.

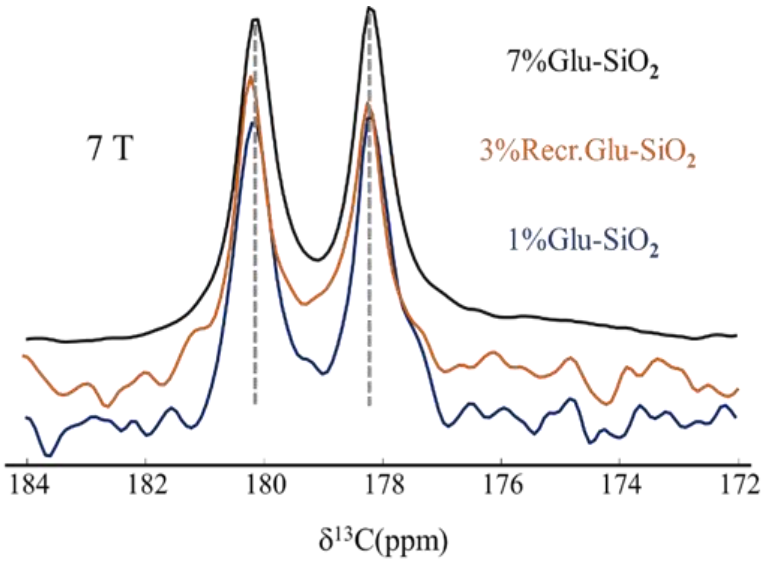

Figure 4.32. ^{13}C CP MAS NMR spectra of natural abundance Glu/SiO_2 at different loadings in the carboxylate region (recorded at 7 T)

Finally, we also prepared 1% Glu/SiO_2 from Glutamic acid enriched solely on the C_1 ([1-$^{13}C_1$]). Its spectrum is compared with that of the non-enriched 1% Glu/SiO_2 in Figure 4.33.

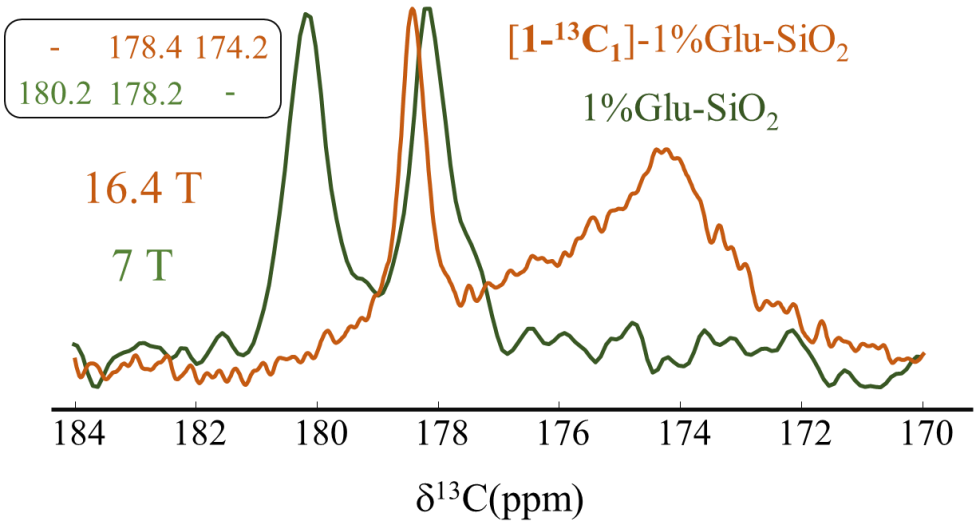

Figure 4.33. ^{13}C CP MAS NMR spectra of 1% [1-$^{13}C_1$] Glu/SiO_2 at 16.4 T compared with a non-enriched 1% Glu/SiO_2 at 7 T in the carboxylate region

The natural abundance sample exhibits two narrow signals at 180.2 ppm and 178.2 ppm. They correspond to C5 and C1 in the β-crystalline form respectively.

In the spectrum of the selectively enriched sample, we expect to see only the signal(s) of the C1 carbon, where the NMR-active nucleus is about 100 times more concentrated than on other positions. Indeed, it does not show the signal at ~180 ppm that we assigned to the C5 –COOH; on the other hand, the narrow signal at 178.2 due to the C1 carboxylate in the β crystal form is observed. But we also see a signal at 174.2 ppm that would then correspond to C1 in the "solution-like" form that we have already mentioned. This signal is now significantly broader than in solution, suggesting that even if C1 is surrounded with water molecules, it's nonetheless relatively rigid.

It is a challenging task to propose a model able to rationalize all these various observations. The most likely possibility is that Glu can easily pass from a solution-like environment to a state with restricted mobility, perhaps depending on small differences in the hydration state that are not perfectly controlled in the ND drying procedure – more on this in the next paragraph. The reader may remember that Leucine-containing samples (Leu/SiO_2, see Chapter III, § III.3.2.2 i) showed a predominant broad component that we assigned to the molecularly adsorbed form, already after ND drying. In the case of Glu/SiO_2, the only spectrum that shows a broad signal is the one at 174 ppm in Figure 4.33: perhaps it captures the inception of Glu adsorption, involving the C1 carboxylate but not the C5 carboxylic acid.

IV.3.2.3.ii ^{13}C DP MAS NMR

We have previously determined (Figure 4.26) that the T_1 relaxation time of both crystalline forms of Glu is high, over 200 s. Thus, performing direct polarization acquisition with short recycle delays should remove the NMR signals of the crystals, possibly preserving those of Glu adsorbed on silica and/or in solution-like environments as previously observed in the case of Leucine. This was done for two differently enriched samples: 1% [1-^{13}C, ^{15}N] Glu/SiO_2 (Figure 4.34) and 1% [$^{13}C_5$, ^{15}N] Glu/SiO_2 (Figure 4.35).

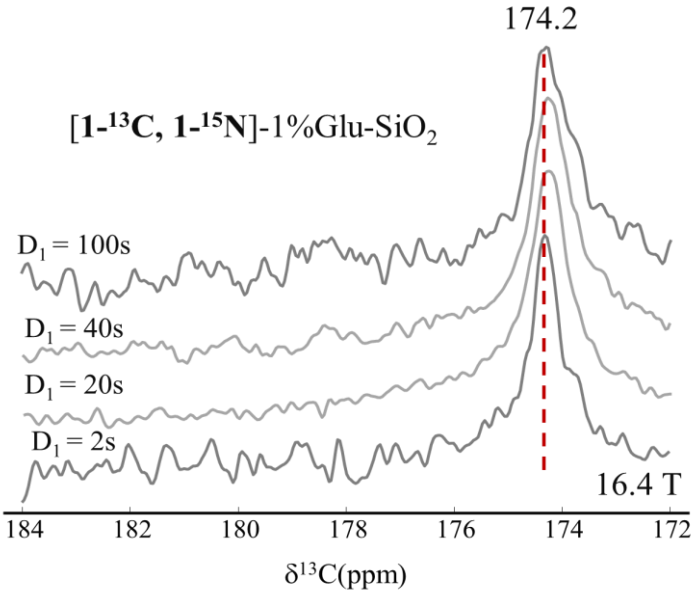

Figure 4.34. ^{13}C DP MAS NMR spectra of 1% [1-^{13}C, 1-^{15}N] Glu/SiO_2 in the carboxylate region at 16.4 T at different recycling delay times (D_1)

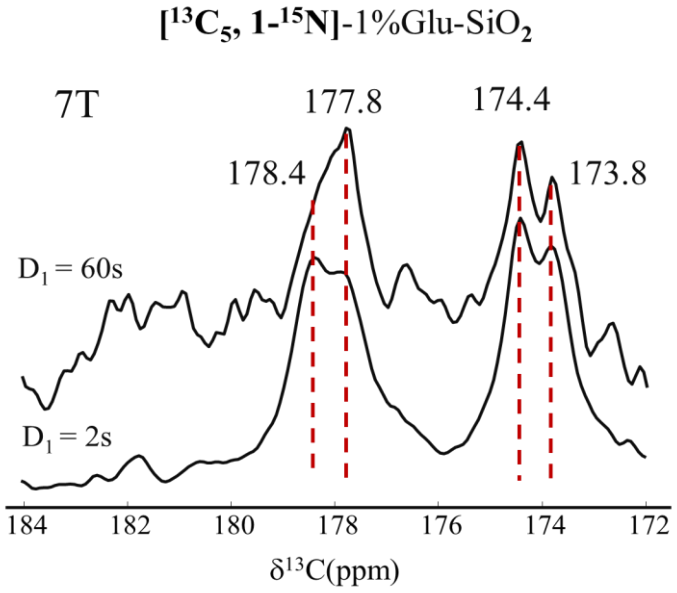

Figure 4.35. ^{13}C DP MAS NMR spectra of 1% [$^{13}C_5$, 1-^{15}N] Glu/SiO_2 in the carboxylate region at 7 T at different recycling delay times (D_1)

In both cases, the observed signals positions are consistent with those observed in aqueous solution. For 1% [1-^{13}C, ^{15}N] Glu/SiO_2, only the C1 carboxylate signal can be observed because the C5 position is not enriched. For 1% [$^{13}C_5$, ^{15}N] Glu/SiO_2, both are visible (with J coupling since all carbons are ^{13}C).

In summary, as anticipated, short recycle delay DP experiments erase the signals of crystalline Glu. They did not eliminate the peak at 174.2 ppm (Figure 4.21), nor the liquid-like peak at 178 ppm (visible when the C5 was enriched).

A question arises here. DP experiments reveal that a substantial amount of the species giving a resonance at 174 ppm is present in 1% Glu/SiO_2. Why then is no such signal detected e.g. in the CP spectrum of Figure 4.32? We believe that in high hydration conditions, the liquid-like species cannot be evidenced by CP, probably because of fast molecular reorientation, causing an efficient averaging of the $^{1}H-^{13}C$ dipolar interactions. The same effect was observed by Folliet *et al.*[91] for Glycine deposited on mesoporous silica. There is possibly a mixture of "rigid solvated", or molecularly adsorbed, Glu in interaction with the surface (which would explain less mobility and CP detection e.g. in the red spectrum of Figure 4.33), "solution like" Glu, more mobile (not detected by CP) and crystalline Glu. Molecularly adsorbed and solution-like Glu could easily transform into one another depending on the water content of the sample. DP and CP-MAS NMR would not “see” the same populations, with DP unable to detect crystalline Glu (at low D1 values), and CP unable to detect the solution-like form.

At low Glu loadings, solution-like/molecularly adsorbed Glu would be present in amounts comparable to crystalline Glu. Even at the lowest loading we tested, crystalline Glu is still detected by NMR (Figure 4.30), while it is not apparent on the X-Ray diffractograms. The signal of the solvated phase of Glutamic acid is dominated by the bulk Glu spectrum in CP at high loadings.

This conclusion is confirmed by the comparison of the CP and DP spectra of 1% in the aliphatic region (Figure 4.36). The DP spectrum only shows peaks at positions very close to Glu in solution; in contrast, the CP spectrum has a strong component at 28.1 ppm that is close to the methylene carbons in the crystalline phases.

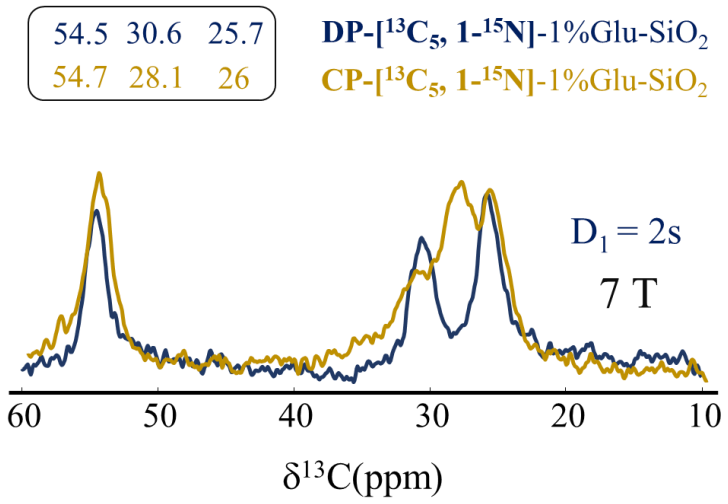

Figure 4.36. ^{13}C DP and CP MAS NMR spectra of 1% [$^{13}C_5$, 1-^{15}N] Glu/SiO_2 in the aliphatic region at 7 T

Finally, the comparison of the CP and DP spectra of a higher-loading, 3% [$^{13}C_5$, 1-^{15}N] Glu/SiO_2 (Figure 4.37) confirms all of the above conclusions.

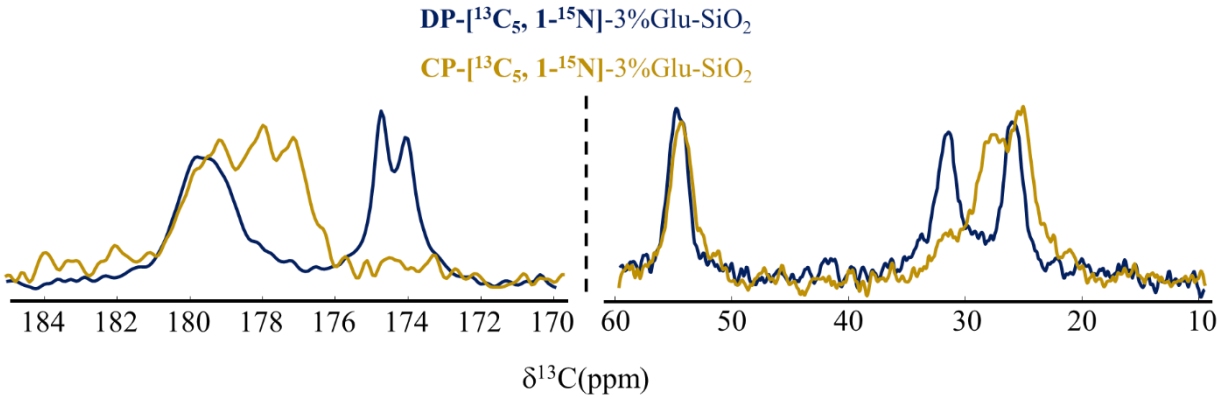

Figure 4.37. ^{13}C DP and CP MAS NMR spectra of 3% [$^{13}C_5$, 1-^{15}N] Glu/SiO_2 in the carboxylate and aliphatic regions at 7 T

IV.3.2.3.iii ^{15}N CP MAS NMR

Figure 4.38 compares the peak positions in two [$^{13}C_5$, ^{15}N] Glu/SiO_2 samples, with high and low loadings, with those in bulk Glu. It also illustrates the effect of the external magnetic field which clearly shows a higher resolution effect and more intense peaks at 16.4 T rather than 7 T.

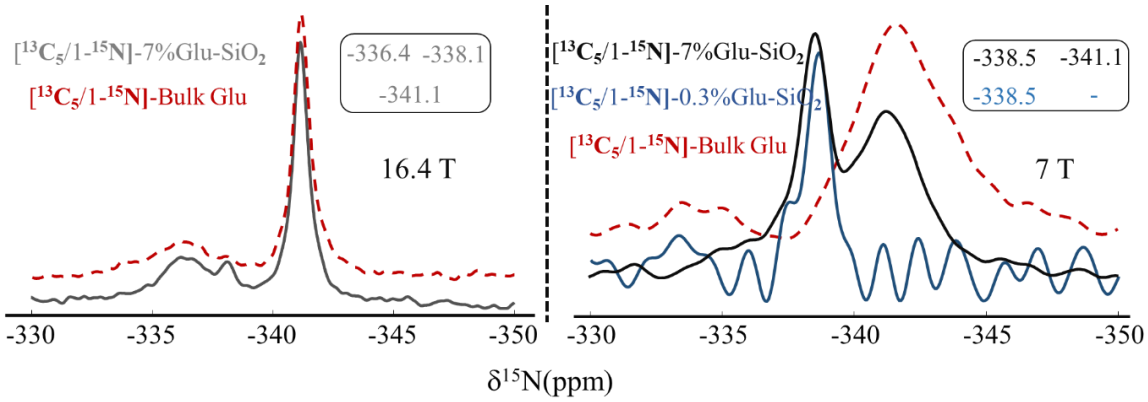

Figure 4.38. ^{15}N CP MAS NMR spectra of different loadings of Glu/SiO_2 at 7 and 16.4 T

At 16.4 T, the spectrum of the high-loading 7% Glu/SiO_2 sample is mostly similar to that of the corresponding bulk Glu, as was also the case for ^{13}C. A small, sharp signal is however apparent at -338.1 ppm. Its sharpness would be compatible with a solution-like form; however, the chemical shift is not exactly the same as that of Glu in aqueous solution (-340.3 ppm).

At 7 T, the same 7% Glu/SiO_2 still shows two signals at the same position, but their respective proportions are very different. The sharp signal at about -338 ppm is much more intense relative to the β crystal form-like one than was the case at high filed.

Finally, the 7 T spectrum of low-loading 0.3% [$^{13}C_5$, 1-^{15}N] Glu/SiO_2 only shows the sharp liquid-like signal, with no peak at the position of the crystal form.

IV.3.2.3.iv ^{1}H MAS NMR

The ^{1}H MAS NMR spectra of ND Glu/SiO_2 samples were not very informative, as they mostly showed a strong peak at + 4.5 ppm due to adsorbed water (in exchange with associated silanols). When the loading was high enough, as already observed for Leu/SiO_2, the protons of the methylene groups in the side chain of Glu gave an additional narrow signal.

IV.3.2.4 Solid-state NMR of Glu/SiO_2 after VD treatment

IV.3.2.4.i ^{13}C CP MAS NMR

Figure 4.39 compares the spectra at 7 T of 0.3% and 1% [$^{13}C_5$, 1-^{15}N] Glu/SiO_2 after vacuum drying (VD), with those previously discussed for the same samples after nitrogen drying. A very broad signal is present after VD, similar to the one observed previously in the case of Leu/SiO_2, and that we had attributed to adsorbed forms in a range of different surface environments. The broadening range extends roughly from 170 ppm to around 183 ppm, including the bulk peak positions of the α and β forms. It is difficult to say if the crystal forms are present too due to the poor signal/noise ratio in these spectra.

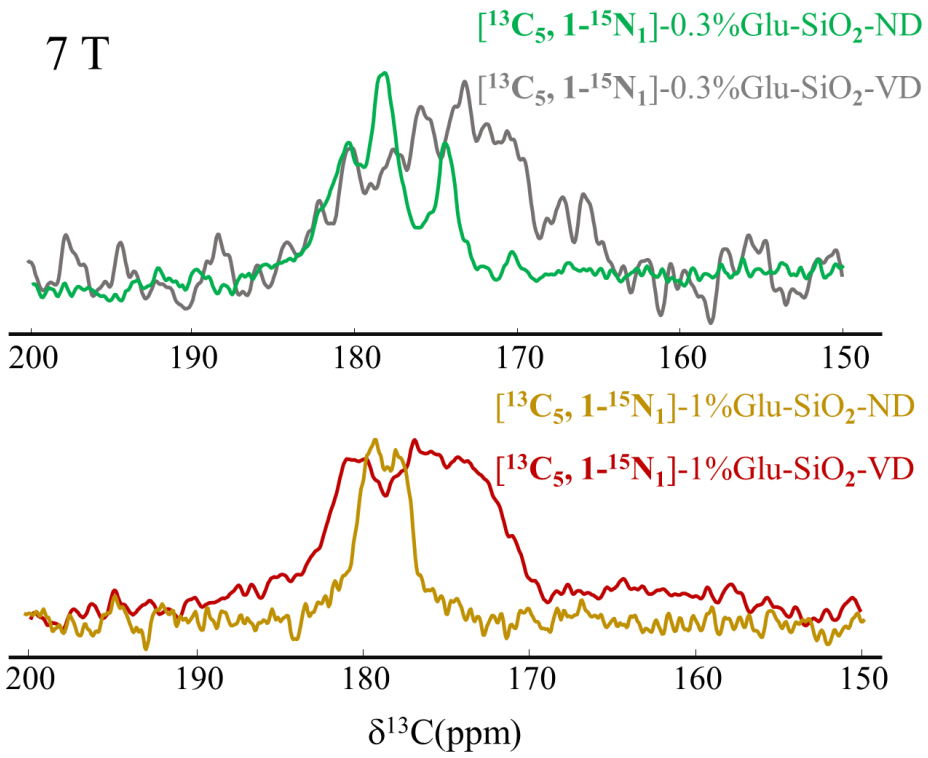

Figure 4.39. ^{13}C CP MAS NMR spectra at 7 T of 0.3% and 1% [$^{13}C_5$, ^{15}N] Glu/SiO_2 in the carboxylate region after VD, compared to the same after ND

At higher magnetic field (16.4 T) the resolution is improved (Figure 4.40). In these conditions, 1% [$^{13}C_5$, ^{15}N] Glu/SiO_2 clearly shows peaks characteristic of crystalline Glu (with the β form in majority but some α form also present) superimposed with the broad component.

In the aliphatic region, the VD treatment resulted in the two methylene carbons (in C3 and C4) giving an overlapped peak around ~27.5 ppm. Rather than to a broadening of the crystal peaks, which is not observed in the carboxylate region, this is probably due to overlap with the methylenes of the adsorbed form.

Thus, Figure 4.40 indicates that for this VD sample, crystalline Glu, which was already observed after the ND treatment, is still present. It seems likely then that the adsorbed form to which we assign the new, broad signal, comes from the solution-like Glu that was also detected in CP spectra (Figure 4.30 and Figure 4.33).

It is apparent again that the use of high fields is very desirable in order to obtain precise information on the speciation of silica-deposited amino acids.

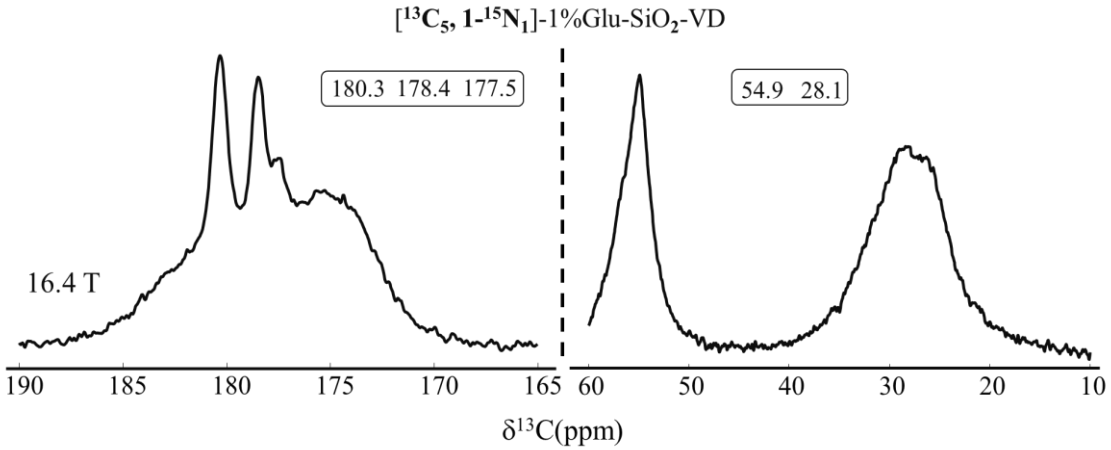

Figure 4.40. ^{13}C CP MAS NMR spectra of 1% [$^{13}C_5$/1-^{15}N] Glu/SiO_2 vacuum dried in the carboxylate and the aliphatic region at 16.4 T at MAS values of 14 kHz

IV.3.2.4.ii ^{13}C DP MAS NMR

Figure 4.41 compares the high-field ^{13}C spectrum of the low-loading Glu/SiO_2 sample obtained by direct polarization with its counterpart obtained by proton cross-polarization (the latter is the same as depicted in Figure 4.40).

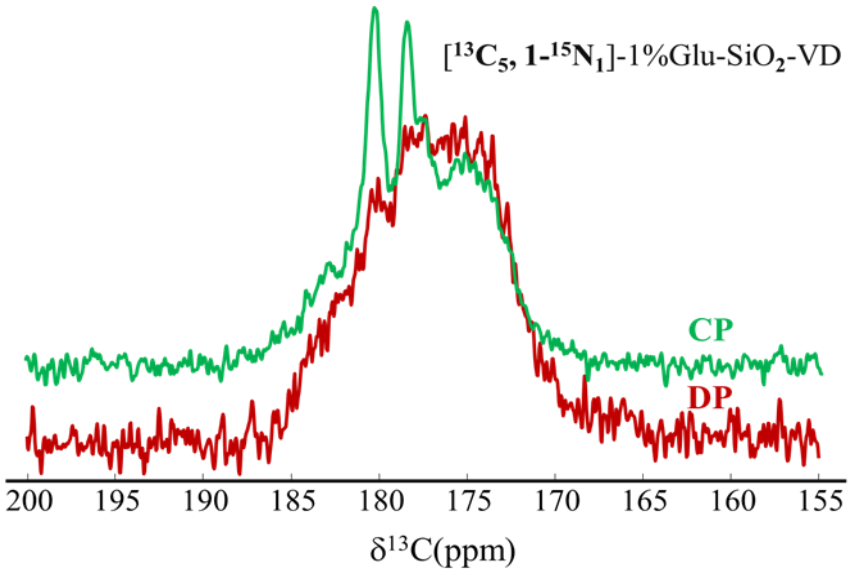

Figure 4.41. ^{13}C MAS NMR spectra at 16.4 T of 1% [$^{13}C_5$, 1-$^{15}N_1$] Glu/SiO_2 after VD treatment in the carboxylate region: comparison of CP and DP

As could be expected, and as already observed for other systems, the sharp signals of the crystal forms disappear, but the broad component we attributed to molecularly adsorbed Glu is still observed.

IV.3.2.4.iii ^{15}N CP-MAS NMR

^{15}N spectra of vacuum dried samples (Figure 4.42) gave consistent results with ^{13}C in that broadening is observed after V.D in both samples (0.3% and 1%).

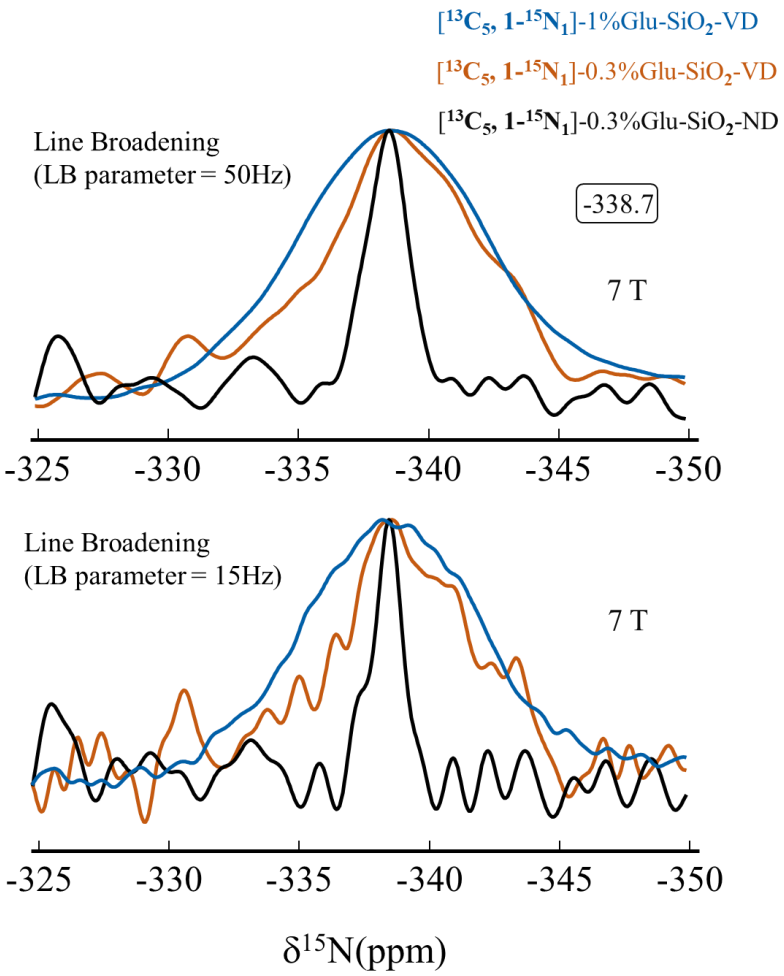

Figure 4.42. ^{15}N CP-MAS NMR spectra of 0.3 and 1 % [$^{13}C_5$, 1-^{15}N] Glu/SiO_2 samples after VD treatment, compared with 0.3 [$^{13}C_5$, 1-^{15}N] Glu/SiO_2 sample after ND

Here, there is no evidence of a sharp peak that could be assigned to a crystal form, even for the 1% loading sample where such signals were apparent in the corresponding ^{13}C samples (Figure 4.41).

IV.3.2.4.iv ^{1}H MAS NMR

Figure 4.43 shows the ^{1}H MAS spectrum of ND and VD 1% Glu/SiO_2 having a spinning speed of 10 kHz but at different fields. The very strong peak at 4.5 ppm in the ND sample decreases and is shifted to 3.4 ppm upon the more severe VD drying, which is probably due to the decrease in the number of water molecules in the H-exchanging clusters between associated silanols and physisorbed waters. A peak appears at 1.8 ppm, the position usually assigned to dehydrated isolated silanols. These phenomena are more strongly marked than for Leu/SiO_2 (§ III.3.2.1.iii). A smaller signal at 1.2 ppm is close to one of the methylene signals in bulk-Glu (§ IV.3.2.1.iii) although at significantly lower chemical shift than the calculated value.

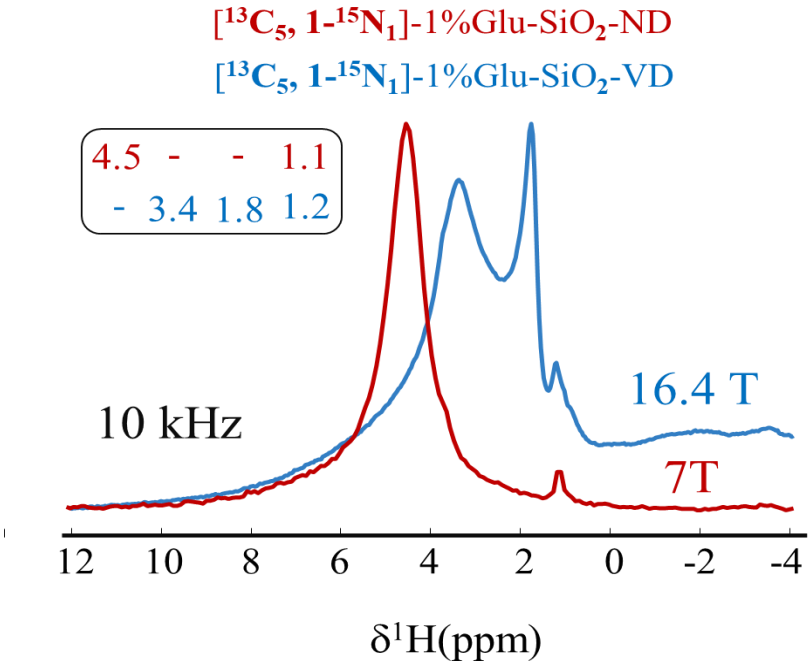

Figure 4.43. ^{1}H MAS NMR spectra of different loadings of [$^{13}C_5$,^{15}N] Glu/SiO_2 after ND and VD drying

IV.3.2.4.v ^{1}H-^{13}C and ^{1}H-^{15}N 2D-HETCOR

Figure 4.44 shows the 2D ^{1}H-^{13}C (carboxylate region) of a low Glu loading sample (1% Glu/SiO_2). The projection onto the ^{13}C chemical shift dimension is very similar to the ^{13}C CP-MAS previously reported (see Figure 4.40), showing the sharp peaks of crystalline Glu forms superimposed to the broad signal of the adsorbed form. We are particularly interested in the adsorbed form, and the examination of the HETCOR pattern shows that peaks in its carboxylate region (around 175 ppm) mostly correlate with the protons resonating at 4.0 and 7.3 ppm. The first set corresponds to the associated silanols + water clusters (suggesting that the carboxylate group is H-bonded to the surface), the second one to the ammonium protons. In comparison, the carboxylate protons in Leu/SiO_2 had a stronger correlation with the C3 methylenes than with the ammonium ones. One possibility is that the carboxylate does not interact with the ammonium of the same molecule, but (through H-bonding) with those of (an)other Glu molecule(s). This would happen if Glu molecules had a strong tendency to form clusters on the surface even at low loadings, a behavior that has already been hypothesized.[86] Finally, the ^{13}C signals above 180 ppm, probably attributable to the C5 carboxylic group of the adsorbed form, do not show any measurable correlation with protons. This might mean that the side chain –COOH does not significantly interact with the surface.

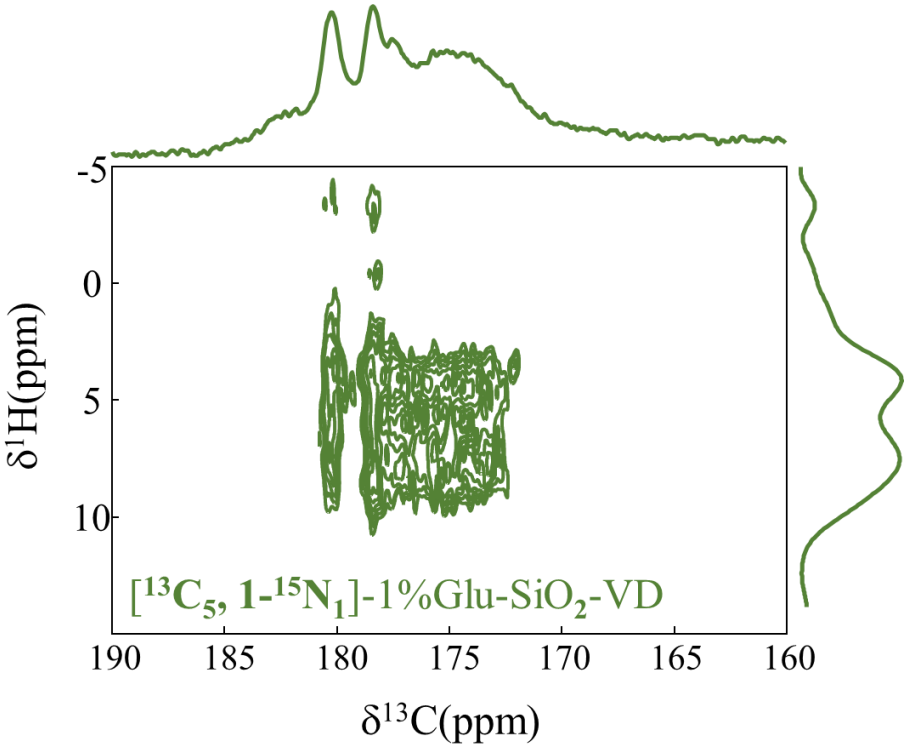

Figure 4.44. 2D ^{1}H-^{13}C HETCOR CP MAS NMR spectra of 1% [$^{13}C_5$, 1-$^{15}N_1$] Glu/SiO_2 after VD

IV.4 Computational Approach

In this part, we report on the designing of models containing the amino acid Glutamic acid (Glu) on the silica surface. As was done in the previous chapter on Leucine, both anhydrous and microsolvated Glutamic acid were investigated. Quantification of the minimal amount of water needed to completely solvate the amino acid was an initial question to be raised. In addition to the two amino acid moieties (carboxylic acid $–COO^-$ and the ammonium $–NH_3^+$), Glutamic acid contains an acidic side chain –COOH which may be able to contribute to adsorption. In solution at natural pH, this moiety remains protonated, as it does in the two crystalline phases. The aqueous phase pKa of the side chain –COOH/$-COO^-$ couple being only 4.07, deprotonation of this side chain certainly cannot be excluded; but the IR evidence presented in § IV.3.1 indicates that –COOH groups are still present in high quantity in Glu/SiO_2. Therefore, we used as an initial configuration Glutamic acid in the $H_2Glu^{\pm}$ zwitterionic form, i.e. a carboxylate, an ammonium and a protonated side chain carboxylic acid group.

Globally 26 different models were run, with 13 of them being anhydrous (containing no water) while the rest (13 models) are microsolvated (containing water). Based on previous experience with the Leu/SiO_2 system, we mostly tested models with 12 co-adsorbed water molecules. This is because we had observed that Leu/SiO_2 was still significantly stabilized up to 10 water molecules per Leu; in addition, Glu has one additional hydrophilic group that might specifically interact with additional water molecules.

IV.4.1 Adsorption energies and molecular configurations

IV.4.1.1 Anhydrous systems

The models designed were based on a simple protocol: to begin with, Glutamic acid was adsorbed in the zwitterionic state. Secondly, we considered all possibilities arising from the interaction of 3 different functional groups on the Glutamic acid and 2 different silanol surface groups as adsorption sites. This gives statistically a distribution of 12 different models to start with. After molecular optimization, energies of adsorption (Ea) and number of hydrogen bonds (HB) were detailed for each model as explained in the paragraphs below.

All 13 anhydrous models (no water) after molecular optimization are shown with their energies of adsorption (Ea) in Figure 4.45.

A

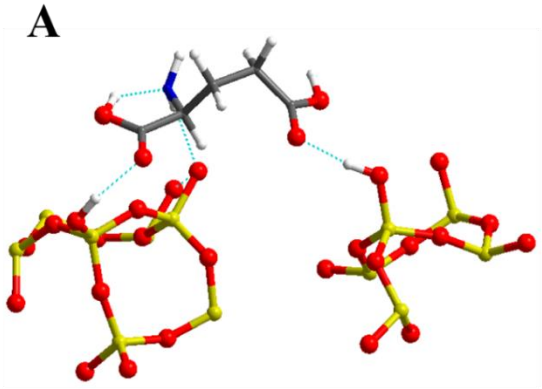

Ea = - 3.71 eV

B

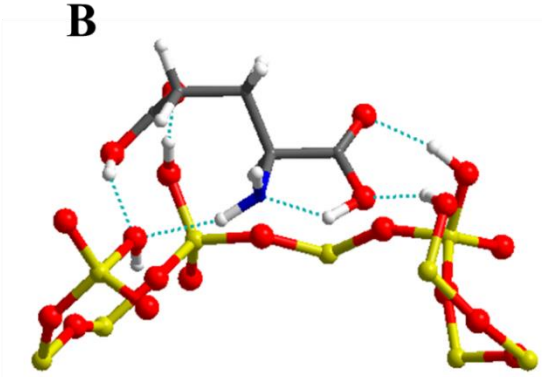

Ea = - 4.06 eV

C

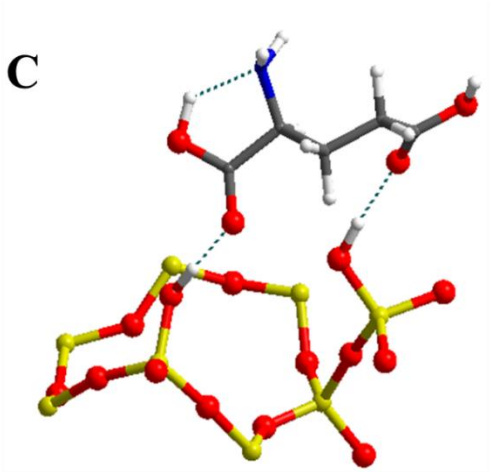

Ea = - 3.06 eV

D

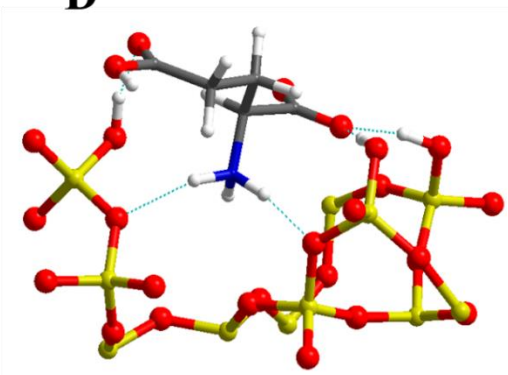

Ea = - 4.08 eV

E

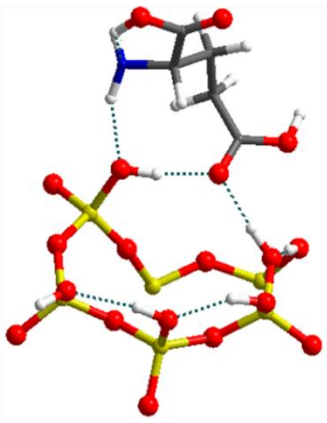

Ea = - 3.60 eV

F

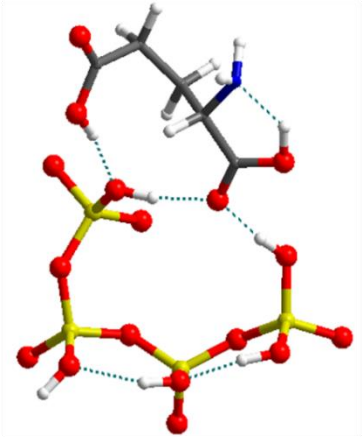

Ea = - 3.74 eV

G

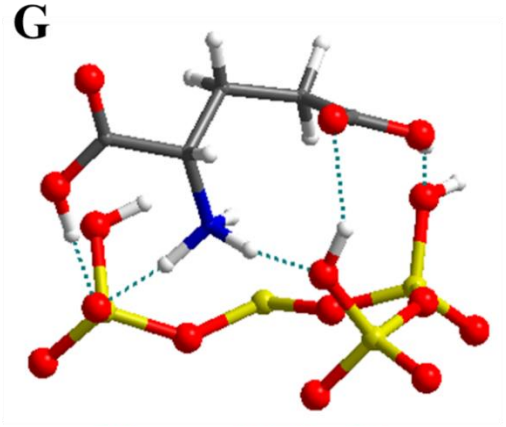

Ea = - 3.71 eV

H

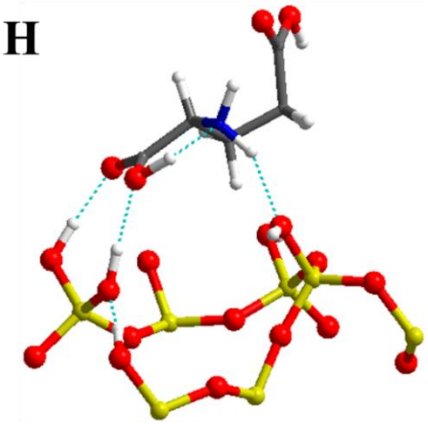

Ea = - 3.97 eV

I

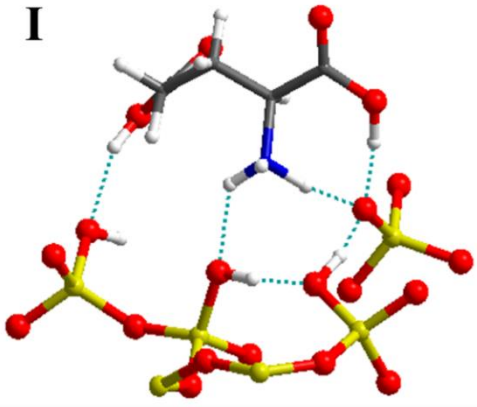

Ea = - 3.70 eV

J

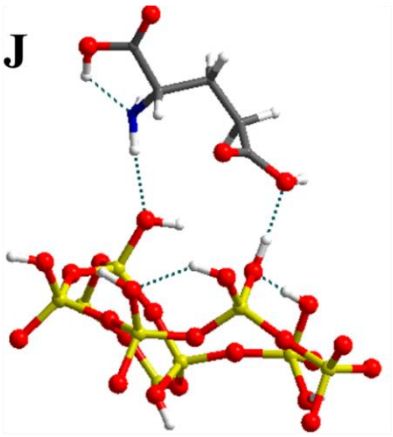

Ea = - 2.68 eV

K

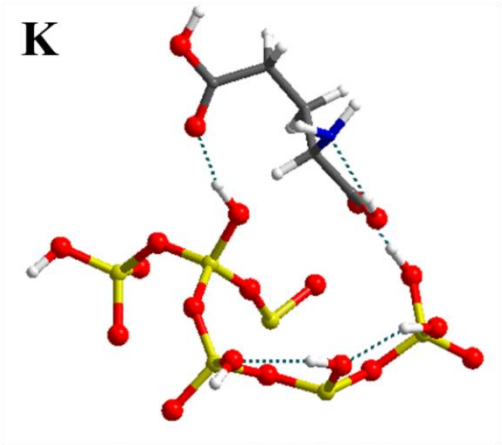

Ea = - 3.34 eV

L

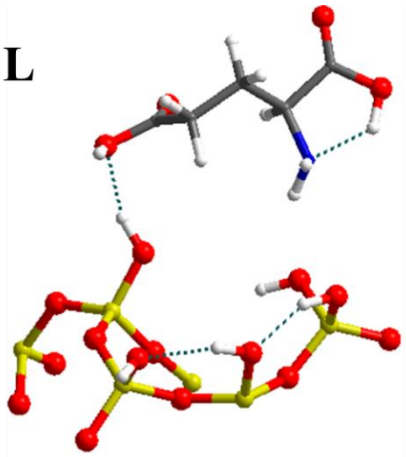

Ea = - 2.75 eV

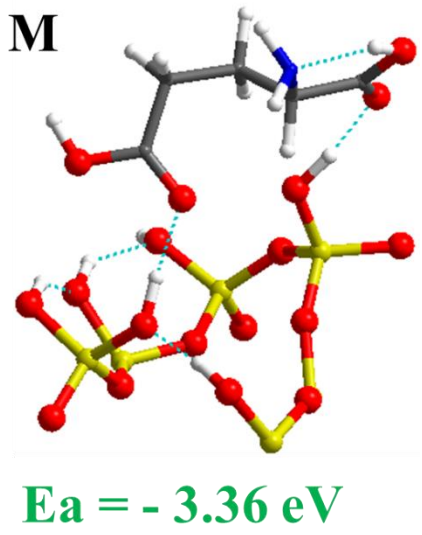

Figure 4.45. Anhydrous models for Glu/SiO_2 with their Ea (Energy of adsorption) after static optimization

Hydrogen bonding seems to be a strong factor in the stabilization of the molecule since increasing numbers of H-bonds result in an increase in the energy of adsorption (in absolute value). Most of the Glutamic acid in the models (A to M) converted to the neutral form, but some preferred to stay zwitterionic or cationic: they correspond to one of the 4-H bond configurations, and both of the 5-H bond configurations.

In Figure 4.46, adsorption energies are plotted for the different models (A to M), as a function of the number of hydrogen bonds and indicating the neutral, cationic or zwitterionic state of Glu.

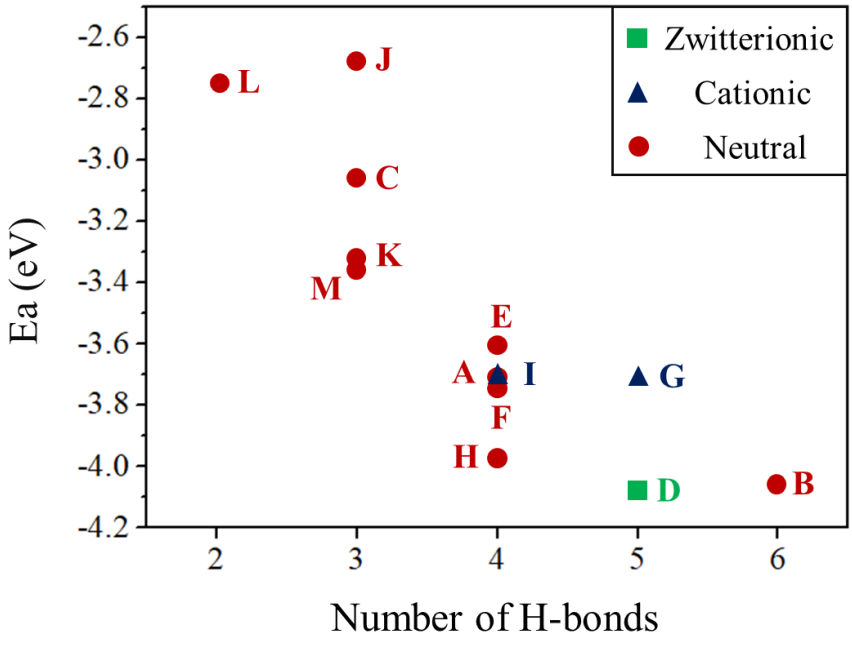

Figure 4.46. Adsorption energy as a function of the number of hydrogen bonds for anhydrous Glu/SiO_2 models

Figure 4.46 shows that energies of adsorption (Ea) increase in absolute value with the number of hydrogen bonds. The most favorable Ea is seen for model D, a zwitterionic form with 5 HB giving an adsorption energy of - 4.08 eV. This is more negative than any model computed for Leu/SiO_2, (most favorable Ea = -3.4 eV, cf. Figure 3.30), even though Leucine also managed to form up to 5 H-bonds.

The single zwitterionic form, as well as the two cationic forms of Glu (see below), are found within models with the higher numbers of H-bonds. However, unexpectedly, model B, with 6 H-bonds, converts to the neutral form. 7 models were selected for further analysis, from which one was in Zwitterionic form, two were cationic and the rest were in the neutral form, based on their high adsorption energies (Ea, in absolute value). They are shown in Figure 4.47.

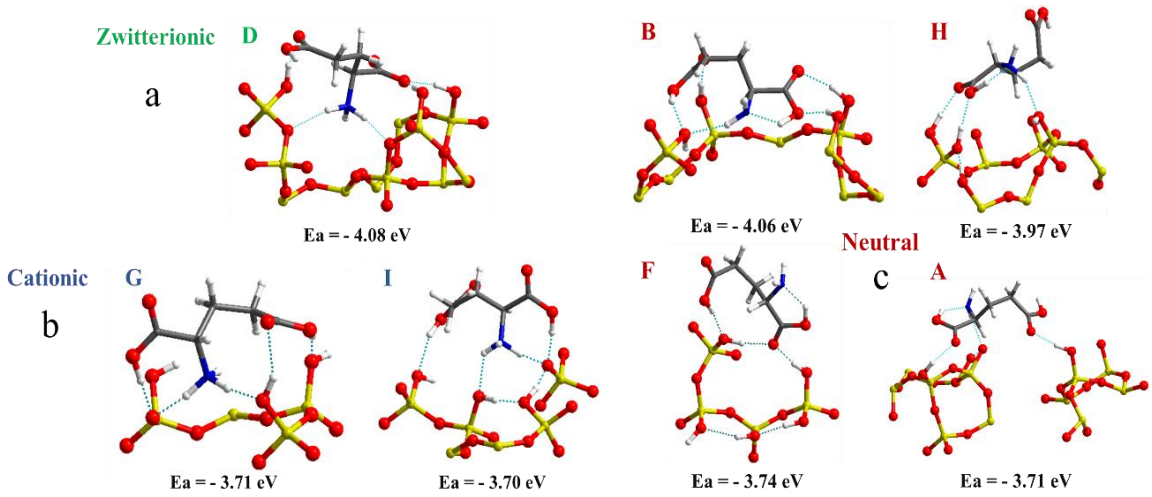

Figure 4.47. Selected models with a. Zwitterionic form, b. Cationic form and c. Neutral form; of Glu adsorbed on the silica nanoparticle surface

In the zwitterionic model D, the Glu molecule is adsorbed with the three functional groups involved in hydrogen bonds with surface silanol groups. The protonated side chain and the carboxylic acid moiety are interacting with isolated and vicinal group respectively, while the ammonium protons interact with silanol groups that are located within the interior of the silicon slab. The ammonium group has been "pushed down" into a silicate ring.

In cationic models G and I, upon optimization, the C1 carboxylate moiety has performed a proton exchange with the hydroxyl of a geminal group, creating a C1 carboxylic acid while the ammonium group remains as $–NH_3^+$. The cationic form of Glutamic acid formed in this way can be denoted as H_3Glu^+, as in Figure 4.1. Colloid chemists would perhaps characterize this form as "electrostatically adsorbed" because the adsorbed molecule and the surface bear opposite charges, but the detailed view of the molecular environment of the amino acid clearly shows that H-bonding plays a crucial role in its stabilization. This kind of proton transfer was not observed for Leucine. In this reaction, adsorbed Glu behaves as a Brönsted base, while the geminal silanols behave as a Brönsted acid. This may look counterintuitive since Glu is generally considered as an acid (recall that the natural pH of its solutions is about 3.4). However, the behavior of a molecule in the absence of water may be different from its behavior in aqueous solution, and for instance in mass spectroscopy, it is known that Glu is more

efficiently protonated than Leu in the gas phase. As regards the surface group that donates a proton, it is not surprising that geminal rather than vicinal or isolated silanols are involved, as they have been shown to be more acidic.[200]

Neutral model B shows the three functional groups adsorbed on the surface, with an adsorption energy close to model D. Model H shows a high Ea, with a carboxylic acid moiety interacting with a geminal group through 2 hydrogen bonds while the protonated side chain is detached from the surface and dangling in vacuum. Thus, the high Ea values obtained for Glu/SiO_2 are not necessarily linked with the adsorption of all three functional groups on the surface. Models F and A show the same number of hydrogen bonds (4 HB) as well as close Ea values, smaller than the previous ones, confirming the correlation between Ea and HB numbers.

IV.4.1.2 Microsolvated systems

The microsolvated models were based initially on the optimized anhydrous systems, with the addition of 12 water molecules: each functional group was surrounded by three water molecules and the remaining three were dispersed alongside the carbon hydrophobic side chain. Afterwards, static optimizations were done in order to reach the energy minima. This number of 12 was obtained based on the previous study on Leucine for which the best NMR calculated values were obtained with models involving 10 water molecules. Since Glu contains an extra protonated side chain with respect to Leu, two additional water molecules were introduced in this case. Figure 4.48 shows all 13 microsolvated models (A' to M'), with the corresponding adsorption energy values (Ea).

The description of the models becomes harder than for anhydrous models since complex patterns of hydrogen bonding are established.

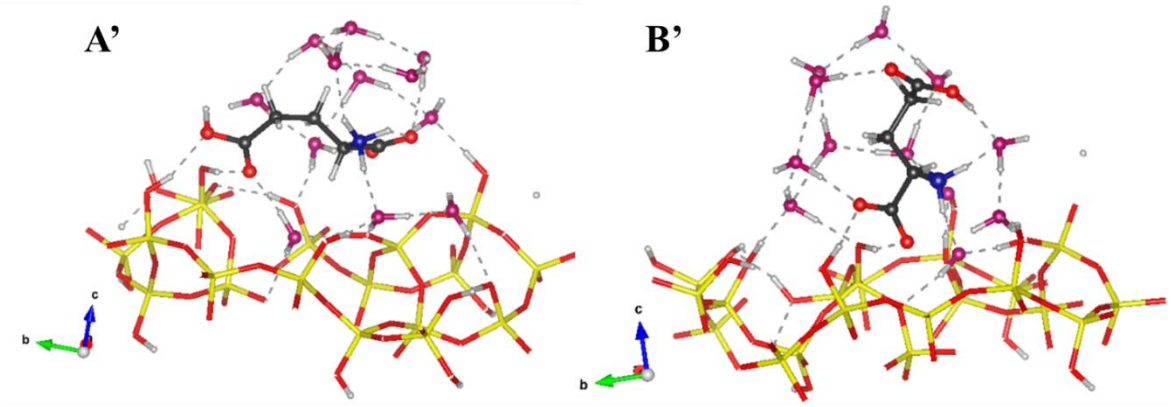

Ea = - 11.17 eV **Ea = - 11.9 eV**

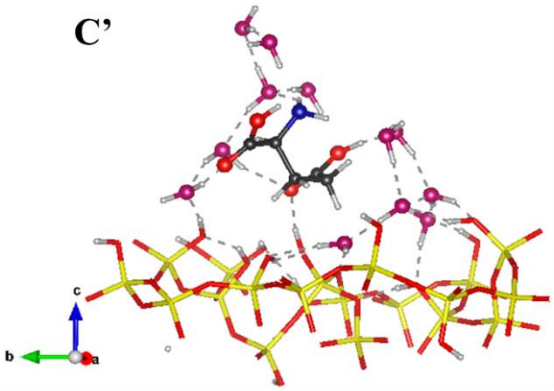

Ea = - 10.58 eV

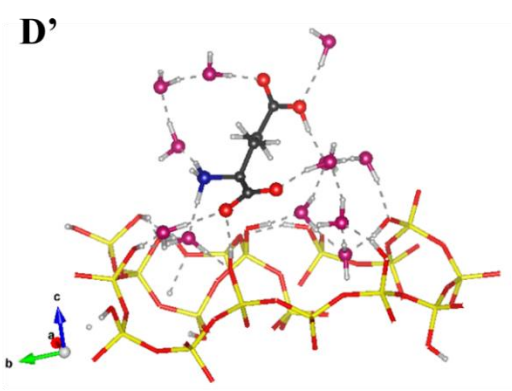

Ea = - 11.46 eV

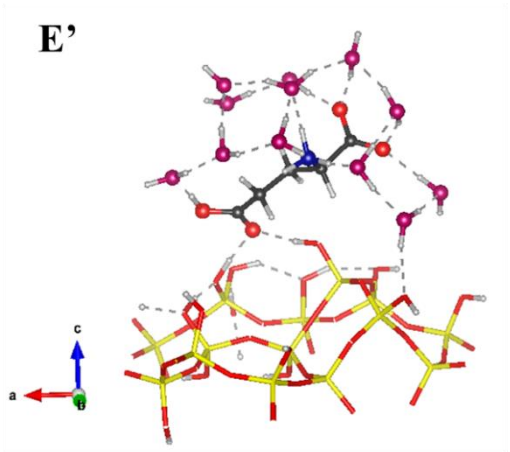

Ea = - 10.73 eV

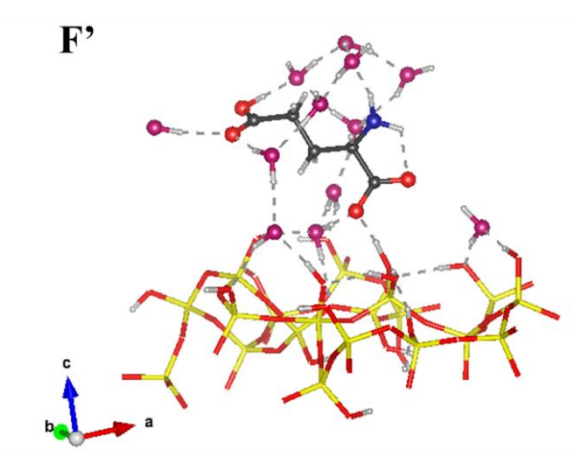

Ea = - 11.73 eV

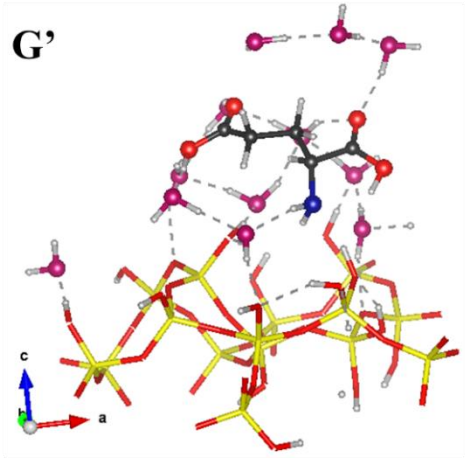

Ea = - 10.33 eV

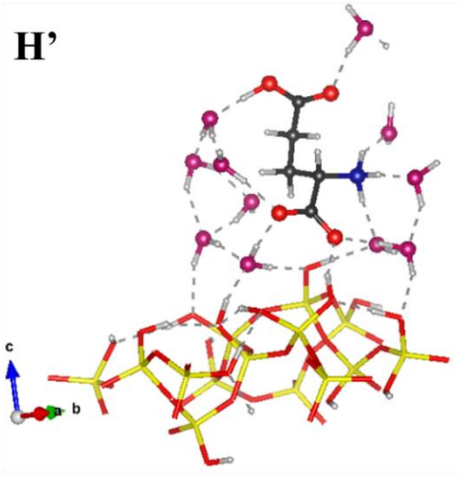

Ea = - 10.95 eV

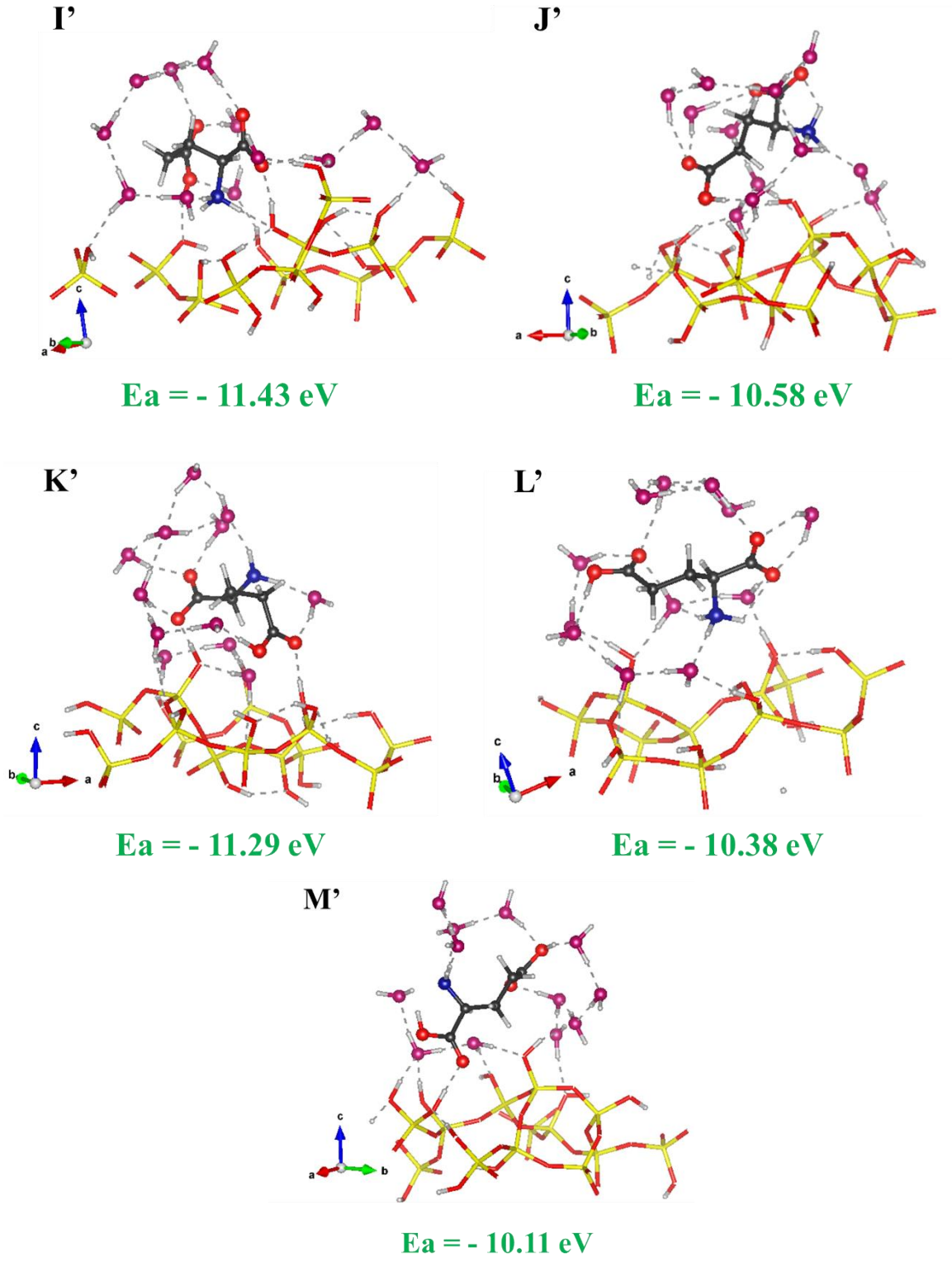

Figure 4.48. 13 microsolvated models for Glu/SiO_2 (12 water molecules per Glu) with their Ea (Energy of adsorption) after static optimization

In Figure 4.49, adsorption energies of all models are plotted as a function of the number of hydrogen bonds (ranging between 22 and 28 HB). The energy difference between the highest and lowest adsorption energy (Ea) is only -1.7 eV. The adsorption energies still generally trend

more negative with increasing numbers of H-bonds, but the correlation is much weaker than for anhydrous models (linear correlation coefficient 0.41 instead of 0.85). Surprisingly, three models (C', G' and M'), among those with the lowest adsorption energies, saw Glu changing to the neutral form upon optimization (recall that for Leu, all hydrated models were zwitterionic).

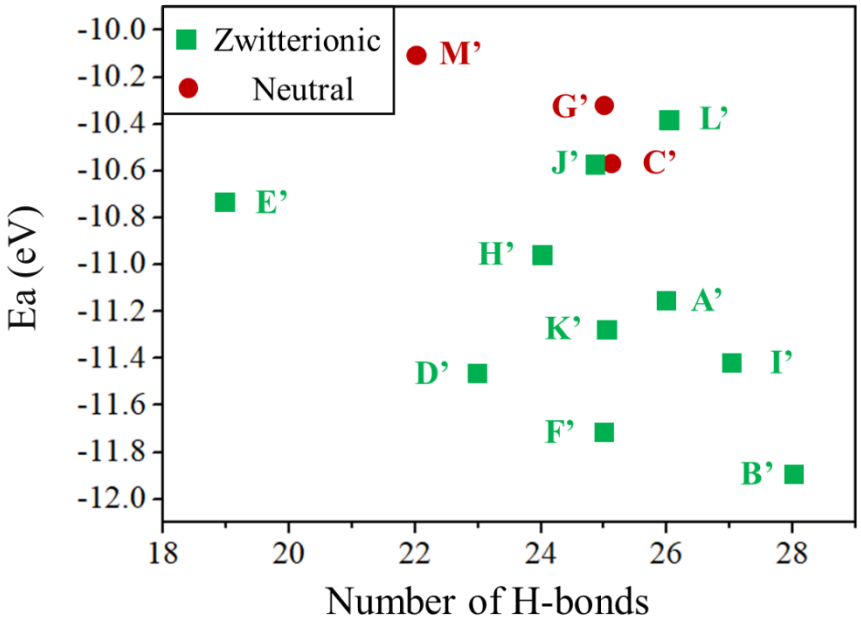

Figure 4.49. Adsorption energy as a function of different models, number of hydrogen bonds are appointed to each model (A' to M')

Models A', B', D', F', I' and K' will be described in some more detail (Figure 4.48) and were selected based on their high adsorption energies (Ea) in absolute value. Due to the large number of water molecules, it is not surprising that the functional groups mainly make hydrogen bonds with neighboring water molecules. Model A' shows that the carboxylate and ammonium moieties are bound to water molecules acting as bridges with the surface hydroxyl groups, while the two oxygens of the side chain carboxylic acid are involved in direct hydrogen bonding with surface vicinal groups. Model B' and D' show the ammonium group surrounded with water acting as bridging molecules with the surface while the carboxylate moiety interacts directly with a vicinal group through either one, or both of its oxygens; meanwhile the protonated side chain is directed away from the surface and surrounded with hydrating waters. Model F' shows one of the carboxylate oxygens interacting with a bridging water molecule while the other oxygen directly interacts with the surface geminal group; both the ammonium and the protonated side chain are directed away from the surface, surrounded by hydrating waters. Model I' shows a direct interaction of both the ammonium and carboxylate groups to the surface geminal silanols, while the side-chain –COOH is directed away from the surface. Finally K' shows a direct interaction between the side-chain -COOH with the surface geminal group and between the C1 carboxylate and a vicinal silanol, while the ammonium is directed away from the surface.

IV.4.2 Calculation of NMR chemical shift values

^{13}C and ^{15}N chemical shift calculations were performed on all 30 models of Glu/SiO_2.

IV.4.2.1 Anhydrous systems

A 2D experimental and theoretical figure is plotted in Figure 4.50 for the 7 anhydrous models previously selected (Figure 4.47).

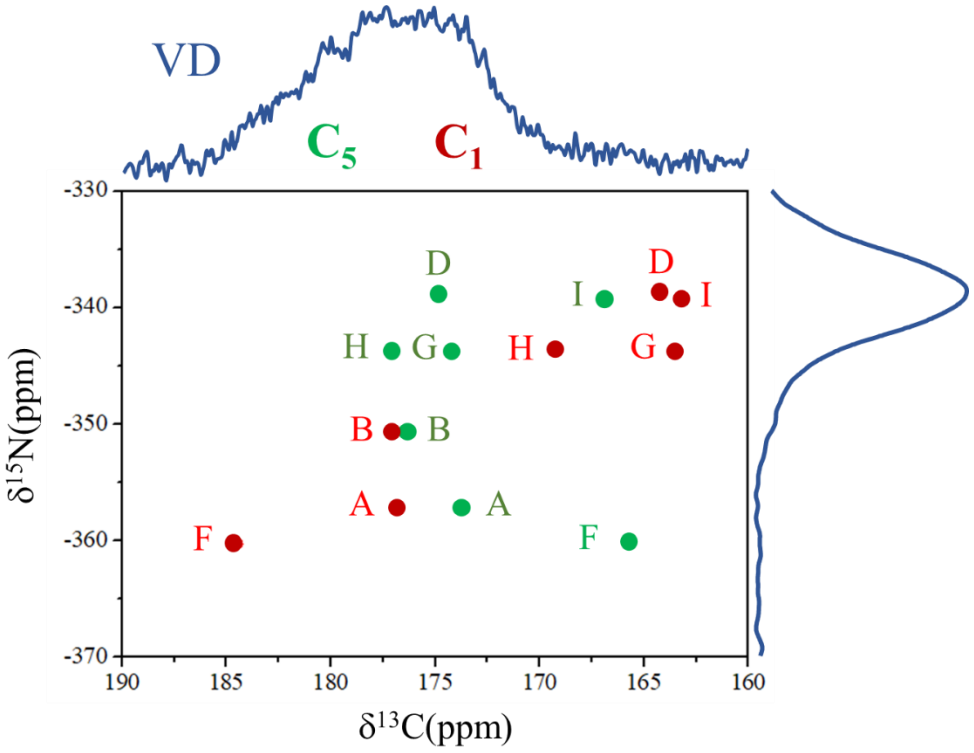

Figure 4.50. A plot correlating experimental ^{13}C (DP) and ^{15}N (CP) spectra of 1% [$^{13}C_5$, 1-^{15}N] Glu/SiO_2 VD with the calculated ^{13}C and ^{15}N chemical shifts for 7 different anhydrous Glu/SiO_2 models

Regarding the fit with the experimental data, three models (A, B and F, all with neutral H_2Glu^0) predict ^{15}N chemical shifts significantly different from the observed one. The other four (D, G, H, I) give an acceptable correspondence from the ^{15}N point of view, but predict peaks for the C1 carboxylate several ppm upfield from any experimentally observed signal. Only model H might be marginally acceptable. Thus, in conformity with the conclusion for Leu/SiO_2, anhydrous models of Glu/SiO_2 do not provide good fits of the experimental NMR data, even for the samples dried in VD conditions.

Even if at this stage, we expect the microsolvated models to be more relevant to be compared with experiments, the anhydrous models are still interesting in looking at for correlations between structural features and NMR characteristics. For instance, models D, G, H, and I (1 with neutral, 1 with zwitterionic, 2 with cationic Glu) predict a more positive chemical shift for

the side-chain C5 carboxylic acid group than for the C1 carboxylate/carboxylic acid, in conformity with the generally accepted peak assignment; of these, two models (D and G) predict a separation between the two signals of about 10 ppm, definitely in excess of the observed value. In contrast, 3 of the 4 models with neutral Glu (A, B and F) predict the opposite order for the signals, with the C5 COOH upfield from the C1. As will be seen in Figure 4.51, this is also the case for several other models with neutral Glu.

The values of the carbon, nitrogen and the proton chemical shifts of the N and C atoms of the 7 selected models are listed in Table 4-7 below; further information regarding the ^{13}C, ^{15}N and ^{1}H chemical shifts of all the 13 anhydrous models are located in Table 2 of the Annex.

Atoms	α-Glu	β-Glu	D	G	I	B	H	F	A
				δ_{iso}					
C1	177.7	178.4	164.1 (2 HB)	163.4 (1 HB)	163.2 (1 HB)	176.6 (2 HB)	169.1 (2 HB)	184.4 (2 HB)	176.8 (1 HB)
C5	180.7	180.5	174.7 (1 HB)	174.2 (2 HB)	166.7 (1 HB)	176.3 (2 HB)	177.1 (0 HB)	165.7 (1 HB)	173.7 (1 HB)
C2	53.6	54.6	57.8	51.3	52.1	54.0	53.2	53.4	53.5
C3	29.8	26.3	21.9	26.9	24.0	29.4	29.0	28.6	25.4
C4	31.9	28.8	27.6	27.7	28.4	32.6	32.87	33.44	31.87
N	-335.6	-339.8	-338.9	-343.5	-339.3	-350.6	-343.5	-360.2	-356.9
Average NH_3	9.9	9	6.5	9.1	8.7	3	9.9	1.9	2.7

Table 4-7. Calculated ^{13}C, ^{15}N and NH_3 ^{1}H chemical shift values of the 7 selected anhydrous models of Glutamic acid adsorbed on the silica surface in comparison with bulk Glu (α and β)

Figure 4.51 shows the calculated ^{13}C, ^{15}N and ^{1}H chemical shift values for each model in graphical form.

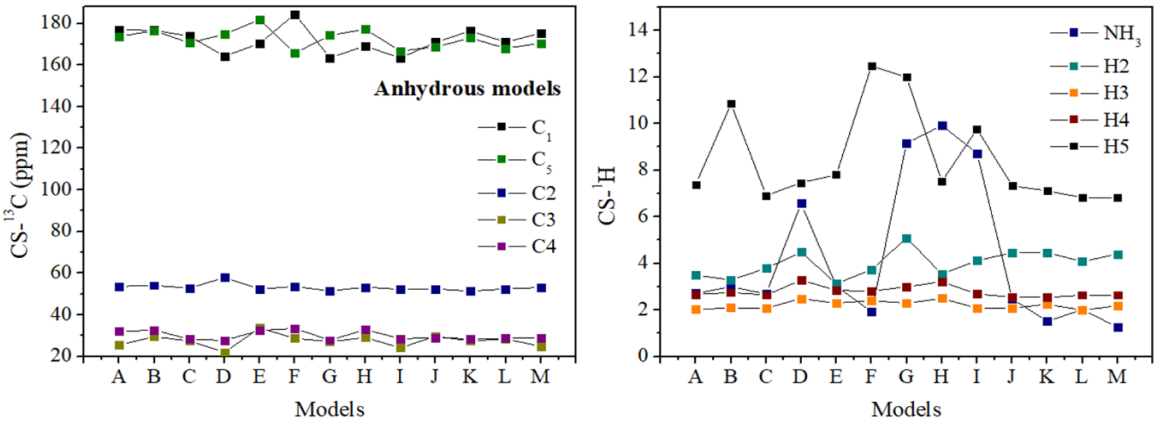

Figure 4.51. ^{13}C, ^{15}N and ^{1}H calculate CS values of 13 anhydrous models of Glu/SiO_2

We have already commented on the relative position of signals from C5 and C1 carboxylic acid/carboxylate groups. ^{13}C selective labelling of one of these positions could allow to assign each peak, and thus provide a probe of the C1 group protonation state. In § IV.3.1, we have seen that IR allows to identify the presence of protonated –COOH, but it cannot easily establish if only the C5 group is protonated, or both the C1 and the C5, something NMR data would help determining.

C2, C3 and C4 ^{13}C NMR signals show little variation, as the corresponding groups cannot be directly involved in H-bonding. Their respective ranges do not overlap; the methylene carbons may shift in a 5 ppm range, but the $–CH_2-$ in C4 is always more deshielded than the one in C3, as expected intuitively (because of the proximity of the electron-withdrawing C5 carboxylic acid group).

As for ^{13}C, ^{1}H chemical shifts of the methylene groups do not vary much between models; those of the C2 methine are somewhat more affected and can vary by about 2 ppm. N-H protons chemical shifts on the other hand strongly depend on the acido-basic speciation of the amine/ammonium moiety. When it is deprotonated (amine), the average NH chemical shift generally falls in the +1 to +3 ppm range. When it is protonated (ammonium), it is found at much higher values (8 to 9 ppm). An apparent exception is model H, which is formally neutral (with an amine group), but has a N-H proton chemical shift of +9.9 ppm. It must be underlined that all our neutral models exhibit an intra-Glu H-bond between the amine and the C1 carboxylic acid groups, i.e. a N---H-OC hydrogen bond. Figure 4.52 shows the close structural proximity between this form and the zwitterion. Now in most neutral models, the N---H distance is longer than 1.75 Å; but in model H, it is found to be 1.55 Å. Apparently, geometrical constraints force the amine group to stay close to the C1 carboxylic acid, so that a strong H-bond results, with the H almost equally shared between the two partners, and the speciation is intermediate between zwitterion and neutral.

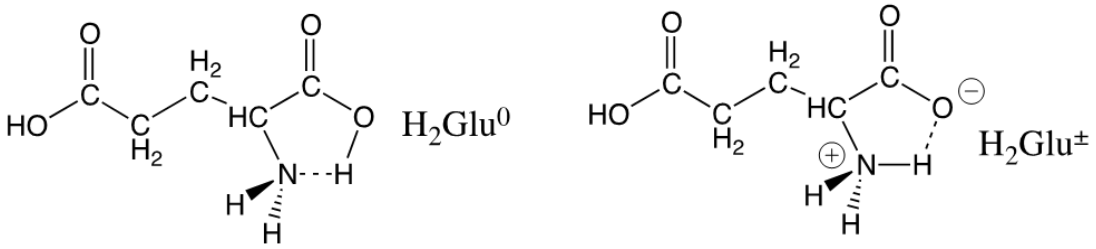

Figure 4.52. Scheme showing the relation between neutral Glu (H_2Glu^0) with strong internal H-bond and zwitterionic Glu ($H_2Glu^{\pm}$)

In an attempt to rationalize the C_1 and C_5 chemical shift evolution, and on the basis of the previous Leucine investigation, we tried to determine if there is a relation between the COO(H) ^{13}C chemical shifts and i) the number of H-bonds they are involved in, and ii) the number of H-bonds the amine/ammonium moiety is involved in. It appears that globally, the C_1 chemical shift value tends to increase with the number of COO---H-X bonds. On the other hand, it seems to decrease with the number of HB involving the amine. For C_5, the tendency is more or less similar.

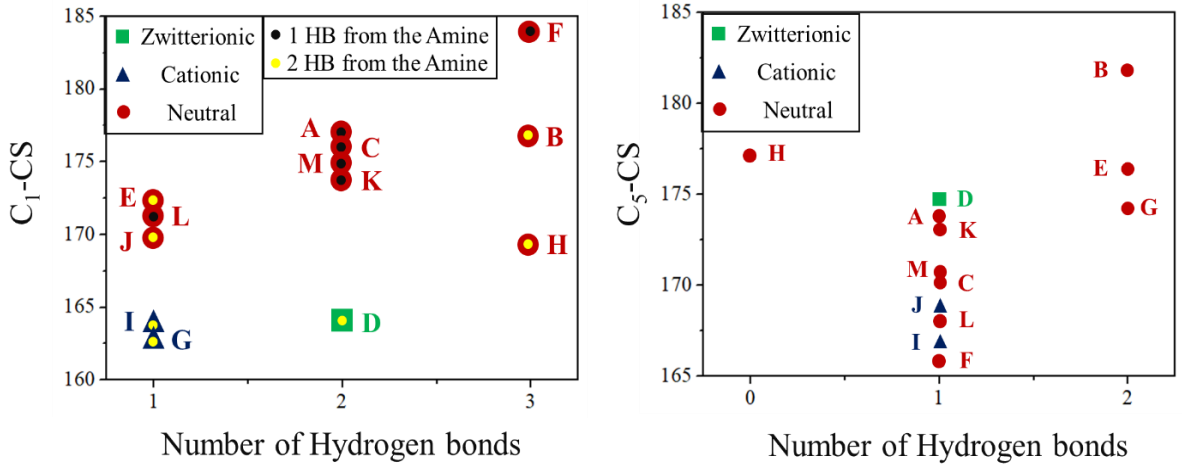

Figure 4.53. Variation of carbon chemical shift for both C_1 and C_5 in all anhydrous models as a function of the number of hydrogen bonds with the C_1OO moiety and C_5OOH side chain. The number of H–bonds involving the NH_2 /NH_3^+ group is also indicated with a color code for C_1

Figure 4.53 examines the relation between the chemical shifts of C1 and C5 and the number of H-bonds they are involved in. For the neutral models, the C1 –COOH is always involved in one internal H-bond as a donor to the amine group. The number of H-bonds as an acceptor is then equal to the total number of H-bonds minus 1. Globally, as the number of hydrogen bonds involving C1 –COOH as an acceptor increases, the chemical shift of C_1 increases as well. This is intuitively reasonable since engaging in H-bonds as an acceptor should decrease the electronic density in the –COOH group, and thus cause a downfield shift.

Unlike C1 –COOH, C5 –COOH protonated side chain can be involved as a donor and as an acceptor of H-bond as shown in Table 4-8 : C5-**O** ending acts as an acceptor of H-bonds and the C5-**OH** ending either may act as a donor or an acceptor of H-bond but cannot be both at the same time (Figure 4.54).

C5OOH side chain		
Models	C5O-**OH**	C5=**O**
A	-	1 HB-Acceptor
B	1 HB-Donor	1 HB-Acceptor
C	-	1 HB-Acceptor
D	-	1 HB-Acceptor
E	-	2 HB-Acceptor
F	-	2 HB-Acceptor
G	1 HB-Donor	1 HB-Acceptor
H	-	-
I	1 HB-Donor	-
J	1 HB-Acceptor	-
K	-	1 HB-Acceptor
L	1 HB-Acceptor	-
M	-	1 HB-Acceptor

Table 4-8. Number of H-Bonds involved as an acceptor or donor from the C5OOH protonated side chain

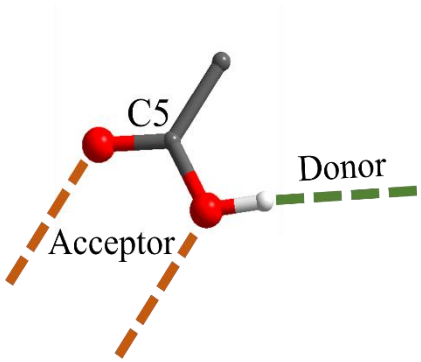

Figure 4.54. Showing the atoms involved in donating or accepting the H-Bond

We also tried to check if the number of H-bonds involving the amine/ammonium moiety influenced the position of the C1 carboxylic acid peak, since such an effect was observed for Leu/SiO_2 (microsolvated models). If we limit ourselves to the neutral models, the evidence is unclear. Among the two models with 3 H-bonds to the C1 –COOH, model B, with 2 H-bonds from the amine, gives a C1 resonance at considerably lower chemical shift than model F, with one H-bond from the amine; but among the two models with 1 H-bond to the C1 –COOH, no influence of the $–NH_2$ bonding state is found. And for models with 2 H-bonds to the C1 –COOH, no comparison can be made because the $–NH_2$ always makes only one H-bond.

Globally, only four neutral models, all with 2 H-bonds to the C1 –COOH and 1 H-bond from the amine, give chemical shifts that fall in the experimentally observed region.

Figure 4.55 shows the calculated ^{15}N chemical shift as a function of the number of hydrogen bonds from the amine/ammonium moiety (acting as a donor): when this number increases, the ^{15}N chemical shift decreases, again as would be expected. Protonation to the ammonium (in models D, G, and I) gives the values closest to the experimental ones (between -330 and -355 ppm for VD systems).

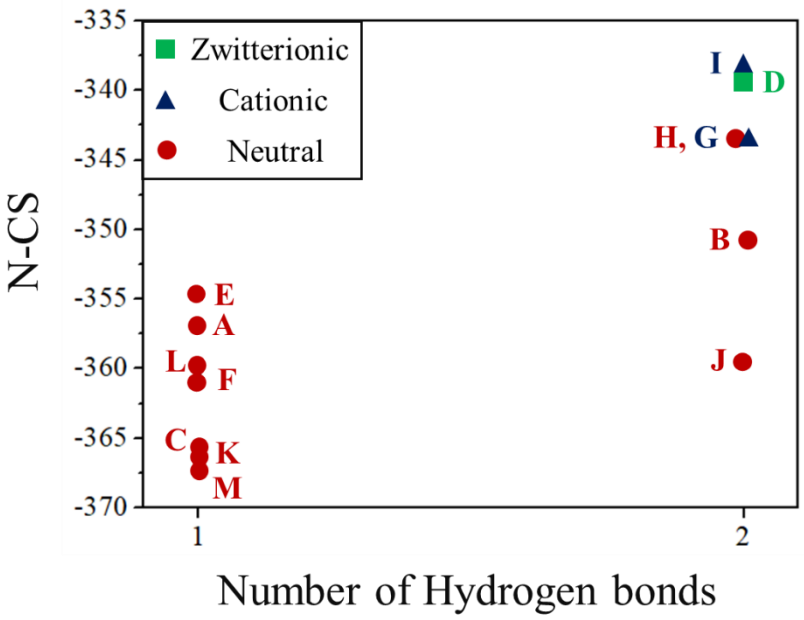

Figure 4.55. Variation of the ^{15}N chemical shift as a function of the number of hydrogen bonds from the NH_3 moiety, for all anhydrous models.

The C-O distance for C_1 and C_5 carbons is consistently also affected by the number of hydrogen bond made by the oxygens. Table 4-9 shows the distance between C_1 and C_5 and their corresponding oxygens in crystalline α- and β-Glu and Figure 4.56 shows the same information on anhydrous models.

Distance (Å)	α-Glu	β-glu
C1---O	1.258 (1 HB)	1.265 (2 HB)
C1---O	1.288 (2HB)	1.277 (1 HB)
C5---O	1.241 (1 HB)	1.245 (1 HB)
C5---OH	1.327 (1 HB)	1.323 (1 HB)

Table 4-9. Distances between C_1 and C_5 carbons and their corresponding oxygens as well as number of hydrogen bonds for crystalline Glu

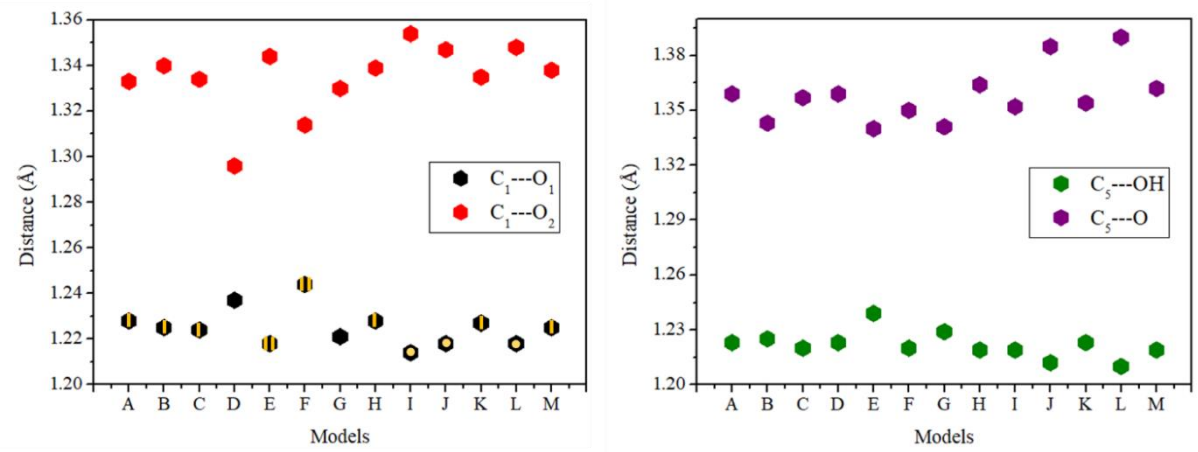

Figure 4.56. Variation of distance between C_1 and C_5 and their corresponding oxygens (number of yellow lines indicate the number of hydrogen bonds)

Figure 4.56 shows the distance between the carbon and the oxygen increases with the hydrogen bonding number. For example, models I, J and L have a C_1---O_1 distance of ~ 1.216 Å and this is correlated with the absence of hydrogen bond involving O_1 for models I, J and L (yellow circle on Figure 4.56). For models A, B, C, H, K and M, one HB involves O_1 resulting in a C_1---O_1 distance of ~ 1.226 Å (1 yellow line). This distance increases to 1.241 Å in models F when the number of hydrogen bonding increases to 2 from the O_1 ending (2 yellow lines) (model E does not follow the same trend as model F). Model I was included because it also has a C_1OOH. On average, the distance between a carbon and a protonated oxygen (C---OH) is ~ 1.34 Å which is always higher than to a deprotonated one (C---O^-). In the case of zwitterionic model D, the distance for the deprotonated C_1-O_2 is 1.296 Å which is significantly lower than for the neutral models exhibiting a C_1-O_2H bond (like model B for example).

IV.4.2.2 Microsolvated systems

The following part focuses on the microsolvated Glutamic acid models. Recall that we had presented above 13 models among which 7 were selected for detailed discussion based on their high adsorption energies (Ea) in absolute value. Figure 4.57 compares the selected models with the experimental spectra of 1% [$^{13}C_5$, 1-^{15}N] Glu/SiO_2 (ND and VD) as well as with the solution NMR spectrum of Glu. The experimental ^{13}C spectrum chosen to represent ND conditions is the DP experiment, which shows the adsorbed forms of Glu only, eliminating the bulk crystalline phase. It is recalled that the adsorbed forms are only detected in significant amounts at relatively low loadings (0.3 to 1%) in ND systems: they are characterized by signals around ~174 ppm for C1, ~178 ppm for C_5 (shifted to lower ppm values compared to crystalline forms) while the ^{15}N signal is observed around ~-338 ppm (corresponding to a shift to higher ppm values compared to crystalline forms).

Knowing that even the vacuum-dried samples contain significant amounts of water, it is important to study microsolvated models. Table 4-10 shows the calculated NMR parameters

for all carbons as well as for the nitrogen, and the average NH_3 proton chemical shifts for the 6 microsolvated models that were selected previously.

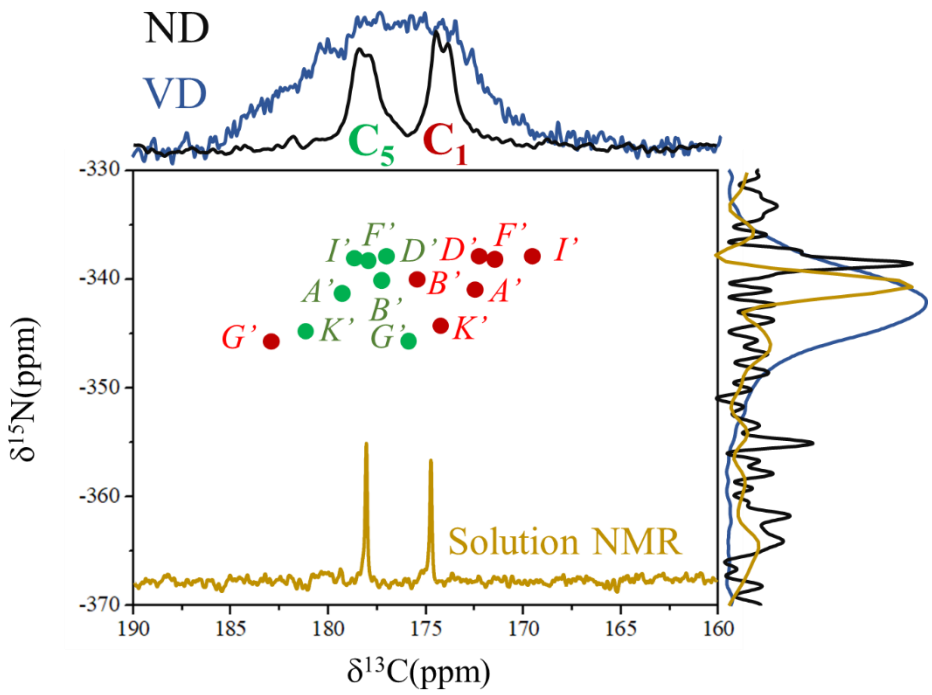

Figure 4.57. 2D plot of calculated ^{15}N and ^{13}C chemical shifts in microsolvated models compared to experimental ^{13}C MAS and ^{15}N CP MAS spectra of 1% [$^{13}C_5$, 1-^{15}N] Glu/SiO_2 (N.D) as well as aqueous solution ^{13}C and ^{15}N liquid NMR spectra of Glu

Regarding the VD spectra, all 6 selected models (and a couple of others) give calculated chemical shifts for both ^{13}C and ^{15}N that fall within the experimentally observed range, with only K' and I' being borderline. Thus, the VD samples could be described by a combination of several hydrated Glu/SiO_2 models, including the ones with highest adsorption energy, which is an encouraging finding.

However, a couple of hydrated models could correspond quite well with the ND spectrum as well – especially, models D' and F'. We have described above the ND spectra as solution-like. Therefore, this means that some of the fully hydrated models result in an environment that cannot be significantly distinguished from Glu in an aqueous solution, at least from the point of view of the NMR probe. For Leu/SiO_2, in contrast, we had found that hydrated models accounted well for VD dried samples, but they were significantly different from the aqueous solution. Figure 4.58 shows the calculated chemical shift of the different protons H-bonded to specific groups, such as the functional moieties of Glu, surface silanols, water molecules, as a function of the relevant H-bond distances.

Microsolvated systems	A'	B'	D'	F'	I'	K'
	Sigma Total (ppm)					
C1	172.61	175.43	172.12	171.54	169.72	174.21
C5	179.13	177.26	178.35	178.01	176.92	181.09
Cα	54.33	54.44	55.78	53.59	52.67	53.86
Cβ	25.21	30.16	26.09	26.73	28.83	28.48
Cγ	31.54	33.28	33.07	33.68	31.51	29.36
N	-341.09	-340.15	-338.11	-338.23	-337.89	-344.54
Average NH_3	8.87	10.13	9.12	9.06	9.50	8.64

Table 4-10. Calculated ^{13}C, ^{15}N and ^{1}H of the 6 selected microsolvated models of Glu/SiO_2

Figure 4.58 shows a similar pattern for all cases: as their hydrogen bonding distance decreases, the chemical shift of the protons increases, in good agreement with previous observations on Leucine (Chapter III, Fig 3.3.2). Water protons H-bonded to the amino acid functional groups have chemical shifts above 5 ppm. There is a high variability for those H-bonded to the C1

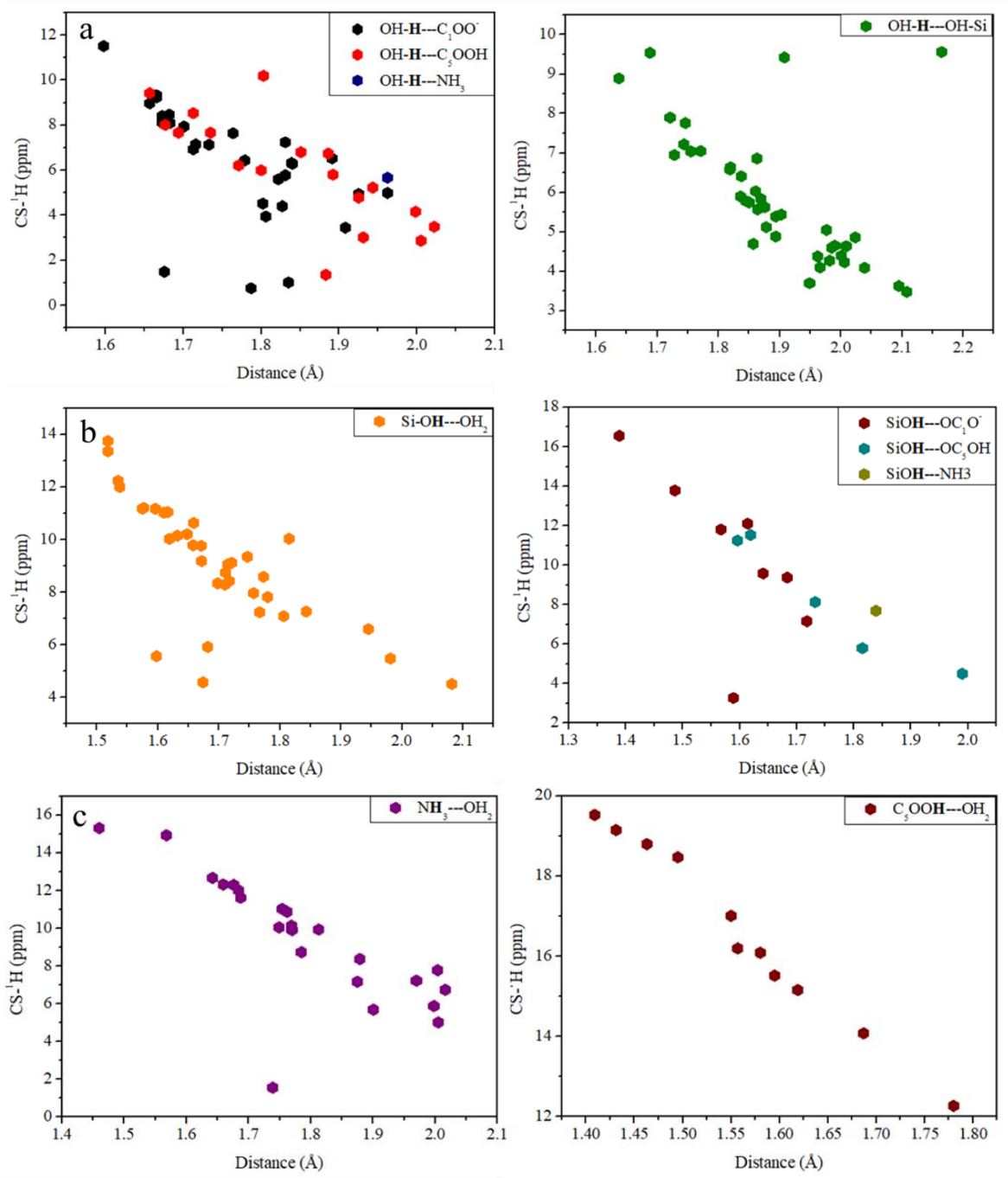

Figure 4.58. Calculated ^{1}H chemical shift values as a function of the H-bonding distance to the acceptor group, for a) protons of water, b) protons of surface silanols, c) protons of ammonium and carboxylic acid groups

carboxylate, while those H-bonded to the surface silanols are most often located below 6 ppm.

The results listed in Figure 4.58 may be used to put some bounds on the type of H-bonds the adsorbed Glu molecule may be engaged in, based on the ^{1}H-^{13}C HETCOR shown in Figure

4.27. C5 carboxylic acid and C1 carboxylate groups were correlated exclusively with protons resonating between +2 and +10 ppm. This would exclude models with SiOH-OC_1O below 1.6Å, but also, most of the models where –COOH makes a donor H-bond to water molecules. It would be quite a stringent restriction; however, it is probably more likely that the expected correlations above 12 ppm (proton dimension) are not seen because the –COOH protons are in fast exchange.

IV.5 Conclusions on the Glu/SiO_2 system

Glu/SiO_2 presents both similarities and differences to Leu/SiO_2. It also presents more challenges to the experimental characterization of the amino acid speciation, and in particular high fields are needed for NMR characterization.

At first sight, XRD seems to indicate that no crystal phases are present up to a given loading, somewhat under 3% by weight. Thus, like for Leucine, Glutamic acid would adsorb molecularly until a saturation coverage, and additional molecules would precipitate as bulk crystals. But ^{13}C NMR forces to reconsider this view since bulk-like signals are observed for loadings as low as 0.3%. We believe that small crystal-like nuclei may form competitively even at low activities of adsorbing Glu. They would not be detectable by XRD, but the local environment of Glu carbons would be very similar to the crystal form(s) and give the same NMR signals. It should be noted that this existence of small, XRD-silent crystal nuclei had already been proposed by Bouchoucha *et al.*,[86] from a somewhat different line of reasoning. An additional remark regarding crystal-like forms in Glu/SiO_2 is that the crystal phase (α or β) seems to exhibit a memory effect with respect to the starting material, which may also be consistent with the existence of small, resilient nuclei consisting of a few Glu molecules.

There is also evidence however for different non-crystalline forms, which can be observed clearly only for loadings of 1% or lower. IR indicates that they are predominantly zwitterionic, with unionized side-chain –COOH. The distribution of Glu between these forms is highly sensitive to the hydration state of the sample – thus, the first conclusion that we drew from the Leu/SiO_2 study ("water matters") is even more valid here. Quantitatively, the amounts of retained water as determined by TG are not very different from those measured for Leu/SiO_2: they increase with the amino acid loading up to a plateau for samples in ND conditions, and they are approximately constant, at a similarly low value, in VD conditions.

In ND conditions, a small amount of Glu is present as "liquid-like" species that are not observed by CP MAS NMR because of too high mobility, but may be seen by DP excitation. Probably as a function of minor, uncontrolled changes in the water content of the sample, these Glu molecules may become visible by CP MAS NMR, indicating reduced mobility, or even (for lower water contents) exhibit significant line broadening without a significant peak shift.

In VD conditions, a broad NMR signal is observed in the carboxyl region, meaning that adsorbed forms in a range of different environments (a range of chemical shifts) coexist on the surface. Contrary to Leucine, there is no clear indication that the ammonium group is more intimately interacting with the surface than the other two functional groups.

Overall, the interaction of Glu with the silica surface seems to be more labile, and to concern a more limited amount of amino acid, than that of Leu. At any rate, both IR and NMR data suggest

interaction through hydrogen bonding, without any covalent bond formation, as was also the case for Leucine.

Regarding the potential of characterization techniques, the comparison of the two crystal forms of bulk Glu indicates that ^{13}C NMR is very sensitive to small differences in the H-bonding state; its applicability to the supported Glu/SiO_2 case is only limited by the heterogeneity of the system. ^{13}C-^{1}H HETCOR is also interesting in this respect as it shows strong intermolecular correlation peaks in some cases. Interestingly, when applied to Glu/SiO_2, HETCOR shows limited but suggestive evidence that clustering of Glu molecules may occur even for the "adsorbed" form.

Molecular modeling confirmed the favorability of adsorption by H-bonding. In the case of anhydrous models, the adsorption energies were more negative than for Leu. This may seem to be in contradiction with the conclusion from experimental data that the adsorbed form of Glu appears "less competitive" (with respect to both the crystal and solution-like forms) than in the case of Leu. But it must be remembered that Ea values are calculated with respect to amino acid molecules in a vacuum. What would be needed would be a comparison with the energy of molecules in the solution and in the energy of association with the crystal phase of Glu. Adsorption energies are correlated to the number of H-bonds for anhydrous, but only weakly for hydrated models.

As for Leu, anhydrous models are mostly neutral. But in some cases, cationic H_3Glu^+ forms through proton exchange with the surface, a fact which has no parallel for Leu. As for Leu again, chemical shifts calculated for the anhydrous models do not agree well with the experiment (either in ND nor VD conditions), in conformity with the finding that even samples in VD conditions contain residual water.

On the other hand, the hydrated models with the highest adsorption energies fit well the ^{13}C and ^{15}N experimental values for VD drying conditions; but a couple of them could equally well fit the values of samples in ND conditions. Broadly speaking, it may be said that some of the best configurations for Glu interacting with the surface are very "liquid-like". ^{1}H chemical shifts calculations indicate that they could be sensitive probes of the H-bonding state, but their interpretation is non-trivial due to strong overlap of the resonances of protons on different groups. It seems that models where the carboxylate is strongly H-bonded to silanols can be excluded on the basis of the correlations found: this would explain why experimental evidence of carboxylate/surface interaction is only seen when most of the water is removed from the system.

In summary, Glutamic acid molecules have a lesser affinity to the silica surface than do Leucine molecules – or Glu with each other.

Chapter V: Thermal activation of amino acids on the SiO_2 surface

Previous chapters have detailed the individual adsorption of Glutamic acid and Leucine on the silica surface of nanoparticles, through hydrogen bonds between the carboxylate and the amine moiety (and from the side chain as well in the case of Glutamic acid) and the silanols and/or water at the silica surface.

This chapter will be first focused on studying the outcome of these amino acids after thermal activation under two different environments as mentioned before: nitrogen dried and vacuum dried. The objective is to observe and compare the effect of a hydrated system initially having a high water activity (N.D) with that of one containing minimal amounts of water (V.D), regarding among others the overall mobility and the dynamics of the amino acids towards peptide bond formation.

Finally, after discussing each amino acid separately, the co-adsorption of these amino acids on the silica nanoparticle surface will be investigated, as well as their thermal activation.

IR spectroscopy and solid state NMR spectroscopy were used to characterize and understand the adsorption phenomena and the condensation of amino acids to polymeric biomolecules after thermal activation.

V.1 Thermal activation of Leu/SiO_2

V.1.1 IR study of the activation of a low-loading 1% Leu/SiO_2

The adsorption of Leucine on the silica nanoparticle surface was reported in the second chapter. XRD suggested that a loading of 3% Leu on silica was the limit above which bulk Leu appeared. However, NMR indicated that at this loading, small amounts of crystalline material were still present. For that reason, 1% Leu/SiO_2 was used in the present Chapter, in order to study exclusively the behavior of molecularly adsorbed Leucine interacting with the silica surface – especially since IR spectroscopy is sensitive to crystalline phases and any form of crystallinity will inhibit the performance of the IR radiation to observe the surface of silica. This choice has a drawback of course, in that the bands of adsorbed molecules will be very weak compared to those of the support. Nevertheless, we will see that important information can still be obtained. Leu/SiO_2 was thermally activated under 2 different conditions as previously described: nitrogen dried and vacuum dried (N.D and V.D). Figure 5.1 presents the two sets of IR spectra recorded for these different samples, after thermal activation at increasing temperatures.

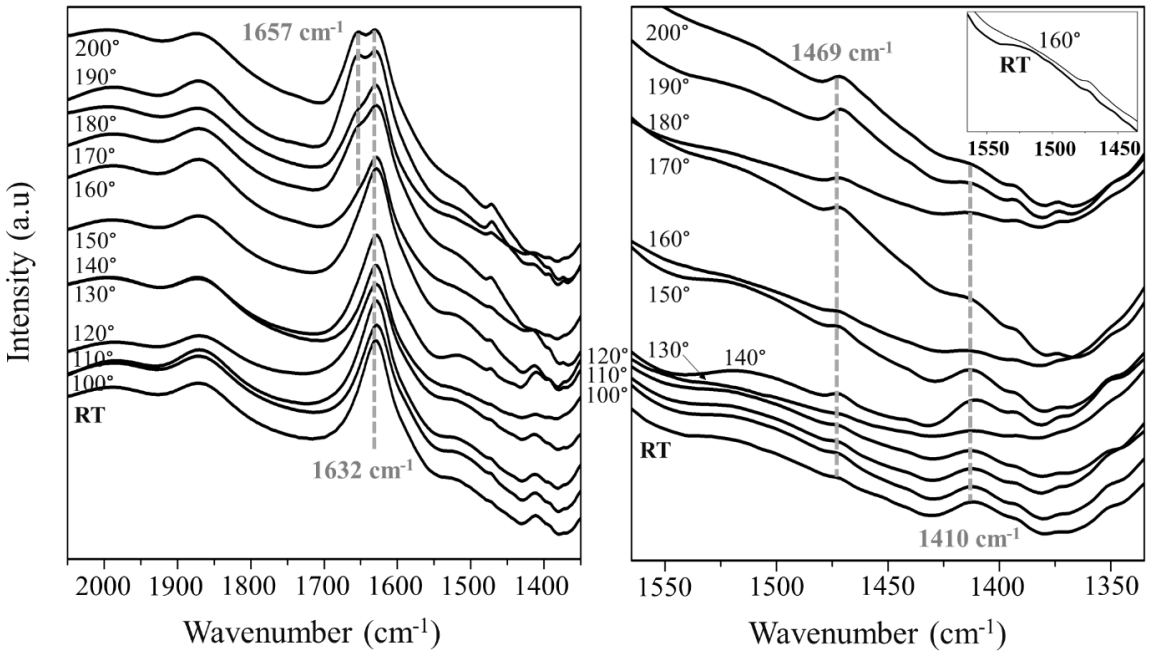

Figure 5.1. IR spectroscopy of 1% Leu/SiO_2 ND, thermally activated at increasing temperatures. Left: general view of the fingerprint region, right: close-up on the 1350-1550 cm^{-1} region

The region represented in the left-hand part of Figure 5.1 contains the two fingerprint bands of the silica support, at 1867 cm-and 1975 cm^{-1}. Their intensity is a good indicator of the total amount of solid material in the IR beam. The water bending vibration at 1630 cm^{-1} is still present in the N.D dried samples and only decreases at the highest activation temperatures tested, even though in the TG apparatus the physisorbed water was essentially eliminated at 100°C. The bands attributable to adsorbed Leucine are broad and weak, essentially $\delta_s(NH_3^+)$ in the 1525-1515 cm^{-1} region, and $\nu_s(COO^-)$ at 1410 cm^{-1}, with $\nu_a(COO^-)$ apparent as a shoulder around 1590 cm^{-1}, and $\delta_s(NH_3^+)$ overlapping with the water bending. A significant modification is obvious between 160°C and 170°C, with the appearance of a strong, rather sharp new band at 1657cm^{-1}, which is attributable to the amide I mode, and the concomitant weakening of the $\delta_s(NH_3^+)$ and $\nu_s(COO^-)$. These observations are compatible with those by Sakhno *et al.*[92] They claimed that their spectra were indicative of the formation of the cyclic dimer cyclo(Leu-Leu), since no band was observed in the region around 1550 cm^{-1} where the amide II mode would be expected: this would be a consequence of the centrosymmetric character of the cyclic dimer.[309] Specifically, the spectrum reported by Sakhno *et al*. contained two bands they attributed to cyclo(Leu-Leu), the amide I at 1657 cm^{-1} and a band at 1469 cm^{-1} attributable to degenerate vibrations of the alkyl groups. We do indeed observe absorbance maxima at exactly the same positions after high-temperature treatments, although a small feature was already apparent around 1470 cm^{-1} for the initial Leu/SiO_2. In bulk cyclo(Leu-Leu), these two bands are situated at 1668 cm^{-1} and 1456 cm^{-1}, respectively.[310]

Figure 5.2 shows the effect of the thermal treatments of samples prepared in VD conditions.

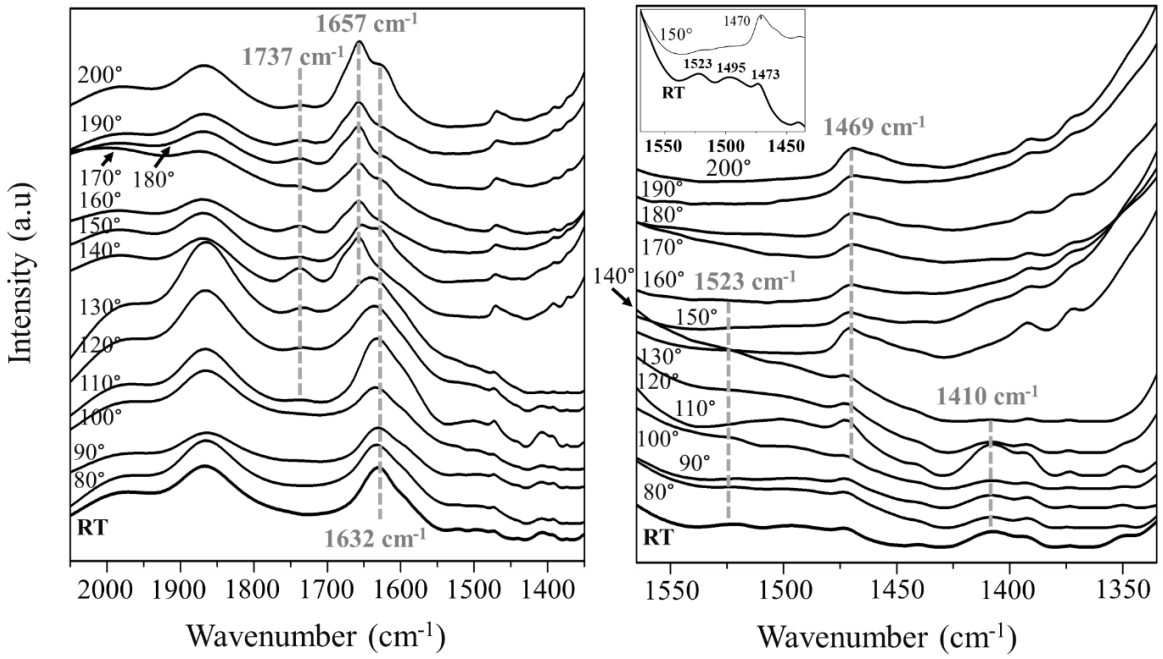

Figure 5.2. IR spectroscopy of 1% Leu/SiO_2 VD, thermally activated at increasing temperatures. Left: general view of the fingerprint region, right: close-up on the 1350-1550 cm^{-1} region

From the start, the intensity of the band at 1632 cm^{-1} is significantly lower than after ND, due to the lower amount of water, which was already remarked in Chapter III. As in ND samples, two new bands appear at 1657 and 1469 cm^{-1} upon heating, while simultaneously the $\delta_s(NH_3^+)$ (see inset) and $\nu_s(COO^-)$ bands disappear. However, this change is apparent at lower temperatures than for ND, already at 140°C, which is at least 20°C lower than in ND conditions; and the amide I band seems to exhibit a shoulder at higher wavenumbers that was not present in ND samples. But the most conspicuous difference between ND and VD is the clear appearance in the latter case of a band at 1737cm^{-1} (the maximum absorbance varies between 1735 and 1739 cm^{-1}). While its appearance also appears to be thermally activated, it is already present at 110°C, i.e., a temperature 30°C lower than for the amide band.

There are two possible attributions for this band. First, it could be due to the formation of a "surface mixed anhydride" or SMA, i.e. to the condensation of the carboxylic acid moiety with a surface silanol, giving a R–CO-O-Si covalent bond to the surface. This possibility has been proposed a long time ago.[311] On silica, Rimola *et al.*[205] proved that it could only be energetically favorable if the SMA formation was accompanied by the opening of a strained "D3" cycle of three siloxane tetrahedra. In recent experimental work[312], IR signals that could convincingly be assigned to SMAs were observed when formic acid was reacted with pristine silica AOX50, provided the latter had not been exposed to water; their C=O stretching vibration resonated between 1723 and 1730 cm^{-1}. We do not believe that such species could be formed here, because the D3 rings necessary to form SMAs are highly unstable in the presence of water and would be destroyed by the aqueous deposition procedure. Reforming them by silanols condensation upon thermal activation is possible but needs high treatment temperatures, and therefore no D3 rings are expected to be present at the low temperature of 110°C where the 1737 cm^{-1} band is first observed.

The second possible attribution is to the C=O stretching mode in protonated –COOH groups. This group vibrates at 1722 cm^{-1} in cationic Leucine (H_2Leu^+) in aqueous solution.[313] For the

neutral species $HLeu^0$, no experimental data in condensed phase are available to the best of our knowledge, but theoretical calculations on the most stable conformers gave ν_{CO} vibration wavenumbers between 1709 and 1740 cm^{-1}. Now the neutral form ($HLeu^0$ or H_2N-CHR-COOH) would seem to constitute a logical intermediate in the peptidic condensation of Leucine, or any amino acid, because a nucleophilic attack of the N-terminal group on the C-terminal group of another amino acid (see Figure 5.3) is only possible if the N-terminal is deprotonated to -NH_2, and certainly favored if the C-terminal is protonated to –COOH.

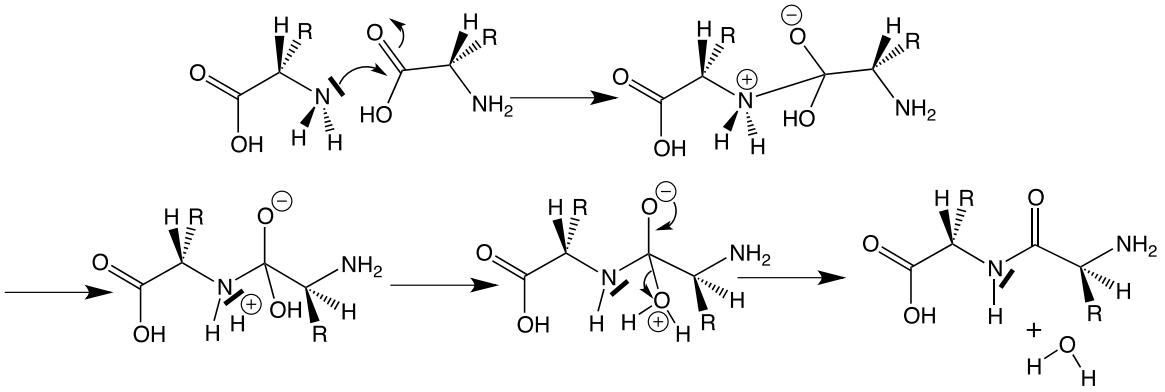

Figure 5.3. A probable mechanism for the peptidic condensation of two amino acids, starting from the neutral forms[314]

Besides, as we have discussed in Chapter III, the zwitterionic form of Leucine remains predominant as long as the surface is hydrated; and TG shows that most of the physisorbed water is gone at 100°C. It is logical to expect that at the slightly higher temperature of 110°C, the last strongly held water molecules are eliminated, forming anhydrous Leu/SiO_2 surface complexes, which contain neutral Leu ($HLeu^0$) in most cases. Further thermal activation would cause the condensation between two neutral Leu. This mechanism is illustrated in Figure 5.4; it goes through two successive reaction intermediates, neutral Leu and the linear dimer H-Leu-Leu-OH. The latter is supposed to be unstable and quickly transformed to the cyclic dimer, as was indeed observed for Glycine.[87]

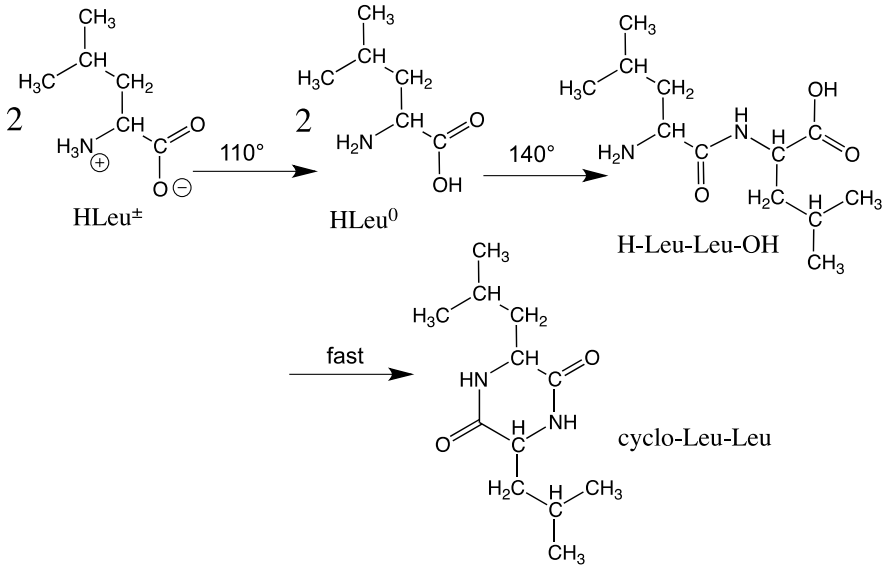

Figure 5.4. Steps in cyclo(Leu-Leu) formation

Even though the existence of a $HLeu^0$ intermediate is not surprising in this context, its observation had never been reported before to our knowledge. Furthermore, our data only evidence it in the VD samples, i.e. when the whole activation procedure is carried out in vacuum. One possible rationalization would be that diffusion phenomena are different on silica surfaces according to the drying conditions. As underlined in Chapter III, if Leucine molecules are uniformly distributed on the surface, they would be quite distant from each other at 1% loading. They would exist at a density of 1 per 8.2 nm^2, i.e. an average distance of 28 Å between molecules centers. Now to react together, two molecules must of course meet each other. It is also likely that surface diffusion of adsorbed molecules would be easier on a hydrated than on an anhydrous surface. Therefore, in low-hydration VD conditions, neutral $HLeu^0$ might form more easily (at 110°C), but their diffusion would only become fast enough for reaction at more elevated temperatures (140°C). In contrast, in higher water activity ND activation, the transition from zwitterionic to neutral would only happen at higher temperatures (160°C), but they would then be able to dimerize immediately because of fast diffusion.

Another feature that might be explained by diffusional limitations is the persistence of the neutral $HLeu^0$ even after the dimer has started to form. It is unexpected in the frame of the mechanism shown in Figure 5.4: if $HLeu^0$ is a reaction intermediate, it should decrease and disappear when the following reaction product becomes predominant. But once again it has to diffuse to another $HLeu^0$ in order to react, and on a fully dehydrated surface, diffusion probably requires "jumping" of the molecule from one silanol (or silanols group) anchoring point to another silanol. On the amorphous silica surface, the distances between neighboring silanols groups would be randomly distributed, and some $HLeu^0$ might not be able to diffuse because the nearest neighbors are too far away. These considerations are of course speculative, but they are in line with what is generally known about silica surfaces.

V.1.2 IR study of the rehydration of activated forms

We investigated the modifications of a Leu/SiO_2 VD sample when it was re-exposed to water vapor at room temperature after thermal activation. This study was carried out on the 3% loading sample that had been extensively characterized by NMR. In addition, we varied the thermal activation protocol by maintaining the final temperature for either 30 or 60 minutes.

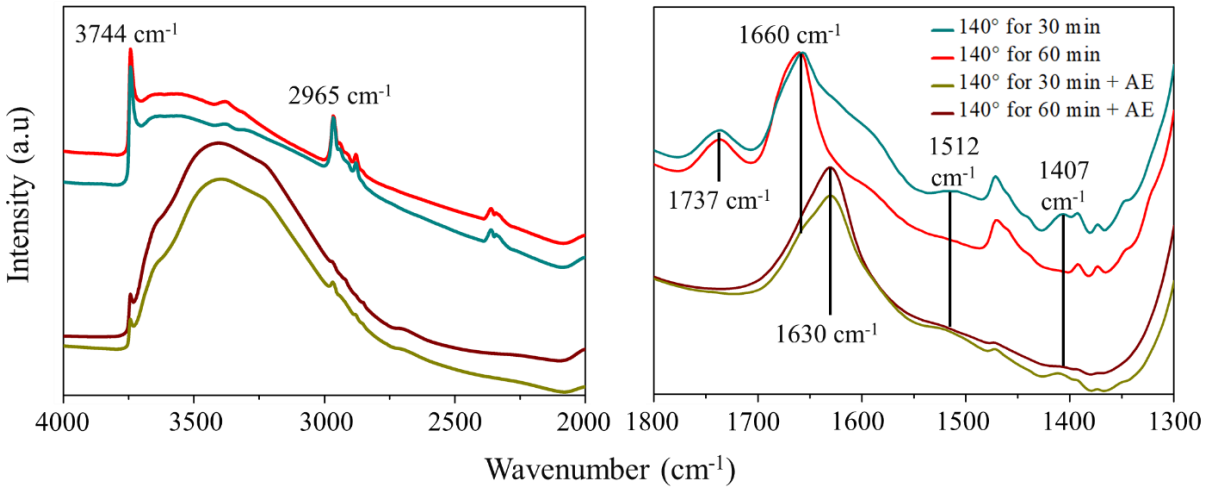

Figure 5.5. IR spectroscopy of 3% Leu/SiO_2 VD samples after thermal activating at 140°C during 30 and 60 min, and subsequent exposure to ambient atmosphere (AE)

Figure 5.5 shows the IR spectra immediately after thermal treatment, then after re-exposure to ambient air for about 5 minutes (by puncturing a hole in the paraffin film that isolated the sample). The temperature for thermal activation was set at 140 °C because the initial study had revealed that dimerization started at this temperature.

In the 4000 cm^{-1}-2000 cm^{-1} region (Figure 5.5, left panel), VD samples after activation clearly show the narrow and intense peak at 3744 cm^{-1} due to the isolated silanols on the surface. The broad absorption in the 3600-3200 cm^{-1} range typical of water and hydrated silanols is weak and allows to see NH stretching bands at 3293 and 3380 cm^{-1}, the former one decreasing upon prolonged activation. Reexposure to air obviously caused considerable rehydration, with the broad water band now dominating this region. This is confirmed by the appearance of the combination band of water at around 5300 cm^{-1} (not shown).

In the mid-IR (Figure 5.5, right panel), the water bending vibration at 1630 cm^{-1} significantly decreases when the activation time is increased, so that the amide I band appears much more prominent. This is also the case for the bands typical of uncondensed $H_2Leu^{\pm}$ monomers, the $\nu_a(COO^-)$ shoulder at around 1590-1600 cm^{-1}, the $\delta_s(NH_3^+)$ at 1512 cm^{-1} and the $\nu_s(COO^-)$ at 1407 cm^{-1}: monomers are obviously disappearing due to condensation. Meanwhile, the 1737 cm^{-1} band remains essentially unchanged.

Re-exposure to air induces remarkable changes in this region. The water band at 1630 cm^{-1} increases again and becomes dominant. It must be underlined, though, that the amide band at 1660 cm^{-1} is still present: the amide bonds are not hydrolyzed in these conditions, meaning that the dimerization is irreversible. In stark contrast, the band at 1737 cm^{-1} completely disappears. This is certainly relevant for the assignment of the latter band. Two different hypotheses were in line: the C=O stretching vibration either in a surface mixed anhydride (SMA), or in the neutral form $HLeu^0$. Upon surface rehydration, $HLeu^0$ should certainly quickly revert to the zwitterionic form $HLeu^{\pm}$ as proton transfer reactions are very quick (see Chapter III, especially the molecular modeling results that showed proton transfer to be unactivated). For SMAs, relevant data are scarce. Ola Samrout has prepared SMAs with formic acid by gas phase deposition on AMX50 silica, with a $\nu_{C=O}$ at 1730 cm^{-1}.[312] Re-exposure to water vapor caused the hydrolysis of part, but not all, of these SMAs. Thus, in summary, the fast and complete suppression of the at 1737 cm^{-1} feature upon rehydration is more compatible with its attribution to $HLeu^0$ than to SMA, although the matter remains arguable.

V.1.3 Deuterium and thermal activation

Another way of characterizing adsorbed Leucine is by deuteration. An exchange of H for D should induce strong modification in the vibration frequencies of H-containing functional groups, which can be easily identified by IR spectroscopy. Figure 5.6 shows the spectra of the

samples considered in Figure 5.5 (3% Leu/SiO_2 VD), that had been deuterium exchanged prior to thermal activation.

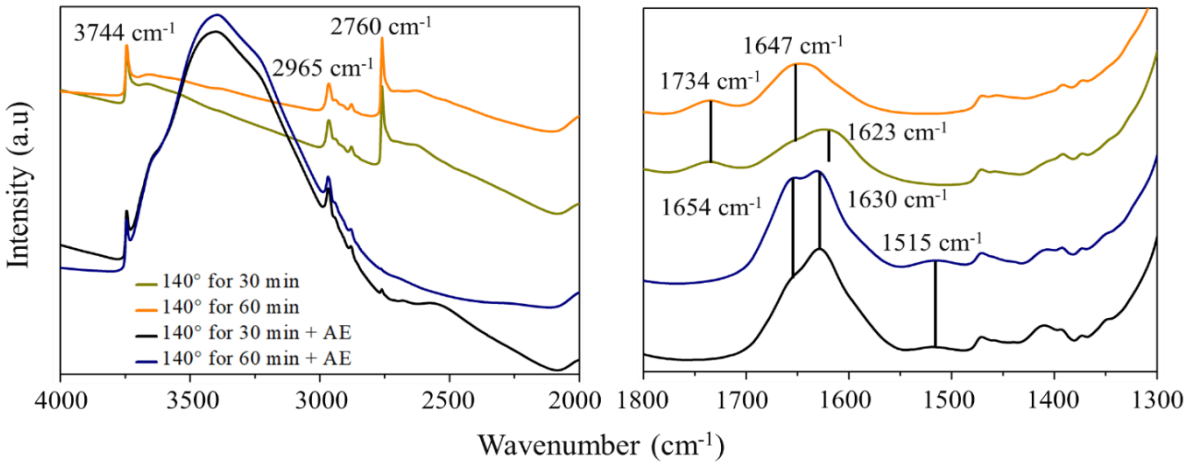

Figure 5.6. IR spectra of deuterated 3% Leu/SiO_2 VD samples activated 30 min and 60 min (1 hr) at 140°C, before and after exposure to air

In the 2000-4000 cm^{-1} region, the intense peak corresponding to isolated Si-OH silanols is still present at 3744 cm^{-1}, while its deuterated counterpart (stretching vibration of isolated Si-OD) has been downshifted to 2760 cm^{-1} – the vibration energy is decreased by a factor 1.36 (not very different from $\sqrt{\frac{m_D}{m_H}} = \sqrt{2} = 1.41$). The band at 2965 cm^{-1} is not affected, because the corresponding vibrator (C-H stretching) only involves non-exchangeable hydrogens.

In the fingerprint region, two bands are apparent at 1734 cm^{-1} and 1647 cm^{-1}. These positions are very close to the –COOH C=O stretching, and amide I bands in non-deuterated samples. Since the vibrational modes corresponding to these bands do not involve H atoms (to a significant extent), they would indeed be expected not to shift much upon H-D exchange.

When these samples are exposed to ambient air, they take up a lot of natural abundance water as can clearly be seen in the OH vibrator region, and this also results in back exchange of the deuterated silanols. The OD vibrations are still seen, but as a small minority. In the fingerprint region, the H-O-H bending vibration is seen at 1630 cm^{-1}, and the amide I reverts to its unmarked position at 1654 cm^{-1} (cf. 1657 cm^{-1} in Figure 5.1). The C=O stretching completely disappears, in keeping with the previous observation that the corresponding species are unstable

in conditions of high hydration. In other words, H/D exchange has no noticeable influence on the speciation and reactivity of silica supported Leucine.

We also duplicated the variable-temperature activation experiments on 1% Leu/SiO_2 (cf. Figure 5.1) after initial deuteration. The spectra are shown in Figure 5.7.

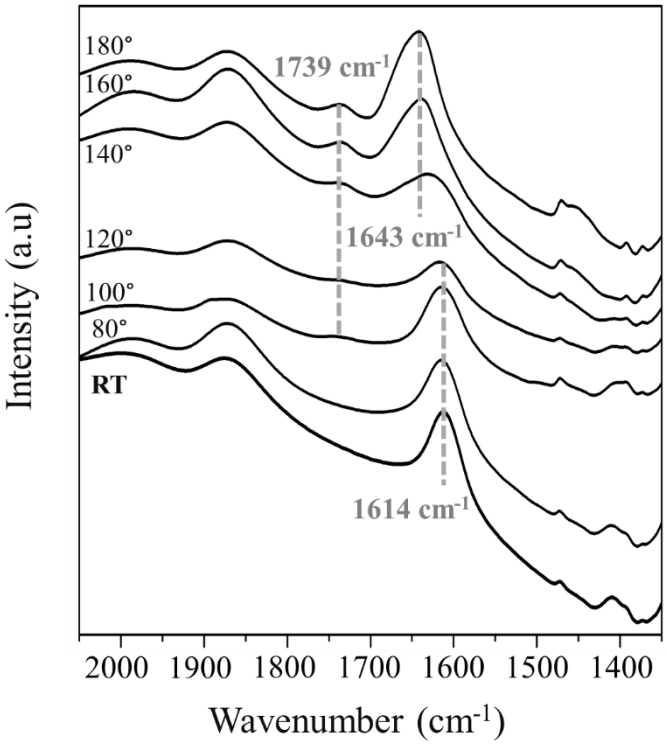

Figure 5.7. IR spectra of the deuterated 1% Leu/SiO_2 samples after thermal activation in VD conditions from 80°C to 200°C

This Figure may be compared to Figure 5.2. Apart from the already noticed band shifts (amide I at 1643 cm^{-1} instead of 1657 cm^{-1}, water bending at 1614 instead of 1630 cm^{-1}), very similar evolutions are observed: the feature that we attributed to the –COOH C=O stretching of the neutral form appears at temperatures as low as 100°C, and the amide I only follows suit at 140 to 160°C. In the 2000 cm^{-1}-4000 cm^{-1} region, the spectra are essentially identical to the ones shown in Figure 5.7 (unhydrated samples).

V.1.4 ^{13}C NMR of thermally activated samples

We also tried to follow the thermal reactions of supported Leucine by ^{13}C CP MAS NMR spectroscopy.

Figure 5.8 depicts the spectra of 3% [$^{13}C_6$, $^{15}N_1$] Leu/SiO_2 and 3% Leu/SiO_2 activated at 105°C for 120 min, at 140°C for 30 min and at 140°C for 60 min. The signal to noise ratio for the activated samples remained poor because non-enriched Leucine was used (while the RT reference – black spectrum- was obtained from fully enriched Leucine). To begin with, the sample thermally activated at the lowest temperature (105°C) shows only a broad feature

between 172 and 180 ppm comparable to the signal we assigned to molecularly adsorbed Leucine (cf. e.g. Figure 3.18), without any trace of crystalline Leu. The first observation is not too surprising: this species was present even in ND samples at RT. As regards the absence of crystal-like peaks, the latter was not systematically observed at low field, possibly due to less resolution compared to high field. At 140°C, a significant intensity appears at lower chemical shift values, and after 60 minutes the maximum of the signal is around 173 ppm. Recall that IR suggested that amide formation occurred between 140°C and 160°C according to drying conditions: one can then surmise that this signal corresponds to silica-supported cyclo(Leu-Leu). For supported Glycine, cyclodimerization caused a comparable upfield shift of +4.5 ppm with respect to the carbonyl in the monomer.[87] In the aliphatic region, the signals of most carbons (C2, C4, C5 and C6) remain unchanged; only in the methylene carbon (C3) region do we see a new signal slowly forming with time at 140°C, and it is then likely to correspond to the methylenes of the cyclo(Leu-Leu) molecules (no genuine cyclo(Leu-Leu) was available to check this). Altogether, the effect of peptide bonds formation on the ^{13}C NMR spectra are not very spectacular; the phenomenon is more easily evidenced by IR.

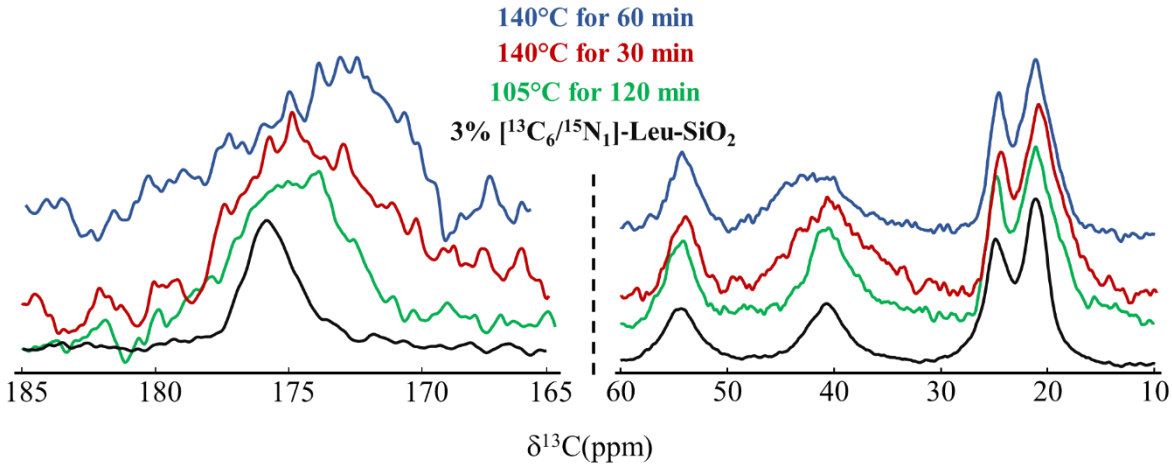

Figure 5.8. ^{13}C CP MAS NMR spectra at 7 T of 3% [$^{13}C_6$,$^{15}N_1$] Leu/SiO_2 at RT and 3% Leu/SiO_2 heated under ND conditions.

V.1.5 Activating the linear dimer H-Leu-Leu-OH on silica

The mechanism we have proposed previously implies that the linear dipeptide H-Leu-Leu-OH is an unstable intermediate: in the conditions where it is supposed to be formed (140°C), it would directly cyclize to cyclo(Leu-Leu). In order to check this hypothesis, we have deposited commercial H-Leu-Leu-OH on silica and studied its thermal reactivity (Figure 5.9).

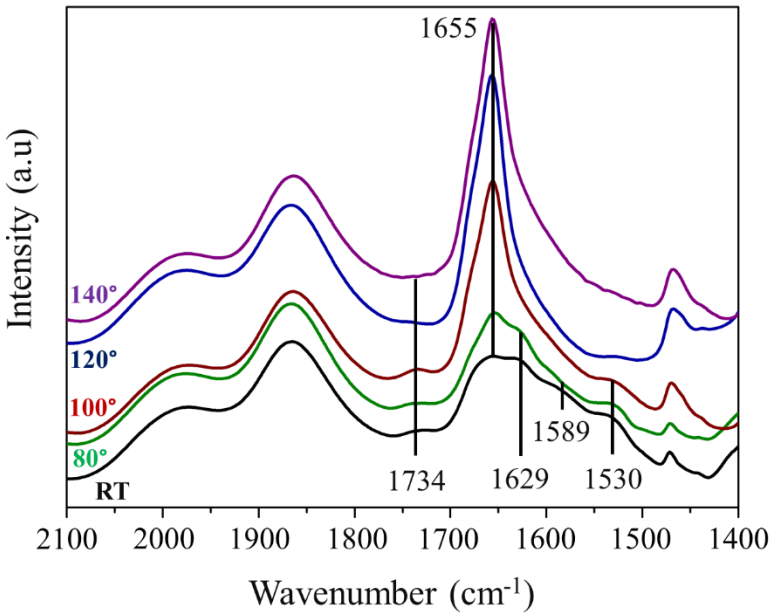

Figure 5.9. Thermal activation of Leu-Leu/SiO_2 under VD conditions

In order to facilitate the observation of the relevant features, we subtracted a 2nd order polynomial baseline and normalized the spectra to the silica band at 1867 cm^{-1}. H-Leu-Leu-OH has many bands in the fingerprint region because it combines one peptide bond with still free carboxylate/carboxylic and amine/ammonium termini. A well-defined maximum at 1655 cm^{-1} probably corresponds to the amide I mode – it is observed at 1674 cm^{-1} in Raman in bulk H-Leu-Leu-OH.[315] As usual, the band at 1629 cm^{-1} is the sum of several contributions, possible including the δ_a of $-NH_3^+$, but certainly also the bending mode of water. The latter must be predominant since this maximum has all but disappeared at 100°C, when the surface is anhydrous. The band at 1530 cm^{-1} could be due to the δ_s of $-NH_3^+$, but since it seems to lie at a rather high wavenumber, it is possible that it contains a contribution of the amide II – the linear dimer is not centrosymmetric, so this vibration should not be extinguished. The evidence is unclear concerning the speciation of the C-terminus. The 1587 cm^{-1} could be the ν_a of $-COO^-$, but the small feature at 1734 cm^{-1} certainly looks like the C=O stretching of a carboxylic acid (-COOH). Maybe both protonation states coexist; altogether, the evidence suggests that H-Leu-Leu-OH deposited on SiO_2 exists as a mixture of cationic and zwitterionic forms. The pKa values of this compound are not known, so they cannot serve to evaluate this hypothesis.

A significant change is observed in the spectrum between 100°C and 120°C. All four bands at 1734 cm^{-1}, 1629 cm^{-1}, 1587 cm^{-1} and 1530 cm^{-1} disappear while the amide I at 1655 cm^{-1} remains as an intense and sharp band. This is in line with the disappearance of uncondensed termini, i.e. with quantitative transformation to cyclo(Leu-Leu). At the same time, and in contrast with the amide I, the band we assigned to amide II also disappears. In conclusion, H-Leu-Leu-OH on a silica surface cyclizes to cyclo(Leu-Leu) at a lower temperature (by at least 20°C) than the point where it can be formed from two Leu molecules, confirming its status as a fleeting intermediate in the Leu dimerization mechanism. We kept on recording the IR spectra

of the sample at temperatures up to 200°C, but no further changes were observed with respect to 120°C.

V.2 Thermal activation of Glutamic acid on SiO_2

V.2.1 IR study of the activation of a low-loading 1% Glu/SiO_2

This part is dedicated to thermal activation of Glu/SiO_2, both under ND and VD conditions, with a special focus on VD systems. Contrary to Leucine, Glutamic acid adsorbs molecularly only in small quantities on the silica surface and tends to crystallize even for rather low loadings (see Figures 4.39 and 4.40, where the signals of crystalline Glu were present for loadings as low as 1%).

Figure 5.10 and 5.12 show two different sets of IR spectra of 1% Glu/SiO_2 thermally activated at different temperatures (from 80 to 200°C) and under different atmospheric conditions (ND and VD). In ND conditions (Figure 5.10), two bands are initially observed, at 1632 cm^{-1} (intense) and 1739 cm^{-1} (weak). The first one, as usual, contains a strong component of adsorbed water, the bands of the Glutamic acid molecules being hidden under it. The 1739 cm^{-1} band is in the region typical for the C=O stretching of a carboxylic acid. We have already mentioned that while the amino acid function of the Glutamic acid is zwitterionic after deposition, the carboxylic moiety in the side chain is protonated: it constitutes a logical attribution for this band.

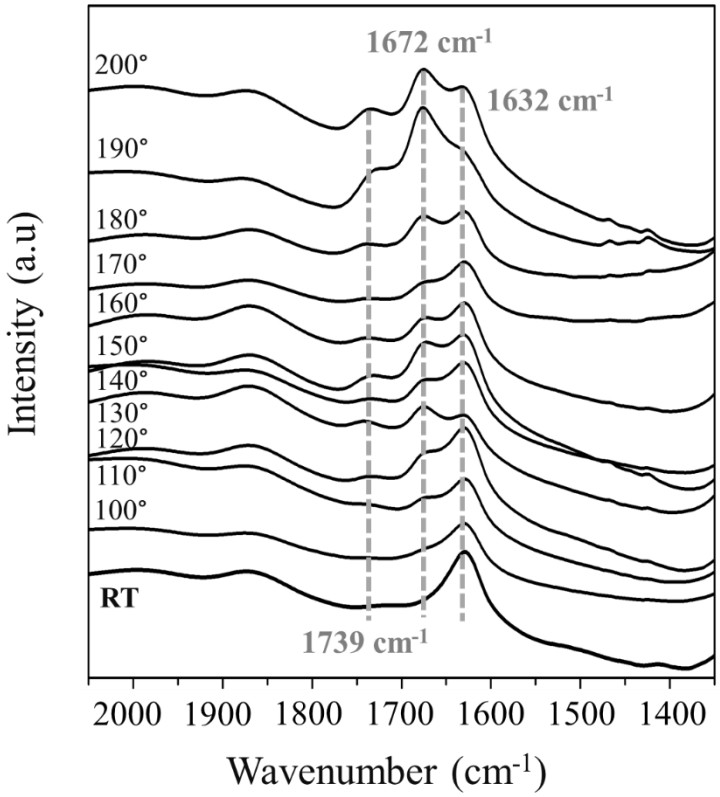

Figure 5.10. IR spectra of Glu/SiO_2 samples thermally activated from 80 to 200°C under ND conditions

From the start of the thermal activation (100 °C), an additional band is observed at 1672 cm^{-1}, likely an amide bond. Its temperature of appearance is much lower than for the corresponding band in Leu/SiO_2, and its position is significantly different (1672 instead of 1657 cm^{-1}). According to previous work,[86] and to our own verification using genuine PyroGlu deposited on silica (see below, § V.2.2), this could be attributable to the internal cyclization of Glu to Pyroglutamic acid (see Figure 5.11). The lactam ring formed in this way contains an amide bond, but in an environment significantly different from that of a peptide chain. In our discussion of DTG traces (§ IV.2.2), we have already mentioned PyroGlu formation as a likely attribution for a low temperature event observed at 120°C in samples with low Glu loadings. It is an internal chemical reaction between the protonated side chain (COOH) and the ammonium moiety (NH_3^+) and from an entropic point of view, it is much easier than a reaction between two separate molecules since no previous diffusion of one molecule towards another is needed (compare with our conclusions on the cyclization of H-Leu-Leu-OH vs. the formation of a peptide bond between two monomeric Leu in § V.1.5).

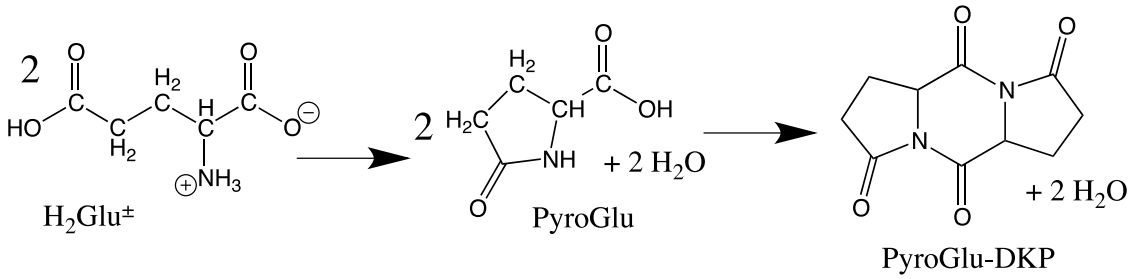

Figure 5.11. Possible steps in the thermal evolution of Glutamic acid according to Bouchoucha *et al*. The second step is not observed here

After this initial transformation, no significant modification is observed in the IR spectra up to 180°C. This may appear contradictory with the work of Bouchoucha *et al*. already cited where the second step in Figure 5.11 was claimed to happen at 160-170°C, namely the condensation of two PyroGlu to the polycyclic molecule PyroGluDKP. In our own DTG traces, a second thermal event is indeed observed at 160 to 170°C for low Glu loading samples. In the IR spectra, a modification of the spectral profile is apparent after heating at 190 and 200°C, but the bands that were considered as typical of PyroGluDKP by Bouchoucha *et al*. (1380, 1720 and 1780 cm^{-1}) are definitely not evident – this may be due however to the low loading we used for our study (1% Glu/SiO_2 as against 2.6% in the former study).

In VD conditions (Figure 5.12), the band at 1634 cm^{-1} is initially less intense than in ND, because the amount of water is lower. The C=O stretching band of the side chain –COOH in $H_2Glu^{\pm}$ is found at 1726 instead of 1739 cm^{-1}. The transformation to PyroGlu is obvious already at 80°C, with extensive formation of the amide I band of PyroGlu at 1682 cm^{-1}, i.e. significantly higher than for ND, and exactly at the same position as in the work of Bouchoucha *et al*. where spectra were also recorded after a treatment in vacuum. Assuming that the transformation to PyroGlu is almost complete, the band at 1745 cm^{-1} may be assigned to the C=O stretching band of the –COOH in PyroGlu. It is then definitely distinct from that of the COOH in $H_2Glu^{\pm}$, which was not the case under ND conditions. These shifts in peak positions between ND and VD indicate that PyroGlu, like the original amino acid, is able to interact with the silica surface upon dehydration, likely by H-bonding.

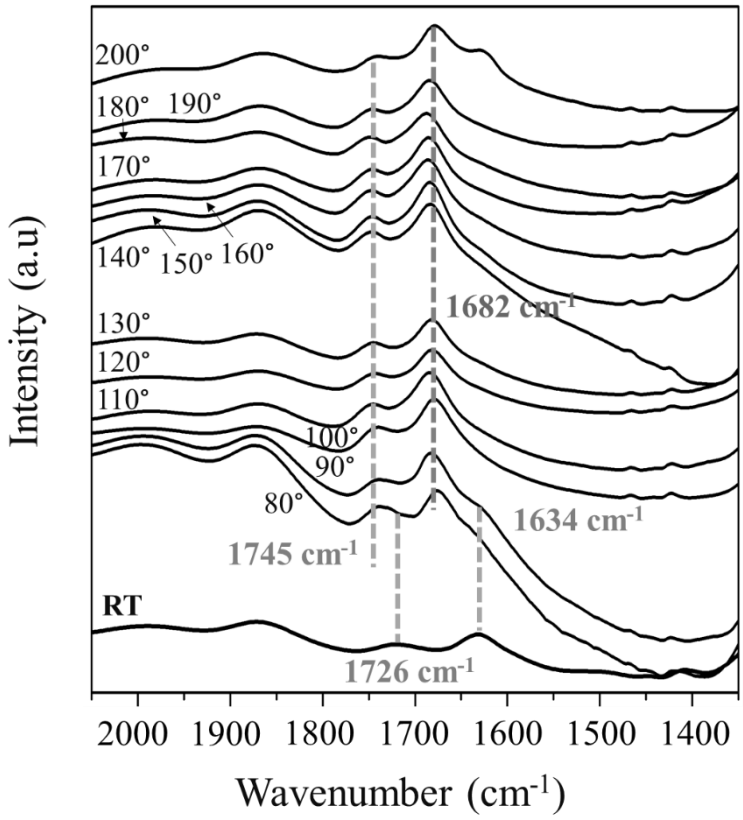

Figure 5.12. IR spectra of Glu/SiO_2 samples thermally activated from 80 to 200°C under VD conditions

As in the case of ND, while the first step of thermal transformation in Figure 5.11 (Glu to PyroGlu) is quite obvious, the occurrence or not of the second (dimerization to PyroGluDKP) cannot be confirmed with certainty: the highest temperature spectrum (200°C) shows a significant transformation with the reappearance of a maximum at about 1630 cm^{-1}, but this is difficult to interpret.

One thing that can be underlined is the difference between Glu/SiO_2 and Leu/SiO_2. For Leu/SiO_2, the –COOH stretching band was assigned to the neutral reaction intermediate $HLeu^0$. For Glu/SiO_2, a –COOH stretching band is also observed, but we have seen that it is most likely due to PyroGlu. In fact, it is possible that $H_2Glu^{\pm}$ first isomerizes to H_2Glu^0 when the surface is dehydrated, but then immediately evolves further to PyroGlu because of the possibility of facile internal cyclization (cf. Figure 5.13). The latter is responsible for the peculiar reactivity of Glu.

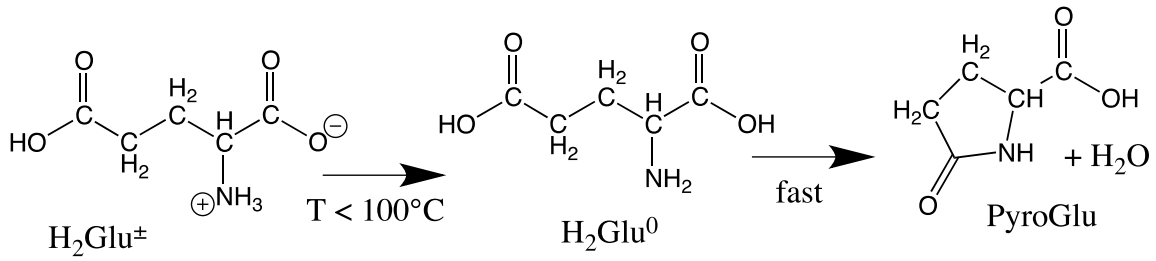

Figure 5.13. Possible additional intermediate step in the thermal evolution of silica-supported Glutamic acid

V.2.2 IR study of PyroGlu/SiO_2

In order to check the assignments made in the previous section, we deposited commercial PyroGlu on silica so as to be able to observe the IR vibrations of the genuine molecule on silica. We then recorded the spectra of 1%PyroGlu/SiO_2 at room temperature and after thermal activation at increasing temperatures. Figure 5.14 shows some of these spectra, compared with the outcome of Glu/SiO_2 activation (from Figure 5.12).

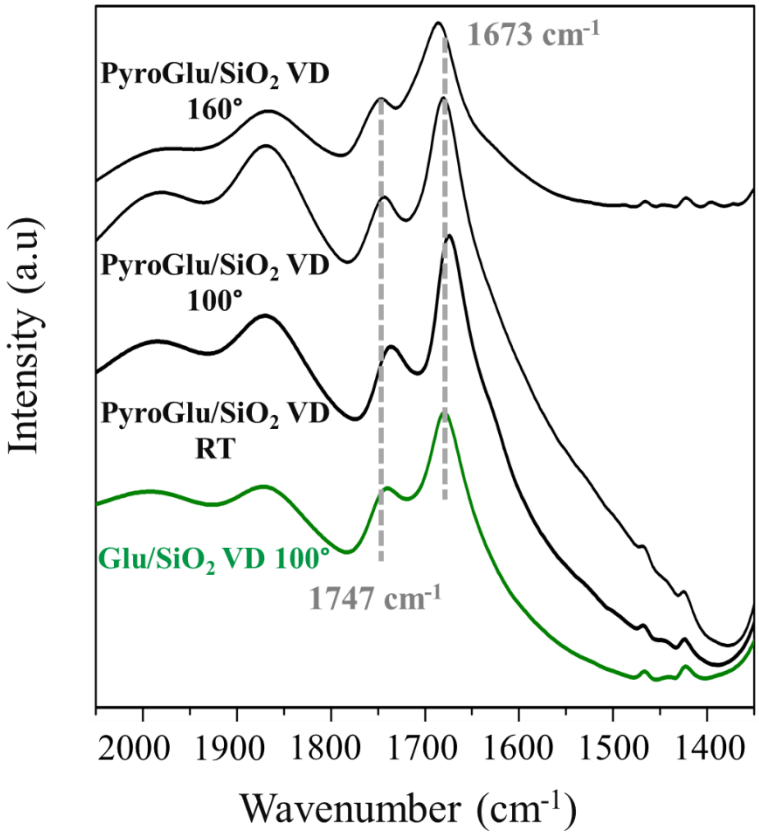

Figure 5.14. IR spectra of 1% PyroGlu/SiO_2 under VD conditions, at RT and thermally activated at increasing temperatures, compared with the product of Glu/SiO_2 activation

The overall aspect of the spectra is very similar to those obtained by activation of Glu/SiO_2. They are dominated by two bands at 1673 cm^{-1}-1682 cm^{-1} and 1730 cm^{-1}-1747 cm^{-1}, corresponding to the amide I and side –chain COOH C=O stretching of PyroGlu. The only modification from RT up to 160° is a progressive blueshift of these two bands, comparable to the one seen when going from ND to VD conditions in thermally treated Glu/SiO_2. Thus, we have a confirmation that i) the species formed at 100°C or lower upon activation of Glu/SiO_2 is supported PyroGlu, ii) upon dehydration, specific interactions are established between PyroGlu and the silica surface, affecting both the amide and –COOH moieties.

V.2.3 IR study of H-Glu-Glu-OH/SiO_2

Another possible intermediate in the thermal transformations of Glu would be the linear dimer H-Glu-Glu-OH (cf. Figure 5.15). Since this compound is commercially available, we have also deposited it on SiO_2. It contains an amide bond, three carboxylic/carboxylate groups (whose protonation state is uncertain), and one terminal amine/ammonium.

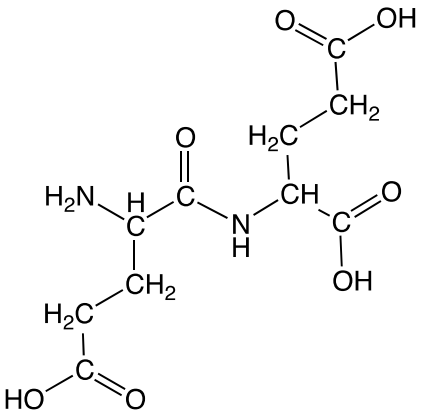

Figure 5.15. The H-Glu-Glu-OH molecule

The spectra of H-Glu-Glu-OH/SiO_2 and the products of its thermal activation at increasing temperatures are shown in Figure 5.16.

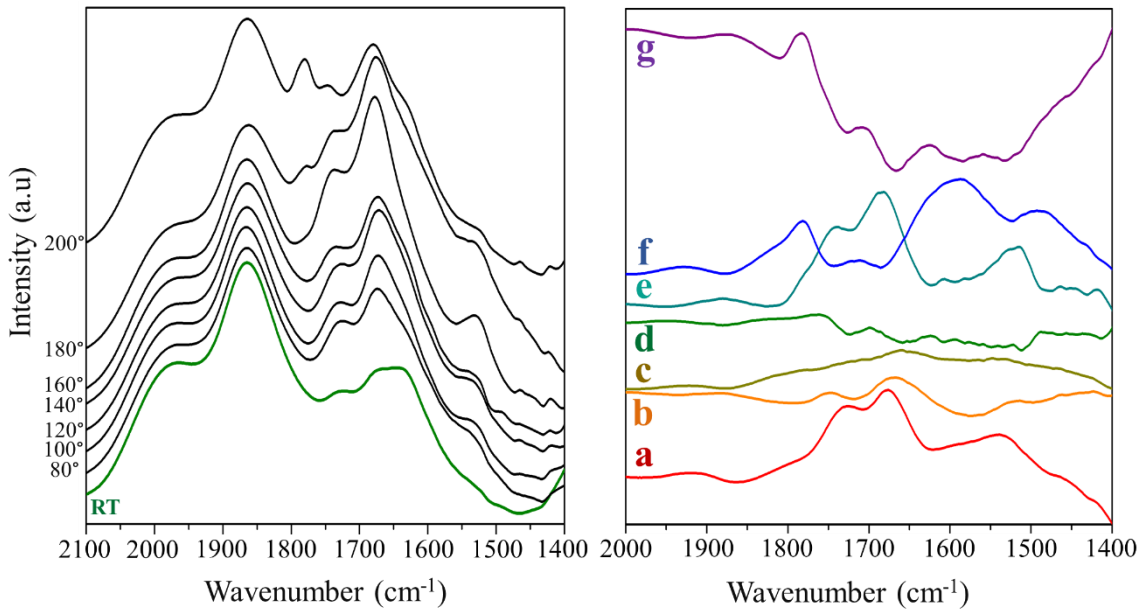

Figure 5.16. Thermal activation of 1%H-Glu-Glu-OH/SiO2 under VD conditions. Left: IR spectra, corrected for 2nd order polynomial background and normalized to the silica band at 1867 cm^{-1}; right: successive difference spectra – a. 80°C – RT, b. 100°C-80°C, c. 120°C-100°C, d. 140°C-120°C, e. 160°C-140°C, f. 180°C-160°C, g. 200°C-180°C

The initial spectrum shows bands typical of side-chain –COOH (1731 cm^{-1}), amide I (1671 cm^{-1}), adsorbed water + $\delta_a(NH_3^+)$ (1638 cm^{-1}) and amide II + $\delta_s(NH_3^+)$ (1530 cm^{-1}). This pattern is not exactly seen in the thermal evolution of supported Glu/SiO_2, and therefore H-Glu-Glu-OH does not seem to be an intermediate in the evolution of the latter, contrary to PyroGlu. Modifications of the spectrum upon heating are best seen by performing subtractions of successive spectra (see right hand side of Figure 5.16). A set of new bands appear between RT and 100°C, with maxima at 1728 cm^{-1}, 1677 cm^{-1} and 1538 cm^{-1}. No significant modifications are observed between 100°C and 140°C; then between 140°C and 160°C, an increase in absorbance is observed at 1744 cm^{-1}, 1682 cm^{-1} and 1514 cm^{-1}, rather close to the first modification – and to bands we assigned to PyroGlu, at least for the first two ones. At 180°C, new bands appear at 1781 cm^{-1}, 1716 cm^{-1} (weak), 1592 cm^{-1} and 1488 cm^{-1}, and at 200°C several bands decrease in intensity. The first two of these bands could be due to PyroGluDKP, specifically to ν(C=O) bands of the succinimide moiety. To explain these observations, we propose that H-Glu-Glu-OH evolves in three steps: closing of a first lactam ring at 80°C -100°C, closing of the second lactam between 140°C and 160°C, and finally formation of the PyroGluDKP tricyclic structure at 180°C, close to the inception of deeper degradation reactions. We will not elaborate any further because H-Glu-Glu-OH is not a likely intermediate in the thermal evolution of monomeric Glu.

V.3 Thermal treatment of co-adsorbed systems: Glu+Leu/SiO_2

V.3.1 IR study of the activation of 3%Glu+Leu/SiO_2

As shown previously for both Leu and Glu adsorbed separately on SiO_2, the formation of cyclic forms is inevitable as the temperature increases. In the case of Leucine, this happens immediately after the formation of the first peptide bond between two Leu molecules, while those molecules that are too isolated on the surface remain "stuck" at the neutral monomer stage. In the case of Glutamic acid, the neutral form is perhaps formed as an intermediate but it is not observed, because it can immediately transform to PyroGlu through internal cyclization. Neither amino acid alone gave rise to linear peptide bond formation, be it under ND or VD conditions, which is not promising to explain the evolution of peptides at the early stages of life.

Therefore, we moved on to the study of (Glu+Leu)/SiO_2 systems, that had been previously reported to form indeed linear peptides.[173] Figure 5.17 and 5.18 show the evolution of the IR spectrum of 2.6% (Glu+Leu)/SiO_2 upon thermal activation, respectively in ND and VD conditions.

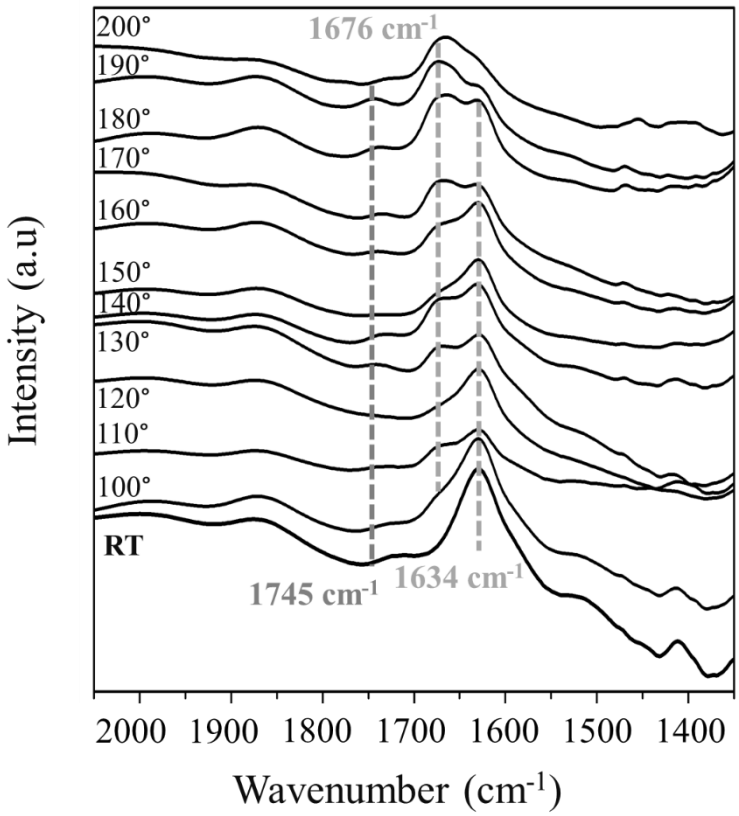

Figure 5.17. IR spectra of 2.6% Glu+Leu/SiO_2 thermally activated under nitrogen drying (ND)

(Glu+Leu) co-adsorbed on SiO_2 initially shows IR peaks at (i) 1726 cm^{-1}, (ii) 1634 cm^{-1}, (iii) 1590 cm^{-1} (shoulder), (iv) 1516 cm^{-1} and (v) 1412 cm^{-1} assigned to (i) ν(C=O) of COOH (ii) superposition of water vibrations and asymmetric deformation of ammonium group $\delta_{as}(NH_3^+)$[316], (iii) $\nu_{as}(COO^-)$, (iv) $\delta_s(NH_3^+)$ and (v) $\nu_s(COO^-)$. Bands (ii) to (iv) could be assigned to either amino acid, while the –COOH group responsible for band (i) is only found in Glu. In ND conditions, the vibration of the side-chain –COOH had been observed at 1738 cm^{-1} in

Glu/SiO_2 (Figure 5.12), which is significantly different. This may indicate that when Leu is present, the side-chain –COOH of Glu is engaged in a different H-bond lattice than when Glu is alone on the surface.

Upon heating in ND conditions, a band appears in the amide I region as early as 100°C, and gradually becomes predominant while the bands of the free termini (-COO^- and –NH_3^+ groups) weaken. Its position is in the 1668 cm^{-1}-1676 cm^{-1} range, i.e. closer to those observed in Glu/SiO_2 than in Leu/SiO_2 systems (although this band may be composite; this is difficult to determine due to overlap). A –COOH ν(C=O) band is still present but it shifts to a different position from the RT one. ν(C=O) band positions as a function of treatment temperature are plotted in Figure 5.19, for both ND and VD conditions. The final value is closer to that in PyroGlu/SiO_2 and $HLeu^0$/SiO_2 than to Glu/SiO_2 RT, i.e., it denotes amino acid C-terminal carboxylic groups (-NH-CHR-COOH) rather than side chain carboxylic acids (R-CH_2-CH_2-COOH). Finally, it would seem that a new band centered in the 1520 cm^{-1}-1530 cm^{-1} region (amide II?) is present at least for the highest treatment temperatures, but since it consists in a rather broad and weak shoulder, its position is difficult to locate.

Moving on to the VD systems (Figure 5.18), the RT spectrum shows the same bands as for the previously discussed ND dried sample, with some slight shifts.

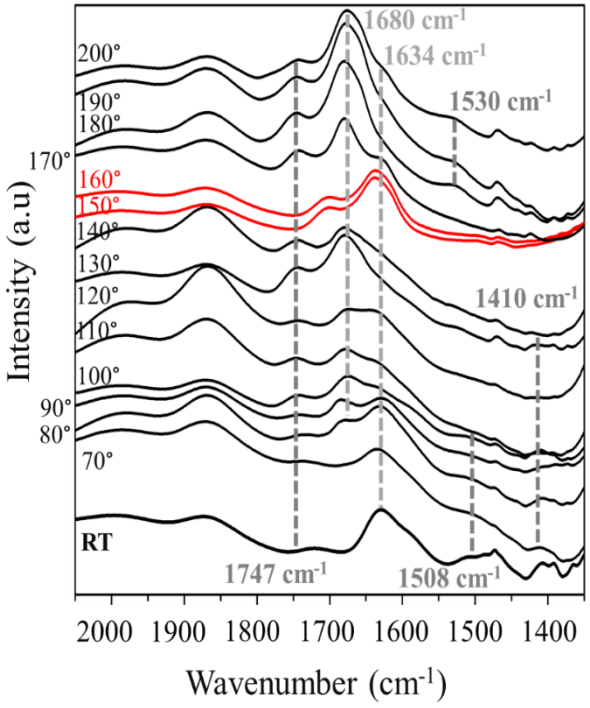

Figure 5.18. IR spectra of 2.6% Glu+Leu/SiO_2 thermally activated under vacuum drying (VD)

The ν(C=O) of COOH in the Glu side chain is located at 1722 cm^{-1} and the $\delta_s(NH_3^+)$ at 1508 cm^{-1}. Upon VD heating, the amide I band appears with a maximum at 1680 cm^{-1}, between 70 and 80°C. Then the COOH ν(C=O) shifts to 1747 cm^{-1}, and the bands of the free N and C termini decrease in intensity until they are no longer discernible at 120°C. For some unidentified reason 150°C and 160°C VD (open circles) show significantly different vibrations than the rest having an unprecedented intense peak at 1700 cm^{-1} (discussed more below).

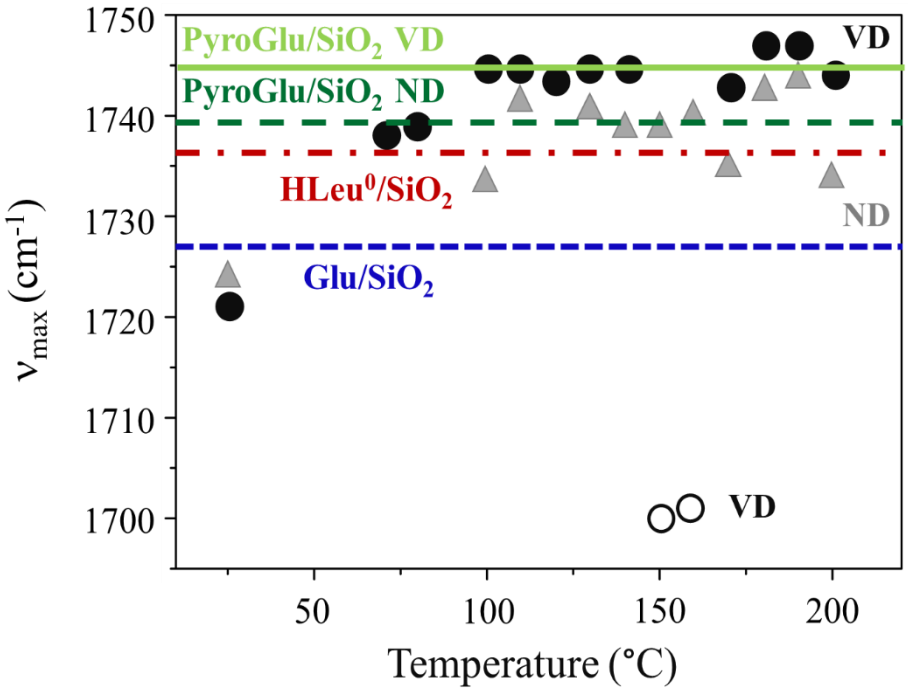

Figure 5.19. ν (C=O) band positions as a function of treatment temperature for both ND and VD conditions

The significance of the final position for ν(C=O) has already been discussed in the comments of the ND spectra and VD data are perfectly compatible with the previous conclusion: what we are seeing is C- terminal –COOH groups, and the Glu side chains have been reacted, no doubt through lactam ring (PyroGlu) formation at lower temperatures.

In VD, more clearly than for ND conditions, a new band appears at 1530 cm^{-1} upon thermal treatment. However, it is only discernible at 180°C and higher. This observation is particularly interesting because a band in this region has been assigned to the amide II.[92] It was not discernible in either single amino acid system (Leu/SiO_2 or Glu/SiO_2) and it indicates the formation of asymmetrical molecules, including linear oligopeptides. While the latter phenomenon has already been reported, the data presented here show that linear peptides formation can happen as a second step, at temperatures significantly higher than the initial amide formation. Thus, species such as PyroGlu may constitute intermediates in linear peptides formation.

Finally, it must be noted that two VD spectra, those at 150°C and 160°C, represent a clear break from the tendency exhibited by the other ones. They show a distinctive profile including a band at 1700 cm^{-1} that was not shown in any other spectra. It must be recalled that all spectra represent successive stages in the treatment of the same sample, and that excludes explanations based e.g. on sample contamination. One tentative explanation would be that the sample was accidentally partly rehydrated after these two treatments, and this rehydration caused a reversible change in adsorbed peptides – subsequent drying steps and thermal treatments would cause the samples to return to the "normal course" of events. This explanation is weakened by the lack of any obvious band of adsorbed water either in the 3400 cm^{-1} or the 5300 cm^{-1} region. Further experiments, including controlled rehydration studies after different activations, would be needed to elucidate this point.

Figure 5.20 compares at 190°C the IR signature of the co-adsorbed (Glu+Leu) with single amino acids Glu and Leu under VD conditions.

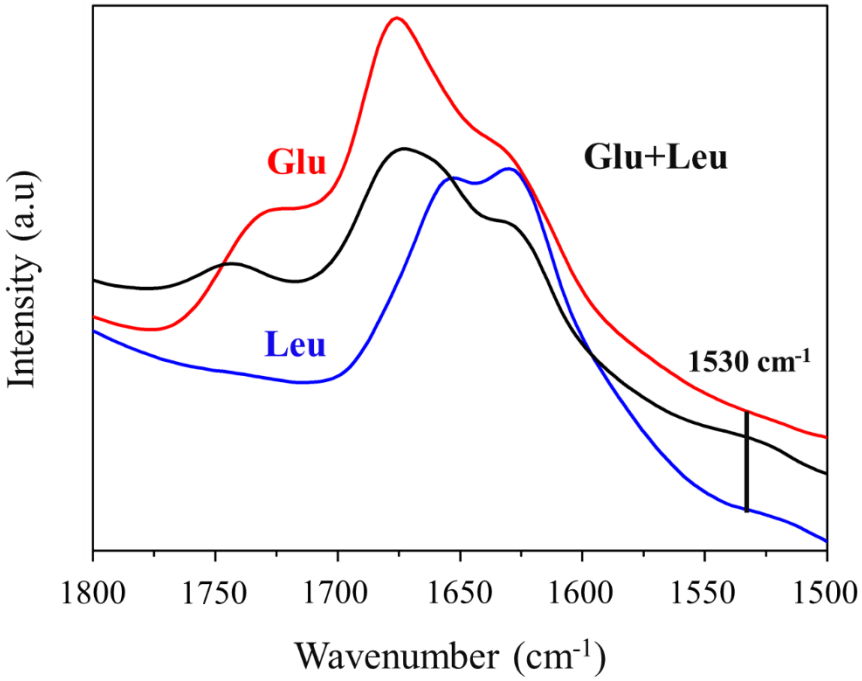

Figure 5.20. IR spectra of co-adsorbed (Glu+Leu) and single amino acids on SiO_2 thermally activated at 190°C in VD conditions

The spectrum of the mixed system (co-adsorbed Glu+Leu) is not simply the sum of the contributions of the two amino acids, confirming that the presence of a second amino acid with different side chain opens new pathways for thermal transformation. It would be worth investing more in the mathematical treatment of the IR spectra in order to identify individual components in the global absorption spectrum.

V.4 ^{13}C solid-state NMR of co-adsorbed systems (Glu+Leu)/SiO_2

V.4.1 ^{13}C NMR

Co-adsorption of (Glu+Leu) amino acids on SiO_2 surface was also investigated by solid state NMR spectroscopy. Initially, experiments were conducted on high loadings such as 7% and 10% with natural abundance amino acids. Let us recall that these figures refer to the total weight loadings in (Glu+Leu), with a 1:1 molar ratio; thus, the 7% (Glu+Leu)/SiO_2 contains an approximately 3.7% loading of Glu and a 3.3% loading of Leu.

Figure 5.21 shows the ^{13}C CP MAS NMR spectra recorded for 7 and 10%(Glu+Leu)/SiO_2 under ND conditions. The carboxylate region shows intense peaks at 180 ppm and 178 ppm corresponding mainly to Glutamic acid in the crystalline phase, and it is mostly the β-phase of

Glu that is present, as was observed for non-enriched Glu/SiO_2. In addition, a relatively broad peak is observed between 176 ppm and 173 ppm, that could correspond to adsorbed species, but the lack of resolution and the presence of superimposed crystalline signals prevents a deeper analysis. It must also be noted that only the peaks of bulk Glu are observable, not those of bulk Leu, although the Leucine loading is > 3%.

The aliphatic region essentially looks like a superposition of the spectra previously described for Leu/SiO_2 and Glu/SiO_2 of comparable loadings. One remark of possible significance is the existence of a small signal at 31.04 ppm in 7% Glu+Leu / SiO_2 (but not of 10% Glu+Leu / SiO_2). This position has been observed for the C4 methylene carbon in the α polymorph of bulk Glu (Figure 4.20). The peak was also present in low-loading Glu/SiO_2 samples (Figures 4.36 and 4.37).

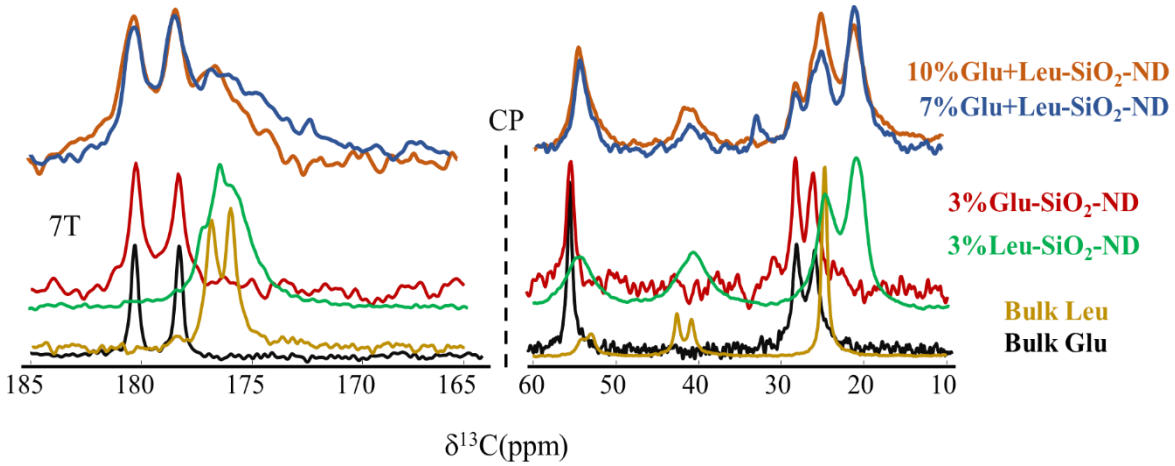

Figure 5.21. ^{13}C CP-MAS NMR spectra of 7% and 10% (Glu+Leu)/SiO_2 in the carboxylate (left) and the aliphatic (right) regions, compared to the spectra of bulk Glu, bulk Leu and the single amino acids systems Glu/SiO_2 and Leu/SiO_2

To avoid crystalline contributions (especially of Glutamic acid), low loadings of Glu+Leu were taken into consideration, using both nitrogen and vacuum drying. The corresponding ^{13}C CP MAS NMR spectra are shown in Figure 5.22 and 5.23.

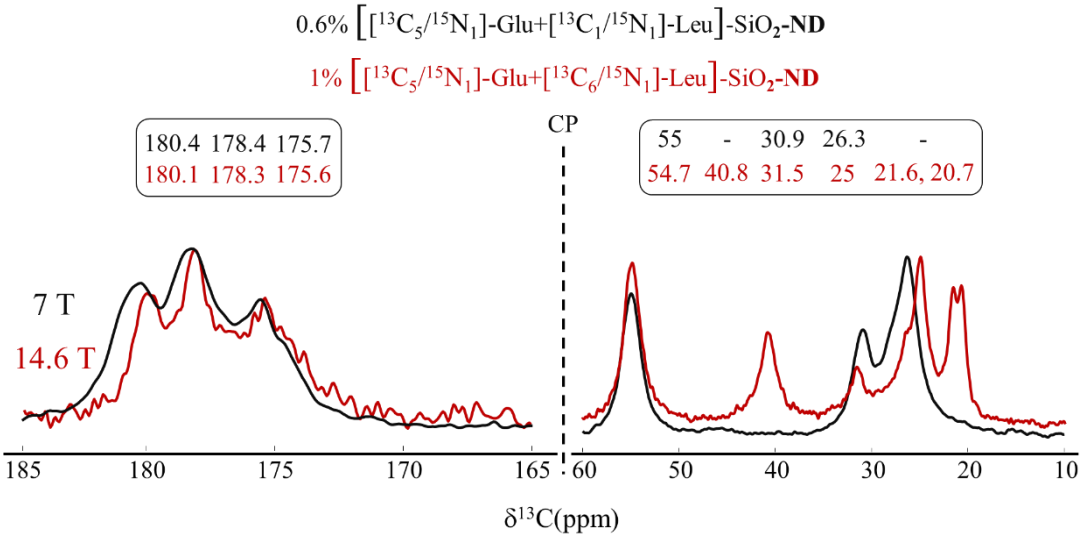

Figure 5.22. ^{13}C CP MAS NMR spectra of 0.6% [$^{13}C_5$,$^{15}N_1$]-Glu + [$^{13}C_1$,$^{15}N_1$]-Leu and 1% [$^{13}C_5$,$^{15}N_1$]-Glu + [$^{13}C_6$,$^{15}N_1$]-Leu/SiO_2 in the carboxylate (left) and in the aliphatic region (right) under ND conditions, recorded at 7 T and 14.6T respectively

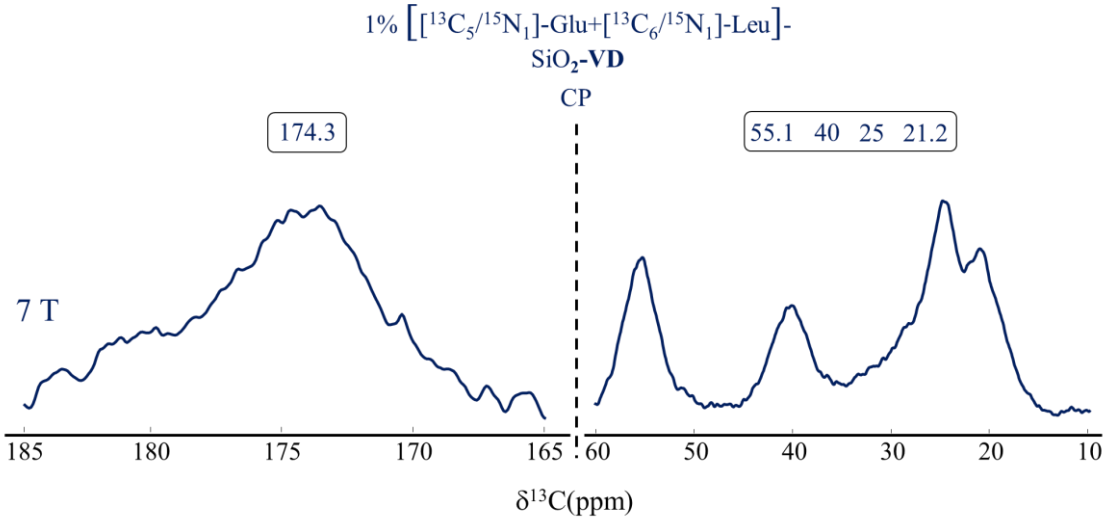

Figure 5.23. ^{13}C CP MAS NMR spectra of 1% [$^{13}C_5$, $^{15}N_1$]-Glu + [$^{13}C_6$, $^{15}N_1$]-Leu/SiO_2 in the carboxylate (left) and in the aliphatic region (right) under VD conditions, recorded at 7 T

The intensity of the crystalline peaks is reduced for 0.6% and 1% loadings in ND conditions, and a peak around ~175.6/175.7 ppm appears that was not present at high loadings. This broad peak may contain contributions from the adsorbed forms of Leu on SiO_2 as seen in chapter III; in contrast, traces of adsorbed Glu are not obvious at the expected peak position around 174.5 ppm (Cf Chapter IV).

Furthermore, this peak is significantly broadened after VD and at 1% loading, a new peak ~ 174.3 ppm emerges and appears to be dominant in the region of the carboxylate. Previously, in chapter IV, 174.5 ppm was attributed to the adsorbed forms of Glu, nonetheless 174.3 ppm is also located within the broad signal of Leu/SiO_2 after VD. Perhaps this signal is as

superimposition of peaks indicating the coexistence for both amino acids (Glu and Leu) with the possible formation of a specific hydrogen bonding pattern between the two.

In the aliphatic region (right), the spectrum looks a lot like a superimposition of Leu and Glu individually adsorbed (it should be noticed that for the 0.6% co-adsorbed sample, Leucine was enriched only on the carboxylate group which explains why some aliphatic signals are "missing" from the spectrum). The signal at > 30 ppm is clearly visible in ND conditions, and disappears under VD conditions. Previously, it was attributed to the C4 of α-Glu (cf. supra); however, here, the corresponding signal of α-Glu in the carbonyl region is not obviously present. Furthermore, it is hard to see why VD would remove the > 30 ppm signal if it was due to a crystalline phase. One should investigate the possibility that a particular adsorbed form (of Glu, most likely) exists with a resonance in this region.

V.4.2 ^{15}N NMR

Figure 5.24 shows the ^{15}N CP MAS NMR spectra of (Glu+Leu) on SiO_2 under ND and VD conditions from high to low loadings (from 10% on non-enriched amino acids to 0.6% on ^{15}N-enriched ones). It reveals a single ammonium nitrogen peak around -339 ppm. The peak position ~ -339 ppm is consistent with the one observed for low loading of Glu / SiO_2 both in ND and VD conditions (-338.7 ppm, cf Fig 4.42) and of Leu / SiO_2 (-338 ppm, cf Fig 3.19). At 0.6% loading, this peak is narrower and allows to observe a broader component centered around -341 ppm. This could be due to the presence of two NH_3^+ groups in different environments. As observed by ^{13}C NMR, it is difficult to conclude from these spectra whether co-adsorption induces differences in the ammonium interaction with the surface by comparison with single adsorption.

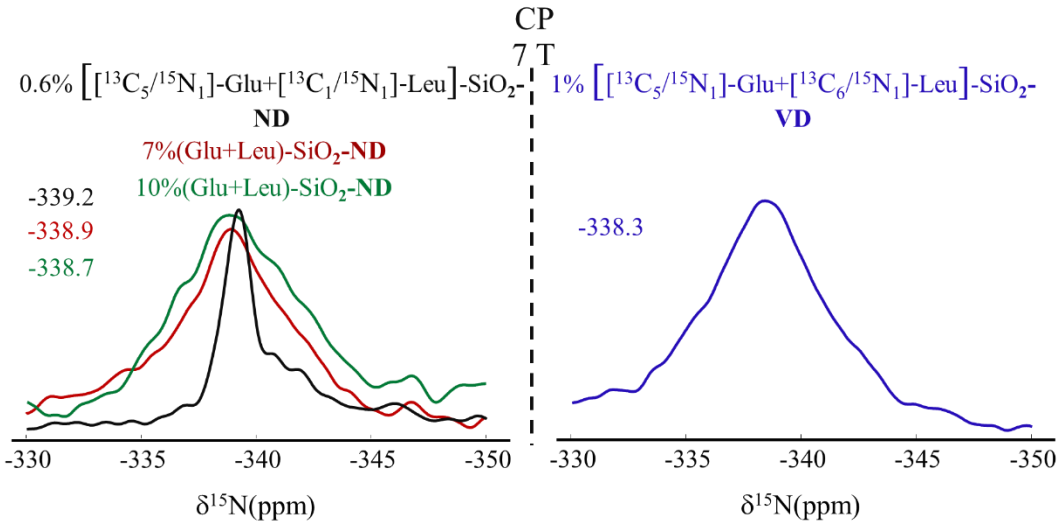

Figure 5.24. ^{15}N CP MAS NMR spectra of the co-adsorbed amino acids on SiO_2 under ND (left) and VD conditions (right), recorded at 7 T

V.4.3 ^{1}H - ^{13}C 2D HETCOR

$^{1}H \rightarrow {}^{13}C$ 2D-HETCOR CP-MAS NMR spectra were recorded on 1% [$^{13}C_5$, $^{15}N_1$]-Glu + [$^{13}C_6$, $^{15}N_1$]-Leu / SiO_2 sample (ND and VD conditions), i.e. for enrichment on all the atoms of Glu and Leu (Figures 5.25 and 5.26).

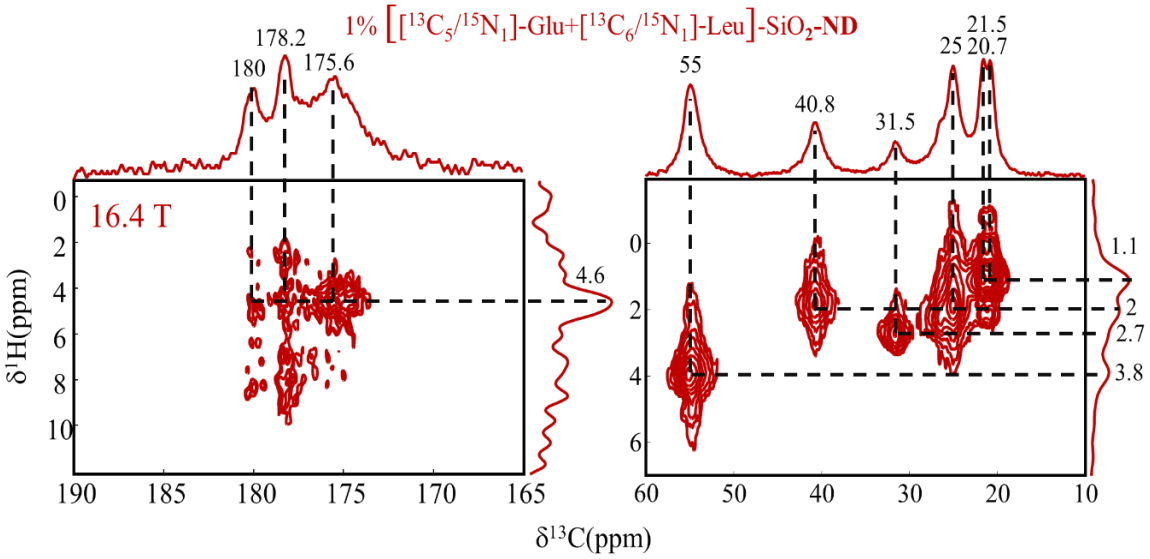

Figure 5.25. $^{1}H \rightarrow {}^{13}C$ 2D-HETCOR CP MAS NMR spectra (16.4 T, 14 kHz) of 1% [$^{13}C_5$, $^{15}N_1$] Glu + [$^{13}C_6$, $^{15}N_1$] Leu / SiO_2 under ND conditions (carboxylate and aliphatic regions)

In ND conditions (Figure 5.25), in the carbonyl region, the signal around 175 ppm assigned to molecularly adsorbed amino acids has a main cross peak at 4.6 ppm on the proton dimension, suggesting that adsorbed forms are mainly interacting with water. Unsurprisingly, in the aliphatic region, the cross peaks correspond mainly to the aliphatic protons (1.1 ppm → 3.8 ppm), with no obvious water signal (expected above 4 ppm). Cross peaks are well-resolved and their position is generally in agreement with the assignments of both ^{13}C and ^{1}H signals.

In VD conditions (Figure 5.26), in the carbonyl region, cross peaks on the ^{1}H dimension are observed at 2.5 ppm corresponding to the aliphatic protons, 5 ppm as a shoulder corresponding to the residual amount of water after VD, 8.3 ppm corresponding to the ammonium and finally 12 ppm and 15 ppm probably corresponds to protonated side chain of the Glutamic acid (-COOH). The strong correlation between the carboxylic/carboxylate carbons and the ammonium protons is definitely suggestive of H-bonding between different amino acid molecules (see § IV.3.2.2.v for a similar observation in crystalline Glu).

The aliphatic region C2, C3 of Glu and Leu shows cross peaks with the nearby ammonium and aliphatic protons. It is less well-resolved than in ND conditions.

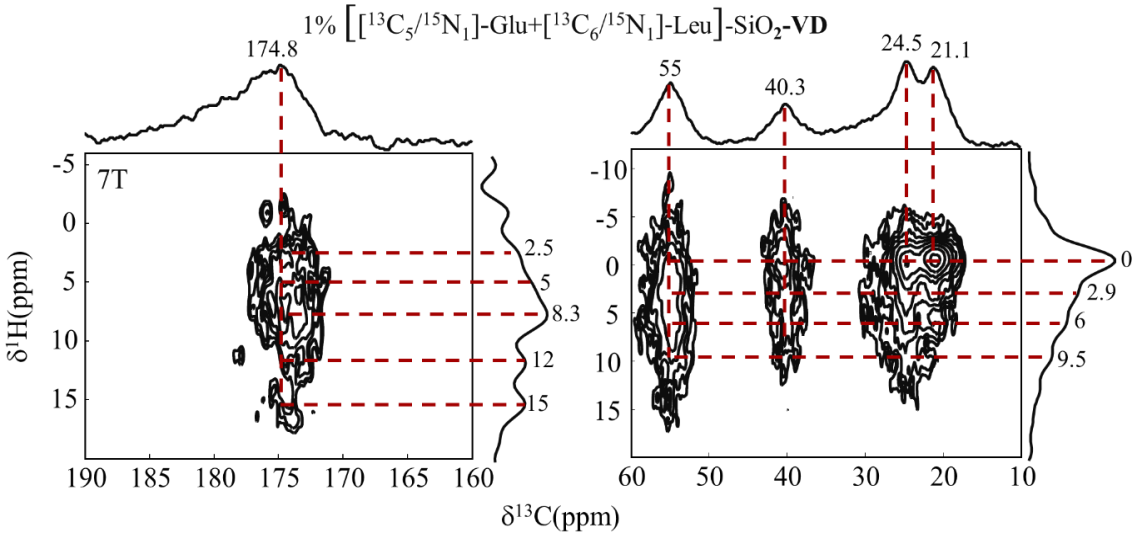

Figure 5.26. $^{1}H \rightarrow {}^{13}C$ 2D-HETCOR CP MAS NMR spectra (7 T, 14 kHz) of 1% [$^{13}C_5$, $^{15}N_1$]-Glu + [$^{13}C_6$, $^{15}N_1$]-Leu / SiO_2 under VD conditions (carboxylate and aliphatic regions)

V.4.4 ^{1}H - ^{15}N 2D HETCOR

^{1}H - ^{15}N 2D-HETCOR CP-MAS NMR spectrum (Figure 5.27) of 1% [$^{13}C_5$, $^{15}N_1$]-Glu + [$^{13}C_6$, $^{15}N_1$]-Leu / SiO_2 (VD) shows that the single peak observed in the ^{15}N CP spectrum (Figure 5.24-right) exhibits a main cross peak at 5 ppm corresponding to the residual water present, consistent with the proposition already presented in § V.4.2 that a small amount of water remains even after VD, in specific interaction with the adsorbed amino acids.

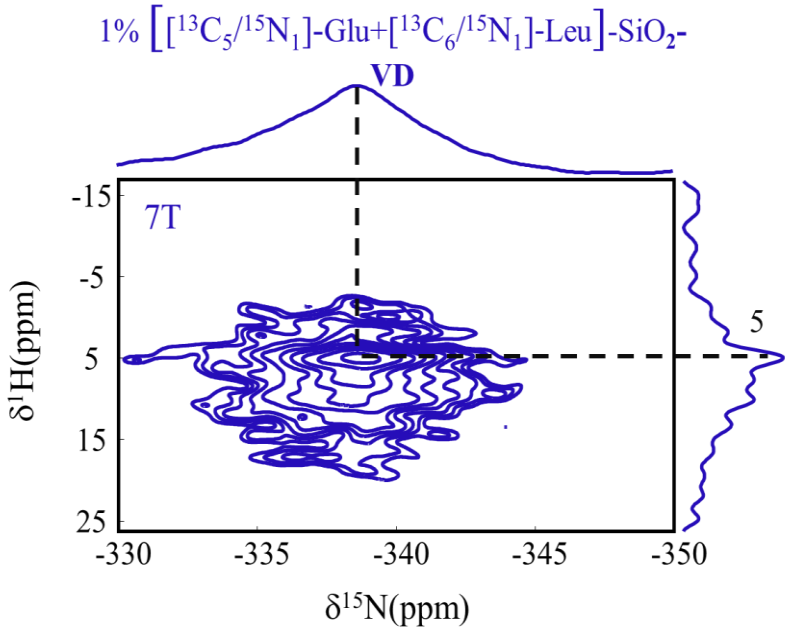

Figure 5.27. $^{1}H \rightarrow {}^{15}N$ 2D-HETCOR CP MAS NMR spectrum of 1% [$^{13}C_5$, $^{15}N_1$]-Glu + [$^{13}C_6$, $^{15}N_1$]-Leu / SiO_2 under VD conditions recorded at 7 T

Altogether, the NMR spectra contain some hints of new environments due to the interactions between the two amino acids, but because of signal broadening and overlap they remain uncertain until further experiments are carried out. More NMR experiments on co-adsorbed and activated systems were planned but could unfortunately not be conducted due to COVID crisis.

V.5 Conclusion and perspectives

In this chapter single and co-adsorbed Glu and Leu on silica surface were studied using mainly IR and NMR spectroscopy.

Both Leu and Glu adsorbed separately on SiO_2 undergo condensation reactions to cyclic forms as the temperature increases. These are clearly revealed by IR where the appearance of the amide I band is obvious, but they are harder to observe by NMR which is hindered by its high sensitivity – slightly different environments give rise to heterogeneous broadening of the signals, and thus to a low signal/noise ratio and strong signal overlap.

In the case of Leucine, amide bond formation is observed at temperatures higher than 160°C in ND conditions, compatible with the thermal event observed in TG (§ III.2.2). The result is mostly the cyclic dimer (cyclo-Leu-Leu or DKP). In VD conditions, where physisorbed water removal is more efficient, we observe the isomerization of the zwitterion $HLeu^{\pm}$ to the neutral form $HLeu^{0}$ at temperatures as low as 110°C – this isomerization had been postulated previously but never directly observed. Upon further heating, $HLeu^{0}$ partly transforms to the cyclic dimer at 140°C, but a residual amount of monomer is still present even at 200°C. Apparently, this reaction is limited by diffusion on the silica surface.

In the case of Glutamic acid, the neutral form is perhaps formed but it is not observed, because it can immediately transform to PyroGlu through internal cyclization. Contrary to previously published data,[86] we did not see any evidence of further transformation to the tricyclic dimer PyroGluDKP. When the genuine linear dimer H-Glu-Glu-OH (containing a preexisting peptide bond between two Glu groups) was deposited on silica and activated, we observed successive internal cyclization, and (probably) ring closure to PyroGluDKP at higher temperatures; but this pathway is not followed when starting from monomeric Glu.

In both cases, the outcome of thermal activation may be considered as a “dead end” from the prebiotic point of view. It remains possible that more interesting peptides could be obtained by complex scenarios involving wetting-and-drying cycles, which we did not investigate.

On the other hand, once these amino acids are co-adsorbed, linear chains of peptides are formed. The IR spectra of the mixed system (co-adsorbed Glu+Leu) is not simply the sum of the contributions of the two amino acids, confirming that the presence of a second amino acid with different side chain opens new pathways for thermal transformation. The amide I band appears at even lower temperatures (80°C) than for Glu/SiO_2, and is probably initially due to PyroGlu formation. But a different phenomenon is observed at higher temperatures (170°C), where the appearance of an amide II band suggests the formation of linear polymers. This hypothesis is confirmed by an ongoing study by advanced MS methods of the polymerization products.[317]

Concerning solid-state NMR, only limited data have been obtained on mixed Glu+Leu/SiO_2 systems. They provide some tantalizing clues of specific interactions between the two amino acids, but a more complete investigation is in order to confirm these initial observations.

The next step would be a more detailed identification of the thermally activated compounds, both experimentally (in particular by NMR) and theoretically. Instead of a "blind" study of activated samples at regularly spaced activation temperatures, one should concentrate on the temperatures at which the IR spectra have been observed to exhibit significant changes. Additional input may be provided by the already mentioned MS studies of activation products – it has been demonstrated recently that in the particular case of Glu+Leu/SiO_2, the peptides formed can be quantitatively desorbed by simple washing with distilled water. Selective enrichment of a single amino acid, and/or amino acids enriched on a single position, may help overcome the difficulties due to signal overlap. In this way, it may become possible to identify specific interactions between functional groups of the two amino acids, that would help explain the special reactivity of the (Glu + Leu) system toward linear oligopeptides formation.

Theoretically, models containing both amino acids together could be constructed, possibly doubling the silica cell used in this study to have enough adsorption sites, and optimized. The challenge to this approach is the very high number of starting configurations that may be imagined when two amino acids, each one with two or three reactive groups, are interacting simultaneously with the surface and with each other; but every specific piece of information provided by IR and NMR will help constrain the models to a manageable list of possibilities. The same approach that we used in previous chapters for single adsorbed amino acids may then be applied: select the energetically most favorable configurations, calculate their theoretical chemical shifts, and compare with the experimental values in order to select the best models.

General Conclusion

During the course of this thesis, we tried to develop an original approach to the understanding and characterization of hybrid systems consisting in bioorganic molecules such as amino acids (Leucine and Glutamic acid) deposited on the surface of silica. Our attention was devoted to this particular system because these two amino acids have different chemical and physical properties and had been singled out before, in our research team, as being an 'interesting couple' to study: namely, upon thermal treatment, they can combine to form rather long linear oligopeptides, a possible key step of the evolution of Life on the primordial Earth.

We combined experimental characterization by *in situ* techniques, mainly solid state NMR, IR spectroscopy, X-Ray diffraction and thermogravimetric analysis with ab-initio structural modeling. A defining feature of our approach is that we systematically compared the theoretical models with the experimental reality, chiefly by NMR chemical shifts calculation.

In both cases (Leu and Glu), the main type of bond between the organic molecule and the inorganic surface is H-bonding, at the exclusion of covalent bonding. This represents a challenge for spectroscopic characterization techniques since individual H-bonds have only limited effects on the position of NMR peaks and IR bands, but at the same time this situation presents an interesting parallel with biochemistry, where lattices of H-bonds play essential roles in molecular recognition (e.g. the DNA double helix) and in catalytic reactivity (e.g. defining the interactions between an enzyme and its substrate).

In both cases too, a parameter was crucial to determine the speciation of the amino acids on the silica surface, namely the degree of hydration. For this reason, we devoted some efforts to controlling the water content in the system. We defined two standard procedures of sample pretreatment, drying under nitrogen flow (here called ND conditions), and drying under vacuum (VD). At the same time, we designed two sets of models for the theoretical studies: anhydrous ones, containing only the amino acid and the silica surface, and microsolvated ones, which contained in addition a fixed number of water molecules.

A first experimental difficulty is to unravel spectroscopic signals from different forms of amino acids: molecularly adsorbed (interacting individually with silica surface sites), and

microcrystalline. For Leucine, the amino acid was found to adsorb molecularly up to slightly less than 3% loading (by weight), at which point the adsorption sites were saturated: bulk-like Leucine started to precipitate and became visible by both XRD and NMR. For Glutamic Acid, the situation was different. Samples that did not show any signs of XRD peaks of the bulk amino acids still exhibited unmistakable signals of the crystal phase in solid-state NMR, down to very low Glu loadings. Apparently, the formation of small crystals (or perhaps, nucleation clusters, containing only few molecules and not detectable by XRD) is energetically competitive with site adsorption on silica from the start, contrary to the case of Leu.

As a consequence, samples with very low amino acid loadings (of the order of 1%) have to be studied in order to predominantly observe the signal of the adsorbed Glu, further straining spectroscopic methods. Using isotopically enriched amino acids is essential for solid state NMR spectroscopy, a technique with a low intrinsic sensitivity; high magnetic fields are also desirable.

With these precautions, the spectroscopic studies indicated that for both amino acids, the zwitterionic form predominates after both ND and VD drying, with the side-chain COOH protonated as regards Glu. In other words, the acido-basic speciation was the same as in water solution. In molecular modeling, it was observed that microsolvated models converged to the zwitterionic form, while most (but not all) of the anhydrous models converged to a neutral form (with uncharged –COOH and $–NH_2$ termini). Thus, comparison of experiment and modeling suggests that water is still present and interacting with the amino acids after room-temperature drying, even under vacuum, a conclusion compatible with TG data.

Adsorbed Leucine showed restricted mobility and heterogeneous broadening already in both ND and VD conditions. ^{15}N NMR indicated that the ammonium moiety may establish a more intimate interaction with the silanols of the silica surface upon VD, a conclusion compatible with the “best” microsolvated models (those with the most negative adsorption energy).

Adsorbed Glutamic acid was harder to characterize. It appeared to exhibit at least two different forms (in addition to the crystal-like Glu), a very mobile, “solution-like” form that was only detected by DP-MAS, and not by CP-MAS NMR, and a form with restricted mobility that was observable by CP. The interconversion of these two forms seems to be highly dependent on the hydration state of the system. Overall, Glu appears to have a lower affinity for the silica surface

than Leu, in keeping with the conclusions of the XRD-NMR study mentioned above. Calculation of the spectroscopic parameters (chemical shifts) showed that the models most compatible with AA/SiO_2 dried at RT were some of the microsolvated ones, confirming the subsistence of strongly co-adsorbed water at room temperature.

We also obtained some data, chiefly from IR, on the thermal reactions of Leu, Glu, and co-adsorbed Glu+Leu. In the case of Leucine, we believe that we have observed the transition from the zwitterionic form present at RT ($HLeu^{\pm}$) to the neutral form ($HLeu^{0}$) predicted by modeling ($HLeu^{\pm}$) upon complete dehydration. Upon further heating, the latter form partly converts to the cyclic dimer cyclo(Leu-Leu), in a reaction that is probably limited by diffusion on the silica surface. In the case of Glutamic acid, the neutral form is not observed because it immediately converts to the product of internal cyclization, pyroglutamic acid (PyroGlu).

In both cases, the predominant product of reaction (cyclo(Leu-Leu), and PyroGlu, respectively) may be considered as a "dead end" as regards the potential for creating complex prebiotic molecules. But for the mixed system (Glu + Leu)/SiO_2, spectroscopic evidence indicates the formation of linear oligopeptides, which is considerably more interesting and confirms data previously obtained in our team and published by Sakhno *et al*. Unfortunately, we did not have enough time to characterize the (Glu + Leu)/SiO_2 systems at the same level of detail as those with a single amino acid, but available evidence shows that the approach we used in the first chapters of this thesis should be applicable here too. Of course, the system is more complex, and the experiments will have to be devised with care; but it is encouraging that the limited data at our disposal already seem to point at localized interactions between different amino acid molecules. Also, concerning the interaction between experimental and modeling results, it will be particularly important to use every piece of spectroscopic evidence to restrict the range of studied models from an otherwise intractable complexity.

Finally, the different behaviors of the two systems we studied in depth should serve to underline the complexity of the interactions between amino acids and mineral surfaces. Each combination is a different story; from a "philosophical" point of view, one may wonder to what degree the complexity of life was constrained and directed by the preexisting complexity of the mineral world.

Annexes

Several models of Leucine and Glutamic acid adsorbed on the silica surface were optimized, both anhydrous and microsolvated and corresponding NMR chemical shift values were calculated.

Model	Carbon (C_1OO^-)	Nitrogen (N)	Average NH_3 protons	C2	C3	C4	C5/C6	H2	H3	H4	H5, H6
Bulk Leucine	175.6/177.3	-334.3/ -336.4	9.6	52.5/ 53.7	41.7/40.1	25.6/25.6	24.6/25	4.6	1.7	1.7	0.9
A	173.3	-335	8	52.4	45.9	22	18.6/25.8	4.7	1.8	1.5	1
B	168.2	-340.6	4.5	55.9	41.9	21.8	17/25.3	3.4	1.7	1.5	0.8
C	169.7	-336.4	7.8	53.8	42.8	21.5	16.6/24.9	3.8	1.7	2.9	0.9
D	164.8	-340.3	1.7	53.2	50.5	20.8	17.9/25	3.7	1.2	1.5	0.8
E	173.3	-334.9	8	52.3	45.9	22	18.6/25.6	4.7	1.3	1.5	1.1
F	173.3	-334.9	8	52.3	45.9	22	18.6/25.6	4.7	1.3	1.5	1.1
G	182.7	-335.3	3.5	52.4	43.1	21.1	20.1/25.2	4.5	1.2	1.7	0.9
H	175.7	-338.3	3.8	53.6	43.6	22	20.6/27.1	4.2	1.4	1.1	1
I	173.3	-345.2	3.4	53.1	42.7	21.1	20.1/24.9	4.3	1.3	1.7	0.9
J	171.3	-343	3.8	52.8	45.2	21.1	18.2/24.9	3.8	1.2	1.6	0.9
K	179.3	-347.1	2.1	51.9	43.6	22.8	19.4/25.8	4.3	1.4	2.2	1

Model	Carbon (C_1OO^-)	Nitrogen (N)	Average NH_3 protons	C2	C3	C4	C5/C6	H2	H3	H4	H5, H6
A'	169	-330.4	8.3	53.6	42.2	25.1	18/21.5	3.7	1.2	1.8	0.9
B'	171.3	-329.2	8	57.4	41.5	25.6	19.4/21.1	3.2	1.8	0.7	1.4
C'	171.8	-331.3	9.5	52.7	36.2	26.7	17.5/20.4	3.4	2	1.2	0.9
D'	167.9	-333.5	8.5	54.8	43.7	26	17.9/21.2	3.8	1.3	1.3	0.9
E'	170.1	-340.1	8.1	55.8	43.6	24.7	18/21.9	4.6	1.3	1.9	1
F'	171.1	-335.9	9.1	53.4	43	24.8	18.4/21.8	5.6	1.2	2	0.9
G'	172.5	-331.7	8.4	57.3	37.8	25.9	17.3/21.9	3.9	1.5	1.4	0.9
H'	170.6	-335.3	9	53.6	39.6	25.8	17.4/21.4	4.2	1.3	1.7	0.8
I'	170.6	-333	8.5	55.7	42.6	25.8	17.1/21.3	3.9	1.3	1.5	0.9
J'	171.8	-334.6	9.1	53.3	40.6	26	17.5/21.1	4.2	1.3	1.7	0.9
K'	169.3	-330.8	8.9	54.4	41.9	25.9	17.4/21.7	3.8	1.4	2.3	0.8
L'	169.1	-336.1	8.2	54.8	41.9	24.7	20.1/21.5	4.7	1.5	1.9	0.9
M'	172.3	-335.9	9.6	51.7	38	20.7	17.3/26.1	3.5	1.4	1.9	0.9
N'	170.6	-329.3	8.9	52.2	42.1	21.7	17.5/26.4	3.7	1.8	1.3	0.9
O'	167.5	-330.2	8.6	53.2	42	21.6	17.4/25.7	3.6	1.3	2.1	0.9
G'-1	170.3	-326.2	7.2	57	40.1	25.8	17.6/21.9	4	1.2	1.5	0.9
G'-2	171	-331.5	7.5	57.2	40	25.7	17.4/21.9	4.1	1.5	1.4	0.9
J'-1	169.4	-329.3	7.1	53.2	40.8	26	17.6/21	4.4	1.3	1.8	0.9
G''	174	-332.9	9.1	56.3	40.1	25.9	17.3/21.6	3.8	1.6	1.3	0.9
O''	175.3	-328.3	9.6	52.4	39.1	26.3	17.2/21.4	3.8	1.4	1.6	1.2
O''-1	174	-330.5	7.6	52.4	40	26.3	17.2/21.4	3.8	1.3	1.7	1.2

Table 1. Calculated ^{13}C, ^{15}N and ^{1}H chemical shift values for all models of Leucine on silica (anhydrous and microsolvated systems)

Model	Carbon (C_1OO^-)	Nitrogen (N)	Average NH_3 protons	C2	C3	C4	C5	H2	H3	H4	H5
α-Bulk Glutamic Acid	177.7	-335.5	9.9	53.6	29.8	31.9	180.7	4.4	2.6	2.7	16.7
β-Bulk Glutamic Acid	178.4	-339.8	9	54.6	26.3	28.8	180.5	4.2	2.4	2.7	19.1
A	176.8	-357	2.7	53.5	25.4	31.8	173.7	3.5	2	2.6	7.3
B	176.6	-350.6	3	54	29.4	32.6	176.3	3.3	2	2.7	10.8
C	173.8	-366	1.3	52.7	27.3	28.2	170.6	3.7	2	2.6	7
D	164.1	-338.7	6.5	57.8	22	27.6	174.7	4.4	2.5	3.2	7.4
E	170.3	-354.7	3	52.3	33.5	32.4	181.8	3.1	2.2	2.8	7.8
F	184.4	-360.2	2	53.4	28.6	33.4	165.7	3.7	2.4	2.8	12.5
G	163.4	-343.5	9.1	51.3	27	27.7	174.2	5	2.2	3	12
H	169.1	-343.5	9.9	53.2	29	32.8	177.1	3.5	2.4	3.2	7.5
I	163.2	-340	8.7	52.1	24	28.4	166.8	4.1	2	2.6	9.7
J	170.9	-359.4	2.4	52.4	29.6	28.8	168.6	4.4	2	2.5	7.3
K	176.3	-366.1	1.5	51.3	27.4	28.4	173	4.4	2.2	2.5	7.1
L	170.9	-360	2	52.3	28.4	28.5	168	4	2	2.6	6.8
M	175.3	-366.1	1.2	53.1	24.6	28.8	170.4	4.4	2.1	2.6	6.8

Model	Carbon (C_1OO^-)	Nitrogen (N)	Average NH_3 protons	C2	C3	C4	C5	H2	H3	H4	H5
A'	172.6	-341	8.8	54.3	25.2	31.5	179.1	3.8	3.2	2.6	23.2
B'	175.4	-340.15	10.1	54.4	30.1	33.2	177.2	3.5	2.9	3	12.2
C'	179.4	-356	4.4	52.2	29.4	31.1	184.6	4.7	2.3	3.1	18.4
D'	172.1	-338.1	9.1	55.7	26	33	178.3	4.7	2.4	3.3	16
E'	173.6	-334.1	9.7	59.9	26.5	30.6	183.6	4.2	2.3	3.1	18.8
F'	171.5	-338.2	9	53.5	26.7	33.6	178	3.9	2.5	2.8	14
G'	182.8	176.7	3.4	55	31.5	30.8	176.7	4.3	2.1	3.8	17
H'	177	176.5	9.4	54.5	29.2	31.8	176.5	3.6	2.7	3	19.5
I'	169.7	177	9.5	52.6	28.8	31.5	177	3.2	2.5	3	15.1
J'	172	181	8	55.7	24.7	31.8	181	4.2	2.5	3.4	15.1
K'	174.2	181	8.6	53.8	28.4	29.3	181	4.5	2.7	2.7	19.1
L'	174.1	185.5	9	51.5	23.3	31.5	185.5	5	2.4	3	15.5
M'	180.7	176.4	5.3	52.1	27	28.4	176.4	5.4	2.2	3.1	16.2

Table 2. Calculated ^{13}C, ^{15}N and ^{1}H chemical shift values for all models of Glutamic acid on silica (anhydrous and microsolvated systems)

Tables 1 & 2 show the calculated ^{13}C and ^{15}N chemical shifts for both Glu and Leu on SiO_2 (anhydrous and microsolvated). Further data and explanations in the coming chapter III and IV will be ultimately based on the following two tables showing all the models prepared doe understing the phenomena of adsorption through DFT simulation by using the QE (Quantum Espresso) software.

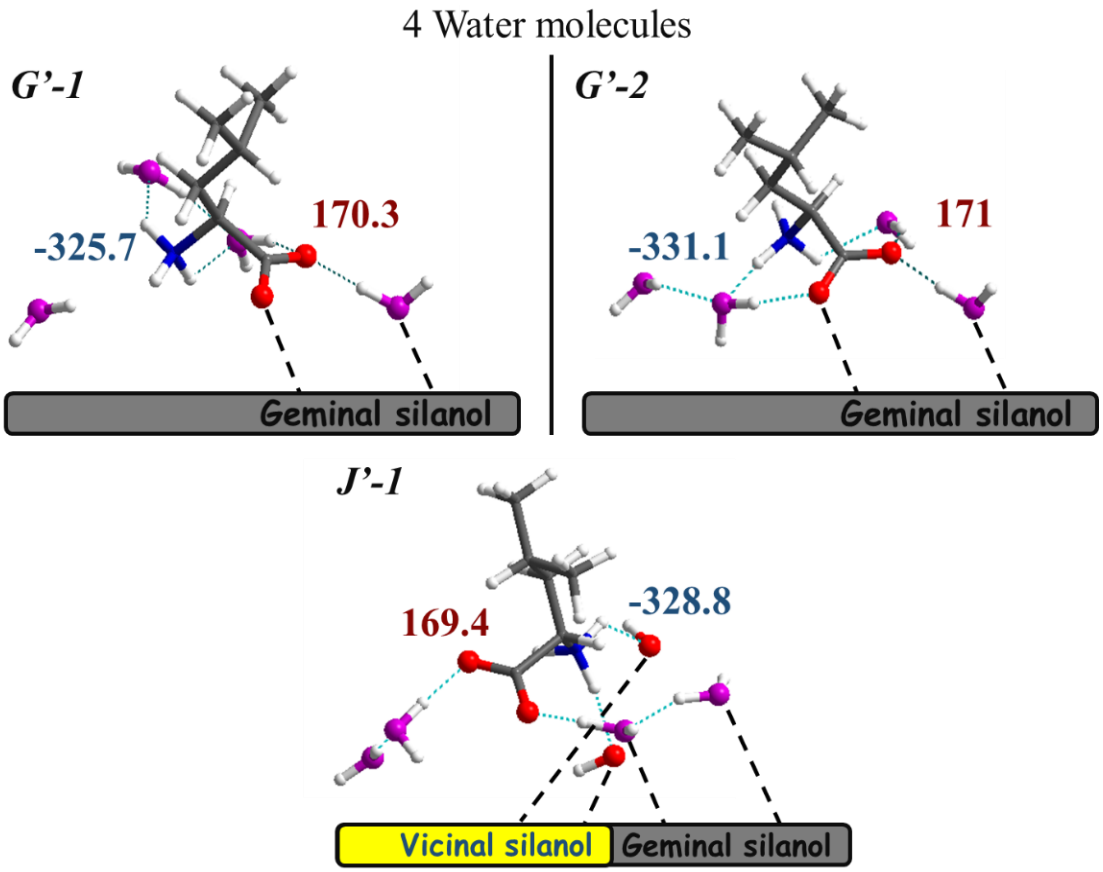

Figure 1. Models of Leu/SiO_2 with forced removal of water molecules

References

(1) Lindstrom, E. W. The Origin of Life. *J. Her**ed.*** **1938, *29*** (12), 465–466.

(2) Miller, S. L. A Production of Amino Acids under Possible Primitive Earth Conditions. *Science*. 1953, pp 528–529.

(3) McCollom, T. M. Miller-Urey and Beyond: What Have We Learned About Prebiotic Organic Synthesis Reactions in the Past 60 Years? *Annu. Rev. Earth Planet. Sci.* **2013**, *41* (1), 207–229.

(4) Kasting, J. F. Earth's Early Atmosphere. *Science (80-.).* **1993**, *5097* (4787), 920–926.

(5) Cleaves, H. J.; Chalmers, J. H.; Lazcano, A.; Miller, S. L.; Bada, J. L. A Reassessment of Prebiotic Organic Synthesis in Neutral Planetary Atmospheres. *Orig. Life Evol. Biosph.* **2008**, *38* (2), 105–115.

(6) Ring, D.; Wolman, Y.; Friedmann, N.; Miller, S. L. Prebiotic Synthesis of Hydrophobic and Protein Amino Acids. *Proc. Natl. Acad. Sci. U. S. A.* **1972**, *69* (3), 765–768.

(7) Miller, S.; Orgel, L. The Origin of Life on the Earth. *Prentice-Hall Inc., Englewood Cliffs, New Jersey* **1974**.

(8) Stribling, R.; Miller, S. L. Energy Yields for Hydrogen Cyanide and Formaldehyde Syntheses: The Hcn and Amino Acid Concentrations in the Primitive Ocean. *Orig. life Evol. Biosph.* **1987**, *17* (3), 261–273.

(9) Walther Löb. No Title. **1913**.

(10) Harada, K. Origin of Life, an Approach from Chemical Evolution (in Japanese). *Univ. Tokyo Press* **1977**, 86–95.

(11) Clark, I. D. The Chemical Kinetics of CO 2 Atmospheres. *Journal of the Atmospheric Sciences*. 1971, pp 847–858.

(12) Noble, J. A.; Theule, P.; Borget, F.; Danger, G.; Chomat, M.; Duvernay, F.; Mispelaer, F.; Chiavassa, T. The Thermal Reactivity of HCN and NH3 in Interstellar Ice Analogues. *Mon. Not. R. Astron. Soc.* **2013**, *428* (4), 3262–3273.

(13) Engel, M. H.; Nagy, B. Distribution and Enantiomeric Composition of Amino Acids in the Murchison Meteorite. *Nature* **1982**, *296*, 837–840.

(14) Nakashima, S.; Kebukawa, Y.; Kitadai, N.; Igisu, M.; Matsuoka, N. Geochemistry and the Origin of Life: From Extraterrestrial Processes, Chemical Evolution on Earth, Fossilized Life's Records, to Natures of the Extant Life. *Life* **2018**, *8* (4), 39.

(15) Pikuta, E. V.; Hoover, R. B. Microbiological Study of the Murchison CM2 Meteorite. *Instruments, Methods, Mission. Astrobiol. XV* **2012**, *8521* (June 2014), 852105.

(16) Hayatsu, R.; Studier, M. H.; Oda, A.; Fuse, K.; Anders, E. Origin of Organic Matter in Early Solar System-II. Nitrogen Compounds. *Geochim. Cosmochim. Acta* **1968**, *32* (2), 175–190.

(17) Gilbert, W. The RNA World Superlattices Point Ahead. *Nature* **1986**, *319*, 618.

(18) Lazcano, A.; Miller, S. L. The Origin and Early Evolution of Life: Prebiotic Chemistry, the Pre-RNA World, and Time. *Cell* **1996**, *85* (6), 793–798.

(19) Sutherland, J. D. Ribonucleotides. **2015**, 1–14.

(20) Cech, T. R. The Ribosome Is a Ribozyme. *Science (80-.).* **2000**, *289* (5481), 878–879.

(21) Goldford, J. E.; Hartman, H.; Smith, T. F.; Segrè, D. Remnants of an Ancient Metabolism without Phosphate. *Cell* **2017**, *168* (6), 1126-1134.e9.

(22) Arrhenius, G.; Sales, B.; Mojzsis, S.; Lee, T. Entropy and Charge in Molecular Evolution - The Case of Phosphate. *J. Theor. Biol.* **1997**, *187* (4), 503–522.

(23) Bean, H. D.; Sheng, Y.; Collins, J. P.; Anet, F. A. L.; Leszczynski, J.; Hud, N. V. Formation of a β-Pyrimidine Nucleoside by a Free Pyrimidine Base and Ribose in a Plausible Prebiotic Reaction. *J. Am. Chem. Soc.* **2007**, *129* (31), 9556–9557.

(24) Strazewski, P. Prebiotic Chemical Pathways to RNA and the Importance of Its Compartmentation. *Handb. Astrobiol.* **2019**, *Kolb, V.*, 235–263.

(25) Oro, J. Synthesis of Adenine from Ammonium Cyanide. *Biochem. Biophys. Res. Commun.* **1960**, *2* (6), 407–412.

(26) Oró, J.; Kimball, A. P. Synthesis of Purines under Possible Primitive Earth Conditions. I. Adenine from Hydrogen Cyanide. *Arch. Biochem. Biophys.* **1961**, *94* (2), 217–227.

(27) Orgel, L. E. The Origin of Life: A Review of Facts and Speculation. *Nat. Life Class. Contemp. Perspect. from Philos. Sci.* **1998**, *0004* (December), 491–495.

(28) Butlerov, A. C. No Title. *Comptes Rendus* **1861**, *53*, 145.

(29) Kopetzki, D.; Antonietti, M. Hydrothermal Formose Reaction. *New J. Chem.* **2011**, *35* (9), 1787–1794.

(30) Delidovich, I. V.; Simonov, A. N.; Taran, O. P.; Parmon, V. N. Catalytic Formation of Monosaccharides: From the Formose Reaction towards Selective Synthesis. *ChemSusChem* **2014**, *7* (7), 1833–1846.

(31) Patel, B. H.; Percivalle, C.; Ritson, D. J.; Duffy, C. D.; Sutherland, J. D. Common Origins of RNA, Protein and Lipid Precursors in a Cyanosulfidic Protometabolism. *Nat. Chem.* **2015**, *7* (4), 301–307.

(32) Deamer, D. The Role of Lipid Membranes in Life's Origin. *Life* **2017**, *7* (1).

(33) Deamer, D. W.; Oro, J. Role of Lipids in Prebiotic Structures. *BioSystems* **1980**, *12* (3–4), 167–175.

(34) Segré, D.; Ben-Eli, D.; Deamer, D. W.; Lancet, D. The Lipid World. *Orig. Life Evol. Biosph.* **2001**, *31* (1–2), 119–145.

(35) Oro, J. Chemical Synthesis of Lipids and the Origin of Life. *J. Biol. Phys.* **1995**, *20* (1–4), 135–147.

(36) Lancet, D.; Zidovetzki, R.; Markovitch, O. Systems Protobiology: Origin of Life in Lipid Catalytic Networks. *J. R. Soc. Interface* **2018**, *15* (144).

(37) Maury, C. P. J. Amyloid and the Origin of Life: Self-Replicating Catalytic Amyloids as Prebiotic Informational and Protometabolic Entities. *Cell. Mol. Life Sci.* **2018**, *75* (9), 1499–1507.

(38) Zaia, D. A. M.; Zaia, C. T. B. V.; De Santana, H. Which Amino Acids Should Be Used in Prebiotic Chemistry Studies? *Orig. Life Evol. Biosph.* **2008**, *38* (6), 469–488.

(39) Fishkis, M. Steps towards the Formation of a Protocell: The Possible Role of Short Peptides. *Orig. Life Evol. Biosph.* **2007**, *37* (6), 537–553.

(40) Holm, N. . Marine Hydrothermal Systems and the Origin of Life. *Kliiwer, Acad. Dordr.* **1992**, 221–241.

(41) Huber, C.; Eisenreich, W.; Hecht, S.; Wächtershäuser, G. A Possible Primordial Peptide Cycle. *Science (80-.).* **2003**, *301* (5635), 938–940.

(42) Shock, E. L. Stability of Peptides in High-Temperature Aqueous Solutions. *Geochim. Cosmochim. Acta* **1992**, *56* (9), 3481–3491.

(43) Bruce Martin, R. Free Energies and Equilibria of Peptide Bond Hydrolysis and Formation. *Biopolymers* **1998**, *45* (5), 351–353.

(44) Lyons, J. R.; Vasavada, A. R. Flash Heating on the Early Earth. *Orig. Life Evol. Biosph.* **1999**, *29* (2), 123–138.

(45) Rode, B. M. Peptides and the Origin of Life. *Peptides* **1999**, *20* (6), 773–786.

(46) De Duve, C.; Miller, S. L. Two-Dimensional Life ? **1991**, *88* (November), 10014–10017.

(47) Hill Jr., A. R.; Bohler, C.; Orgel, L. E. Polymerization on the Rocks: Negatively-Charged Alpha-Amino Acids. *Orig Life Evol Biosph* **1998**, *28* (3), 235–243.

(48) Gerstner, J. A.; Bell, J. A.; Cramer, S. M. Gibbs Free Energy of Adsorption for Biomolecules in Ion-Exchange Systems. *Biophys. Chem.* **1994**, *52* (2), 97–106.

(49) Marshall-Bowman, K.; Ohara, S.; Sverjensky, D. A.; Hazen, R. M.; Cleaves, H. J. Catalytic Peptide Hydrolysis by Mineral Surface: Implications for Prebiotic Chemistry.

Geochim. Cosmochim. Acta **2010**, *74* (20), 5852–5861.

(50) Lambert, J. F.; Stievano, L.; Lopes, I.; Gharsallah, M.; Piao, L. The Fate of Amino Acids Adsorbed on Mineral Matter. *Planet. Space Sci.* **2009**, *57* (4), 460–467.

(51) Fox, S. W.; Harada, K. The Thermal Copolymerization of Amino Acids Common to Protein. *J. Am. Chem. Soc.* **1960**, *82* (14), 3745–3751.

(52) Rodriguez-Garcia, M.; Surman, A. J.; Cooper, G. J. T.; Suárez-Marina, I.; Hosni, Z.; Lee, M. P.; Cronin, L. Formation of Oligopeptides in High Yield under Simple Programmable Conditions. *Nat. Commun.* **2015**, *6*.

(53) Zaia, D. A. M. A Review of Adsorption of Amino Acids on Minerals : Was It Important for Origin of Life ? Short Communication. **2004**, 113–118.

(54) Bernal, J. D. *The Physical Basis of Life.*; Routledge and Paul: London, 1951.

(55) Anderson, D, M.; Banin, A. SOIL AND WATER AND ITS RELATIONSHIP TO THE ORIGIN OF LIFE. *D. Reidel Publ. Company, Dordrecht-holl.* **1975**, *6*, 23–36.

(56) Poch, O.; Jaber, M.; Stalport, F.; Nowak, S.; Georgelin, T.; Lambert, J. F.; Szopa, C.; Coll, P. Effect of Nontronite Smectite Clay on the Chemical Evolution of Several Organic Molecules under Simulated Martian Surface Ultraviolet Radiation Conditions. *Astrobiology* **2015**, *15* (3), 221–237.

(57) Hansma, H. G. Possible Origin of Life between Mica Sheets. *J. Theor. Biol.* **2010**, *266* (1), 175–188. https://doi.org/10.1016/j.jtbi.2010.06.016.

(58) Cairns-Smith, A. G. Seven Clues to the Origin of Life: A Scientific Detective Story. *Cambridge Univ. Press Cambridge* **1985**.

(59) Hazen, R. M. Genesis: The Scientific Quest for Life's Origin. *Washingt. DC, Joseph Henry Press* **2005**.

(60) Peptide Formation in the Prebiotic Era : Thermal Condensation of Glycine in Fluctuating Clay Environments Author (s): N . Lahav , D . White and S . Chang Published by : American Association for the Advancement of Science Stable URL : Http://Www.Jstor.Or. **2016**, *201* (4350), 67–69.

(61) Bujdák, J.; Faybíková, K.; Eder, A.; Yongyai, Y.; Rode, B. M. Peptide Chain Elongation: A Possible Role of Montmorillonite in Prebiotic Synthesis of Protein Precursors. *Orig. Life Evol. Biosph.* **1995**, *25* (5), 431–441.

(62) Bujdák, J.; Rode, B. M. Silica, Alumina, and Clay-Catalyzed Alanine Peptide Bond Formation. *J. Mol. Evol.* **1997**, *45* (5), 457–466.

(63) Bujdák, J.; Rode, B. M. Silica, Alumina and Clay Catalyzed Peptide Bond Formation: Enhanced Efficiency of Alumina Catalyst. *Orig. Life Evol. Biosph.* **1999**, *29* (5), 451–461.

(64) Ertem, G.; Ferris, J. P. Template-Directed Synthesis Using the Heterogeneous Templates Produced by Montmorillonite Catalysis. A Possible Bridge between the Prebiotic and RNA Worlds. *J. Am. Chem. Soc.* **1997**, *119* (31), 7197–7201.

(65) Smith, J. V. Biochemical Evolution. I. Polymerization on Internal, Organophilic Silica Surfaces of Dealuminated Zeolites and Feldspars. *Proc. Natl. Acad. Sci. U. S. A.* **1998**, *95* (7), 3370–3375.

(66) Munsch, S.; Hartmann, M.; Ernst, S. Adsorption and Separation of Amino Acids from Aqueous Solutions on Zeolites. *Chem. Commun.* **2001**, *1* (19), 1978–1979.

(67) Titus, E.; Kalkar, A. K.; Gaikar, V. G. Equilibrium Studies of Adsorption of Amino Acids on NaZSM-5 Zeolite. *Colloids Surfaces A Physicochem. Eng. Asp.* **2003**, *223* (1–3), 55–61.

(68) Krohn, J. E.; Tsapatsis, M. Amino Acid Adsorption on Zeolite β. *Langmuir* **2005**, *21* (19), 8743–8750.

(69) Krohn, J. E.; Tsapatsis, M. PhenylAlanine and Arginine Adsorption in Zeolites X, Y, and β. *Langmuir* **2006**, *22* (22), 9350–9356.

(70) Wijntje, R.; Bosch, H.; de Haan, A. B.; Bussmann, P. J. T. Influencing the Selectivity of Zeolite Y for Triglycine Adsorption. *J. Chromatogr. A* **2007**, *1142* (1 SPEC. ISS.), 39–47.

(71) Phuakkong, O.; Bobuatong, K.; Pantu, P.; Boekfa, B.; Probst, M.; Limtrakul, J. Glycine Peptide Bond Formation Catalyzed by Faujasite. *ChemPhysChem* **2011**, *12* (11), 2160–2168.

(72) Stückenschneider, K.; Merz, J.; Hanke, F.; Rozyczko, P.; Milman, V.; Schembecker, G. Amino-Acid Adsorption in MFI-Type Zeolites Enabled by the PH-Dependent Ability to Displace Water. *J. Phys. Chem. C* **2013**, *117* (37), 18927–18935.

(73) Liu, G.; Wright, M. M.; Zhao, Q.; Brown, R. C.; Wang, K.; Xue, Y. Catalytic Pyrolysis of Amino Acids: Comparison of Aliphatic Amino Acid and Cyclic Amino Acid. *Energy Convers. Manag.* **2016**, *112*, 220–225.

(74) Wächtershäuser, G. Before Enzyme and Templates: Theory of Surface Metabolism. *Microbiol. Rev.* **1988**, *52* (4), 452–484.

(75) Boehme, C.; Marx, D. Glycine on a Wet Pyrite Surface at Extreme Conditions. *J. Am. Chem. Soc.* **2003**, *125* (44), 13362–13363.

(76) Nair, N. N.; Schreiner, E.; Marx, D. Glycine at the Pyrite-Water Interface: The Role of Surface Defects. *J. Am. Chem. Soc.* **2006**, *128* (42), 13815–13826.

(77) Pollet, R.; Boehme, C.; Marx, D. Ab Initio Simulations of Desorption and Reactivity of Glycine At a Water-Pyrite Interface At “Iron-Sulfur World” Prebiotic Conditions. *Orig. Life Evol. Biosph.* **2006**, *36* (4), 363–379.

(78) Schreiner, E.; Nair, N. N.; Wittekindt, C.; Marx, D. Peptide Synthesis in Aqueous Environments: The Role of Extreme Conditions and Pyrite Mineral Surfaces on Formation and Hydrolysis of Peptides. *J. Am. Chem. Soc.* **2011**, *133* (21), 8216–8226.

(79) Hazen, R. M.; Sverjensky, D. A. Mineral Surfaces, Geochemical Complexities, and the Origins of Life. *Cold Spring Harb. Perspect. Biol.* **2010**.

(80) Lahav, N.; White, D.; Chang, S. Peptide Formation in the Prebiotic Era: Thermal Condensation of Glycine in Fluctuating Clay Environments. *Science (80-.).* **1978**, *201* (4350), 67–69.

(81) Stievano, L.; Yu Piao, L.; Lopes, I.; Meng, M.; Costa, D.; Lambert, J.-F. Glycine and Lysine Adsorption and Reactivity on the Surface of Amorphous Silica. *Eur. J. Mineral.* **2007**, *19* (3), 321–331.

(82) Basiuk, V. A.; Gromovoy, T. Y.; Golovaty, V. G.; Glukhoy, A. M. Mechanisms of Amino Acid Polycondensation on Silica and Alumina Surfaces. *Orig. Life Evol. Biosph.* **1990**, *20* (6), 483–498.

(83) Vladimir, A.; Gromovoy, T. Y. U.; Glukhoy, A. M.; Golovaty, V. G. Chemical Transformations of Proteinogenic Amino Acids during Their Sublimation in the Presence of Silica. **1991**, 129–144.

(84) Meng, M.; Stievano, L.; Lambert, J. F. Adsorption and Thermal Condensation Mechanisms of Amino Acids on Oxide Supports. 1. Glycine on Silica. *Langmuir* **2004**, *20* (3), 914–923.

(85) Lopes, I.; Piao, L.; Stievano, L.; Lambert, J. F. Adsorption of Amino Acids on Oxide Supports: A Solid-State NMR Study of Glycine Adsorption on Silica and Alumina. *J. Phys. Chem. C* **2009**, *113* (42), 18163–18172.

(86) Bouchoucha, M.; Jaber, M.; Onfroy, T.; Lambert, J. F.; Xue, B. Glutamic Acid Adsorption and Transformations on Silica. *J. Phys. Chem. C* **2011**, *115* (44), 21813–21825.

(87) Lambert, J. F.; Jaber, M.; Georgelin, T.; Stievano, L. A Comparative Study of the Catalysis of Peptide Bond Formation by Oxide Surfaces. *Phys. Chem. Chem. Phys.* **2013**, *15* (32), 13371–13380.

(88) Jaber, M.; Spadavecchia, J.; Bazzi, H.; Georgelin, T.; Costa-Torro, F.; Lambert, J.-F. Non-Biological Selectivity in Amino Acids Polymerization on TiO2 NanoParticles Amino Acids. *Amino Acids* **2013**.

(89) Jaber, M.; Georgelin, T.; Bazzi, H.; Costa-Torro, F.; Lambert, J. F.; Bolbach, G.; Clodic, G. Selectivities in Adsorption and Peptidic Condensation in the (Arginine and Glutamic Acid)/Montmorillonite Clay System. *J. Phys. Chem. C* **2014**, *118* (44), 25447–25455.

(90) Georgelin, T.; Akouche, M.; Jaber, M.; Sakhno, Y.; Matheron, L.; Fournier, F.; Méthivier, C.; Martra, G.; Lambert, J. F. Iron(III) Oxide Nanoparticles as Catalysts for the Formation of Linear Glycine Peptides. *Eur. J. Inorg. Chem.* **2017**, *2017* (1), 198–

211.

(91) Folliet, N.; Gervais, C.; Costa, D.; Laurent, G.; Babonneau, F.; Stievano, L.; Lambert, J. F.; Tielens, F. A Molecular Picture of the Adsorption of Glycine in Mesoporous Silica through NMR Experiments Combined with DFT-D Calculations. *J. Phys. Chem. C* **2013**, *117* (8), 4104–4114.

(92) Sakhno, Y.; Battistella, A.; Mezzetti, A.; Jaber, M.; Georgelin, T.; Michot, L.; Lambert, J.-F. One Step up the Ladder of Prebiotic Complexity: Formation of Non-Random Linear Polypeptides from Binary Systems of Amino Acids on Silica. *Chem. - A Eur. J.* **2018**.

(93) Bedoin, L.; Alves, S.; Lambert, J.-F. Origins of Life and Molecular Information: Selectivity in Mineral Surface-Induced Prebiotic Amino Acid Polymerization. *ACS Earth Sp. Chem.* **2020**, *4* (10), 1802–1812.

(94) Guo, C.; Holland, G. P. Investigating Lysine Adsorption on Fumed Silica Nanoparticles. *J. Phys. Chem. C* **2014**, *118* (44), 25792–25801.

(95) Guo, C.; Holland, G. P. Alanine Adsorption and Thermal Condensation at the Interface of Fumed Silica Nanoparticles: A Solid-State NMR Investigation. *J. Phys. Chem. C* **2015**, *119* (45), 25663–25672.

(96) Guo, C.; Holland, G. P.; Yarger, J. L. Lysine-Capped Silica Nanoparticles: A Solid-State NMR Spectroscopy Study. *MRS Adv.* **2016**, *1* (31), 2261–2266.

(97) Guo, C.; Jordan, J. S.; Yarger, J. L.; Holland, G. P. Highly Efficient Fumed Silica Nanoparticles for Peptide Bond Formation: Converting Alanine to Alanine Anhydride. *ACS Appl. Mater. Interfaces* **2017**, *9* (20), 17653–17661.

(98) Shir, I. Ben; Kababya, S.; Amitay-Rosen, T.; Balazs, Y. S.; Schmidt, A. Molecular Level Characterization of the Inorganic-Bioorganic Interface by Solid State NMR: Alanine on a Silica Surface, a Case Study. *J. Phys. Chem. B* **2010**, *114* (18), 5989–5996.

(99) Ben Shir, I.; Kababya, S.; Schmidt, A. Binding Specificity of Amino Acids to Amorphous Silica Surfaces: Solid-State NMR of Glycine on SBA-15. *J. Phys. Chem. C* **2012**, *116* (17), 9691–9702.

(100) Ben Shir, I.; Kababya, S.; Schmidt, A. Molecular Details of Amorphous Silica Surfaces Determine Binding Specificity to Small Amino Acids. *J. Phys. Chem. C* **2014**, *118* (15), 7901–7909.

(101) Lomenech, C.; Bery, G.; Costa, D.; Stievano, L.; Lambert, J. F. Theoretical and Experimental Study of the Adsorption of Neutral Glycine on Silica from the Gas Phase. *ChemPhysChem* **2005**, *6* (6), 1061–1070.

(102) Costa, D.; Lomenech, C.; Meng, M.; Stievano, L.; Lambert, J.-F. Microsolvation of Glycine by Silanol Ligands and Water : A DFT Study. *Theochem* **2007**, *806*, 253–259.

(103) Costa, D.; Tougerti, A.; Tielens, F.; Gervais, C.; Stievano, L.; Lambert, J. F. DFT Study of the Adsorption of Microsolvated Glycine on a Hydrophilic Amorphous Silica Surface.

Phys. Chem. Chem. Phys. **2008**, *10* (42), 6360–6368.

(104) Rimola, A.; Tosoni, S.; Sodupe, M.; Ugliengo, P. Peptide Bond Formation Activated by the Interplay of Lewis and Brønsted Catalysts. *Chem. Phys. Lett.* **2005**, *408* (4–6), 295–301.

(105) Rimola, A.; Sodupe, M.; Tosoni, S.; Civalleri, B.; Ugliengo, P. Interaction of Glycine with Isolated Hydroxyl Groups at the Silica Surface: First Principles B3LYP Periodic Simulation. *Langmuir* **2006**, *22* (15), 6593–6604.

(106) Rimola, A.; Sodupe, M.; Ugliengo, P. Amide and Peptide Bond Formation: Interplay between Strained Ring Defects and Silanol Groups at Amorphous Silica Surfaces. *J. Phys. Chem. C* **2016**, *120* (43), 24817–24826.

(107) Pantaleone, S.; Ugliengo, P.; Sodupe, M.; Rimola, A. When the Surface Matters: Prebiotic Peptide-Bond Formation on the TiO2 (101) Anatase Surface through Periodic DFT-D2 Simulations. *Chem. - A Eur. J.* **2018**, *24* (61), 16292–16301.

(108) Rimola, A.; Fabbiani, M.; Sodupe, M.; Ugliengo, P.; Martra, G. How Does Silica Catalyze the Amide Bond Formation under Dry Conditions? Role of Specific Surface Silanol Pairs. *ACS Catal.* **2018**, *8* (5), 4558–4568.

(109) Rimola, A.; Sodupe, M.; Ugliengo, P. Role of Mineral Surfaces in Prebiotic Chemical Evolution. In Silico Quantum Mechanical Studies. *Life* **2019**, *9* (1), 10.

(110) Rimola, A.; Tosoni, S.; Sodupe, M.; Ugliengo, P. Does Silica Surface Catalyse Peptide Bond Formation? New Insights from First-Principles Calculations. *ChemPhysChem* **2006**, *7* (1), 157–163.

(111) Rimola, A.; Sodupe, M.; Ugliengo, P.; Ifm, C.; Uni, V. Aluminosilicate Surfaces as Promoters for Peptide Bond Formation : An Assessment of Bernal ' s Hypothesis by Ab Initio Methods Earliest Ones , Based on the Pioneering Work of Miller , 5 Miller Along the Same Line of Thought Is a Suggestion Based on The. *Jacs* **2007**, *129* (6), 8333–8344.

(112) Rimola, A.; Civalleri, B.; Ugliengo, P. Neutral vs Zwitterionic Glycine Forms at the Water/Silica Interface: Structure, Energies, and Vibrational Features from B3LYP Periodic Simulations. *Langmuir* **2008**, *24* (24), 14027–14034.

(113) Rimola, A.; Sodupe, M.; Ugliengo, P. Affinity Scale for the Interaction of Amino Acids with Silica Surfaces. *J. Phys. Chem. C* **2009**, *113* (14), 5741–5750.

(114) Rimola, A.; Ugliengo, P. The Role of Defective Silica Surfaces in Exogenous Delivery of Prebiotic Compounds: Clues from First Principles Calculations. *Phys. Chem. Chem. Phys.* **2009**, *11* (14), 2497–2506.

(115) Rimola, A.; Sakhno, Y.; Bertinetti, L.; Lelli, M.; Martra, G.; Ugliengo, P. Toward a Surface Science Model for Biology: Glycine Adsorption on Nanohydroxyapatite with Well-Defined Surfaces. *J. Phys. Chem. Lett.* **2011**, *2* (12), 1390–1394.

(116) Jimenez-Izal, E.; Chiatti, F.; Corno, M.; Rimola, A.; Ugliengo, P. Glycine Adsorption at

Nonstoichiometric (010) Hydroxyapatite Surfaces: A B3LYP Study. *J. Phys. Chem. C* **2012**, *116* (27), 14561–14567.

(117) Rimola, A.; Costa, D.; Sodupe, M.; Lambert, J.-F.; Ugliengo, P. Silica Surface Features and Their Role in the Adsorption of Biomolecules: Computational Modeling and Experiments. *Chem. Rev.* **2013**, *113* (6), 4216–4313.

(118) Lopes, I.; Piao, L.; Stievano, L.; Lambert, J. F. Adsorption of Amino Acids on Oxide Supports: A Solid-State NMR Study of Glycine Adsorption on Silica and Alumina. *J. Phys. Chem. C* **2009**, *113* (42), 18163–18172.

(119) Georgelin, T.; Jaber, M.; Onfroy, T.; Hargrove, A. A.; Costa-Torro, F.; Lambert, J. F. Inorganic Phosphate and Nucleotides on Silica Surface: Condensation, Dismutation, and Phosphorylation. *J. Phys. Chem. C* **2013**, *117* (24), 12579–12590.

(120) Martra, G.; Deiana, C.; Sakhno, Y.; Barberis, I.; Fabbiani, M.; Pazzi, M.; Vincenti, M. The Formation and Self-Assembly of Long Prebiotic Oligomers Produced by the Condensation of Unactivated Amino Acids on Oxide Surfaces. *Angew. Chemie - Int. Ed.* **2014**, *53* (18), 4671–4674.

(121) Bloch, F. Nuclear Induction. *Phys. Rev.* **1946**, *70* (7–8), 460–474.

(122) Purcell, E. M. Resonance Absorption by Nuclear Magnetic Moments in a Solid. *Phys. Rev* **1946**, *69* (681).

(123) Pellecchia, M.; Sem, D. S.; Wüthrich, K. NMR in Drug Discovery. *Nat. Rev. Drug Discov.* **2002**, *1* (3), 211–219.

(124) Zhu, G. *NMR of Proteins and Small Biomolecules Preface*; 2012; Vol. 326.

(125) Wang, S.; Ladizhansky, V. Recent Advances in Magic Angle Spinning Solid State NMR of Membrane Proteins. *Prog. Nucl. Magn. Reson. Spectrosc.* **2014**, *82*, 1–26.

(126) Lauterbur, P, S. Image Formation by Induced Local Interactions: Examples Employing Nuclear Magnetic Resonance. *Nat. Phys. Sci.* **1973**, *242*, 190–191.

(127) Hore, P, J. Nuclear Magnetic Resonance. *Oxford Univ. Press. Oxford*, **2015**.

(128) Levitt, M. H. Spin Dynamics: Basics of Nuclear Magnetic Resonance. *John Wiley Sons Ltd*, **2001**.

(129) Duer, M, J. Introduction to Solid-State NMR Spectroscopy,. *Blackwell Publ. Oxford* **2004**.

(130) Abragam, A. Principles of Nuclear Magnetism. *Oxford Univ. Press. Oxford*, **1961**.

(131) Apperley, D, C.; Harris, R, K.; Hodgkinson, Paul. Solid-State NMR: Basic Principles & Practice,. *Momentum Press. New York*, **2012**.

(132) Keeler, J. Understanding NMR Spectroscopy. *Wiley, Chichester* **2010**.

(133) Frydman, L. S PIN -1/2 AND B EYOND : A Perspective in Solid State NMR Spectroscopy . *Annu. Rev. Phys. Chem.* **2001**, *52* (1), 463–498.

(134) Kentgens, A. P. M. A Practical Guide to Solid-State NMR of Half-Integer Quadrupolar Nuclei with Some Applications to Disordered Systems. *Geoderma* **1997**, *80* (3–4), 271–306.

(135) Lowe, I. J. Free Induction Decays of Rotating Solids. *Phys. Rev. Lett.* **1959**, *2* (7), 285–287.

(136) Andrew, E. R.; Bradbury, A. Removal of Dipolar Broadening of Nuclear Magnetic Resonance Spectra of Solids by Specimen Rotation. *Eades, R. G. Nat.* **1959**, *183*, 1802–1803.

(137) Hahn, E. L. Spin Echoes. *Phys. Rev.* **1950**, *80* (4), 580–594.

(138) Demco, D. E.; Blümich, B. Solid-State NMR Imaging Methods. Part II: Line Narrowing. *Concepts Magn. Reson.* **2000**, *12* (5), 269–288.

(139) Stöver, H. D. H.; Stover Fréchet, J. M. J. Direct Polarization 13C and 1H Magic Angle Spinning NMR in the Characterization of Solvent-Swollen Gels. *Macromolecules* **1989**, *22* (4), 1574–1576.

(140) Hartmann, S. R.; Hahn, E. L. Nuclear Double Resonance in the Rotating Frame. *Phys. Rev.* **1962**, *128* (5), 2042–2053.

(141) Pines, A.; Gibby, M. G.; Waugh, J. S. Proton-Enhanced Nuclear Induction Spectroscopy. a Method for High Resolution Nmr of Dilute Spins in Solids. *J. Chem. Phys.* **1972**, *56* (4), 1776–1777.

(142) Stejskal, E. O.; Schaefer, J.; Waugh, J. S. Magic-Angle Spinning and Polarization Transfer in Proton-Enhanced NMR. *J. Magn. Reson.* **1977**, *28* (1), 105–112.

(143) Rovnyak, D. Tutorial on Analytic Theory for Cross-Polarization in Solid State NMR. *Harv. Bus. Rev* **2008**, No. December, 1–6.

(144) Ashbrook, S, E.; Dawson, D, M.; Griffin, J, M. Local Structural Characterisation. *Eds. D. W. Bruce, D. O'Hare R. I Walton, Wiley, Chichester* **2014**.

(145) Field, L, D.; Li, H, L.; Magill, A, M. *Organic Structures from 2D NMR Spectra*; 2015.

(146) Bonhomme, C.; Gervais, C.; Laurencin, D. Recent NMR Developments Applied to Organic-Inorganic Materials. *Prog. Nucl. Magn. Reson. Spectrosc.* **2014**, *77*, 1–48.

(147) Gervais, C.; Dupree, R.; Pike, K. J.; Bonhomme, C.; Profeta, M.; Pickard, C. J.; Mauri, F. Combined First-Principles Computational and Experimental Multinuclear Solid-State NMR Investigation of Amino Acids. *J. Phys. Chem. A* **2005**, *109* (31), 6960–6969.

(148) Prabhu, V.; Chatson, B.; Abrams, G.; King, J. 13C Chemical Shifts of 20 Free Amino

Acids and Their Use in Detection by NMR of Free Amino Acids in Intact Plants of Arabidopsis. *J. Plant Physiol.* **1996**, *149* (3–4), 246–250.

(149) Wishart, D. S.; Bigam, C. G.; Holm, A.; Hodges, R. S.; Sykes, B. D. 1H, 13C and 15N Random Coil NMR Chemical Shifts of the Common Amino Acids. I. Investigations of Nearest-Neighbor Effects. *J. Biomol. NMR* **1995**, *5* (1), 67–81.

(150) Alberts, B.; Bray, D.; Lewis, J.; Raff, M.; Roberts, K.; Watson, J, D. Molecular Biology of the Cell. *Garl. Publ. New York, NY* **1994**, *11* (3), 121–122.

(151) Amitay-Rosen, T.; Kababya, S.; Vega, S. A Dynamic Magic Angle Spinning NMR Study of the Local Mobility of Alanine in an Aqueous Environment at the Inner Surface of Mesoporous Materials. *J. Phys. Chem. B* **2009**, *113* (18), 6267–6282.

(152) Amitay-Rosen, T.; Vega, S. A Deuterium MAS NMR Study of the Local Mobility of Dissolved Methionine and Di-Alanine at the Inner Surface of SBA-15. *Phys. Chem. Chem. Phys.* **2010**, *12* (25), 6763–6773.

(153) Loja, V. S.; Pz, T. S. A N U C L E A R M A G N E T I C R E S O N A N C E (NMR) A N D FOURIER- T R A N S F O R M I N F R A R E D (FTIR) S T U D Y OF GLYCINE SPECIATION ON A Cd-RICH M O N T M O R I L L O N I T E. **2000**, *48* (5).

(154) Arrondo, J. L. R.; Muga, A.; Castresana, J.; Goñi, F. M. Quantitative Studies of the Structure of Proteins in Solution by Fourier-Transform Infrared Spectroscopy. *Prog. Biophys. Mol. Biol.* **1993**, *59* (1), 23–56.

(155) Barth, A. Infrared Spectroscopy of Proteins. *Biochim. Biophys. Acta - Bioenerg.* **2007**, *1767* (9), 1073–1101.

(156) Chirgadze, Y. N.; Fedorov, O. V.; Trushina, N. P. Estimation of Amino Acid Residue Side-chain Absorption in the Infrared Spectra of Protein Solutions in Heavy Water. *Biopolymers* **1975**, *14* (4), 679–694.

(157) Venyaminov, S. Y.; Kalnin, N. N. Quantitative IR Spectrophotometry of Peptide Compounds in Water (H2O) Solutions. I. Spectral Parameters of Amino Acid Residue Absorption Bands. *Biopolymers* **1990**, *30* (13–14), 1243–1257.

(158) Rahmelow, K.; Hübner, W.; Ackermann, T. Infrared Absorbances of Protein Side Chains. *Anal. Biochem.* **1998**, *257* (1), 1–11.

(159) Goormaghtigh, E.; Cabiaux, V.; Ruysschaer, J, M. Determination Ofsoluble and Membrane Protein Structure by Fourier Transform Infrared Spectroscopy. I. Assignments and Model Compounds. *Subcell. Biochem* **1994**, *23*, 329–362.

(160) Wright, W. W.; Vanderkooi, J. M. Use of IR Absorption of the Carboxyl Group of Amino Acids and Their Metabolites to Determine PKs, to Study Proteins, and to Monitor Enzymatic Activity. *Biospectroscopy* **1997**, *3* (6), 457–467.

(161) Derbel, N.; Hernández, B.; Pflüger, F.; Liquier, J.; Geinguenaud, F.; Jaïdane, N.;

Lakhdar, Z. Ben; Ghomi, M. Vibrational Analysis of Amino Acids and Short Peptides in Hydrated Media. I. L-Glycine and L-Leucine. *J. Phys. Chem. B* **2007**, *111* (6), 1470–1477.

(162) Groenewegen, J. A.; Sachtler, W. M. H. Infrared Spectra of Some Amino Acids Adsorbed on Silica and on Silica-Supported Nickel. *J. Catal.* **1974**, *33* (2), 176–183.

(163) Baratova, L. A.; Goldanskii, V. I.; Kosigin, M. J.; Yampolskii, E. A. Baratova, L. A., Goldanskii, V. I., Kosigin, M. J., and Yampolskii, E A.: 1970, Biokhimiya 35, 1216 (Russian). *Biokhimiya* **1970**, *35*, 1216 (Russian).

(164) Rohlfing, D. L.; McAlhaney, W. W. Rohlfing, D. L. and McAlhaney, W. W.: 1976, BioSystems 8, 139. *BioSystems* **1976**, *8*, 139.

(165) Fouche Jr, clarence and Rohlfing, D. L. THERMAL POLYMERIZATION OF AMINI ACIDS UNDER VARIOUS ATSOPHERES OR AT LOW PRESSURES. *North-holl. Publ. Company, Amsterdam* **1976**, *8*, 57–65.

(166) Basyuk, V. A. IR SPECTRA OF BIFUNCTIONAL α-AMINO ACIDS SORBED ON DEHYDRATED AEROSIL. **1990**, *26* (1), 89–93.

(167) Gromovoy, T. Y.; Basiuk, V. A.; Chuiko, A. A. Growth of Peptide Chains on Silica in Absence of Amino Acid Access from Without. *Orig. Life Evol. Biosph.* **1991**, *21* (3), 119–128.

(168) Basiuk, Vladimir A.; Gromovy, T. Y.; Chuiko, A. A.; Soloshonok, V. A.; Kukhar, V. P. . A Novel Approach to the Synthesis of Symmetric Optically Active 2,5-Dioxopiperazines. pp 5, 449–451.

(169) Basiuk, V. A.; Gromovoy, T. Y. Reactions of Vaporous Proteinogenic α-Amino Acids an Silica and Alumina Surfaces. *React. Kinet. Catal. Lett* **1993**, *50* (1–2), 297–303.

(170) Basiuk, V. A.; Gromovoy, T. Y. The Gas-Solid-Phase 2,5-Dioxopiperazine Synthesis. Cyclization of Vaporous Dipeptides on Silica Surface. *Collect. Czechoslov. Chem. Commun.* **1994**, *59* (2), 461–466.

(171) Basiuk, V. A.; Navarro-Gonzalez, R.; Basiuk, E. V. Behavior of Amino Acids When Volatilized in the Presence of Silica Gel and Pulverized Basaltic Lava. *Orig. Life Evol. Biosph.* **1998**, *28* (2), 167–193.

(172) Fabbiani, M.; Rebba, E.; Pazzi, M.; Vincenti, M.; Fois, E.; Martra, G. Solvent-Free Synthesis of Ser–His Dipeptide from Non-Activated Amino Acids and Its Potential Function as Organocatalyst. *Res. Chem. Intermed.* **2018**, *44* (3), 1797–1810.

(173) Rimola, A.; Fabbiani, M.; Sodupe, M.; Ugliengo, P.; Martra, G. How Does Silica Catalyze the Amide Bond Formation under Dry Conditions? Role of Specific Surface Silanol Pairs. *ACS Catal.* **2018**, *8* (5), 4558–4568.

(174) Kitadai, N.; Yokoyama, T.; Nakashima, S. ATR-IR Spectroscopic Study of L-Lysine Adsorption on Amorphous Silica. *J. Colloid Interface Sci.* **2009**, *329* (1), 31–37.

(175) Mermut, O.; Phillips, D. C.; York, R. L.; McCrea, K. R.; Ward, R. S.; Somorjai, G. A. In Situ Adsorption Studies of a 14-Amino Acid Leucine-Lysine Peptide onto Hydrophobic Polystyrene and Hydrophilic Silica Surfaces Using Quartz Crystal Microbalance, Atomic Force Microscopy, and Sum Frequency Generation Vibrational Spectroscopy. *J. Am. Chem. Soc.* **2006**, *128* (11), 3598–3607.

(176) Hammond, R. B.; Lai, X.; Roberts, K. J.; Thomas, A.; White, G. Application of In-Process X-Ray Powder Diffraction for the Identification of Polymorphic Forms during Batch Crystallization Reactions. *Cryst. Growth Des.* **2004**, *4* (5), 943–948.

(177) Fleck, M.; Petrosyan, A. M. *Salts of Amino Acids: Crystallization, Structure and Properties*; 2014; Vol. 9783319062.

(178) Schrödinger, E. An Undulatory Theory of the Mechanics of Atoms and Molecules. *Phys. Rev.* **1926**, *28* (6), 1049–1070.

(179) Schleich, W. P.; Greenberger, D. M.; Kobe, D. H.; Scully, M. O. Schrödinger Equation Revisited. *Proc. Natl. Acad. Sci. U. S. A.* **2013**, *110* (14), 5374–5379.

(180) Born, M.; Oppenheimer, R. J. On the Quantum Theory of Molecules (English Translation). *Ann. Phys.* **1927**, *457* (1927), 1–32.

(181) Born, M.; Huang, K. Dynamical Theory of Crystal Lattices. *Acta Crystallogr.* **1956**, *9* (10), 837–838.

(182) Jensen, F. Introduction to Computational Chemistry. *Wiley, Chichester* **2007**.

(183) Hartree, D. R. The Wave Mechanics of an Atom with a Non-Coulomb Central Field Part I Theory and Methods. *Math. Proc. Cambridge Philos. Soc.* **1928**, *24* (1), 89–110.

(184) Hohenberg, P.; Kohn, W. Inhomogeneous Electron Gas. *Phys. Rev* **1964**, *136*, B864–B871.

(185) Kohn, W.; Sham, L. J. Self-Consistent Equations Including Exchange and Correlation Effects. *Phys. Rev* **1965**, *140*, A1133–A1138.

(186) Ceperley, D. M.; Alder, B. J. Ground State of the Electron Gas by a Stochastic Method. *Phys. Rev. Lett.* **1980**, *45* (7), 566–569. https://doi.org/10.1103/PhysRevLett.45.566.

(187) Koch, W.; Holthausen, M. C. *A Chemist's Guide to Density Functional Theory*; 2000.

(188) Perdew, J. P.; Wang, Y. Accurate and Simple Analytic Representation of the Electron-Gas Correlation Energy. *Phys. Rev. B* **1992**, *45*, 13244.

(189) Perdew, J. P.; Ernzerhof, M.; Burke, K. Errata: Generalized Gradient Approximation Made Simple. *Phys. Rev. Lett.* **1996**, *77* (18), 3865–3868.

(190) Leung, K.; Rempe, S. B. Ab Initio Molecular Dynamics Study of Glycine Intramolecular Proton Transfer in Water. *J. Chem. Phys.* **2005**, *122* (18).

(191) Ullah, A. D.; Kapsokalivas, L.; Mann, M.; Steinhöfel, K. Protein Folding Simulation by Two-Stage Optimization. *Commun. Comput. Inf. Sci.* **2009**, *51* (October 2009), 138–145.

(192) Bonhomme, C.; Gervais, C.; Babonneau, F.; Coelho, C.; Pourpoint, F.; Azaïs, T.; Ashbrook, S. E.; Griffin, J. M.; Yates, J. R.; Mauri, F.; *et al*. First-Principles Calculation of NMR Parameters Using the Gauge Including Projector Augmented Wave Method: A Chemists Point of View. *Chem. Rev.* **2012**, *112* (11), 5733–5779.

(193) ICSD. The Royal Society of Chemistry.

(194) Verlet, L. Computer "Experiments" on Classical Fluids. I. Thermodynamical Properties of Lennard-Jones Molecules. *J. Phys. D. Appl. Phys.* **1976**, *159* (98).

(195) Sauer, J. Molecular Structure of Orthosilicic Acid, Silanol, and H3SiOH·AlH3 Complex: Models of Surface Hydroxyls in Silica and Zeolites. *J. Phys. Chem.* **1987**, *91* (9), 2315–2319.

(196) Zhanpeisov, N. U. Cluster Quantum Chemical Study of Triaminotoluene Interaction with a Model Clay Surface. *Struct. Chem.* **1999**, *10* (4), 285–294.

(197) Chizallet, C.; Raybaud, P. Density Functional Theory Simulations of Complex Catalytic Materials in Reactive Environments: Beyond the Ideal Surface at Low Coverage. *Catal. Sci. Technol.* **2014**, *4* (9), 2797–2813.

(198) Ceresoli, D.; Bernasconi, M.; Iarlori, S.; Parrinello, M.; Tosatti, E. Two-Membered Silicon Rings on the Dehydroxylated Surface of Silica. *Phys. Rev. Lett.* **2000**, *84* (17), 3887–3890.

(199) Ugliengo, P.; Sodupe, M.; Musso, F.; Bush, I. J.; Orlando, R.; Dovesi, R. Realistic Models of Hydroxylated Amorphous Silica Surfaces and MCM- 41 Mesoporous Material Simulated by Large-Scale Periodic B3LYP Calculations. *Adv. Mater.* **2008**, *20* (23), 4579–4583.

(200) Tielens, F.; Gervais, C.; Lambert, J. F.; Mauri, F.; Costa, D. Ab Initio Study of the Hydroxylated Surface of Amorphous Silica: A Representative Model. *Chem. Mater.* **2008**, *20* (10), 3336–3344.

(201) Halbert, S.; Ispas, S.; Raynaud, C.; Eisenstein, O. Modeling the Surface of Amorphous Dehydroxylated Silica: The Influence of the Potential on the Nature and Density of Defects. *New J. Chem.* **2018**, *42* (2), 1356–1367.

(202) Gierada, M.; De Proft, F.; Sulpizi, M.; Tielens, F. Understanding the Acidic Properties of the Amorphous Hydroxylated Silica Surface. *J. Phys. Chem. C* **2019**, *123* (28), 17343–17352.

(203) Gierada, M.; Petit, I.; Handzlik, J.; Tielens, F. Hydration in Silica Based Mesoporous Materials: A DFT Model. *Phys. Chem. Chem. Phys.* **2016**, *18* (48), 32962–32972.

(204) Macià Escatllar, A.; Ugliengo, P.; Bromley, S. T. Modeling Hydroxylated Nanosilica:

Testing the Performance of ReaxFF and FFSiOH Force Fields. *J. Chem. Phys.* **2017**, *146* (22).

(205) Rimola, A.; Ugliengo, P.; Sodupe, M. Strained Ring Motif at Silica Surfaces: A Quantum Mechanical Study of Their Reactivity towards Protic Molecules. *Comput. Theor. Chem.* **2015**, *1074*, 168–177.

(206) Nonella, M.; Seeger, S. Investigating Alanine-Silica Interaction by Means of First-Principles Molecular-Dynamics Simulations. *ChemPhysChem* **2008**, *9* (3), 414–421.

(207) Zhao, Y. L.; Köppen, S.; Frauenheim, T. An SCC-DFTB/MD Study of the Adsorption of Zwitterionic Glycine on a Geminal Hydroxylated Silica Surface in an Explicit Water Environment. *J. Phys. Chem. C* **2011**, *115* (19), 9615–9621.

(208) Han, J. W.; Sholl, D. S. Enantiospecific Adsorption of Amino Acids on Hydroxylated Quartz (0001). *Langmuir* **2009**, *25* (18), 10737–10745.

(209) Mian, S. A.; Khan, Y.; Ahmad, U.; Khan, M. A.; Rahman, G.; Ali, S. Investigating the Adsorption Mechanism of Glycine in Comparison with Catechol on Cristobalite Surface Using Density Functional Theory for Bio-Adhesive Materials. *RSC Adv.* **2016**, *6* (115), 114313–114319.

(210) Costa, D.; Tougerti, A.; Tielens, F.; Gervais, C.; Stievano, L.; Lambert, J. F. DFT Study of the Adsorption of Microsolvated Glycine on a Hydrophilic Amorphous Silica Surface. *Phys. Chem. Chem. Phys.* **2008**, *10* (42), 6360–6368.

(211) Tranca, I.; Smerieri, M.; Savio, L.; Vattuone, L.; Costa, D.; Tielens, F. Unraveling the Self-Assembly of the (S)-Glutamic Acid "Flower" Structure on Ag(100). *Langmuir* **2013**, *29* (25), 7876–7884.

(212) Pickard, C. J.; Mauri, F. All-Electron Magnetic Response with Pseudopotentials: NMR Chemical Shifts. **2001**, *63*, 1–13.

(213) Giannozzi, P.; Baroni, S.; Bonini, N.; Calandra, M.; Car, R.; Cavazzoni, C.; Ceresoli, D.; Chiarotti, G. L.; Cococcioni, M.; Dabo, I.; *et al*. QUANTUM ESPRESSO: A Modular and Open-Source Software Project for Quantum Simulations of Materials. *J. Phys. Condens. Matter* **2009**, *21* (39).

(214) Stievano, L.; Tielens, F.; Lopes, I.; Folliet, N.; Gervais, C.; Costa, D.; Lambert, J. F. Density Functional Theory Modeling and Calculation of NMR Parameters: An Ab Initio Study of the Polymorphs of Bulk Glycine. *Cryst. Growth Des.* **2010**, *10* (8), 3657–3667.

(215) Vulcu, A.; Berghian Grosan, C.; Chiriac, M.; Almasan, V. The 15N Labelled L-Glutamic Acid: Experimental and Computational NMR Studies. *Rev. Roum. Chim.* **2011**, *56* (6), 667–674.

(216) Charpentier, T. The PAW/GIPAW Approach for Computing NMR Parameters: A New Dimension Added to NMR Study of Solids. *Solid State Nucl. Magn. Reson.* **2011**, *40* (1), 1–20.

(217) Brás, A. R.; Fonseca, I. M.; Dionísio, M.; Schönhals, A.; Affouard, F.; Correia, N. T. Influence of Nanoscale Confinement on the Molecular Mobility of Ibuprofen. *J. Phys. Chem. C* **2014**, *118* (25), 13857–13868.

(218) Shizu, K.; Noda, H.; Tanaka, H.; Taneda, M.; Uejima, M.; Sato, T.; Tanaka, K.; Kaji, H.; Adachi, C. Highly Efficient Blue Electroluminescence Using Delayed-Fluorescence Emitters with Large Overlap Density between Luminescent and Ground States. *J. Phys. Chem. C* **2015**, *119* (47), 26283–26289.

(219) Lejaeghere, K.; Bihlmayer, G.; Björkman, T.; Blaha, P.; Blügel, S.; Blum, V.; Caliste, D.; Castelli, I. E.; Clark, S. J.; Dal Corso, A.; *et al*. Reproducibility in Density Functional Theory Calculations of Solids. *Science (80-.).* **2016**, *351* (6280).

(220) Marquardt, D.; Heberle, F. A.; Miti, T.; Eicher, B.; London, E.; Katsaras, J.; Pabst, G. 1H NMR Shows Slow Phospholipid Flip-Flop in Gel and Fluid Bilayers. *Langmuir* **2017**, *33* (15), 3731–3741.

(221) Wiench, J. W.; Avadhut, Y. S.; Maity, N.; Bhaduri, S.; Lahiri, G. K.; Pruski, M.; Ganapathy, S. Characterization of Covalent Linkages in Organically Functionalized MCM-41 Mesoporous Materials by Solid-State NMR and Theoretical Calculations. *J. Phys. Chem. B* **2007**, *111* (15), 3877–3885.

(222) Mineva, T.; Gaveau, P.; Galarneau, A.; Massiot, D.; Alonso, B. 14N: A Sensitive NMR Probe for the Study of Surfactant-Oxide Interfaces. *J. Phys. Chem. C* **2011**, *115* (39), 19293–19302.

(223) Sautet, P.; Delbecq, F. Catalysis and Surface Organometallic Chemistry: A View from Theory and Simulations. *Chem. Rev.* **2010**, *110* (3), 1788–1806.

(224) Meynen, V.; Cool, P.; Vansant, E. F. Verified Syntheses of Mesoporous Materials. *Microporous Mesoporous Mater.* **2009**, *125* (3), 170–223.

(225) Emami, F. S.; Puddu, V.; Berry, R. J.; Varshney, V.; Patwardhan, S. V.; Perry, C. C.; Heinz, H. Prediction of Specific Biomolecule Adsorption on Silica Surfaces as a Function of PH and Particle Size. *Chem. Mater.* **2014**, *26* (19), 5725–5734.

(226) Somorjai, G. A.; Frei, H.; Park, J. Y. Advancing the Frontiers in Nanocatalysis, Biointerfaces, and Renewable Energy Conversion by Innovations of Surface Techniques. *J. Am. Chem. Soc.* **2009**, *131* (46), 16589–16605.

(227) Breen, N. F.; Weidner, T.; Li, K.; Castner, D. G.; Drobny, G. P. A Solid-State Deuterium NMR and Sum-Frequency Generation Study of the Side-Chain Dynamics of Peptides Adsorbed onto Surfaces. *J. Am. Chem. Soc.* **2009**, *131* (40), 14148–14149.

(228) Hsiao, J. K.; Tsai, C. P.; Chung, T. H.; Hung, Y.; Yao, M.; Liu, H. M.; Mou, C. Y.; Yang, C. S.; Chen, Y. C.; Huang, D. M. Mesoporous Silica Nanoparticles as a Delivery System of Gadolinium for Effective Human Stem Cell Tracking. *Small* **2008**, *4* (9), 1445–1452.

(229) Rosen, J. E.; Gu, F. X. Surface Functionalization of Silica Nanoparticles with Cysteine: A Low-Fouling Zwitterionic Surface. *Langmuir* **2011**, *27* (17), 10507–10513.

(230) Logunov, S.; Kuchinsky, S. Experimental and Theoretical Study of Bulk Light Scattering in Ca F 2 Monocrystals. *J. Appl. Phys.* **2005**, *98* (5).

(231) Hayashi, S.; Hayamizu, K. Chemical Shift Standards in High-Resolution Solid-State NMR (1) 13 C, 29 Si, and 1 H Nuclei. *Bulletin of the Chemical Society of Japan*. 1991, pp 685–687.

(232) Hayashi, S.; Hayamizu, K. Chemical Shift Standards in High-Resolution Solid-State NMR (2) 15 N Nuclei. *Bull. Chem. Soc. Jpn.* **1991**, *64* (2), 688–690.

(233) Kresse, G. Ab Initio Molecular Dynamics for Liquid Metals. *J. Non. Cryst. Solids* **1995**, *192–193* (1), 222–229.

(234) Kresse, G.; Hafner, J. Ab Initio Molecular-Dynamics Simulation of the Liquid-Metalamorphous- Semiconductor Transition in Germanium. *Phys. Rev. B* **1994**, *49* (20), 14251–14269.

(235) Vojta, M. Reports on Progress in Physics Related Content. *Rep. Prog. Phys.* **1996**, *59*, 1665–1735.

(236) Perdew, J. P.; Burke, K.; Ernzerhof, M. Generalized Gradient Approximation Made Simple. *Phys. Rev. Lett.* **1996**, *77* (18), 3865–3868.

(237) Blöchl, P. E.; Jepsen, O.; Andersen, O. K. Improved Tetrahedron Method for Brillouin-Zone Integrations. *Phys. Rev. B* **1994**, *49* (23), 16223–16233.

(238) Joubert, D. From Ultrasoft Pseudopotentials to the Projector Augmented-Wave Method. *Phys. Rev. B - Condens. Matter Mater. Phys.* **1999**, *59* (3), 1758–1775.

(239) Blöchl, P. E. Projector Augmented-Wave Method. *Phys. Rev. B* **1994**, *50* (24), 17953–17979.

(240) Troullier, N.; Martins, J. L. Efficient Pseudopotentials for Plane-Wave Calculations. *Phys. Rev. B* **1991**, *43* (3), 1993–2006.

(241) Bylander, D. M.; Kleinman, L. Efficacious Form for Model Pseudopotentials. *Phys. Rev. Lett.* **1982**, *48* (20), 1425–1428.

(242) Jönsson, P. G.; Kvick, Å. ;. Precision Neutron Diffraction Structure Determination of Protein and Nucleic Acid Components. III. The Crystal and Molecular Structure of the Amino Acid α-Glycine. *Acta Crystallogr. Sect. B Struct. Crystallogr. Cryst. Chem.* **1972**, *28* (6), 1827–1833.

(243) Lehmann, M. S.; Koetzle, T. F.; Hamilton, W. C. Precision Neutron Diffraction Structure Determination of Protein and Nucleic Acid Components. I. The Crystal and Molecular Structure of the Amino Acid L-Alanine. *J. Am. Chem. Soc.* **1972**, *94* (8), 2657–2660.

(244) Görbitz, C. H.; Dalhus, B. Redetermination of L-Leucine at 120 K. *Acta Crystallogr. Sect. C Cryst. Struct. Commun.* **1996**, *52* (7), 1754–1756.

(245) Lehmann, M. S.; Nunes, A. C. A Short Hydrogen Bond between near Identical Carboxyl Groups in the α-Modification of L-Glutamic Acid. *Acta Crystallogr. Sect. B Struct. Crystallogr. Cryst. Chem.* **1980**, *36* (7), 1621–1625.

(246) Hirokawa, S. A New Modification of L-Glutamic Acid and Its Crystal Structure. *Acta Crystallogr.* **1955**, *8* (10), 637–641.

(247) Alaeddine, S.; Nygren, H. The Adsorption of Water and Amino Acids onto Hydrophobic Quartz Surfaces. *Coll. Surf* **1996**, *6*, 71–79.

(248) Gao, Q.; Xu, W.; Xu, Y.; Wu, D.; Sun, Y.; Deng, F.; Shen, W. Amino Acid Adsorption on Mesoporous Materials: Influence of Types of Amino Acids, Modification of Mesoporous Materials, and Solution Conditions. *J. Phys. Chem. B* **2008**, *112* (7), 2261–2267.

(249) Basiuk, V. Thermodynamics of Adsorption of Amino Acids, Small Peptides, and Nucleic Acid Components on Silica Adsorbents. *Cheminform* **2004**, *35*.

(250) Rai, A. K.; Xu, X.; Lin, Z.; Rai, D. K. Conformational Search for Zwitterionic Leucine and Hydrated Conformers of Both the Canonical and Zwitterionic Leucine Using the DFT-CPCM Model. *Vib. Spectrosc.* **2011**, *56* (1), 74–81.

(251) Elfassy, E.; Basel, Y.; Mastai, Y. Crystallization of Amino Acids at the Chiral Ionic Liquid/Water Interface. *CrystEngComm* **2016**, *18* (45), 8769–8775.

(252) Burneau, A.; Gallas, J. P. *In The Surface Properties of Silicas*; Legrand, A. P., J. W. & S. C., Ed.; 1998.

(253) Harding, M, M.; Howieson, R, M. L-Leucine. *Acta Cryst.* **1976**, *32*, 632–633.

(254) Coll, B. Y. M.; Solans, X.; FONT-ALTABA, M. Structure of L-Leucine: A Redetermination. *Acta Cryst. C* **1986**, *42*, 599–601.

(255) Faanha Filho, P. F.; Jiao, X.; Freire, P. T. C.; Lima, J. A.; Dos Santos, A. O.; Henry, P. F.; Yokaichiya, F.; Kremner, E.; Bordallo, H. N. Structure-Property Relations in Crystalline l-Leucine Obtained from Calorimetry, X-Rays, Neutron and Raman Scattering. *Phys. Chem. Chem. Phys.* **2011**, *13* (14), 6576–6583.

(256) Binns, J.; Parsons, S.; McIntyre, G. J. Accurate Hydrogen Parameters for the Amino Acid l -Leucine. *Acta Crystallogr. Sect. B Struct. Sci. Cryst. Eng. Mater.* **2016**, *72* (6), 885–892.

(257) Tadeusiak, E. J.; Ciesielski, W.; Olejniczak, S. Determination of Enantiomeric Excess of Leucine By13C CP-MAS Solid-State NMR. *Appl. Magn. Reson.* **2008**, *35* (1), 155–161.

(258) Hollingsworth, M. D.; Cyr, N. High Resolution Solid-State NMR Spectra of Leucine: A Re-Examination. *J. Chem. Soc. Chem. Commun.* **1990**, No. 7, 578–580.

(259) Ye, C.; Fu, R.; Hu, J.; Hou, L.; Ding, S. Carbon-13 Chemical Shift Anisotropies of Solid Amino Acids. *Magn. Reson. Chem.* **1993**, *31* (8), 699–704.

(260) Taylor, R. E. 13C CP/MAS: Application to Glycine. *Concepts Magn. Reson. Part A Bridg. Educ. Res.* **2004**, *22* (2), 79–89.

(261) Bixel, M. G.; Engelmann, J.; Willker, W.; Hamprecht, B.; Leibfritz, D. Metabolism of [U- 13C]Leucine in Cultured Astroglial Cells. *Neurochem. Res.* **2004**, *29* (11 SPEC. ISS.), 2057–2067.

(262) Liu, C. C.; Maciel, G. E. The Fumed Silica Surface: A Study by NMR. *J. Am. Chem. Soc.* **1996**, *118* (21), 5103–5119.

(263) de la Caillerie, E.; Raouf Aimeur, M.; El Kortobi, Y.; Pierre Legrand, A. Water Adsorption on Pyrogenic Silica Followed by 1H MAS NMR. *J. Colloid Interface Sci.* **1997**, *194* (194), 434–439.

(264) Hu, J. Z.; Kwak, J. H.; Herrera, J. E.; Wang, Y.; Peden, C. H. F. Line Narrowing in 1H MAS Spectrum of Mesoporous Silica by Removing Adsorbed H2O Using N2. *Solid State Nucl. Magn. Reson.* **2005**, *27* (3), 200–205.

(265) Trébosc, J.; Wiench, J. W.; Huh, S.; Lin, V. S.-Y.; Pruski, M. Solid-State NMR Study of MCM-41-Type Mesoporous Silica Nanoparticles. *J. Am. Chem. Soc.* **2005**, *127* (9), 3057–3068.

(266) Iwahara, J.; Jung, Y. S.; Clore, G. M. Heteronuclear NMR Spectroscopy for Lysine NH3 Groups in Proteins: Unique Effect of Water Exchange on 15N Transverse Relaxation. *J. Am. Chem. Soc.* **2007**, *129* (10), 2971–2980.

(267) Shir, I. Ben; Kababya, S.; Amitay-Rosen, T.; Balazs, Y. S.; Schmidt, A. Molecular Level Characterization of the Inorganic-Bioorganic Interface by Solid State NMR: Alanine on a Silica Surface, a Case Study. *J. Phys. Chem. B* **2010**, *114* (18), 5989–5996.

(268) Kassab, E.; Langlet, J.; Evleth, E.; Akacem, Y. Theoretical Study of Solvent Effect on Intramolecular Proton Transfer of Glycine. *J. Mol. Struct. THEOCHEM* **2000**, *531* (1–3), 267–282.

(269) Rimola, A.; Civalleri, B.; Ugliengo, P. Neutral vs Zwitterionic Glycine Forms at the Water/Silica Interface: Structure, Energies, and Vibrational Features from B3LYP Periodic Simulations. *Langmuir* **2008**, *24* (24), 14027–14034.

(270) Remesal, E. R.; Amaya, J.; Graciani, J.; Márquez, A. M.; Sanz, J. F. Adsorption of Prototypical Amino Acids on Silica: Influence of the Pre-Adsorbed Water Multilayer. *Surf. Sci.* **2016**, *646*, 239–246.

(271) Bolis, V.; Cavenago, A.; Fubini, B. Surface Heterogeneity on Hydrophilic and Hydrophobic Silicas: Water and Alcohols as Probes for H-Bonding and Dispersion Forces. *Langmuir* **1997**, *13* (5), 895–902.

(272) Tudela, D.; Marx, D. Water-Induced Zwitterionization of Glycine: Stabilization

Mechanism and Spectral Signatures. **2016**.

(273) Siskos, M. G.; Choudhary, M. I.; Gerothanassis, I. P. Hydrogen Atomic Positions of O-H•••O Hydrogen Bonds in Solution and in the Solid State: The Synergy of Quantum Chemical Calculations with 1H-NMR Chemical Shifts and X-Ray Diffraction Methods. *Molecules* **2017**, *22* (3).

(274) Dračínský, M.; Unzueta, P.; Beran, G. J. O. Improving the Accuracy of Solid-State Nuclear Magnetic Resonance Chemical Shift Prediction with a Simple Molecular Correction. *Phys. Chem. Chem. Phys.* **2019**, *21* (27), 14992–15000.

(275) Surprenant, H. L.; Sarneski, J. E.; Key, R. R.; Byrd, J. T.; Reilley, C. N. Carbon-13 NMR Studies of Amino Acids: Chemical Shifts, Protonation Shifts, Microscopic Protonation Behavior. *J. Magn. Reson.* **1980**, *40* (2), 231–243.

(276) Day, P. N.; Pachter, R. A Study of Aqueous Glutamic Acid Using the Effective Fragment Potential Method. *J. Chem. Phys.* **1997**, *107* (8), 2990–2999.

(277) Sebben, D.; Pendleton, P. Analysis of Ionic Strength Effects on the Adsorption of Simple Amino Acids. *J. Colloid Interface Sci.* **2015**, *443*, 153–161.

(278) Sebben, D.; Pendleton, P. (Amino Acid + Silica) Adsorption Thermodynamics: Effects of Temperature. *J. Chem. Thermodyn.* **2015**, *87*, 96–102.

(279) Ostwald, W. F. No Title. *Z. Phys. Chem.* **1897**, *22*, 289.

(280) Boistelle, R.; Astier, J. P. Crystallization Mechanisms in Solution. *J. Cryst. Growth* **1988**, *90* (1–3), 14–30.

(281) Veesler, S.; Puel, F.; Fevotte, G. Polymorphisme Dans Les Procédés de Cristallisation En Solution. *S.T.P. Pharma Prat.* **2005**, *15* (1), 53–84.

(282) Agatonovic-Kustrin, S.; Wu, V.; Rades, T.; Saville, D.; Tucker, I. G. Ranitidine Hydrochloride X-Ray Assay Using a Neural Network. *J. Pharm. Biomed. Anal.* **2000**, *22* (6), 985–992.

(283) Guengerich, F. P. Mechanisms of Drug Toxicity and Relevance to Pharmaceutical Development. *HHS Public Access* **2011**, *26* (1), 3–14. h

(284) Vippagunta, S. R.; Brittain, H. G.; Grant, D. J. W. Crystalline Solids. *Adv. Drug Deliv. Rev.* **2001**, *48* (1), 3–26.

(285) Brittain, H. G.; Byrn, S. R.; Lee, E. *Polymorphism in Pharmaceutical Solids*; 2016; Vol. 192.

(286) Davey, R. J.; Blagden, N.; Potts, G. D.; Docherty, R. Polymorphism in Molecular Crystals: Stabilization of a Metastable Form by Conformational Mimicry. *J. Am. Chem. Soc.* **1997**, *119* (7), 1767–1772.

(287) Threlfall, T. L. Analysis of Organic Polymorphs. *Analyst* **1995**, *120* (10), 2435–2460.

(288) Cameron, M.; Zhou, G. X.; Hicks, M. B.; Antonucci, V.; Ge, Z.; Lieberman, D. R.; Lynch, J. E.; Shi, Y. J. Employment of On-Line FT-IR Spectroscopy to Monitor the Deprotection of a 9-Fluorenylmethyl Protected Carboxylic Acid Peptide Conjugate of Doxorubicin. *J. Pharm. Biomed. Anal.* **2002**, *28* (1), 137–144.

(289) Liu, W.; Wei, H.; Black, S. An Investigation of the Transformation of Carbamazepine from Anhydrate to Hydrate Using in Situ FBRM and PVM. *Org. Process Res. Dev.* **2009**, *13* (3), 494–500.

(290) Gu, C. H.; Young, V.; Grant, D. J. W. Polymorph Screening: Influence of Solvents on the Rate of Solvent-Mediated Polymorphic Transformation. *J. Pharm. Sci.* **2001**, *90* (11), 1878–1890.

(291) Bernal, J. D. The Crystal Structure of the Natural Amino Acids and Belated Compounds. *Kürzere Orig. und Notizen* **1931**, 363–369.

(292) Hirokawa, S. A New Modification of L-Glutamic Acid and Its Crystal Structure. *Acta Crystallogr.* **1955**, *8* (10), 637–641.

(293) Palanisamy, D.; Karuppannan, S. Nucleation Control and Growth of Metastable α-l-Glutamic Acid Single Crystals in the Presence of l-PhenylAlanine. *Procedia Eng.* **2016**, *141*, 70–77.

(294) Sakata, Y. Studies on the Polymorphism of L-Glutamic Acid. *Agric. Biol. Chem.* **1961**, *25* (11), 829–837.

(295) Sano, C.; Kashiwagi, T.; Nagashima, N.; Kawakita, T. Effects of Additives on the Growth of L-Glutamic Acid Crystals (β-Form). *J. Cryst. Growth* **1997**, *178* (4), 568–574.

(296) Hasegawa, M.; Fukuda, N.; Higuchi, H.; Noguchi, S.; Matsubara, I. The Isolation and Identification of γ-Glutamylpeptides from L-Glutamic Acid Fermentation Broths and Their Actions to the Crystallization of the Amino Acid. *Agric. Biol. Chem.* **1977**, *41* (1), 49–56.

(297) Bernstein, J. Polymorphism of L-Glutamic Acid: Decoding the α–β Phase Relationship via Graph-set Analysis. *Acta Crystallogr. Sect. B* **1991**, *47* (6), 1004–1010.

(298) Dharmayat, S.; Calderon De Anda, J.; Hammond, R. B.; Lai, X.; Roberts, K. J.; Wang, X. Z. Polymorphic Transformation of L-Glutamic Acid Monitored Using Combined on-Line Video Microscopy and X-Ray Diffraction. *J. Cryst. Growth* **2006**, *294* (1), 35–40.

(299) Lai, T. T. C.; Ferguson, S.; Palmer, L.; Trout, B. L.; Myerson, A. S. Continuous Crystallization and Polymorph Dynamics in the l -Glutamic Acid System. *Org. Process Res. Dev.* **2014**, *18* (11), 1382–1390.

(300) Srinivasan, K.; Dhanasekaran, P. Separation and Nucleation Control of α and β Polymorphs of L-Glutamic Acid by Swift Cooling Crystallization Process. *Amino Acids* **2011**, *40* (4), 1257–1260.

(301) Croker, D.; Hodnett, B. K. Mechanistic Features of Polymorphic Transformations: The Role of Surfaces. *Cryst. Growth Des.* **2010**, *10* (6), 2808–2816.

(302) Moshe, H.; Levi, G.; Mastai, Y. Polymorphism Stabilization by Crystal Adsorption on a Self-Assembled Monolayer. *CrystEngComm* **2013**, *15* (44), 9203–9209.

(303) Quang, K. C.; Truong Giang, D.; Thi, T.; Huyen, T.; Tuan, N. A. Crystallization of L-Glutamic Acid: Mechanism of Heterogeneous β-Form Nucleation. *Res. Inven. Int. J. Eng. Sci.* **2017**, *7* (1), 2319–6483.

(304) Nunes, R. S.; Cavalheiro, É. T. G. Thermal Behavior of Glutamic Acid and Its Sodium, Lithium and Ammonium Salts. *J. Therm. Anal. Calorim.* **2007**, *87* (3), 627–630.

(305) Battistella, A. " THE ROLE OF THE INORGANIC SURFACE IN PROMOTING OLIGOPEPTIDES FORMATION . VIBRATIONAL SPECTROSCOPIC STUDIES ". **2017**.

(306) Hirayama, N.; Shirahata, K.; Ohashi, Y.; Sasada, Y. Structure of α Form of L-Glutamic Acid. α-β Transition. *Bulletin of the Chemical Society of Japan*. 1980, pp 30–35.

(307) Ruggiero, M. T.; Sibik, J.; Zeitler, J. A.; Korter, T. M. Examination of l -Glutamic Acid Polymorphs by Solid-State Density Functional Theory and Terahertz Spectroscopy. *J. Phys. Chem. A* **2016**, *120* (38), 7490–7495.

(308) Wang, Y.; Wilson, D.; Harbison, G. S. Solid-State NMR and the Crystallization of Aspartic and Glutamic Acids. *Cryst. Growth Des.* **2016**, *16* (2), 625–631.

(309) Bellamy, L. J. *The Infrared Spectra of Complex Molecules*; 1975.

(310) Ziganshin, M. A.; Safiullina, A. S.; Gerasimov, A. V.; Ziganshina, S. A.; Klimovitskii, A. E.; Khayarov, K. R.; Gorbatchuk, V. V. Thermally Induced Self-Assembly and Cyclization of l -Leucyl- l -Leucine in Solid State. *J. Phys. Chem. B* **2017**, *121* (36), 8603–8610.

(311) White, D. H.; Kennedy, R. M.; Macklin, J. Acyl Silicates and Acyl Aluminates as Activated Intermediates in Peptide Formation on Clays. *Orig. Life* **1984**, *14* (1–4), 273–278.

(312) El Samrout, O. Personal Communication.

(313) Poopari, M. R.; Zhu, P.; Dezhahang, Z.; Xu, Y. Vibrational Absorption and Vibrational Circular Dichroism Spectra of Leucine in Water under Different PH Conditions: Hydrogen-Bonding Interactions with Water. *J. Chem. Phys.* **2012**, *137* (19).

(314) Van Dornshuld, E.; Vergenz, R. A.; Tschumper, G. S. Peptide Bond Formation via Glycine Condensation in the Gas Phase. *J. Phys. Chem. B* **2014**, *118* (29), 8583–8590.

(315) Silva, C. B.; da Silva Filho, J. G.; Pinheiro, G. S.; Teixeira, A. M. R.; de Sousa, F. F.; Freire, P. T. C. High-Pressure Studies on L,L-DiLeucine Crystals by Raman

Spectroscopy and Synchrotron X-Ray Diffraction Combined with DFT Calculations. *Spectrochim. Acta - Part A Mol. Biomol. Spectrosc.* **2020**, *229*, 117899.

(316) Biswas, A.; Mallik, B. S. Distinctive Behavior and Two-Dimensional Vibrational Dynamics of Water Molecules inside Glycine Solvation Shell. *RSC Adv.* **2020**, *10* (11), 6658–6670.

(317) Bedoin, L. Ph.D. Thesis, Sorbonne Université, to be defended in 2021.

Résumé de la thèse

Contexte et état de l'art

En 1924, Alexander Oparine a proposé que la synthèse abiotique de composés organiques sur une longue période de temps a constitué une condition préalable à l'émergence de la vie sur terre[1], établissant ainsi un lien entre les processus biochimiques fondamentaux et la chimie « prébiotique », et posant des questions intrigantes pour les générations à venir. Il a fallu près de 30 ans pour que le modèle d'Oparine de réduction de l'atmosphère primordiale soit testé expérimentalement par Miller et Urey, dans les années 1950. Les biochimistes Stanley Miller et Harold Urey ont tenté de simuler ces conditions hypothétiques de la Terre archéenne, en effectuant une expérience de décharge électrique dans un dispositif expérimental contenant des gaz atmosphériques censés reproduire l'atmosphère primordiale. Après avoir mené l'expérience pendant un certain temps, ils ont réussi à obtenir entre autres des acides aminés!

Pour qu'une condensation se produise entre deux acides aminés ou même des acides aminés présents à grande échelle, la précipitation et l'évaporation continues ncorporées dans l'expérience de Miller-Urey ne sont pas suffisantes. La formation d'amides nécessite une énergie élevée car elle ne se produit pas spontanément et, par conséquent, une source d'énergie externe est nécessaire. Au fil des années, beaucoup ont postulé des scénarios de condensation des acides aminés.

Ainsi, il a été suggéré depuis longtemps que les surfaces minérales ont joué un rôle crucial dans l'évolution chimique de la vie, agissant comme un lieu prometteur pour la transition de la géochimie chimique à la biochimie. Le rôle essentiel des matériaux inorganiques dans les origines de la vie a été proposé pour la première fois par J. D. Bernal en 1949 dans une communication influente intitulée *"The Physical Basis of Life"* et publiée ultérieurement, en 1951. Initialement, la justification qu'il a donnée d'un possible rôle des surfaces minérales était la suivante. La formation d'une liaison peptidique entre deux acides aminés peut s'écrire:

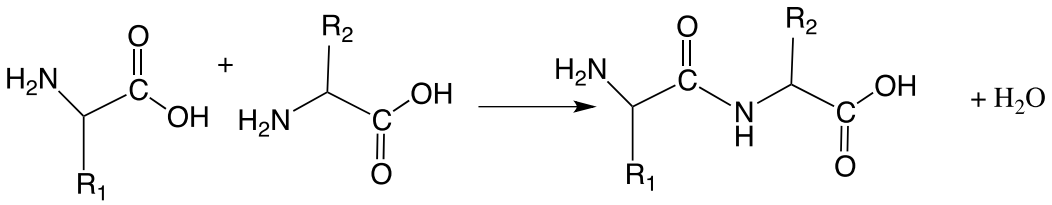

Ou de façon plus condensée:

A + B ⟶ A-B + H_2O, avec une constante d'équilibre $K = \frac{a_{A-B}a_{H_2O}}{a_A a_B}$

Comme il s'agit d'une réaction de condensation, une concentration de la solution augmentera le rapport dimère / monomère à l'équilibre. Cela vaut également pour toutes les étapes suivantes de polymérisation. Bernal a fait valoir que l'effet de l'adsorption serait d'augmenter la concentration locale en acides aminés et favoriserait donc automatiquement davantage la polymérisation dans la «phase adsorbée» que dans la solution. En effet, en thermochimie, l'adsorption est considérée comme une augmentation de concentration locale au voisinage de la surface, et déplace donc l'équilibre vers la polymérisation. Peu de données étaient disponibles sur l'adsorption des acides aminés lorsque Bernal a formulé son hypothèse, mais on pouvait s'attendre à ce que par ex. les minéraux avec des surfaces chargées positivement, comme les hydrotalcites, adsorberaient et concentreraient les acides aminés anioniques tels que les ions glutamates.

Notre thèse porte sur l'adsorption de deux acides aminés (AA) aux propriétés différentes, la leucine et l'acide glutamique, sur la surface de la silice amorphe. Elle illustre une approche générale des systèmes hybrides qui combine des informations expérimentales et la modélisation moléculaire afin de caractériser au niveau moléculaire l'interaction de molécules organiques avec des sites d'adsorption à la surface de minéraux inorganiques.

Des techniques spectroscopiques de pointe, principalement la spectroscopie IR et la RMN du solide, ont été utilisées pour recueillir des informations sur les groupes fonctionnels des acides aminés et la manière dont ils sont modifiés par l'adsorption. En conjonction avec des techniques de caractérisation macroscopique telles que la diffraction des rayons X (DRX) et l'analyse thermogravimétrique (ATG), elles ont permis d'identifier les paramètres qui régissent la spéciation de surface - principalement l'activité de l'eau, expliquant l'importance d'une étape de séchage contrôlée - et la compétition entre l'adsorption sur site et la précipitation en tant que phase cristalline distincte. Parmi tous les acides aminés possibles qui auraient pu être étudiés

(et l'ont parfois été effectivement), certains présentent plus d'intérêt que d'autres. Récemment, des chercheurs du LRS ont observé que la co-adsorption de la leucine (Leu) et de l'acide glutamique (Glu) sur la silice conduit à des peptides linéaires assez longs qui semblent présenter une sélectivité de séquence non triviale. Ainsi, nous avons entrepris une caractérisation expérimentale et théorique conjointe de l'interaction de ces deux acides aminés avec une surface de silice.

Leucine/silice

Le chapitre III se concentre sur Leu / SiO_2. Ce système particulier a fait jusqu'à présent l'objet d'études limitées, principalement au niveau macroscopique. Pour comprendre l'adsorption des espèces de leucine, une combinaison de plusieurs techniques spectroscopiques a été appliquée. Pour cela, les spectroscopies IR et RMN à l'état solide ont été choisies, en utilisant notamment des expériences de corrélation hétéronucléaire 2D (HETCOR) pour mettre en évidence les proximités et les connectivités proton-carbone ou proton-azote dans l'espoir de comprendre et d'identifier le type de liaison de la leucine avec la surface. De plus, des états d'hydratation élevés et faibles ont été étudiés et quantifiés par ATG, afin de comprendre l'influence de l'eau sur la spéciation de la leucine et le comportement d'adsorption. Le système a également été étudié en utilisant des simulations DFT avancées. Du point de vue expérimental, la spectroscopie RMN à l'état solide montre que l'interaction leucine-silice est essentiellement régie par l'eau, différents états d'hydratation (séchage sous flux d'azote à température ambiante, ND ou sous vide, VD) induisant différentes spéciations de la leucine. Le séchage sous flux (ND) conduit à des échantillons encore fortement hydratés. Alors que l'élargissement des pics RMN indique une mobilité et un échange diminués et une hétérogénéité significative de l'environnement local, d'autres caractéristiques (résolution des signaux C4 et C5, C6, mobilité de l'ammonium…) sont comparables à celles de la supportée. En revanche, le séchage sous vide (VD) entraîne une diminution significative de la quantité d'eau résiduelle. La quantification par TG suggère que dans cet état, chaque molécule de Leucine conserve encore un nombre limité de molécules d'eau d'hydratation (de l'ordre de 3 à 5 H_2O par Leu). Ceci est corroboré par la comparaison des déplacements chimiques ^{13}C et ^{15}N observés expérimentalement avec les valeurs calculées pour des modèles microsolvatés d'une part (Leucine co-adsorbée avec un nombre limité de molécules d'eau), anhydres d'autre part (Leucine interagissant uniquement avec les groupes silanols de surface). La plupart des modèles offrant une bonne correspondance avec l'expérience sont des modèles microsolvatés. D'un point de vue énergétique, la co-adsorption d'une molécule d'eau

avec la Leucine a un ΔG° plus négatif que son adsorption directe sur la surface de la silice. L'état de la Leucine VD pourrait être décrit comme un ensemble d'adduits de surface à 3 partenaires : Leu.$(H_2O)_n$.(Site de surface), dont la cohésion est assurée par un réseau de liaisons hydrogène assez fortes.

La spectroscopie IR prouve par ailleurs que dans les échantillons séchés sans activation thermique, les espèces prédominantes sont des zwitterions (possédant un carboxylate négatif ainsi qu'un groupe ammonium positif, comme en solution aqueuse) plutôt que des formes neutres. Ceci est fortement corroboré par la comparaison des déplacements chimiques RMN expérimentaux et calculés - tous parmi les modèles donnant une bonne correwpondance, même quand ils sont anhydres, ont un Leu zwitterionique. L'acide aminé adsorbé dans cet état ne doit pas être très réactif car le groupement nucléophile nécessaire à la formation de la lision peptidique ($-NH_2$) est désactivé par protonation. On peut enfin tirer quelques informations plus spécifiques concernant la structure moléculaire des adduits de leucine adsorbés en conditions VD : d'après les calculs théoriques, les modèles où NH_3^+ interagit directement avec la surface sont significativement stabilisés énergétiquement par rapport à ceux qui possèdent des molécules d'eau pontantes. De plus, l'observation des corrélations $\{^1H\text{-}^{15}N\}$ impliquant les protons de l'ammonium indique que ce groupe a une mobilité restreinte, par rapport aux échantillons ND, sans doute en raison de la création d'une interaction spécifique avec la surface. La position de ces protons d'ammonium sur l'échelle des déplacements chimiques ^1H est également compatible avec une liaison directe ammonium-silanols, et l'IR indique que l'ammonium est plus modifié par adsorption que le carboxylate. A l'inverse, pour le groupement carboxylate, les mêmes critères pointent plutôt vers une interaction indirecte carboxylate$\cdots H_2O\cdots$surface. Au-delà de ces caractéristiques, le caractère large des signaux RMN (à l'exclusion des petits signaux fins dus à la leucine massique résiduelle) indique une certaine variabilité structurelle dans les adduits de surface. Tous les silanols ne conviennent pas comme sites d'adsorption, car le recouvrement de saturation de la leucine adsorbée est environ 10 fois inférieur à la densité de silanols (0,36 nm^{-2} contre 4 nm^{-2}), et parmi les sites possibles de nombreux groupes silanols quelque peu différents fourniront des environnements moléculaires eux-mêmes légèrement différents pour l'espèce adsorbée.

Acide Glutamique/silice

Au chapitre IV, nous appliquons la même approche et les mêmes techniques à l'acide glutamique supporté sur silice fumée : DRX, ATG, IR et spectroscopie RMN du solide, ainsi que modélisation moléculaire DFT et comparaison des paramètres expérimentaux et calculés. Glu / SiO_2 présente à la fois des similitudes et des différences avec Leu / SiO_2. Ce système présente plus de défis pour la caractérisation expérimentale de la spéciation des acides aminés, et en particulier des champs élevés sont nécessaires pour la caractérisation RMN. A première vue, la DRX semble indiquer qu'aucune phase cristalline n'est présente jusqu'à une charge d'environ 3% en poids. Ainsi, comme pour la leucine, l'acide glutamique s'adsorberait de manière moléculaire jusqu'à un recouvrement de saturation, et es molécules supplémentaires précipiteraient sous forme de cristaux massiques. Mais la RMN de ^{13}C oblige à reconsidérer ce point de vue puisque des signaux de type massique sont observés pour des charges aussi faibles que 0,3%. Nous pensons que de petits noyaux cristallins peuvent se former de manière compétitive même à de faibles activités du Glu adsorbé. Ils ne seraient pas détectables par XRD, mais l'environnement local des carbones de Glu serait très similaire à la (aux) forme(s) cristalline(s) et donnerait les mêmes signaux RMN. Cette existence de petits noyaux cristallins silencieux en DRX avait déjà été proposée par Bouchoucha et al., à partir d'un raisonnement quelque peu différent. Une remarque supplémentaire concernant les formes cristallines dans Glu / SiO_2 est que la phase cristalline observée (α ou β) semble présenter un effet mémoire par rapport au matériau de départ, ce qui peut également être cohérent avec l'existence de petits noyaux résilients constitués de quelques molécules Glu.

Cependant, il existe également des signatures de différentes formes non cristallines, qui ne peuvent être clairement observées que pour des charges de 1% ou moins. L'IR indique qu'elles sont principalement zwitterioniques, avec une chaîne latérale non ionisée –COOH. La distribution du Glu entre ces formes est très sensible à l'état d'hydratation de l'échantillon - ainsi, la première conclusion que nous avons tirée de l'étude Leu / SiO_2 (« l'eau est déterminante») est encore plus valable ici. Quantitativement, les quantités d'eau retenue déterminées par TG ne sont pas très différentes de celles mesurées pour Leu / SiO_2: elles augmentent avec la charge en acides aminés jusqu'à un plateau pour les échantillons dans des conditions de ND, et elles sont approximativement constantes, et à un niveau comparable, dans des conditions VD.

En conditions ND, une petite quantité de Glu est présente sous forme d'espèces «quasi liquides» qui ne sont pas observées par RMN CP-MAS en raison d'une mobilité trop élevée, mais peuvent l'être par excitation directe. En fonction sans doute de changements mineurs et incontrôlés de la teneur en eau de l'échantillon, ces molécules de Glu peuvent devenir visibles par RMN CP-MAS, indiquant une mobilité réduite, ou même (pour des teneurs en eau plus faibles) présenter un élargissement de signal significatif sans déplacement du pic. En conditions VD, un signal RMN large est observé dans la région carboxyle, ce qui signifie que des formes adsorbées dans une gamme d'environnements différents coexistent à la surface. Contrairement à la leucine, rien n'indique clairement que le groupe ammonium interagisse plus intimement avec la surface que les deux autres groupes fonctionnels. Globalement, l'interaction de Glu avec la surface de la silice semble être plus labile, et concerner une quantité plus limitée d'acides aminés, que celle de Leu. En tout cas, les données IR et RMN suggèrent une interaction par liaison hydrogène, sans aucune formation de liaison covalente, comme c'était également le cas pour la leucine.

En ce qui concerne le potentiel des techniques de caractérisation, la comparaison des deux formes cristallines du Glu massique indique que la RMN ^{13}C est très sensible aux petites différences dans l'état de liaison H; son applicabilité au cas Glu / SiO_2 supporté n'est limitée que par l'hétérogénéité du système. La HETCOR ^{13}C-^{1}H est également intéressante à cet égard car elle montre des pics de corrélation intermoléculaire intenses dans certains cas : en d'autres termes, des preuves limitées mais suggestives que l'agrégation des molécules Glu peut se produire même pour la forme «adsorbée».

La modélisation moléculaire confirme que l'adsorption par liaisons H est thermodynamiquement favorable. Dans le cas des modèles anhydres, les énergies d'adsorption sont plus négatives que pour Leu. Cela peut sembler en contradiction avec la conclusion expérimentale selon laquelle la forme adsorbée de Glu apparaît «moins compétitive» (à la fois vis-à-vis des formes cristallines et en solution) que dans le cas de Leu. Mais il faut se rappeler que les valeurs d'énergies d'adsorption sont calculées par rapport aux molécules d'acides aminés dans le vide. Il faudrait comparer avec l'énergie des molécules en solution et avec l'énergie d'association à la phase cristalline de Glu. Les énergies d'adsorption sont corrélées au nombre de liaisons H pour les modèles anhydres, mais seulement faiblement pour les modèles hydratés. Tout comme pour Leu, les modèles anhydres sont pour la plupart neutres. Mais dans certains cas, H_3Glu^+ cationique se forme par échange de protons avec la surface, possibilité qui

n'a pas de parallèle pour Leu. Comme pour Leu à nouveau, les déplacements chimiques calculés pour les modèles anhydres ne concordent pas bien avec l'expérience (que ce soit en conditions ND ou VD), conformément au constat que même les échantillons en conditions VD contiennent de l'eau résiduelle. D'autre part, les modèles hydratés les plus favorables énergétiquement donnent des déplacements chimiques ^{13}C et ^{15}N qui correspondent bien avec les valeurs expérimentales pour les conditions de séchage VD; mais quelques-uns d'entre eux pourraient tout aussi bien correspondre aux valeurs des échantillons en conditions ND. D'une manière générale, on peut dire que certaines des meilleures configurations d'interaction de Glu avec la surface sont très semblables aux espèces en phase liquide. Les calculs des déplacements chimiques ^{1}H indiquent qu'ils pourraient être des sondes sensibles de l'état de liaison H, mais leur interprétation n'est pas triviale en raison du fort chevauchement des résonances des protons entre différents groupes. Il semble que les modèles où le carboxylate est fortement lié par liaison H aux silanols puissent être exclus sur la base des corrélations trouvées: cela expliquerait pourquoi les preuves expérimentales de l'interaction carboxylate / surface ne sont visibles que lorsque la majeure partie de l'eau est éliminée du système, Les molécules d'acide glutamique ont une affinité moindre pour la surface de la silice que les molécules de Leucine - ou que les Glu les unes avec les autres.

Evolution thermique des systèmes

Le dernier chapitre (V) se concentre sur les transformations des acides aminés par activation thermique dans deux environnements caractérisés par des activités de l'eau différentes. L'objectif est de comparer l'évolution d'un système hydraté ayant initialement une forte activité de l'eau (ND) avec celui d'un système contenant des quantités minimales d'eau (VD), entre autres en ce qui concerne la mobilité globale et la dynamique des acides aminés vis-à-vis de la formation de liaisons peptidiques. Enfin, après avoir discuté de chaque acide aminé séparément, l'activation thermique de ces acides aminés co-adsorbés sur la surface des nanoparticules de silice a été étudiée. La spectroscopie IR et la RMN à l'état solide ont à nouveau été utilisées. Leu et Glu adsorbés séparément sur SiO_2 subissent des réactions de condensation en formes cycliques lorsque la température augmente. Celles-ci sont clairement révélées par IR où l'apparition de la bande amide I est évidente, mais elles sont plus difficiles à observer par RMN car la forte sélectivité de la technique peut se révéler un inconvénient - des environnements légèrement différents donnent lieu à un élargissement hétérogène des signaux, et donc à un faible rapport signal/bruit et à un fort recouvrement des signaux.

Dans le cas de la Leucine, la formation de liaisons amides est observée à des températures supérieures à 160 ° C dans les conditions ND, observation compatible avec l'événement thermique vu en TG (§ III.2.2). Le résultat est principalement le dimère cyclique (cyclo-Leu-Leu ou DKP). Dans les conditions VD, où l'élimination de l'eau physisorbée est plus efficace, nous observons l'isomérisation du zwitterion $HLeu^{\pm}$ en forme neutre $HLeu^{0}$ dès une température de 110 ° C - cette isomérisation avait été postulée auparavant mais jamais directement observée. Lors d'un chauffage ultérieur, $HLeu^{0}$ se transforme partiellement en dimère cyclique à 140° C, mais une quantité résiduelle de monomère est toujours présente même à 200° C. Apparemment, cette réaction est limitée par la diffusion à la surface de la silice. Dans le cas de l'acide glutamique, la forme neutre se forme peut-être mais elle n'est pas observée, car elle peut se transformer immédiatement en PyroGlu par cyclisation interne. Contrairement aux données publiées précédemment, nous n'avons vu aucune preuve d'une transformation ultérieure en dimère tricyclique PyroGluDKP. Lorsque le dimère linéaire H-Glu-Glu-OH (contenant une liaison peptidique préexistante entre deux groupes Glu) a été déposé sur la silice et activé, nous avons observé une cyclisation interne successive et (probablement) une cyclisation à PyroGluDKP à des températures plus élevées; mais cette voie n'est pas suivie en partant du monomère Glu.

Dans les deux cas, l'issue de l'activation thermique peut être considérée comme une «impasse» du point de vue prébiotique. Il reste possible que des peptides plus intéressants puissent être obtenus par des scénarios complexes impliquant des cycles d'humidification/séchage, que nous n'avons pas étudiés.

Par contre, lorsque les deux acides aminés sont co-adsorbés, des chaînes linéaires de peptides se forment. Le spectre IR du système mixte (Glu + Leu co-adsorbé) n'est pas simplement la somme des contributions des deux acides aminés, confirmant que la présence d'un deuxième acide aminé avec une chaîne latérale différente ouvre de nouvelles voies de transformation thermique. La bande amide I apparaît à des températures encore plus basses (80 ° C) que pour Glu/SiO_2, et est probablement initialement due à la formation de PyroGlu. Mais un phénomène différent est observé à des températures plus élevées (170 ° C), où l'apparition d'une bande amide II suggère la formation de polymères linéaires (cette hypothèse est confirmée par une étude en cours utilisant des méthodes avancées de MS des produits de polymérisation). Concernant la RMN à l'état solide, seules des données limitées ont été obtenues sur les systèmes mixtes Glu + Leu / SiO_2. Ils fournissent des indices suggestifs sur d'éventuelles interactions

spécifiques entre les deux acides aminés, mais une enquête plus complète serait nécessaire pour confirmer ces observations initiales.

L'étape suivante serait une identification plus détaillée des composés thermiquement activés, à la fois expérimentalement (en particulier par RMN) et théoriquement. Au lieu d'une étude «à l'aveugle» d'échantillons activés à des températures d'activation régulièrement espacées, on devrait se concentrer sur les températures auxquelles les spectres IR présentent des changements significatifs. Un apport supplémentaire peut être fourni par les études SM déjà mentionnées des produits d'activation - il a été démontré récemment que dans le cas particulier de Glu + Leu / SiO_2, les peptides formés peuvent être désorbés quantitativement par simple lavage à l'eau distillée. L'enrichissement sélectif d'un seul acide aminé, et / ou d'acides aminés enrichis en une seule position, peut aider à surmonter les difficultés dues au chevauchement des signaux. De cette manière, il peut devenir possible d'identifier des interactions spécifiques entre les groupes fonctionnels des deux acides aminés, ce qui aiderait à expliquer la réactivité particulière du système (Glu + Leu) vis-à-vis de la formation d'oligopeptides linéaires. Théoriquement, des modèles contenant les deux acides aminés ensemble pourraient être construits, éventuellement en doublant l'unité élémentaire de silice utilisée dans cette étude pour avoir suffisamment de sites d'adsorption, et optimisés. La difficulté de cette approche réside dans le nombre très élevé de configurations de départ que l'on peut imaginer lorsque deux acides aminés, chacun avec deux ou trois groupes réactifs, interagissent simultanément avec la surface et entre eux; mais chaque information spécifique fournie par IR et RMN aidera à restreindre les modèles à une liste gérable de possibilités. La même approche que nous avons utilisée dans les chapitres précédents pour les acides aminés adsorbés uniques pourra alors être appliquée: sélectionner les configurations énergétiquement les plus favorables, calculer leurs déplacements chimiques théoriques, et comparer avec les valeurs expérimentales afin de sélectionner les meilleurs modèles.

Références

(1) Lindstrom, E. W. The Origin of Life. *J. Hered.* **1938**, *29* (12), 465–466.

(2) Zaia, D. A. M.; Zaia, C. T. B. V.; De Santana, H. Which Amino Acids Should Be Used in Prebiotic Chemistry Studies? *Orig. Life Evol. Biosph.* **2008**, *38* (6), 469–488.

(3) Sakhno, Y.; Battistella, A.; Mezzetti, A.; Jaber, M.; Georgelin, T.; Michot, L.; Lambert, J.-F. One Step up the Ladder of Prebiotic Complexity: Formation of Non-Random Linear Polypeptides from Binary Systems of Amino Acids on Silica. *Chem. - A Eur. J.* **2018**.

(4) Alaeddine, S.; Nygren, H. The Adsorption of Water and Amino Acids onto Hydrophobic Quartz Surfaces. *Coll. Surf* **1996**, *6*, 71–79.

(5) Gao, Q.; Xu, W.; Xu, Y.; Wu, D.; Sun, Y.; Deng, F.; Shen, W. Amino Acid Adsorption on Mesoporous Materials: Influence of Types of Amino Acids, Modification of Mesoporous Materials, and Solution Conditions. *J. Phys. Chem. B* **2008**, *112* (7), 2261–2267.

(6) Basiuk, V. Thermodynamics of Adsorption of Amino Acids, Small Peptides, and Nucleic Acid Components on Silica Adsorbents. *Cheminform* **2004**, *35*.

(7) Bouchoucha, M.; Jaber, M.; Onfroy, T.; Lambert, J. F.; Xue, B. Glutamic Acid Adsorption and Transformations on Silica. *J. Phys. Chem. C* **2011**, *115* (44), 21813–21825.

(8) Bedoin, L. Ph.D. Thesis, Sorbonne Université, to Be Defended in 2021.